Development of a New Strategy for the Modification of Monolithic Stationary Phases used in Capillary Electrochromatography

Jean-Louis Cabral

A thesis

in

The Department

of

Chemistry and Biochemistry

Presented in Partial Fulfillment of the Requirements
for the Degree of philosophae doctor (Ph.D.) of Chemistry at
Concordia University
Montreal, Quebec, Canada

December 2007

Your file Votre référence
ISBN: 978-0-494-37722-2
Our file Notre référence
ISBN: 978-0-494-37722-2

Abstract

In the past two decades, growing research and commercial activity in the fields of biotechnology and medicine has spawned the development of *minore* efficient separation methods capable of handling increasingly complex and smaller samples. In this new research playpen, capillary electrochromatography (CEC), combining both electrophoretic and chromatographic separation mechanisms, has the potential of playing an important role. Nonetheless, the development and optimization of specialized electrochromatographic stationary phases capable of providing high separation efficiencies for specific applications, such as proteomics, is first required.

This Ph.D. research thesis reports on the development of multifunctional monolithic stationary phases employed principally in capillary electrochromatography. In order to enable the fabrication of such multifunctional monoliths, a simple and novel copolymer grafting followed by functionalization strategy for the adjustment of a monolith's properties was developed. The developed methodology was compared to the classical approach based on adjustment of individual polymerization conditions for the fine-tuning of monolithic support. The grafting approach enabled the efficient introduction of functional moieties on an existing monolithic stationary phase while retaining physical and morphological properties critical to its electrochromatographic properties. The classical approach would have required reoptimization of the polymerization conditions. To demonstrate that the developed technique allows easy

fabrication of a multitask monolithic support, selected proteomics applications were developed.

One of these applications was the development of proteolytic microreactors fabricated via direct and linker-mediated immobilization of trypsin, a proteolytic enzyme, on a reactive monolith. The monolith was made reactive by photografting glycidyl moieties. The proteolytic reactors exhibited high proteolytic efficiency, reproducibility and stability. In addition to the enzymatic capacities the monolith preserved its electrochromatographic properties which could enable its implementation for on-line high-throughput digestion of minute amounts of proteins.

The same photografting methodology was used to produce boronate-functionalized monoliths for the (electro)chromatographic differentiation of glycosylated substrates from their non-glycosylated counterparts. Spectroscopic analyses clearly showed the efficient immobilization of boronate and resulted in efficient separation of glycosylated and non-glycosylated proteins.

Finally, an atomic force microscopy (AFM) characterization technique able to provide physical information in wetted and dry conditions was developed in order to address the general lack of information on structural and morphological properties of monolithic stationary phases in their working (electro)chromatographic conditions.

Acknowledgements

This work would have not been possible without the full support of my devoted supervisor, Cameron D. Skinner who assisted, helped and directed my research work. More important than this project itself, he gave me the privilege of continuously challenging my scientific curiosity, debating my point of views while allowing me to develop stronger personal confidence and mind-opening over not only science but human relationships. He, among others but in a way that can not be acknowledged in any sufficient manner, accepted the personal situations in which I have been confronted throughout these tough but enjoyable years.

This work is dedicated to my beloved partner, coach, best and worst supporter, Vilayvanh Tithavong who has shown me to enjoy not only my success but also and mainly the failures, frustrations and defeats of life.

"Science is not everything, but science is very beautiful", J. Robert Oppenheimer

Without the great involvement of all project students and lab colleagues, this thesis would not have been completed:

Lab colleagues: Zack Papachristou, Dirk Bandilla, Pieter Roos, Vincent Lau, Michel Boisvert, Jane Maxwell, Wei Lin

Supervised summer students: Marie-Ève Beaudoin, Erin Templeton, Nick Gold, Anda Vintiliou, Katherine Drolet-Vives, Karine Lamy, Jonathan Dion, Céline Lacroix, Navneet Kaur, Uduak Idiong, Bobby Ernst-Boursiquot & Maria Kaltcheva.

Table of Contents

List of Figures

List of Tables

List of Equations

Chapter 1

Introduction to Capillary Electrochromatography

1.1 History, Facts and Figures

Capillary Electrochromatography (CEC) is at the junction of Capillary Electrophoresis (CE) and micro-Liquid Chromatography (μ-LC) from which it inherits versatility and high separation efficiency. CEC was first described by Pretorius [1] in 1974 as a separation technique that could offer higher efficiency than traditional liquid chromatography (LC). However, it was not until the involvement of Jorgenson [2] and Knox [3] in the early 1980's that the primary practical and mathematical aspects of CEC were described. It has since attracted great attention for a broad range of applications such as environmental to biochemical analyses of endogenous and exogenous molecules. For instance, Haddad's research group has developed elegant CEC methods for the rapid and efficient determination of small inorganic anions and cations [4,5] while other groups such as El Rassi's [6,7] have successfully implemented CEC for pesticide and insecticide determination in water. CEC has also proved efficient in pharmaceutical analyses including separation and quantitation of hormonal steroids [8], acidic [9] and basic drugs [10]. Historically, reversed-phase differentiation has dominated most electrochromatographic applications due to the commercial availability of functionalized silica stationary phases. However, with the development of polymeric stationary phases, other chromatographic differentiation mechanisms have also been validated. These

chromatographic mechanisms include affinity [11], chiral [12,13], ion-exchange [14] and size-exclusion [15] electrochromatography.

An exhaustive description and explanation of the literature related to capillary electrochromatography was already presented by Bandilla [16]. The publication data clearly shows an increase in the number of publications dedicated to CEC over the last two decades. As experience and theoretical knowledge around electrochromatography research improves, an impressive number of reviews have been written in the last ten years on various aspects such as new electrochromatographic supports, applications and more theoretical aspects. Despite the great initial interest in CEC, a quick look at Figure 1–1 clearly shows that there seems to be a decline in the number of reviews and publications published in the CEC literature that might highlight the need for a "second breath" in the CEC domain. As it was the case for HPLC, this second wind will come with the development of dedicated instrumentation, more pervasive usage and recognition of CEC as a powerful analytical technique [17].

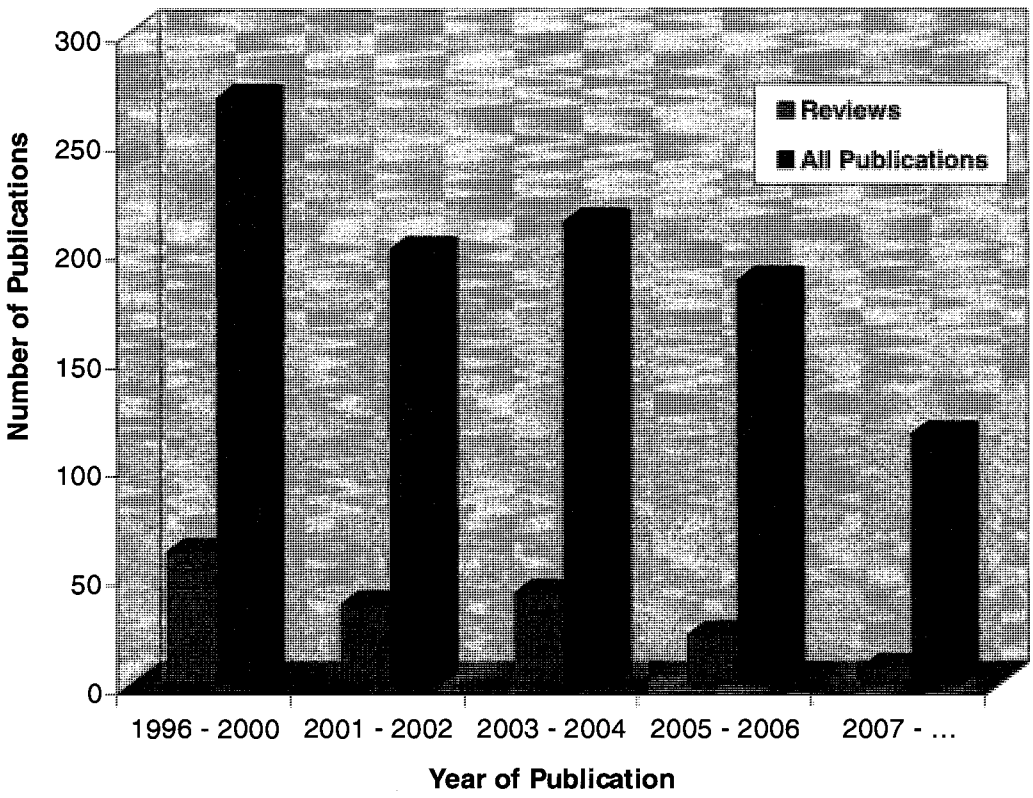

Figure 1–1: Evolution of the number of reviews and all CEC-related publications published solely on capillary electrochromatography including application, theoretical and technical aspects of CEC.

Most of the interest has been, and is still, directly related to electrochromatographic bioanalytical applications where classic one-dimensional separation techniques have not demonstrated sufficient efficiency. It is noteworthy that since 2000 there is a continuous number of publications on novel monolithic CEC stationary phases with an average of 40 yearly publications highlighting the need for improvements in that area.

1.2 Principles of Capillary Electrochromatography

1.2.1 Capillary Electrochromatography Among Other Separation Techniques

Few researchers have seen in CEC a new separation technique that could potentially replace HPLC as the separation technique of first choice in analytical laboratories [18]. Even though CEC offered an improvement in efficiency and significant simplification of instrumental requirements, especially for microvolume samples, the analytical community quickly realized that CEC would become an additional or complementary technique rather than supplanting classic chromatographic and electrophoretic techniques. The reasons for this included more complex method development, lack of fundamental knowledge and absence of specialized electrochromatographic separation supports, *i.e.* dedicated and optimized stationary phases.

There have been a considerable number of reviews elaborating the theoretical advantages of CEC over pressure-driven HPLC [19,20]. A complete overview of the differences in kinetic processes involved between these two techniques is outside the scope of this thesis. However, basic aspects will be discussed in order to allow the reader to understand the potential benefits as well as the advantages and drawbacks of CEC as an analytical separation technique.

The first important question is how do HPLC and CE/CEC differ? The most significant difference between HPLC and electrophoretic techniques such as CE/CEC lies

in how solvent flow is generated in order to enable sample differentiation along the separation channel. HPLC and μ-LC employ an external liquid pump capable of generating a homogeneous liquid flow (hydrodynamic), while flow in CE and CEC is generated via the application of a strong electrical field across the separation capillary leading to electroosmosis, which will be explained below [21]. In addition to the generation of an electroosmotic flow, the electrical field induces electrophoretic differentiation of charged species based on their hydrodynamic size to charge ratio. Thus, analytes are separated based on their difference in mobility with CE and CEC. By comparison, HPLC analyte differentiation occurs strictly based on analytes distribution between an immobilized chromatographic support and a moving mobile phase.

However, CEC differs from CE and other electrophoretic techniques in that it uses separation channels tightly filled with a static solid chromatographic phase similar to that used with liquid chromatographic techniques. Blending of chromatographically active supports and an electrically driven flow allows CEC to take advantage of high separation efficiency found in CE and the powerful versatility of chromatographic techniques.

With regards to size scale, HPLC is commonly performed on 1 to 5 mm internal diameter (I.D.) columns varying between 5 to 25 cm in length [22] and can easily be scaled-up from micro to semi-preparative or preparative scales with samples from sub-nanogram to gram. Increasing demands for the analysis of minute samples has lead to the evolution of HPLC into μ-LC, now widely carried out using capillaries ranging from 10

to 100 cm in length and 5 to 300 μm ID. On the other hand, CE and CEC columns are typically between 20 and 50 cm in length with 5 to 100 μm I.D. but can be longer than a meter together with I.D.'s up to 300 μm if proper capillary cooling techniques are employed. Even though preparative CEC (ID > 300 μm) has been described in the literature, it will stay outside the topic of this thesis due to present limitations in use. Electrodriven separations are limited by the need to dissipate Joule heat associated with the current generated by virtue of application of an electrical field. As it will be explained in Section 1.2.3, dissipation of the electrically-associated joule heating is favoured with the use of capillary channels with smaller internal diameters that possess higher surface area to volume ratio for efficient heat exchange with the external environment. Thus, sub-ng to microgram samples are commonly separated by electrochromatography.

As with liquid chromatography and electrophoretic techniques, CEC has different modes of operation that are distinguished based on the chromatographic support in the separation channel as well as the mechanisms of chromatographic differentiation. CEC, as with other chromatographic techniques, can be performed with separation channels either completely filled or with only the surface modified by a chromatographic moiety. In open-tubular CEC (OTCEC) [23] the stationary phase is formed by means of a chemical reaction within a clean separation channel leading to the formation of a thin functionalized layer sufficient to allow chromatographic differentiation. Due to limited rates of mass transfer with the chromatographic layer on the wall, OTCEC suffers from

lower separation efficiency than packed column CEC where contact between the analyte and stationary phase is much improved. Nonetheless, Wu clearly underlined that OTCEC also offers advantages over packed CEC [24]. As pointed out in his review, higher sensitivity can be observed using capillaries with close to 10 μm inner diameter due to a lack of multipath band broadening from the chromatographic packing. Furthermore, Joule heating is less prevalent in OTCEC due to the higher surface area to volume ratio of capillaries employed in OTCEC allowing the use of higher electrical fields that result in faster separation and less longitudinal band broadening.

All separation mechanisms employed in HPLC have been described for CEC including reversed-phase [25], normal-phase [26], ion-exchange [14], affinity [11], size-exclusion [15], chiral separation [12] and hydrophilic interaction [27] as well as combined chromatographic mechanisms [28,29]. Indeed, all types of chromatographic supports can be easily transferred from HPLC to CEC as long as a sufficient and homogeneous number of ionized moieties are present on the chromatographic media in the operating conditions for a constant and homogeneous electroosmotic flow along the stationary phase, as it will be discussed further below.

The following table summarizes the main characteristics of both μ-LC, CEC and common modes of CE.

Table 1: General aspects of μ–LC, CEC and CZE

Parameters	μ–LC	CEC	CE (CZE, MEKC, CGE, cIEF)
Detection methods	All	All	Buffer interference with MS detection
Versatility	Yes	Yes	Yes
Cost	Expensive columns and instrumentation	Expensive columns	Very affordable
Ease of operation & method development	Relatively easy	Troubleshooting difficult	Relatively easy
Dedicated instrument	Yes	No	Yes
Well described theory	Yes	Partially	Yes
Mode of separation	RP, NP, IE, size-exclusion, affinity, chiral…	As μ–LC + electrophoresis	As μ–LC + electrophoresis (dynamic process requiring additives)

CZE: Capillary zone electrophoresis
MEKC: Micellar electrokinetic capillary electrophoresis
CGE: Capillary gel electrophoresis
cIEF: Capillary isoelectric focussing

1.2.2 CEC Driving Force: Electroosmotic Flow

As explained in the previous section, CEC differs from liquid chromatography in that mobile phase flow is generated by the application of an electrical field in the separation channel, as in capillary electrophoresis (CE). It shall be mentioned here that throughout this thesis, CE refers to capillary zone electrophoresis (CZE) unless otherwise specified.

An experienced chromatographer not familiar with the principles of electrokinetic separations will naturally ask how can a chromatographic support generate a constant and homogenous flow in the separation channel? Flow generation in CEC is explained by the same surface phenomenon allowing CE separations, namely electroosmotic flow (EOF).

When used in combination with the ionized surface of a stationary phase, the application of an electric field leads to the generation of an electroosmotic, or electroendosmotic, flow observed over the entire hydrated surface. To explain how the EOF is generated it is important to bear in mind the two main criteria required: the surface must possess a net homogeneous charge over its entire surface and that there is an accumulation of counter charges in the surrounding mobile phase.

If a surface (*e.g.* silica or a sulfonated stationary phase) is placed in contact with an aqueous phase the surface functional groups may be ionized resulting in a charged solid-liquid interface. To maintain local electroneutrality, the charged hydrated surface naturally attracts ions with an opposite charge from the bulk liquid leading to polarization of the liquid close to the surface. The Helmoltz electric-double layer produced by this polarization, and described by the Stern model, consists of a rigid counter ion plane (Helmoltz plane) near the solid-liquid interface and a more diffuse counter ion region farther away from the surface [30]. The generated electric double-layer δ has a typical thickness of 1 to 10 nm and is associated with the ξ potential and is shown on the right-hand edge of Figure 1–2.

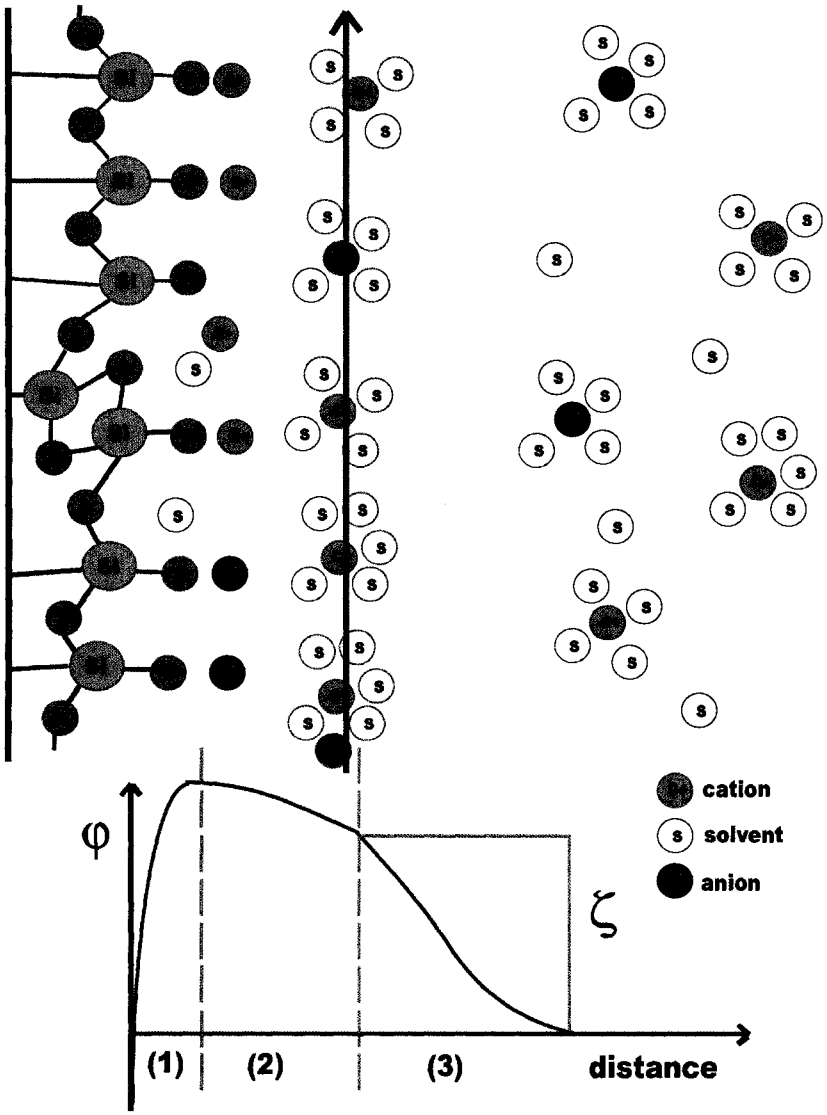

Figure 1–2: Generation of EOF near the surface of a quartz capillary with a graph of the potential (φ) dependency over distance from the silica wall. The potential at the boundary of layers (2) and (3) is the zeta-potential (ξ) of the Helmoltz electric double-layer. Layers: (1) Helmholtz inner plane; (2) Helmholtz outer plane; (3) Diffuse layer.

As shown in Figure 1–2, the Stern layer consists of the combination of charged silanols (SiO^-) from the capillary wall and unsolvated cations close to the surface. The unsolvated cations form a rigid plane in the Helmholtz inner plane while the solvated cations and anions further away from the surface in the Helmholtz outer plane are moving

toward the cathode under the influence of a cathodic electric potential. Through the movement induced in the Helmholtz outer plane, the solvated anions, cations and solvent molecules from the diffuse layer are carried toward the cathode resulting in the EOF.

The Smoluchowski equation describes the magnitude of this flow, expressed as the linear velocity u_{eo} [31]:

(Equation 1) $$u_{eo} = \frac{\varepsilon_0 \varepsilon_r \xi E}{\eta} = \frac{\varepsilon_0 \varepsilon_r \xi V}{\eta L}$$

Equation 1: Smoluchowski equation where ε_0 is the vacuum permittivity constant (8.85×10^{-12} $C^2 J^{-1} m^{-1}$), ε_r is the dielectric constant of the mobile phase, ξ is the zeta potential, E is the electric field strength due to the application of a voltage V across a separation media of length L while η is the viscosity of the mobile phase.

Due to the direct relationship between the electroosmotic velocity and the applied field strength, the most straightforward means used to tune the EOF amplitude is to regulate the applied electric potential. However, the relationship between EOF and electric field deviates from linear at elevated electric fields due to Joule heating effects. The heating resulting from increased electrical current causes a decrease in mobile phase viscosity thus faster electroosmotic velocity than predicted by theory, an important phenomenon that will be discussed in a later section.

For small electric potentials, the zeta potential is also expressed as:

(Equation 2) $$\xi = \frac{\sigma \delta}{\varepsilon_0 \varepsilon_r}$$

Equation 2: Zeta-potential of the Helmoltz electric double-layer where σ is the charge density at the surface and δ is the thickness of the double-layer.

(Equation 3) $$\delta = \left(\frac{\varepsilon_0 \varepsilon_r RT}{2IF^2} \right)^{1/2}$$

Equation 3: Thickness of the double-electric layer where R is the universal gas constant (8.314 J K^{-1} mol^{-1}), F is the Faraday constant (9.6485x10^4 C mol^{-1}), T is the absolute temperature and I is the ionic strength of the mobile phase in mol L^{-1}.

As underlined by the Smoluchowski equation, the EOF amplitude can also be adjusted by modifying the electrical double-layer thickness via the mobile phase (electrolyte solution) composition. Adjustments of the mobile phase pH, viscosity, temperature, ionic strength (concentration) and dielectric constant are the key parameters affecting the flow rate of a CE or CEC separation.

Subtly, the Smoluchowski equation also highlights the significance of the electrochromatographic stationary phase surface properties on the EOF amplitude. More specifically, the pKa and surface density of the surface ionizable moieties that support the EOF have a direct influence on the EOF. Additionally, unreacted silanol groups from the supporting capillary wall can also contribute to CEC EOF [32]. However, efficient electrochromatographic separations require that the CEC stationary phase generates uniform EOF flow over its entire surface otherwise excessive band broadening would result from the mixing due to the mismatch in EOF's [33]. It should also be mentioned that the physical and morphological characteristics of the electrochromatographic support also have a slight impact on the EOF as explained by Choudhary [34], but this topic will not be discussed here.

Unlike the parabolic flow profile in μ-LC, the EOF amplitude remains independent of separation channel diameter (d_c) as long as it is greater than 50δ [35]. When the distance separating two EOF generating surfaces is smaller than 50δ, electric-double layer overlap can occur and results in the formation of stagnant non-mixing zones. In practice, this phenomenon is observed at the junction of two adjacent stationary phase particles or within narrow pores. For instance, Bartle [35] estimated that for a mobile phase consisting of 30/70 (%v/v) aqueous electrolytes/acetonitrile with a 2.5 mM ionic strength, double-layer overlap would occur in voids smaller than 5 nm while in a 1.0 mM ionic strength solution the overlap would happen in pores smaller than 8 nm. Thus, perfusive flow within stationary phase particles is expected to occur with high ionic strength only for sorbents characterized by wide pores (>50 nm). The EOF non-uniformities and stagnant zones result in additional band broadening and lower the chromatographic efficiency. This is quite important to consider in CEC because the distance between chromatographic particles, or mean channel diameter, can approach the electric-double layer overlap limit [15].

When the conditions for generating an EOF are met, a flat flow profile is observed in CE at distances over 1 nm from the capillary wall [36] and significantly reduces the sample band broadening, as depicted in Figure 1–3, but this same flat profile occurs in the smaller inter-particle channels in CEC. Comparatively, pressure-driven separation techniques generate parabolic flow profiles due to the higher resistance to flow

at solid-liquid interfaces. As a result, electrodriven techniques offer a significant improvement in separation efficiency over HPLC and μ-LC.

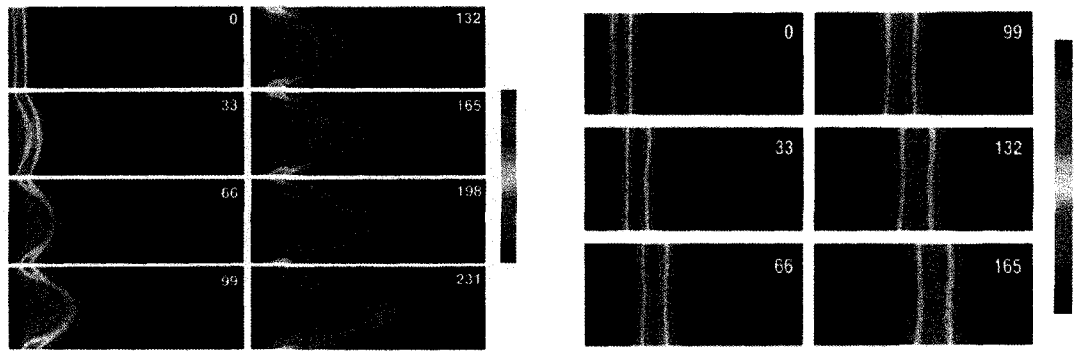

Figure 1–3: Flow profiles in an open channel induced by a pressure (left) and voltage (right) (From ref [37]).

1.2.3 Joule heating in CEC

Using electro-driven separations in packed media has its own non-negligible disadvantages. In CEC, the applied field strength determines the linear velocity as previously noted, but, as with any other resistive object, the chromatographic solvents will dissipate energy producing heat, known as Joule heating. This Coulombic phenomenon is amplified with increasing mobile phase ionic strength, solvent dielectric constant and channel cross-sectional area. Fortunately, CEC, unlike CE, employs organic modifiers that reduce Joule heating significantly due to their lower dielectric constant and have a reduced cross-sectional area making possible the use of higher electrical potentials.

If sufficient cooling of the column/capillary is not achieved, Joule heating causes the generation of a temperature gradient across the channel/capillary leading to gradients in the mobile phase viscosity. Because cooling is less effective at the center of the

separation channel the higher temperature and lower viscosity allow higher EOF and analyte molecules migrate faster than the ones closer to the channel wall. Also, it leads to changes in analyte diffusion coefficient (D_m) across the capillary thus increasing bandbroadening. Indeed, both EOF and analyte mobility are dependent on viscosity while analyte diffusion is dependent on both temperature and viscosity. Additionally, analyte retention is also reduced by increasing temperature due to increased partition into the mobile phase. Thus, the generation of a temperature gradient associated with Joule heating will broaden chromatographic bands through a variety of bandbroadening mechanisms. Once again, this effect is minimized with smaller diameter capillaries that maximize the surface area per cross-sectional area and active capillary cooling that permits better heat transfer.

Problems associated with bed overheating have been one of the many impediments for the early acceptance of CEC. Perhaps more important than the viscosity effect, in CEC, excessive heating also leads to formation of bubbles within the chromatographic bed, or at retaining frits due to difference in EOF between the frit and stationary phase.

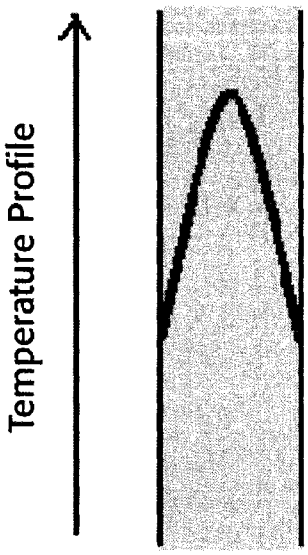

Figure 1–4: Theoretical temperature profile from an insufficiently cooled separation media due to Joule heating. Viscosity follows an inverse relationship with temperature, analyte at the center of the capillary will migrate faster than the ones closer to the cooler capillary wall, where the mobile phase is more viscous.

These bubbles form when mobile phase degassing occurs due to local increase in temperature within the closed microenvironment formed by the packing. Once formed, these bubbles break the electrical continuity and result in electrical discharges within the capillary. The discharge causes further local heating and "cooks" the stationary phase bed.

1.2.4 Chromatographic Theory in Capillary Electrochromatography

The electroosmotic flow has a direct impact on the kinetics of chromatography. Even though CEC differs significantly from HPLC and μ-LC, it follows the same basic

empirical model outlined by the Van Deemter equation that describes chromatographic techniques.

As in all chromatographic techniques, the dispersion of a band during its chromatographic elution is described by the kinetic theory based on the Brownian motion of molecules along with the retention process. More specifically, it corresponds to the summation of all the independent mechanisms leading to variance in the distance that analyte molecules will, statistically, travel along a separation channel. This results in a Gaussian distribution of analyte molecules represented as a peak.

(Equation 4) $\sigma_{total}^2 = \sum_i^n \sigma_i^2$

Equation 4: Summation of all of the independent contributions to sample band broadening, related to peak width, is the observed peak variance.

In common chromatographic experiments, all variances responsible for band spreading including both intra and extracolumn broadening sources are summed. Typical extracolumn band broadening sources are associated with connecting tubing, detector cell volume and injection issues that are not related to the actual properties of the separation media [38]. In this thesis only intracolumn band broadening sources that are representative of a chromatographic media properties are discussed.

The Van Deemter equation is a theoretical model that consolidates all contributions to a chromatographic band distribution expressed as its plate height, where [39]:

(Equation 5) $H = \frac{\sigma^2}{L}$

Equation 5: The relationship between a chromatographic band plate height (H, expressed in cm) and the total variance of the band (cm^2) for a separation channel of a length L (cm).

For both CEC and LC, it is articulated as:

(Equation 6) $H = H_{disp} + H_{e,diff} + H_{i,diff} + H_{t,diff} + H_{kin}$

Equation 6: Van Deemter equation for CEC and LC where H_{disp} is the contribution to band broadening caused by the axial diffusion in the interstitial space, $H_{e,diff}$ is from the resistance to mass transfer in the stationary phase film, $H_{i,diff}$ is from the diffusion of the solute in the intra particle stagnant mobile phase, $H_{t,diff}$ is from the transchannel mass transfer and H_{kin} is from the limited kinetics of interaction between the solute and the stationary phase.

Succinctly, it is simplified and commonly expressed as:

(Equation 7) $H = A + \frac{B}{u} + Cu = 2\lambda d_p + \frac{2\gamma D_m}{u} + \frac{cd_p^2}{D_m}u$

Equation 7: Simplified Van Deemter equation for CEC and LC where A (H_{eddy}) is the Eddy diffusion term, B (H_{diff}) represents the longitudinal diffusion, C ($H_{masstransf}$) the resistance to mass transfer term, λ a factor related to packing d_p the particle diameter, D_m the analyte diffusion coefficient in the mobile phase, γ the obstruction factor of the stationary phase and u the linear flow rate (cm s^{-1}), c is a constant.

The Eddy diffusion term (A) relates to band spreading caused by the stationary phase tortuosity arising from all the different flow paths, thus distances, that the analyte molecules can follow through the packed bed. Its magnitude depends on the packing quality, referred by Knox as "goodness" of column packing [40] and is also related to the homogeneity of the packing and is amplified by increasing interparticle distances, as

shown in Figure 1–5. The knowledge built-up from the use of packed columns for liquid chromatographic separations has demonstrated that the multi-path term can be significantly improved through the use of smaller chromatographic particles combined with a reduction in the total particle size distribution.

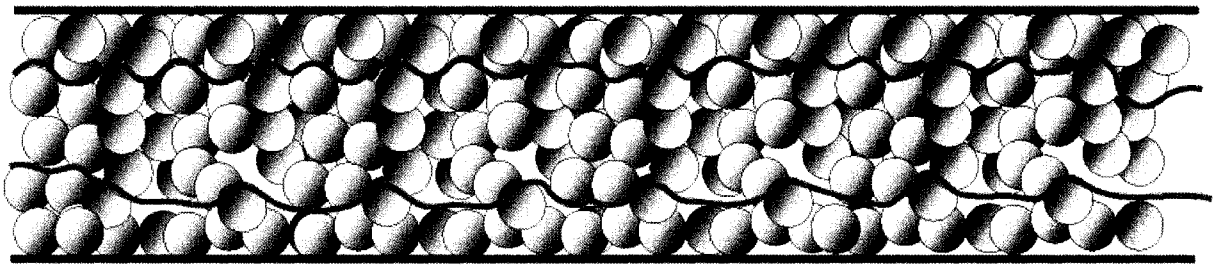

Figure 1–5: Example of band broadening due to different flow paths followed by two molecules. The two molecules will follow paths of different lengths thus arriving at the detector at different times leading to spreading of the chromatographic peak.

Experiments using the same columns for μ-LC and CEC have shown that a net reduction in the Eddy diffusion term was achievable in CEC over μ-LC [41,42,43] due to the flat flow profile associated with electrodriven separation.

The second term of the Van Deemter equation explains the bandbroadening from longitudinal diffusion caused by analyte diffusion from the highly concentrated chromatographic band center to the surrounding liquid media. It thus results in a concentration gradient with a typical Gaussian distribution pattern due to equal diffusion in both axial directions. The extent of diffusion depends on the total time available for diffusion thus the inverse relationship with the mobile phase velocity. Additionally, the chromatographic particles reduce the extent of diffusion by obstructing (γ) the molecules.

Not surprisingly, the longitudinal diffusion term is similar for both CEC and HPLC unlike eddy diffusion.

Finally, the last term of the Van Deemter equation corresponds to the contribution to band spreading (C) caused by resistance to mass transfer which reflects the slow equilibration of an analyte molecule between the mobile phase and stationary phase and vice-versa. With pressure-driven separations, the analyte mixing between the pores and the interstitial mobile phase is relatively slow because it is inherently dependent on analyte diffusion. On porous stationary phase particles, between 50 to 80% of the surface area is enclosed within pores which highlights the mass transfer limitation, especially at high mobile phase velocity which limits the time available for equilibration [44]. This phenomenon is significantly reduced with non-porous and superficially porous chromatographic particles, which on the other hand suffer from low surface area for retention. Alternatively, clear improvements in mass transfer kinetics can be achieved with porous stationary phases in CEC due to the constant mixing to/from within pores ensured by EOF provided that the limits of the electric double-layer overlap are respected.

Considering the minimal impact of the Eddy diffusion term, Equation 7 now simplifies for CEC separation into:

(Equation 8) $$H = \frac{B}{u} + Cu = \frac{2\gamma D_m}{u} + \frac{cd_p^2}{D_m}u$$

Equation 8: Simplified Van Deemter equation for CEC.

Further gains in separation efficiency can theoretically be achieved through the use of smaller chromatographic particles such that band broadening would mainly be caused by longitudinal diffusion (term B). In fact, Dittman and Rozing were among the first to recognize that EOF enables the use of very small particles that would not be practical with pressure driven separations because of the significant increase in operating backpressure (ΔP) at constant linear velocity [43]. The relationship between mobile phase velocity and pressure is:

(Equation 9) $$\Delta P = \frac{u \phi L \eta}{d_p^2}$$

Equation 9: Pressure drop (ΔP) in pressure driven separation where u is the linear velocity, ϕ the pressure resistance factor of the packed channel, L the separation media length and η the mobile phase viscosity.

CEC does not suffer from backpressure issues since flow is generated at the stationary phase surface and throughout the column. Accordingly, the use of very small packing particles combined with high linear velocity can theoretically yield rapid and very efficient separations.

To conclude, the advantages of CEC over HPLC were well demonstrated by Jiang as shown in the Van Deemter curves achieved using the same chromatographic bed [45]:

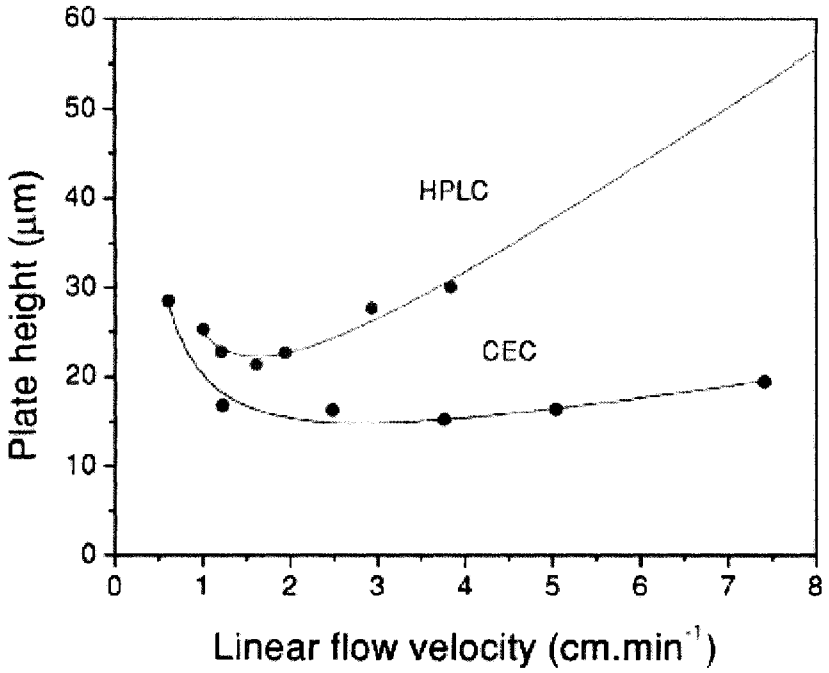

Figure 1–6: Van Deemter curves of a single chromatographic column obtained under electrokinetic (CEC) and pressure-driven conditions (from ref [45]).

1.2.5 Optimization of Electrochromatographic Separation Conditions

Even if LC and CEC differ significantly, they both exploit the same basic chromatographic principles to attain analyte differentiation. However, the combination of electrophoretic and chromatographic differentiation in CEC introduces a new dimension to classic liquid chromatography theory that requires revision of pressure-driven chromatographic expressions. For pressure-driven separations, the extent of retention of an analyte, is defined as the capacity factor *k*:

(Equation 10) $k = \frac{t_r - t_o}{t_o}$

Equation 10: Capacity factor where t_r is the retention time of the selected analyte and t_o the mobile phase retention time often detected using an unretained marker.

Because an unretained marker does not interact with the chromatographic media, by definition, all species will elute with or after this unretained marker ($t_o \leq t_r$) in pressure-driven conditions, therefore k is always positive.

Unlike HPLC, the capacity factor in CEC can have positive, negative or null values for retained species and unretained species since the velocity of an analyte (u_{total}) in CEC is the summation of its electrophoretic (u_{ep}) and electroosmotic (u_{eo}) mobility and a chromatographic "retardation" factor (1/(1+k)), as expressed by Mistry [46], all schematized as vectors in Figure 1–7.

(Equation 11) $u_{total} = \frac{u_{ep} u_{eo}}{(1+k)}$

Equation 11: Velocity of a charged analyte in CEC.

Comparatively, an unretained marker in CEC must be neutral meaning that it has no electrophoretic mobility. In these conditions, it can elute before, with or after a charged species ($0<k<0$) in electrochromatography as shown in Figure 1–7.

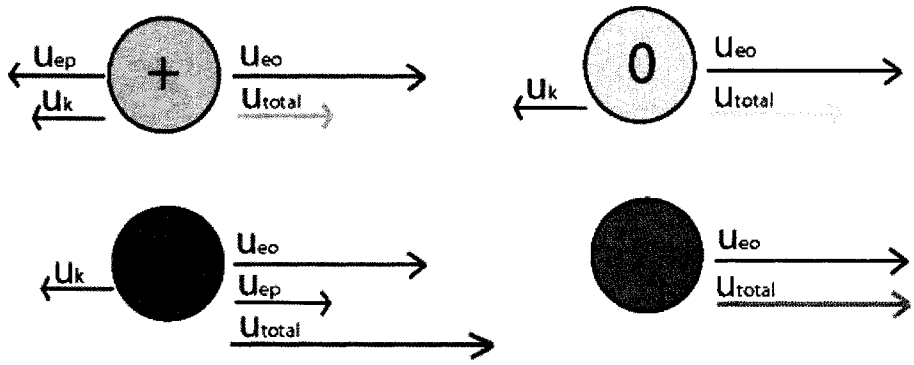

Figure 1–7: CEC differentiation of charged, neutral retained and unretained species where the individual overall mobilities are represented by the coloured arrows. The total mobility of an analyte (u_{total}) is represented as a vector resulting from the vector summation of all individual mobility vectors, *i.e.* its electrophoretic mobility (u_{ep}), electroosmotic mobility (u_{eo}) and retardation/retention factor (u_k) expressed as a counterdirectional vector. Analyte differentiation will occur if individual u_{total} vectors differ significantly.

A few formalisms have been proposed to adapt the classic interpretation of the capacity factor to electrochromatography. Rathore and Horvath proposed a definition based on an electrophoretic formalism that considers the difference in electrophoretic mobility of an analyte and an unretained marker [47].

(Equation 12) $k_{CE} = \frac{t_o - t_r}{t_r}$

Equation 12: Capacity factor following the electrophoretic formalism. An analyte moving faster than the EOF will have a $k_{CE} > 0$ while an analyte eluting after the EOF will exhibit a $k_{CE} < 0$.

However, this latter formalism does not clarify the individual contributions of the chromatographic and electrophoretic components to the retention capacity. Accordingly, a number of publications have dealt with various approaches to develop and validate a

theoretical description that would better fit experimentally observed electrochromatographic parameters [47,48,49,50]. Even though there has been a substantial, and a fundamental, consensus toward the requirement of a better mathematical model for the description of CEC differentiation, this last expression will be used throughout this thesis to describe and compare chromatographic separations and supports due to its simplicity and ease of understanding for comparison of retention/migration.

1.2.5.1 Parameters Influencing Electrochromatographic Retention

Considering the interplay of migration mechanisms in a CEC separation, a chromatographer might find it difficult to convert a pressure-driven analytical separation method to its voltage-driven counterpart. However, taking into account a few basic considerations during initial method development and optimization will allow the separation to benefit from both the electrophoretic and chromatographic components of the electrochromatographic method.

The separation conditions dictate the amplitude and direction of the EOF, the apparent migration of an unretained neutral marker is used to establish the EOF velocity, thus the electroosmotic component of the analyte electrochromatographic mobility. However, consideration must be given to the occurrence of any size-exclusion mechanisms, even with small chromatographically unretained molecules, as it will bias the true EOF value due to a change in the unretained molecule retention time caused by

the size-exclusion mechanism but nonetheless provides a practical framework for CEC measurements.

As in HPLC, a change in the mobile phase composition, for example pH, ionic strength, can affect retention through modification of the equilibrium constant that dictates retention. For example, protonation/deprotonation of either the chromatographic surface and/or analyte molecule can be used to increase or decrease retention. Some CEC stationary phases can exhibit profound variations in EOF amplitude even upon subtle changes in pH or ionic strength as a result of their low acidic or basic capacity, as in weak anionic/cationic exchange electrochromatography. This strategy is the main approach for tuning the chromatographic properties in ion-exchange electrochromatography. Several applications have also shown the benefits of modifying the mobile phase ionic strength in reversed-phase CEC for the differentiation of mildly non-polar compounds [51]. However, when elevated ionic strengths are used, excessive Joule heating may result. One way of avoiding such concerns is the use of zwitterionic additives [52].

In addition to modifying the electrophoretic properties of the separation, CEC allows tuning of the retention kinetics like other retention based chromatographic techniques. Naturally, the most common and appropriate strategy remains modification of the mobile phase organic content, *i.e.* concentration and nature of the organic solvents/modifiers. The mobile phase composition controls analyte partitioning between the mobile and stationary phase. Yet, in reversed-phase electrochromatography a change

in the mobile phase hydrophobicity not only affects the retention kinetics but also affects the dielectric constant, thus the ionic strength that, as explained previously, has a direct influence on the EOF amplitude. The interdependence of chromatographic and electrophoretic factors is cited as one of the chief drawbacks of CEC but even with these limitations there is sufficient independence to allow a wide range of operational conditions to be achieved.

Surprisingly, few researchers have shown the potential of adjusting separation temperature to adjust both the EOF amplitude separation efficiency due to the kinetic nature of the chromatographic retention [53].

Interestingly, other researchers have realized benefits with the use of external pressure to assure control of the mobile phase velocity and avoid dependance on the EOF for flow generation. This hybrid technique is termed pressurized-flow electrochromatography (PEC) [54] and has been employed mainly to prevent bubble formation that particularly hindered the development of CEC in its early stages. In addition, the use of external pressure provided by a liquid pump as in μ-LC enables potential enhancement of separation efficiency via gradient elution, known as gradient elution PEC [55] and described later in Section 1.2.6. Unfortunately, it suffers from the same drawback as pressure-driven separation, that is limitations of column length and inner diameter due to increased backpressure. Even though it was thought that selective application of positive pressure to either the inlet or outlet end of the electrochromatographic channel could introduce another efficient means to adjust the

selectivity [56], a very limited number of references have investigated this added benefit of PEC [57].

At first glance, the inexperienced (electro)chromatographer might be discouraged by the complex interplay between the electroosmotic, chromatographic and electrophoretic mechanisms characteristic to CEC separations. Yet, as just described, CEC offers a wider range of separation parameters that can give access to improved separation efficiencies and selectivities if the multiple parameters are well understood and controlled.

1.2.5.2 CEC On-line Sample Enrichment Techniques

As with other separation techniques based on microchannels, detection limits in CEC methods are naturally limited by the small injection volume and reduced pathlength available for photometric detection. To overcome these limitations sample-stacking techniques, such as isotachophoresis, dynamic pH junctions and low ionic strength sample zones (field-enhanced sample injection or sweeping) that concentrate analyte into a narrow band through manipulations of zonal electrophoretic mobility can be used [58,59]. For example, Zhang [60] employed chromatographic zone-sharpening and field-enhanced sample stacking, inherited from CE and LC, respectively, to improve detection sensitivity by 1600 fold in the CEC analysis of propanetene. Moreover, several publications have described the combination of chromatographic focusing techniques such as step-gradient elution [61] and preparation of sample in non-eluting solvent [62] to

electrophoretic stacking methods improving the detection sensitivity by a factor of up to 1000 fold.

1.2.6 Instrumentation

CEC remains an immature separation technique, not widely implemented in either commercial or even research laboratories. Most pioneers from the electrochromatography and chromatography research fields have blamed the lack of dedicated commercial instruments for the slow improvement and implementation of CEC into non-academic research laboratories [18].

In fact, CE and CEC instruments are quite similar. Basic capillary-based instrumental designs include a high voltage power-supply that provides generation of the separation electric potential, a detector (UV-VIS, diode-array, fluorescence, MS, NMR) either on-column or in-line, a capillary holder and an external pressure source as shown in Figure 1–8.

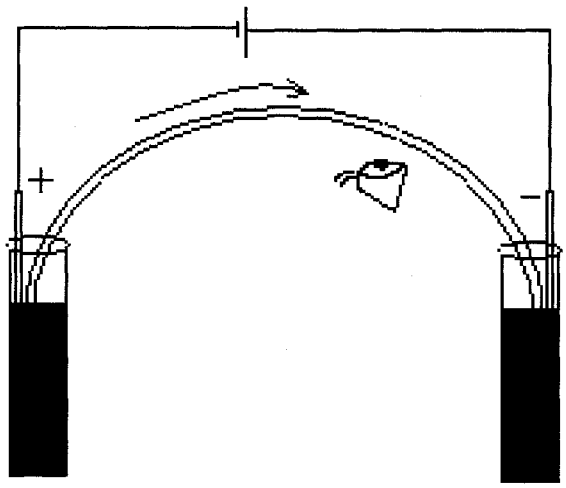

Figure 1–8: Schematic diagram of a basic CE/CEC instrument with cathodic EOF flow. In PCEC, pressure is applied to either both inlet and outlet vials to reduce the extent of bubble formation or applied to a single vial to accelerate (inlet) or slow (outlet) separation.

Sample introduction is through immersion of the inlet in the sample vial and either through application of a positive pressure or application of an electrical potential to generate EOF pumping. Successful hydrodynamic sample injection and capillary conditioning in CEC can only be achieved by using a high pressure source (500-1500 psi) due to the high back pressure caused by the CEC media. In addition to direct capillary injection, high pressure can also be used to accelerate capillary conditioning using low pH and/or high organic content solvents that usually generate very weak electroosmotic flows.

Furthermore, application of moderate external pressure (~50 psi) to both inlet and outlet capillary ends has also been shown to decrease the extent of bubble formation [63]. Unfortunately, only a few commercial instruments can provide the pressures required for injecting/conditioning, which explains the great number of CEC publications that use external HPLC pumps or other high pressure sources. For instance, in order to fully exploit the separation power of CEC, Behnke [64] and Robson et al. [65] as well as Eimer [66] have developed a home-built pressurized flow CEC (PCEC) system that can perform gradient-elution with the assistance of a binary HPLC pump and an electrically grounded tee-junction that allows injection and elution through electroosmosis as shown in Figure 1–9:

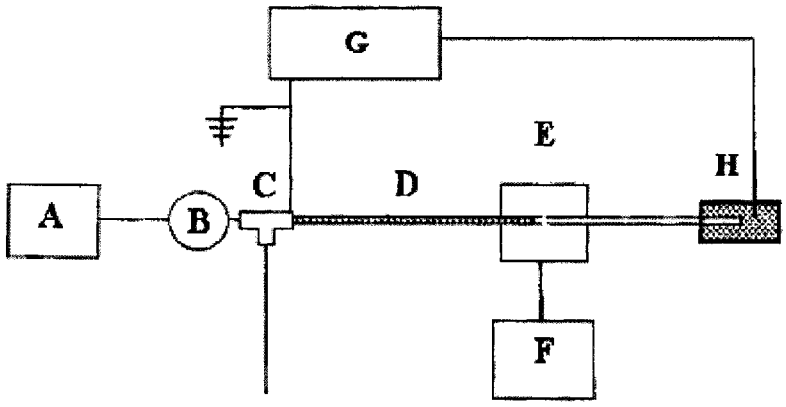

Figure 1–9: Schematic diagram of a gradient-elution CEC instrumental design reproduced from [66]. Instrumental details: (A) HPLC pump, (B) Injector, (C) Tee/flow splitter, (D) Packed separation capillary, (E) Detector, (F) Data acquisition, (G) High voltage power supply, (H) Electrode vessel.

CEC also suffers from the absence of commercially available power supplies able to generate electrical potentials in excess of 30 kV that would allow higher field

strengths, higher EOF's and faster separations. However, at such high electrical potentials CEC could encounter the same limitation as CE, namely excessive Joule heating. As recognized by Simal-Gándara [67], development and further commercialization of instrumentation allowing users to perform, and switch between CE, CEC, HPLC and pressurized CEC with the same instrument would really broaden the horizon of CEC to real-world laboratories. In parallel, special efforts will be required to develop and implement dedicated stationary phases capable of providing similar efficiencies as achieved on existing HPLC columns while giving the possibility of being used in CEC conditions.

In terms of detection techniques, various technical schemes and approaches have been described together with CEC separations. The most prominent are UV-Vis absorbance, laser-induced fluorescence (LIF), mass spectrometry (MS) [68], nuclear magnetic resonance (NMR) [69] and electrochemical (conductimetric) detection [70]. As with any other capillary-based separation technique, absorbance detection sensitivity in CEC is relatively low compared to macrobore separation media due to the restricted path length available for detection. In practice, the combination of higher plate numbers and on-line concentration strategies has shown an interesting improvement in sensitivity, as explained previously.

Other researchers have used their knowledge and experience developed with CE-LIF and investigated different approaches involving native fluorescence [71], pre-

separation [72], on-capillary [73] and post-separation [72] fluorescence labelling coupled to CEC for increasing detection sensitivity.

However, many have recognized that the structure elucidation capability of mass spectrometry and NMR detection, in combination with the separation efficiency of CEC, is ideal for complex analyses and particularly for proteomic applications. Additionally, CEC methods often employ organic solvents, or modifiers, that improve MS and NMR detection, unlike CE mobile phases. In CE, the mobile phase (background electrolyte) is usually aqueous and contains buffer salts or additives that result in poor sample vaporization in the MS source and/or adduct formation for both small molecules and macromolecule analysis. In the case of MEKC methods, the closest electrophoretic technique to CEC, additives essential to differentiation are not compatible with MS detection. Another parent electrophoretic separation technique based on a non-aqueous mobile phase, nonaqueous CE (NACE) first described by Jorgenson in 1980 [74], has also shown great potential with MS detection but usually demonstrates poor migration time reproducibility and band broadening due to destacking phenomena [75, 76]. One of the great benefits of CEC-NMR resides in the characteristic low flow rates enabling the use of expensive deuterated solvents in comparison to HPLC-NMR. Implementation of these detection techniques has already shown great promise in various research fields [68].

1.2.7 Applications of CEC in Proteomics and Other Fields of Research

CEC has been used in various applications where μ–LC and CE methods lacked sufficient efficiency. Haddad and collaborators [77] demonstrated that a wide selection of CEC supports used in ion-exchange chromatography were able to shorten separation time without decreasing separation efficiency for simple ions due to enhanced mass transfer kinetics. Numerous μ–LC reversed-phase separation methods have been successfully implemented in CEC, mainly in the analysis of neutral drugs [78], parabens and PAH's [79] and small biomolecules. Smith [80] for example benefited from the complex interplay of ion-exchange chromatography and electrophoresis for the optimized separation of small charged antidepressants using a strong cation exchange stationary phase.

Even though there is an extensive list of electrochromatographic applications that has been published in the last two decades, the overall achievements of CEC were not sufficient to warrant CEC replacing well-integrated μ–LC and HPLC methods in the routine analytical laboratory. CEC researchers have thus put a stronger focus towards applications where the required level of information is high such as the analysis of complex biological samples.

This is the case in proteomics, biomarker discovery and complex plasma analysis where important information is normally masked by very complex sample patterns. Only with high resolution and efficient separations is the quality of the information high enough that it becomes possible to reveal precise details on the nature and abundance of

the analytes (e.g. biomarkers) constituting the biological image of the subject under investigation.

Smith and coworkers were among the first to demonstrate the robustness of CEC with regards to the analysis of complex plasma samples [81]. In their investigation, they were able to demonstrate that lower LOD's were obtained for the highly reproducible CEC separation of corticosteroids on a hybrid octadecyl (C18)-strong cation exchange (SCX) stationary phase from a plasma sample using MS compared to UV detection. Interestingly, the investigators observed that higher currents could be used with MS over UV detection without observing significant Joule heating, even without capillary pressurization but no further explanation was provided by the authors.

Ion exchange, normal-phase, reversed-phase, size-exclusion and affinity-chromatography are all examples of liquid separation modes that have already demonstrated their efficiencies for both chromatographic and electrochromatographic separations of biopolymers and small analytes [82]. An extensive series of reviews has been published over the last decade dealing with the electrochromatographic differentiation of biomacromolecules (83,84). A number of these have commented on the large number of applications that have shown the great separation efficiency of reversed-phase and ion-exchange electrochromatography [85,86,87]. On the other hand, several groups have applied mixed-mode polymeric stationary phases for the high efficiency electrochromatographic separations of peptide and protein mixtures [46]. Practically, the combination of electroendosmotic, ionic and hydrophobic differentiation gives access to

greater separation flexibility although the basis for the resulting electrochromatographic pattern becomes more complex to explain from a theoretical point.

In cases where a combination of ionic and hydrophobic interaction occurs, investigation of the influence of organic content and ionic strength (salt content) on the analyte logarithmic retention factor (log k') remains a good way to estimate the extent of each mechanism on individual analyte migration behaviour.

However, as described by Haddad [88], the relationship of the logarithmic retention factor (log k') over the mobile phase eluotropic strength and salt content is mostly nonlinear for charged analytes in CEC in comparison to pure reversed-phase and ion-exchange chromatography. Thus, results obtained should be used only as guidelines for method optimization.

In concert with chromatographic mechanisms, electrophoretic differentiation plays an important role on the overall separation mechanism of charged analytes. In the case of proteins, the observed electrochromatographic mobility is the result of both the protein properties (tertiary structure, hydrodynamic radius, accessibility of hydrophobic and ionic moieties) and stationary phase properties in the separation conditions (pore size, surface hydrophobicity and charge). Furthermore, proteins, as well as various natural and synthetic peptides, have also been separated through affinity-based or mixed with ion-exchange, reversed-phase and size-exclusion mechanisms [89]. Even though CEC has clearly shown its capacity for the separation of standard proteins and isoforms as well as smaller biological molecules [89] and other biopolymers [90], no complete

demonstration of CEC efficiency has been shown for biomarker investigation involving dynamic living systems. As underlined by Simal-Gándara [91], CEC would shine in applications where μ–LC, CE or other high-efficiency separation techniques have not been able to provide a high level of information.

CEC has also demonstrated its abilities outside of the biomacromolecule niche and proved to be efficient for a wide class of applications. These include electrochromatographic separations of acidic [92], basic [93] and neutral [94] drugs, antibiotics [95], polyaromatic hydrocarbons (PAH) [96] as well as their DNA-adducts [97], synthetic polymers [98] and other classes of compounds classically analyzed using HPLC, GC or CE.

Alternatively, novel and specialized modes of interactions were also validated for their potential for implementation in the CEC format. These include normal phase, chiral recognition of small molecules using immobilized cyclodextrins [99] and proteins [100], immunological (antigen-antibody, lectin-sugar, enzyme-substrate) interaction, inverse-size exclusion and even affinity chromatography using molecularly-imprinted stationary phases [101].

While the list of proof of principle demonstrations for CEC continues to grow, real advancements in CEC development are greatly hindered by the lack of serious input into the organized development of stationary phases dedicated to CEC.

1.3 CEC supports: from Borrowed HPLC Materials to Custom Supports

1.3.1 History

Jorgenson and Lukacs published the first description of a CEC separation using a capillary channel packed with functionalized silica microspheres [2]. At the time, spherical materials were easily accessible as they were in routine HPLC use. These materials offered, and still offer, very well known surface chemistry and physical properties facilitating direct comparison with similar separations performed in pressurized-mode. To prevent escape of the stationary phase media from the column, researchers prepare retaining frits by sintering a small section of stationary phase in the same way as packed μ–LC columns. With a retaining frit in place, the separation media were packed through conventional high pressure slurry packing [102], electrokinetic loading [103,104], centripetal force [105], supercritical CO_2 [106] and gravity [107]. Early pioneering results obtained with packed columns clearly proved that CEC was able to outperform other separation techniques in certain cases. However, further recognition of CEC as a powerful technique was hindered by problems associated with the retaining frits that were known to cause bubble formation. Even today retaining frits are commonly used in CEC but the technique used for their fabrication has evolved significantly. Chen and coworkers [108] demonstrated that photoinitiated polymeric frits offered a better alternative to sintered ones due to better homogeneity, reproducibility and the possibility of achieving their polymerization anywhere along the separation channel.

In order to circumvent the drawbacks caused by the presence of sintered retaining frits, researchers worked on the development of open-tubular CEC (OTCEC) separation media as already briefly introduced. Matyska *et al.* [109] evaluated the potential of OTCEC by etching of silica capillary inner wall followed by functionalization of the walls via silane chemistry. This CEC method showed that relatively high plate numbers could be obtained without the use of a packed stationary phase. To accomplish this though, a narrow separation channel (<10 μm) had to be used which enabled increased access to the chromatographically-active capillary wall but also inevitably reduced the detection sensitivity [110]. Even though this mode of CEC is still being investigated, it did not attract any significant attention mainly due to its inherent limited sample loading and separation efficiency.

It is through the work of polymer chemists such as Fréchet and Svec in the mid 1990's that CEC really gained notoriety with the incorporation of functional porous polymers as CEC chromatographic supports [111,112,113,114]. At the same time, development of monolithic silica rods as chromatographic supports in CEC and LC invigorated the analytical community who discovered a novel way to perform high-efficiency chromatographic separations.

1.3.2 Silica-based CEC: Silica Microspheres and Monolithic Silica Supports

The functionalization chemistry of silica-based materials is a well-known science that has been developed extensively by the chromatographic industry since the late

1950's. The functionalization of silica microspheres, or silica surfaces, is most commonly done through reaction of the exposed silanol moieties from the silica network. Classically, reactive mono- or tri-chlorosilane reagents are employed due to their fast and reproducible reactivity but also high crosslinking efficiency. The newly formed silica surface inherits the chromatographic properties acquired from the silane functional groups.

Depending on the type of application, silica substrate particles are fabricated with either spherical or irregular shapes possessing specific porous or non-porous surfaces. Most chromatographic silica microspheres are synthesized by a sol-gel process involving the polycondensation/polymerization of a liquid alkoxide precursor such as triethoxysilane (TEOS) or trimethoxysilane (TMOS) through acidic or basic catalysis. Upon gelification of the silica colloids to form a polymer made of O-Si-O linkage, the silica particles acquire their final physical properties (sphericity, surface defects and porosity) through a final step of slow drying in a casting solvent. Even though a strong theoretical basis has evolved during the last fifty years, the preparation of silica particles remains a combination of both art and science. Nonetheless, the methodologies developed to properly adjust the condensation conditions, *i.e.* pH, acid/base catalysis, water:alkoxide ratio, temperature, solvent in order to obtain desired properties have enabled the fabrication and commercialization of silica particles characterized by a wide range of particle and pore sizes, shapes and chemistries [115].

In the mid 1990's, a new type of silica material, monolithic silica, with very interesting porous properties was introduced by Tanaka's research group [116]. Monolithic silica materials are fabricated through a similar sol-gel process where the gelification includes the addition of a porogenic or a template substance that acts as a mold around which a well defined macroporous and mesoporous network is formed. In the first publication detailing the fabrication of a monolithic silica, Nakanishi *et al.* [117] employed polyethylene oxide (PEO) as a template during polycondensation of TMOS resulting in a well defined mesoporous and macroporous structure. In order to allow solidification of the sponge-like network without cracking the fragile structure, aging and/or thermal processes were performed in controlled conditions together with aging solvents. For chromatographic usage, the synthesized monolithic silica network, which is a solid rod, is usually housed in a polyether ether ketone (PEEK) tube to be employed for CEC or μ–LC separations. Another approach developed by Aissie *et al.* [118] is based on the *in-situ* sintering of pre- or non-functionalized silica particles in a capillary channel at high temperature creating a strongly bound stationary phase without requiring fabrication/integration of a retaining frit. Even though this latter approach is a clear simplification and allows a net improvement in surface area over its packed counterpart without affecting the inner porous structure of the sintered particles, it has not been exploited extensively in the literature. This approach still requires the homogeneous introduction of chromatographic particles into the channel which remains fairly complex.

As shown in Figure 1–10, the resulting chromatographic rod has a well defined macro- and meso- porous network that provides improved mass transfer kinetics and is capable of generating higher separation efficiencies than similar particulate stationary phases. In conjunction with higher surface area, silica monoliths exhibit higher permeability resulting in very low column backpressure thus allowing their exploitation in fast μLC. One of the major technological breakthroughs in monolithic silica preparation is the ability to easily and independently tailor the mesopore and macropore dimensions.

Chemically, monolithic silica is very similar to particulate silica in that it also consists of a silica network with exposed silanol moieties at its external surface. For this reason, functionalization strategies developed for particulate silica have been extensively applied to monolithic silica [119].

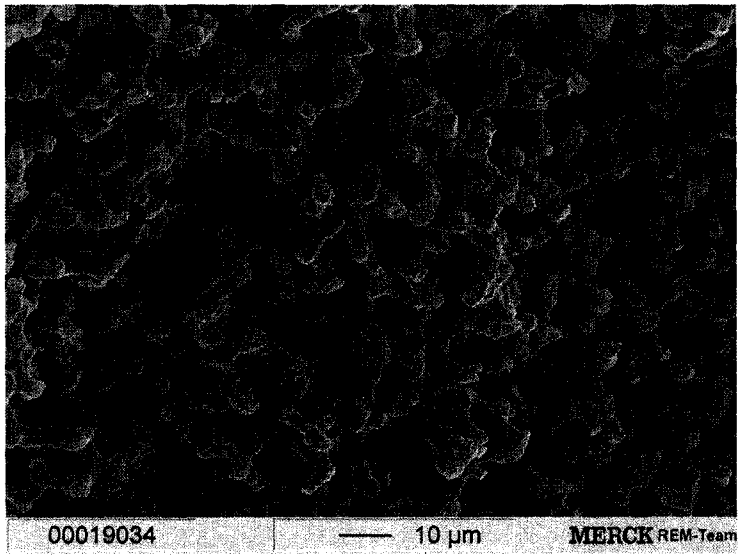

Figure 1–10: Monolithic silica fabricated through sol-gel process [from reference 120].

Integration of monolithic silica materials into CEC has also been investigated. In 2003, Allen published a good review describing state-of-the-art fabrication and functionalization of monolithic silica, especially for CEC, emphasizing the specific issues related to improving chromatographic retention while preserving EOF generation capacity [121]. Intrigued and teased by their ease of fabrication, virtually capable of being synthesized in any size and shape, many researchers have quickly developed several applications in both microfluidic and capillary formats [122].

The main advantages of silica-based stationary phases are their ease of functionalization and their well-known physical properties. Silica particles, in contrast to polymeric particles, which will be described later, demonstrate a high mechanical strength combined with chemical inertness to most chromatographic solvents. Monolithic silica materials also show the same chemical inertness but with enhanced separation efficiency associated with their improved bimodal porous structures. Due to their very interesting properties, these supports are gaining in popularity not only for chromatographic applications but also for catalytic applications and potentially as drug delivery substrates [123]. Nonetheless, their low sample capacity still hampers their implementation in routine chromatographic applications. Further, since all monolithic silica columns are prepared and functionalized *in-situ*, their high cost also impedes integration into research and industrial laboratories.

1.3.3 Organic-Polymer Based Monolithic CEC Stationary Phases

In parallel to the development of silica-based monoliths, intensive work has been directed toward organic-based materials that could surpass limitations related to the use of silica-based materials as chromatographic supports, namely limited pH stability, hydrophobicity and surface loading.

From the early 1990's, the combined input of the polymer and analytical communities have greatly improved the knowledge and expertise on the fabrication, properties and chromatographic use of polymeric stationary phases. The pioneering work of Hjerten and coworkers demonstrated the first use of a modified acrylamide polymeric CEC stationary phase [124]. Historically, acrylamide gels have demonstrated great potential for the efficient separation of proteins but their low porosity combined with their low mechanical strength prevented their use in HPLC. For this reason Hjerten, and later other researchers, polymerized acrylamide gel *in-situ* to incorporate additional charged monomers allowing substantial EOF while increasing the porosity of the acrylamide gel. Later, different strategies were also explored in order to increase gel hydrophobicity including incorporation of hydrophobic monomers and functionalization of precast acrylamide gel [125]. Still, one of the main limitations of acrylamide gels is their low mechanical strength that does not allow application of external pressure required for hydrodynamic injection and faster column conditioning.

Organic-based chromatographic stationary phases, or organic monoliths, are now fabricated and classified through five different classes of polymeric beds: divinyl benzene (DVB), acrylate, methacrylate, acrylamide and polystyrene-based stationary phases.

One of many advantages of polymeric stationary phases is in the almost unlimited access to various types of chemistry due to the wide selection of commercially available monomers and crosslinkers. Moreover, their fabrication is very simple, inexpensive and faster than derivatized silica gel because chromatographic functionalities are directly incorporated through selection of the monomers. However, as it will be discussed later, reactive polymers can easily be synthesized and further functionalized to allow introduction of chromatographic moieties not available as monomers. They can either be manufactured directly within the separation channel (*in-situ*) or in bulk then packed into the separation channel. Most polymeric stationary phases possess a specific mesostructured porous network that allows higher mass transfer kinetics than their silica packed counterparts. Their physical properties (pore, channel and particle size) are easily modified through careful selection and modification of the polymerization conditions but also results in modification of the final chemical properties.

In terms of chemical properties, polymer stationary phases will generally exhibit extended pH stability in both acidic and basic conditions due to the absence of hydrolysable groups within the backbone, unlike silica networks. For this reason, they have become the materials of choice for purification and extraction of big biomacromolecules requiring extreme pH conditions for elution or washing of the bed

[126]. Nevertheless, unlike silica, they are not compatible with almost all types of solvents. Some solvents can cause irreversible swelling, or melting, of the polymer bed resulting in loss of its three-dimensional structure.

With regards to CEC applications, polymeric materials represent a clear advantage over silica materials because the ionizable groups necessary to sustain sufficient EOF are incorporated within the bed during polymerization and are not buried during functionalization of the chromatographic bed, as they are for silica gel. For instance, functionalization of the free silanols with octadecylsilane (C18) significantly decreases EOF on silica because the silanols are also necessary for EOF generation [127,128].

For the most part, organic monolith fabrication methodologies are based on standard polymer synthesis knowledge and protocols while their integration as stationary phases is performed through two main approaches. In the first approach, polymerization is performed in bulk solution followed by sequential washing, conditioning and drying of the porous polymer particles. In certain cases, polymerization produces a very solid and compact agglomerate of particles requiring grinding. As for particulate silica employed in HPLC columns, the material is suspended in a slurry solvent and introduced into the separation capillary either through application of high pressure, electrokinetic loading, centripetal force, supercritical CO_2 or gravity in conjunction with a retaining frit within the separation channel. However, this approach has proven to be less effective due to issues of problematic packing in the capillary-based format.

In the second approach, these limitations are avoided with *in-situ* fabricated silica or organic polymers. As the name implies, in the *in-situ* fabrication process the polymer is prepared by reacting a precursor mixture of monomers and solvents in the separation channel. In order to prevent extrusion of the polymeric bed from applied pressure, or EOF, *in-situ* polymerization of organic-based monoliths usually starts by introducing reactive functional groups that will anchor the polymer onto the silica capillary wall with a silanization agent. The capillary is then filled with a polymerization mixture that consists of one, or more, crosslinking and functionalizing monomers homogenized in a porogenic solvent mixture. A photolabile or thermolabile initiator is included within the mixture that enables polymerization until reaction of monomers or of the polymer structure is complete. Other modes of polymer initiation, for example, gamma-irradiation that is commonly used in plastic manufacturing, is occasionally used even in monolith fabrication [129,130].

The widespread use of thermoinitiation has shown that this method is technically easier for fabricating *in-situ* monoliths but occurs over the entire length of the separation capillary/channel. Since the separation channel is completely filled by the polymer, which is highly scattering and opaque, off-capillary detection or connection with an empty capillary for on-line detection is necessary. Photoinitiation, on the other hand, avoids such complicated capillary interfacing procedures because polymerization only occurs where the polymerization mixture is exposed directly to UV light. Thus it is easy to control the bed length by masking zones off where no polymerization is to occur.

Formation of the polymeric stationary phase by photopolymerization can typically be performed in a very short time using commercially available UV lamps. However, photopolymerization requires the use of UV transparent capillary moulds such as Teflon or polyacrylate coated fused silica capillaries or glass microfluidics to let sufficient light energy to penetrate through the separation walls, triggering and sustaining the polymerization in a homogeneous way.

As it is used in the electronic industry for the photopatterning of microelements, photoinitiation is well suited for the incorporation of monoliths within very defined areas. Accordingly, it has shown great promise for the implementation of electrochromatography in microfluidic interfaces. For example, Yu *et al.* [131,132] adopted photoinitiation for the fabrication of a polymethacrylate monolith within a microfluidic chip as a proof of concept. Because only the irradiated microchannels undergo polymerization, this concept enables production of complex separation interfaces combining various types of support and chemistry, commonly referred as micrototal analytical systems (μTAS).

Other polymerization methodologies have also shown their potential for the *in-situ* fabrication of monolithic stationary phases. For example, a different class of monolithic chromatographic supports was recently introduced by Sinner and coworkers based on ring-opening metathesis polymerization (ROMP) [133]. Other cited methodologies include molecular imprinting (MIP) [134] and microemulsion polymerization [135].

1.3.4 Development and Modification of Organic-based Monolithic Stationary Phases

In opposition to silica-based stationary phases, most organic-based polymers gain both their final morphological and chemical properties during their polymerization. This is achieved through the complex interplay between polymerization parameters: the nature of the porogenic solvents, monomers and crosslinkers and their concentrations, type of initiation, temperature, and intensity of polymerization initiation source (UV light, temperature). However, there are no exact rules governing the relationship between individual polymerization conditions and final properties. Thus, optimization experiments are performed for each new set of conditions under investigation. Nonetheless, a few basic rules can still be employed to modify the porous properties as outlined by Svec [136].

The morphology and porous properties of a polymeric stationary phase are closely related to the solubility of the growing polymer chain as well as the kinetics of the free radical polymerization. Typical strategies have looked into modifying the temperature and has shown that, depending on the type and decomposition rate of the polymerization initiator, an increase in temperature typically leads to an increase in nucleation sites thus to higher numbers of particles and smaller pores. This is typically the case with initiators with very short half-lives/fast cleavage. Theoretically, such a strategy should only impact the morphology of the polymer because the chemical nature and ratio of the monomeric constituents responsible for the chemical properties of the polymer are not changed.

On the other hand, the nature and concentration of solvents, monomers and crosslinkers as well as the addition of solubilizing agents are all directly responsible for the polymer chemical and morphological properties. Because of the unique behaviour of individual polymerization systems, a few research groups have started to apply rational and factorial experimental designs and chemometrically-derived models to predict polymer properties based on the starting reagents/conditions [137,138,139]. This allows for simplification together with higher-throughput polymer development and optimization but still requires extensive development work for each new polymer. An alternative to the complete reoptimization of a stationary phase is achievable through the integration or addition of reactive functionalities onto/into the polymer permitting further reaction with any number of desired chromatographic moieties. Because a so-called "reactive polymer" already possesses its definitive morphology, it then becomes possible to simply introduce new functionalities without changing its physical characteristics.

This strategy is the basis of restricted-access media (RAM) stationary phases possessing at least two different chromatographic functionalities physically segregated to the interior/exterior of the pores. For RAM, functionalization of the pore interiors and the external surface of the chromatographic particle are performed independently allowing incorporation of two different functionalities on the same stationary phase. To do so, the first functionalization agent is selected to have a diameter exceeding the pore size so that it may only react with the external surface(s) of the particle. Accordingly, the size of the second functionalizing compound is small enough to allow derivatization of

the inner pores. The combination of chromatographic and size differentiation has found its use in applications involving extraction of specific compounds from complex matrices. For example, direct extraction and analysis of drugs and metabolites from diluted serum and urine samples have been performed on RAM stationary phases thus avoiding time-consuming sample extraction and manipulation [140].

However, all strategies based on modification of reactive polymers are limited to the development of stationary phases with a single additional functionality throughout the length of the column due to lack of geometric selection. Yang and Rånby [141] introduced a somewhat similar strategy but based on copolymer grafting of additional monomeric and polymeric moieties on an existing polymeric stationary phase. As for reactive polymers, this methodology has the advantage of keeping the same basic morphological properties of the polymer while being able to introduce a wide selection of chromatographic or reactive functionalities onto the monolith. In comparison to reactive polymers, it has the advantage of enabling modification of a wider class of already existing polymers. It allows geometrically selective functionalization that is not possible with reactive monoliths, thus the fabrication of a multifunctional stationary phase on a single monolithic rod.

Copolymer grafting allows a new layer of monomers and/or polymer to be grafted onto an existing polymeric surface through initiation of a second polymerization reaction in the presence of the initial monolithic stationary phase. In practice, a polymerization mixture containing selected monomer(s), initiator and solvents, in contact with the

monolithic stationary phase, is used for the polymerization. The grafting can occur through two different initiation mechanisms. Radicals trapped within the monolith, due to lack of mobility of the growing chain, can be used to initiate a second grafting polymerization [142] or the more popular route is the initiation of additional radicals to induce efficient grafting of new material/polymer onto an existing monolithic material. The degree of unsaturation in the monolith's backbone, type and concentration of initiator, chemical nature of monomers and the presence of steric hindrance influence the extent of copolymer grafting. As underlined very recently by Eeltink *et al.* [143] in a very pertinent publication, the source intensity employed for grafting initiation also has an impact on extent of grafting as well as blocking of pores. Blocked pores are caused by the excessive formation of polymer in solution and can lead to complete blockage and significant loss in EOF and retention surface.

In terms of applications, Hilder *et al.* have employed this approach for the shielding of EOF-supporting functionalities by a hydrophobic layer in order to suppress undesirable electrostatic interaction with analytes [144]. Researchers have not yet shown customization of a separation media for a specific application requiring a surface chemistry not initially available on the base separation media, *i.e.* through a significant change the chemical and/or chromatographic properties of a monolithic stationary phase.

1.4 Physical and Chemical Characterization of Monolithic Stationary Phases

As previously underlined, both the chemical and physical properties of a stationary phase strongly contribute to the chromatographic retention of an analyte. Thus, in order to properly evaluate and compare stationary phases, efficient and accurate physical and chemical characterization methods have to be employed.

1.4.1 Physical Characterization: Destructive and Non-Destructive Methods

Techniques such as scanning electron microscopy (SEM) [145], mercury intrusion porosimetry (MIP) [146], Brunauer-Emmet-Teller (BET) and Barrett-Joyner-Halenda (BJH) gas adsorption-desorption isotherms and high-resolution optical microscopy (HROM) [147] have increased the understanding of how chemistry affects the monolith morphology. Given that the stationary phase surface morphology plays such an important role in the separation process, these techniques are the primary methods for the characterization of novel polymeric separation supports used in electrochromatography. However, the main drawback of SEM, MIP, BET and BJH stems from their inability to test wetted material and cannot provide information about the monolith in its functional state. Also, they are destructive and do not allow multiple analysis to be performed on the same polymeric material. This is especially important with *in-situ* fabricated monoliths that are only synthesized in very low amounts. Moreover, MIP, BET and BJH need large masses of sample that cannot be prepared in conditions exactly the same as those achieved in a capillary mould. It is also important to note that the non-imaging

characterization techniques determine the material's physical characteristics based on the filling of available pores by probe species. For this reason, differences in results are often due to the size or nature of the probe used in the individual techniques [148]. For example, MIP only allows the determination of macropores (width > 50 nm) size while techniques such as BJH permit characterization of mesopores (2 nm < width < 50 nm). Micropores (width < 2 nm) usually are inaccessible and therefore, to date, can not be characterized even though they are critical in chromatography. Therefore, the results from these methods are semi-quantitative and not always indicative of the polymer behaviour when used for chromatography [149,150].

Marŭska [151] demonstrated that HROM provides access to details from porous media with maximum resolution down to 1-2 μm in both dry and wet conditions. As they have shown, HROM also has the advantages of not requiring complex sample preparation as with other intrusive techniques. Nonetheless, its limited resolution limits its capacity to access much finer details of porous structure.

Due to its simplicity, SEM, a non-contact imaging technique, is the most widespread imaging method used for studying the physical aspects of new monoliths down to 500 nm. However, detailed structures smaller than about 50 nm cannot be resolved. In this technique, a focused electron beam scans the surface leading to the emission of secondary-electrons that are collected by electro-optical lenses. For the best resolution the scanned surface must be thermally stable, relatively flat and conductive to reduce surface charge inhomogeneity. In the case of a polymeric monolith, the surface

possesses none of these features. Sufficient conductivity can be achieved by sputtering a thin layer of either gold or carbon onto the surface but the thermal sensitivity of the polymer limits the voltage that can be applied for imaging.

As an alternative to SEM imaging, AFM is a direct probing technique that allows the study of surface morphology, regardless of conductivity. It is based on the deflection of a flexible tip during its scanning movement on a surface [152], as depicted in Figure 1–11. Three operational modes prevail: contact, non-contact and intermittent (tapping) modes. In contact mode, the tip is engaged directly on a surface and dragged along a scan pattern to measure surface topography. To minimize imaging noise due to the adsorption of sample onto the tip in contact mode, a vibration can be applied to the tip such that the tip only touches the surface intermittently. This latter mode is called intermittent contact, or tapping mode, and is capable of resolving structures of 20 nm depending on surface hardness and morphology. Interactions between a derivatized, or non-derivatized, AFM tip and the surface can also be monitored by applying an oscillation to a tip close to the sample surface. The observed frequency of oscillation is influenced by Van der Waals forces between the sample and the tip. Unfortunately, this technique is not suited to the study of morphological properties of rough surfaces since the frequency is also dependant on the distance to the surface.

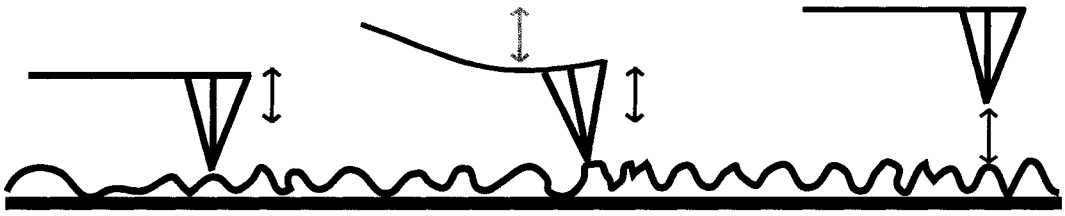

Figure 1–11: Probing of a surface with an AFM tip in three conventional operational modes: (left) Contact (middle) Intermittent (tapping) (right) Non-contact.

AFM permits a higher resolution in the depth, or z, direction than SEM leading to more accurate surface roughness values, but care must be taken when imaging structures that are similar in size, or smaller, than the tip radius. In these cases, the side of the tip can make contact with the structure before the tip thus leading to an erroneous measurement. A distinct advantage of AFM is its ability to analyze the surface of the monolith in a wetted state. Thus conditions similar to those used in a chromatographic separation may be investigated.

A limited number of other methods can also be used to describe monolithic polymer materials in wetted conditions. Chromatography based techniques such as Inverse Size-Exclusion Chromatography (ISEC) and Inverse Size-Exclusion Electrochromatography (ISEEC) measure porosity parameters in the working state [153,154]. Morphology parameters are calculated from the retention behaviour of molecules, with known hydrodynamic radius, separated on the stationary phase. Chromatography based techniques are able to assess the full range of three-dimensional porosity characteristics compared to imaging techniques which are limited to

characteristics at, and close to, the probed surface. However, they typically use operating conditions that are not representative of typical chromatographic conditions (e.g. strong solvents such as THF) and that may affect the morphology of the polymer. Additionally, the limited size range and nature of the standards available hampers their widespread application.

Rathore [155] and Chen [156] described the calculation of porosity values extrapolated from electrokinetic measurements. This approach has the main advantage of providing information on the monolithic polymer material in the same conditions, *i.e.* same solvent and under an electrical field, as it is used normally in CEC separation experiments. However, this approach only allows the calculation of a factor representative of the total porosity. Also, it does not allow the distinction between intra- and inter-particle/skeleton sizes as available from imaging techniques.

Pesek and Matyska [157,158] have shown a good comparison between information obtained by SEM and AFM for silica surfaces modified for open-tubular capillary electrochromatography (OTCEC). AFM allowed to measure the surface area as well as the surface-tip forces of attraction, which is not possible by the latter technique. In another paper, Kornyšova [159] imaged a novel self-assembled monolithic support, *i.e.* a polyrotaxane based monolith, by both AFM and SEM together with HROM. They successfully demonstrated that an increase in ionic strength during polymerization resulted in a net increase of channel size. Nonetheless, the monolithic media had to be dried prior to both AFM and SEM experiments and no experiments were performed in

wetted conditions. Few studies have been published assessing the effect of pore size of monolithic media on chromatographic stationary phases in part due to difficulties of measuring their true porous properties in their wetted state [160]. However, our group has recently shown that a monolith morphology could easily be investigated in various solvent systems allowing accurate determination of its morphological properties in working conditions employing a straightforward AFM methodology [150].

Overall, only a few limited physical characterization techniques are available for the analysis of *in-situ* fabricated monolith as summarized in Table 2 and present their own advantages and disadvantages as just discussed.

Table 2: Physical characterization techniques

	Techniques	**Advantages**	**Disadvantages**
Destructive	BET, BJH	Accurate pore size and distribution determination	Dry conditions
	MIP		
	SEM	High resolution, large scan size	Dry conditions, general information
Non-Destructive	ISEEC, ISEC	Wetted conditions	Limited by standards size
	HROM	Large scan size	Dry conditions, limited in resolution
	AFM	High resolution	Small scan size and slow

1.4.2 Chemical & (Electro)Chromatographic Characterization

In HPLC, the effective chromatographic properties are determined using standard probe compounds. Common separation media are chromatographically characterized by the manufacturer for their relative hydrophobicity using standard hydrophobic molecules,

residual silanol activity for silica based packings (surface acidity) and ion-exchange capacity for ion-exchange stationary phases. For example, standard compounds are commonly used to evaluate and compare various commercially available C18 stationary phases, such as those popularized by Tanaka and Engelhardt [161]. However, data extrapolated from such measurements only provide an approximation of surface properties and not quantitative data on the exact chemical nature or surface concentration of a chromatographic moiety.

Surface loading, or concentration, on a functionalized stationary phase is determined after functionalization. This is often achieved through elemental analysis of the carbon, nitrogen, oxygen and sulphur content upon heating of the functionalized particles at very high temperature combined with catalytic conversion of the generated gases (CHNO analysis). In the case of functionalized silica particles or monoliths, results from elemental analysis are usually accurate in terms of surface loading calculation due to thermal stability and lack of signal from the silica support. On the other hand, elemental analysis of organic polymers for determination of their surface loading is tedious because of their lower thermal stability and organic nature. Nonetheless, it is possible to approximate the total concentration of a specific chromatographic moiety in a polymeric backbone and at its surface if the number of different monomers and crosslinkers is limited, or their elemental composition is significantly different than the chromatographic moieties. In the case of reactive polymers, this does not cause any issue

because the surface loading can be determined through differential elemental analyses of functionalized and non-functionalized polymers.

Other surface characterization strategies have also been investigated. These include elemental analysis based on X-ray spectroscopic probing of surfaces, such as Energy Dispersive X-Ray Spectroscopy (EDX), Wavelength Dispersive X-Ray Spectroscopy (WDX) and X-Ray Photoelectron Spectroscopy (XPS). Briefly, by impacting the surface with a beam of either high-energy electrons, or X-rays, of a fixed energy, a secondary X-ray spectrum is are emitted from the surface that corresponds to the surface atoms. Depending on the nature of the atoms emitting the X-rays, analysis can either be quantitative or semi-quantitative. Heavier atoms are stronger X-ray emitters due to their higher number of electrons and lower energy of ionization. These techniques are commonly employed to determine concentration and localization of heavy metals on the surface. The metals can be impurities or intentionally reacted onto the surface as probes. The only other commonly employed trace metal technique, inductively coupled plasma mass spectrometry (ICP-MS), would require digestion of the chromatographic support for analysis and would not provide any information on surface distribution of the atoms measured as in X-ray spectroscopic imaging. For example, Hilder *et al.* [144] employed EDX to assess surface distribution of sulphur atoms grafted to a polymeric surface using a sulfonated monomer.

On the other hand, titration of surfaces combined with solid state spectroscopic measurements such as solid state nuclear magnetic resonance (NMR) and Raman

spectroscopy has proven useful for both direct qualitative and quantitative analysis of polymers [162,163,164].

Even though chemical analysis can enable identification and quantification of the functional groups of a polymer, further analyses are required to determine the capacity of a polymer to be employed for electrochromatographic purposes. In fact, conclusions extrapolated from chemical analysis of a polymeric stationary phase do not necessarily correlate with its aptitude to sustain a substantial EOF. Electrochromatographic characterization of a stationary phase involves measurements of its EOF amplitude as well as its response to pH. Lower than expected EOF can be caused by electrical double-layer overlap or the lack of accessibility of the ionizable groups, two characteristic that are not readily observed through chemical analyses. Thus, these additional measurements are crucial to determine the operational limits of an electrochromatographic stationary phase while permitting calculation of its electrokinetic porosity, as described earlier.

To summarize, while chemical and physical analyses of a polymer provides a good overall description of its expected chemical properties and are essential tools in polymeric stationary phase development, the assessment of its chromatographic and electrochromatographic properties offers a more accurate means to probe the effectivness of a polymeric stationary phase. However, depending on the type of application, preliminary knowledge of the targeted analytes as well as the sample matrix will enable

determination of the required stationary phase properties and govern the choice of starting materials and preparation methods.

1.5 CEC and Monolithic Supports in Proteomics: Sample Treatment and Separation

1.5.1 History and State of Knowledge/Practice

A number of publications in the last decade have dealt with the use of monolithic supports, both in CEC and μ-LC modes, directed specifically at proteomic applications. The complexity and heterogeneity of proteins produced in living systems requires sophisticated separation and analysis tools. The combination of enhanced mass transfer kinetics that yields higher separation efficiencies, improved stability at extreme working pH and compatibility with mass spectrometric detection makes polymeric stationary phases, and in particular CEC separations on polymeric monoliths, a very promising proteomics analytical tool.

A good review was published in 2004 by Bandilla [165] that summarized the accumulated knowledge and practices of protein and peptide electrochromatography. As it is still the case today, a great number of the reported CEC publications were based on the use of columns packed with functionalized silica particles, mostly due to their commercial availability. Also, capillary-based separations were predominant while today greater attention is directed toward microfluidic devices that can implement multiple

tasks on the same platform/device. From what is observed in the current literature, organic-based monoliths have gained momentum over silica-based stationary phases due to their enhanced morphological and chemical properties. Further, the scientific community has quickly realized the benefits, time and cost wise, of *in-situ* fabricated monoliths as well the easy access to a wide variety of chemistries.

Thus, a significant number of publications have appeared in the last ten years dealing with very interesting approaches and stationary phases for both model and real-life proteomic applications. The reader is invited to consult the above review for an extensive coverage of the literature.

1.5.2 Differentiation by Reversed-Phase and Ion-Exchange CEC

Most of CEC proteomic separations are still performed using reversed-phase (RP) mechanisms. Based on tuning of an analyte hydrophobic or electrostatic interaction with the monolithic support, model proteins as well as tryptic digests have been separated on functionalized and non-functionalized poly(methacrylate-divinylbenzene) [166], poly(aspartic acid) [167], polyacrylate [168] and polymethacrylate [169] polymeric beds or coated capillaries (OTCEC). Interestingly, because a stationary phase requires ionized moieties in electrochromatography, protein separations are usually achieved through a combination of hydrophobic, electrostatic interactions with the stationary phase and electrophoretic differentiation.

1.5.3 Affinity Electrochromatography: On-line Enrichment and Separation

Outside the more classic RP and ion-exchange (IE) mechanisms, great achievements have been made towards implementation of affinity-based strategies in the CEC format that allows selective differentiation of proteins and their post-translationally modified (PTM) counterparts. Affinity chromatography is the result of either weak, medium or strong interactions between very specific molecules and substrates. Because of these differences in strength, they can be used for selective sample-enrichment or directly for separation of complex samples. Practically, weak interactions differ from medium and stronger interaction in that the mobile phase allows moderate to sufficient differentiation between the target molecules and other compounds in the sample. Alternatively, medium and strong affinity interactions require an eluting phase to dislodge target molecules from the immobilized substrate leading to very efficient and highly selective extractions but poor differentiation of similar species such as PTM's. In order to allow further differentiation of these species, extraction is commonly conjugated to an (electro)chromatographic separation. Among common affinity-based interactions, immobilized metal affinity chromatography (IMAC), antibody-antigen (immunoaffinity), lectin, sugar-based and aptamer affinity have been extensively employed in preparative chromatography of proteins, as reviewed by Okanda and El Rassi [170].

Briefly, IMAC uses the very specific interaction between Ni(II) and proteins engineered, or tagged, to contain six consecutive histidine (His) amino acid subunits [171]. Recently, Slentz [172] replaced nickel by Cu(II) which also exhibits strong

interaction with histidines containing proteins or fragments for the sequential microfluidic proteolytic digestion, Cu(II)-IMAC trapping and RP separations of histidine-containing proteins for their identification. Specifically applicable to the separation of engineered proteins, IMAC has not found much use in real-world sample CEC applications.

In this regard, other modes of affinity (electro)chromatography could theoretically exhibit increased potential for investigation of endogenous protein post-translational modifications or isolation and analysis of specific substrates. For instance, immunological interactions based on antibody-antigen binding have been used extensively in purification, concentration and analysis of specific substrates through various modes of chromatography [277]. With immobilization of monoclonal antibodies, highly specific interactions are possible permitting isolation of particular substrates from heterogeneous sample mixtures while decreasing the extent of non-specific interactions with other molecules.

Unfortunately, the major drawback of immobilized complex biomacromolecules, such as antibodies, is the limited stability of most immobilized biological substrates due to loss of their specific three-dimensional structure essential to specific target recognition mechanism of immunological interactions. As in free solution, loss of immobilized enzyme activity can be caused by pH, solvent and temperature effects even though immobilization has been shown to increase enzyme stability [173]. Also, immobilization

can also lead to undesirable interactions between the immobilized biomacromolecule and supporting surface resulting in loss of activity [174].

Novel stationary phases have been developed in order to investigate PTM of proteins. Post-translational reactions include various biochemical modifications of proteins responsible for the triggering of a wide number of biological responses. These include alkylation, glycosylation, hydroxylation, methylation, phosphorylation as well as more complex mechanisms such as the conjugation of proteins or proteolytic cleavages [175].

One important class of PTM is glycosylation which has gained great interest in the last decade due to increasing incidence of diabetes in both the adult and youth population. The higher level of non-assimilated glucose puts diabetic patients at higher risk of atherosclerosis and other diabetic complications caused by glycosylation of proteins and subsequent loss of protein function. Important research has thus been directed toward development of analytical tools allowing selective extraction and analysis of glycosylated proteins for investigation of their specific modifications and their use as potential biomarkers of disease [176].

Two principal technologies have been evaluated for their specific affinity for glucose moieties. Lectins, a class of naturally occurring proteins from plants, have high affinities for carbohydrates and have been used to isolate both sugars and glycosylated biomolecules. Already well implemented in HPLC since the 1980's, Madera [177] and Okanda [178] have shown the efficiency of lectin affinity for the electrochromatographic

and chromatographic capture and separation of model glycosylated proteins. In both cases, capture was performed using an optimized buffer system while elution was achieved by using specific sugars to compete for the surface-bound lectins. Unfortunately, lectins exhibit the same stability issues as for other biomacromolecules.

Alternatively, boronates have also been employed since the 1970's for isolation and separation of molecules differentiated by the presence of sugar moieties such tRNA, nucleotides and their sugar derivatives as well as glycosylated proteins [179,180]. Boronate affinity chromatography works through the specific interaction observed between borate and adjacent cis-diols as depicted in Figure 1–12. It has been suggested that the binding mechanism was caused by reversible formation of a five-member ring [181].

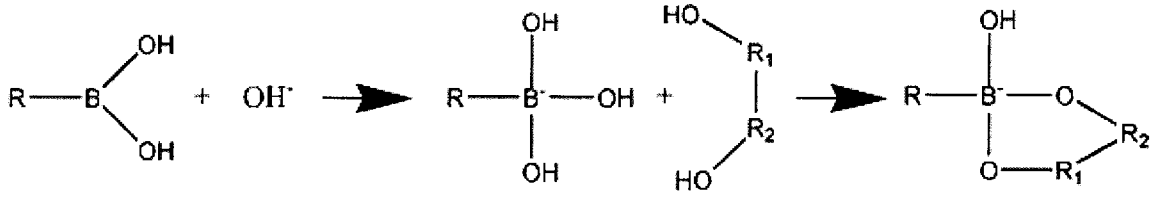

Figure 1–12: Interaction between borate and coplanar cis-diols responsible for boronate-affinity chromatography.

For this purpose, 3-aminophenyl boronic acid (APBA) has been extensively used as an immobilized ligand for boronate affinity chromatography of carbohydrates, nucleosides, nucleotides as well as glycosylated proteins. The improved stability of boronate functionalities, over lectins and other macromolecular chelators, for sugar recognition with respect to pH, temperature and solvents have led to its use in

chemosensors [182]. Many glyco-selective fluorogenic dyes are also based on boronic acids [183]. Also, compared to lectin-based affinity columns, boronic acid columns can be regenerated easily at very low pHs that are potentially problematic with lectins.

Optimal HPLC retention and analysis of cis-diol containing molecules is usually performed at pH greater than 7.5 while elution is achieved using competing molecules such as borate buffers, mannitol or sorbitol at pH lower than 6.5. The optimal pH for diol binding is generally higher than the pKa of the boronic acid used. Even though boronate exhibits a strong affinity for cis-diols due to its locked sp3 orientation, it can also form tridentate complexes with molecules possessing three properly aligned hydroxyl groups such as D-ribose.

Well integrated in HPLC, boronate-affinity has not yet been investigated thoroughly in CEC separations. Very recently, Potter et al. [184] functionalized a monolith through photografting of a glycidyl methacrylate monomer followed by the reaction of an aminophenylboronic acid group and demonstrated isolation of model glycosylated proteins. However, details as to the behaviour of the boronate-affinity monolith in CEC conditions, *i.e.* efficiency, reproducibility and stability of the stationary phase and resulting separation were not given.

Through a combination of the highly specific interactions provided by boronate-affinity and higher electrochromatographic separation efficiencies, it is thought that boronate-affinity electrochromatography could become a complimentary tool for

investigation of low-level glycosylated proteins and provide higher throughput for the field of glycomic research.

1.5.4 Proteolytic Bioreactors: From Glass Beads to On-line Multifunctional Monolithic Supports

Affinity techniques are essential tools for simplifying the level of complexity of biological samples required for many of the new –omics research fields. In order to achieve high accuracy and efficient identification of each individual isolated substrate, on-line or off-line strategies and tools are available. For samples consisting of a very limited number of known targets, monoclonal antibodies combined with fluorogenic dyes are commonly employed to confirm identity and concentration. Unfortunately, complex samples such as those subjected to proteomic investigation typically consist of a very large number of proteins and peptides, as well as their post-translational conjugates, which would require an untenable number of monoclonal antibodies. Clearly, a general purpose tool that allows sequencing of differentiated substrates is required.

One key method that was essential for the development of proteomics has been, and continues to be, peptide mapping of individual substrates. Peptide mapping is commonly performed through sequential separation, isolation and proteolytic cleavage of the isolated substrate and identification of the generated peptides by mass spectrometric methods. Identification of the protein is then achieved through comparison of expected peptide mass spectra maps from accessible databases (*e.g.* Swissprot) and experimental mass spectra. Only a few proteases are routinely employed in peptide mapping because

of their high specificity for cleavage at specific amino acid residues. Their specificity allows calculation of the expected peptides and many accessible and commercial databases use these proteases. For example, trypsin, the most extensively exploited protease, is a serine protease that exhibits very high specificity for proteolytic cleavage at the carboxylic side of arginine and lysine residues.

Proteolysis is routinely performed in-solution by digestion of isolated proteins at fixed substrate:enzyme ratios. Advantages of in-solution proteolytic digestion include ease-of-use, controlled reaction conditions as well as specificity of proteolytic enzymes now available. On the other hand, since the amount of protease has to be kept relatively high to allow efficient proteolytic digestion, it also leads to generation of autolytic peptides, *i.e.* peptides caused by the autoproteolysis of the protease, which can become problematic in the investigation of low-abundance proteins.

Scientists have thus looked at alternatives such as surface-immobilized proteases. Due to the limited degrees of freedom, immobilization of proteases on various types of solid substrates decreased autolytic susceptibility and also increases the interaction between proteins and substrates. Indeed, proteolytic efficiency is mainly limited by diffusion in in-solution digestion while the increased surface area with immobilized proteases allows significant improvement in protein-substrate interactions. Optimization of the digestion conditions and contact time allows greater digestion efficiency to be achieved quickly. Further, immobilization of proteases also permits their reuse but requires special attention due to limited enzyme stability; care must thus be exercised

with respect to solvent, pH and temperature during use and regeneration. Additional benefits of proteolytic reactors include minimal sample requirement, minimized sample handling, possible direct coupling to separation or mass spectrometric detectors, increased digestion efficiency through multiple passages of the sample on the same reactor and the potential for successive exposure to reactors comprising different proteases.

A wide number of chemical strategies have been employed for the immobilization of biomolecules and are also applicable to protease immobilization. Depending on the nature of the supporting surface, immobilization can be performed through different approaches. In the case of monoliths possessing reactive surfaces, direct immobilization through nucleophilic reaction of the protease primary amines and surface electrophiles is possible. Due to their relatively high reactivity, epoxides have been used extensively in the literature for direct immobilization of biomolecules [185,186,187].

Even though direct linkage is a very convenient and straightforward method for immobilization of both small and large (bio)molecules, reactive group proximity to the surface can hamper immobilization efficiency of larger molecules. Further, biomolecules immobilized close to the supporting surface can suffer from steric hindrance or non-specific interaction with the surface leading to lower activity. For this reason, linker arms, or spacer arms, have been designed to distance the reactive moieties from the surface and allow immobilization of biomolecules further away from the surface. Practically, linkers are available in different lengths, hydrophobicity and nature of the

two reactive moieties located at the extremities. They can be initially reacted with the substrate of interest followed by immobilization on the surface or *vice-versa.*

Fabrication of proteolytic reactors has been achieved on various types of surfaces using many different types of reactive functionalities and linkers. For example, Bonneil *et al.* [188] employed commercially-available porous glass beads activated with diisothiocyanate for trypsin immobilization for the fabrication of a proteolytic reactor coupled on-line to CE. More recently, Fréchet and Novotny's research groups have investigated different monolith backbones and reactive moieties for the same purpose while carefully investigating the resulting proteolytic efficiencies through both on-line and off-line (electro)chromatographic separation and mass spectrometric analysis [189,190,191,192,193,194]. In these studies, both off-line collection followed by MALDI-TOF MS identification and direct on-line ESI-MS of generated peptides have been demonstrated. Improved proteolytic efficiency of immobilized trypsin over conventional in-solution approach was shown.

As reviewed by Massolini [195], on-line coupling of proteolytic reactors with various separation techniques has shown great utility and potential for high-throughput proteomic applications. The combination of minimal sample volume required for proteolytic microreactors and easy interfacing with (electro)chromatographic separations for "shotgun" proteomic applications gives this technology a good advantage over conventional time-consuming off-line proteolytic approaches. Following this interest, Applied Biosystems have marketed the Poroszyme® cartridges based on a porous

poly(styrene-divinylbenze) on which trypsin has been immobilized as reusable high-efficiency tryptic digestors [196].

Integration of extraction, digestion and separation of proteins have also been described in the literature but mainly through chromatographic mechanisms involving complex sample handling strategies [197]. In most cases, these examples were based on the combination of sequential columns and reactors achieved through eluate transfer from one column to another via switching valves placed between each column. However, an increasing number of research groups are now working toward development of microfluidic devices integrating all these techniques while allowing direct coupling to mass spectrometric detectors, essential for high-throughput proteomics and biomarker discovery [198, 199,200].

1.6 Contribution to Original Knowledge

CEC remains an immature separation technique that can become a very useful method for situations where other techniques cannot meet the needs of the analyst. In order to improve the potential benefits that CEC could bring to the general scientific community further work is required on different facets including theoretical understanding of separation mechanisms, development of dedicated instrumentation and stationary phases as well as applications that illustrate the strengths of CEC.

Thus the work detailed in this thesis is not based on a single aspect of CEC but on a combination of facets. In the first section, the reader will be introduced to the

experimental details and instrumentation that have allowed the development and employment of the monolithic stationary phases used throughout the thesis.

In the remainder of the thesis, a more extensive emphasis has been directed toward the importance of dedicated stationary phases for electrochromatographic applications. Starting with Chapter 3, practical aspects of CEC will be described including important aspects related to the use of UV-transparent capillaries as described in one of our publications [201].

In Chapter 4, the development of the first atomic force microscopy methodology for the assessment of an electrochromatographic monolith morphological properties in both dry and wetted conditions will be described. The results were compared to other common modes of characterization (MIP, flow-based methods) while further details were also provided to determine the accuracy of the AFM methodology [150]. In the same chapter the modification of the monolithic stationary phase will be described through conventional tuning of the polymerization conditions in order to determine the effect of this common approach. To provide contrast, Chapter 5 will show results obtained through photografting for the modification of a model monolith through a similar approach as initially demonstrated by Hilder, who employed a different monolith, poly(butyl acrylate-co-ethylene dimethacrylate) [144]. However, this approach was taken a step further and Chapter 6 reports on the fabrication and extensive characterization of a monolithic proteolytic reactor through the same basic photografting strategy. Preliminary (electro)chromatographic characterization of the grafted proteolytic

reactor will also be depicted. The proteolytic efficiency of photografted proteolytic reactors were compared to two microreactors fabricated with reactive poly(glycidyl methacrylate-co-trimethylolpropane trimethacrylate) monoliths. The first reactor was made via direct immobilization of protease on the monolith while a novel linker, N-succinimidyl-S-acethylthioacetate (SATA), was used in the second reactor.

Chapter 6 also summarizes the first example, and characterization, of boronate-affinity electrochromatography based on the immobilization of aminophenylboronic acid on a reactive monolith. Two distinctive approaches are described, namely direct immobilization and photografting. Spectroscopic characterization (NMR and Raman) of the functionalized monoliths is reported in addition to its electrochromatographic behaviour.

Chapter 2

Experimental

In this chapter, all details related to the fabrication, modification, characterization and utilization of monolithic stationary phases for (electro)chromatographic and proteolytic purposes are described. In order to allow replication of experiments detailed in this thesis, all manufacturer and distributors of chemicals as well as identification and description of equipment are also included.

All aqueous solutions were prepared using HPLC grade ultrapure deionized water (18 MΩ, Millipore, Billerica, MA) while organic solvents employed for (electro)chromatographic separation were all of the same grade. Mobile phases, sample solutions and working standards were prepared on a daily basis while aqueous buffers and standard stock solutions were kept at 4°C unless otherwise recommended by the vendors. All mobile phases were mixed to their final concentration on a volume basis and are reported accordingly. Also important to mention is the fact that the pH of mobile phases are taken from the aqueous portion exclusively using a pH meter (Thermo Fisher Scientific, Ottawa, ONT, Canada) standardized daily through a 3 point calibration.

To prevent clogging of monolithic capillary columns, all buffers employed for CEC were filtered using 0.45 μm Nylon filters (Millipore) then mixed volumetrically if required with the appropriate HPLC grade organic solvent. In most cases, sample solutions were prepared just prior to injection through dilution of standard stock solutions with the appropriate solvent or buffer. As for mobile phase, sample and standard

solutions were aliquotted individually in 1.5 mL amber polypropylene vials for electrochromatographic injections and separations. To eliminate the effects of electrolysis buffer and sample vials were replaced after each injection and run.

2.1 Characterization and Practical Limitations of Teflon-Coated Capillaries

An increasing number of research groups have discovered the advantage of Teflon-coated capillaries due to their high UV transmittance enabling formation of monolithic stationary phases of any desired geometric dimensions. These UV-transparent capillaries become an excellent model for the development of monoliths that can then be reproduced in microfluidic microchannels.

However, Teflon-coated capillaries suffer from certain drawbacks as shown in Chapter 3 and reference [201]. Experiments described in this chapter employed UV-transparent and polyimide-coated capillaries. Also reported are the results of a series of experiments where Teflon capillaries/monoliths were kept immersed for prolonged periods in typical CEC solvents.

2.1.1 Cutting Teflon Coated Capillaries

Four different cutting techniques were investigated and are described in Chapter 3. Imaging of monolith ends was achieved using the scanning electron microscopy (SEM) instrumentation and prior coating with gold as described in Section 2.4.2.

2.2 μ-LC and Electrochromatographic Instrumentation

Capillary chromatographic separations and pressure-driven experiments were accomplished by connecting the separation capillaries to a zero dead-volume tee junction using standard HPLC finger-tight fittings, ferrules and PEEK sleeves (part F-385X), all from Chromatographic Specialties (Brockville, ONT, Canada) except for the tee purchased from Valco (Houston, TX, USA). The tee union was alternatively connected to a Spectra Physics P4000 HPLC pump (now part of Thermo Fisher Scientific) while a 15 cm x 0.46 cm Spherisorb-Octyl 5 μm column (Chromatography Sciences Company, Montreal, QUÉ, Canada) was employed as flow resistor. Also, for experiments that required comparison of pressure and voltage-driven separation pattern, an ESA Model 580 μ-LC binary pump (Chelmsford, MA) was employed instead of the previous pump and the HPLC column was replaced with various lengths of fused silica capillaries to allow different split flow ratios (Polymicro Technologies, Phoenix, AZ, USA). With both pumps, a Thermo Separation Products SpectraSYSTEM AS3000 cooled sample compartment autosampler (San Jose, CA, USA) equipped with a 20 μL stainless steel sample loop was used for injection of samples.

Some electrochromatographic experiments were conducted on a lab-built system consisting of a Spellman Model CZE 1000R high-voltage power supply (Happauge, NY, USA) operated through a LabView 5.1 program written in-house (National Instruments, Austin, TX, USA). The voltage required for injection and separation were triggered through an analog output from a lab-built interface board connected to a PCI-1200 (12 bit

resolution) data acquisition board (National Instruments). The voltage for injection and separation was applied using 0.5 mm platinum wire electrodes from Goodfellow (Cambridge, UK). Capillary current was measured using the previously described board during separation through a current to voltage converting resistor connected to the ground end of the HV circuit. The same board was used to acquire the absorbance signal output from a Unicam 4225 UV variable wavelength detector (Mississauga, ONT, Canada) or an ISCO CV4 Variable Wavelength Capillary Electrophoresis Detector (Lincoln, NE, USA) operated at 214 or 254 nm with a rise time of 0.1 s and 0.1 absorbance unit full scale. The same detectors, acquisition/control hardware and program were also employed for μ-LC experiments. However, synchronization of injection and data acquisition were done manually for the chromatographic experiments while the synchronization was done automatically using the electrochromatographic interface. All data was collected at 20 Hz and processed using IGOR Pro version 3.15 (WaveMetrics, Lake Oswego, OR, USA) or GRAMS/32 Version 4.01 (Thermo Galactic, Salem, NH, USA).

Light-emitting diode fluorescence experiments were performed on a lab-built system mounted on an optical table. A Lumileds Luxeon III Royal-Blue LED was used for fluorescence excitation, operated at a fixed current of 100 mA, filtered through a 510 nm short-pass excitation filter and a 520 ± 15 nm bandpass emission filter (520DF15, Omega Optical, Battleboro, VT, USA). Detection was achieved with a model R1477 Hamamatsu photomultiplier tube (Shizuoka, Japan) using confocal spatial filtering.

2.3 Fabrication and Modification of Monolithic Stationary Phases

2.3.1 Reagents for Polymerization and Grafting

The chemicals used were: glycidyl methacrylate (GMA), butyl acrylate (BAC), 1,3-butanediol diacrylate (BDDA), (3-methacryloyloxypropyl)trimethoxysilane (MTS), 2-acrylamido-2-methyl-1-propanesulfonic acid 99% (AMPS), trimethylolpropane trimethacrylate (TRIM) technical grade, Amberlite IRA-900 ion-exchange resin, ethanol (EtOH) ACS grade, isooctane ACS grade, HPLC grade toluene and sodium hydroxide (NaOH). The photoinitiator, benzoin methyl ether (BME), was purchased from Fluka (available through Sigma-Aldrich, Oakville, ONT, Canada) while acetonitrile and methanol, both HPLC grade, were from Fisher Scientific (Thermo Fisher, Ottawa, ONT, Canada).

2.3.2 Monolithic Stationary Phases Preparation

All monoliths were prepared in 360 μm O.D. and 100 μm I.D. Teflon coated UV-transparent capillaries from Polymicro Technologies unless otherwise noted.

Manual washing, introduction of silanization and polymerization mixtures into empty capillaries was achieved using a sleeve, finger-tight fittings and a quick-connect male luer lock adapter (P-656) from Upchurch Scientific (Oak Harbor, WA, USA). Once filled, the capillaries were sealed at both ends using regular GC septa.

Silanization and introduction of anchoring methacrylate moieties was achieved by reacting (3-methacryloyloxypropyl)trimethoxysilane (MTS) with free silanols from the

silica through an acid catalyzed reaction. The reaction mixture consisted of 20% MTS, 30% glacial acetic acid and 50% water (%v/v) and was left overnight with the capillary ends sealed. Following washing of the silanized capillary with HPLC grade water, the polymerization mixtures were introduced manually. Silanized capillaries of 55 cm total length were then filled with the polymerization mixture and a minimum length of 25 cm of monomer-filled capillary section was exposed to UV light. The length of the exposed and polymerized section was selected to allow a monolith of 20 to 23 cm while avoiding bubbles commonly found at both capillary tips during polymerization. Following polymerization, the monoliths were washed successively with water, ACN and the separation buffer hydrodynamically or electrokinetically with the separation buffer.

Two base model monoliths were employed in the course of this thesis. Briefly, the polymerization mixture for the fabrication of the poly(AMPS-co-BAC-co-BDDA) monolith consisted of 340 μL BAC, 150 μL BDDA, 3.0 mg AMPS and 15.0 mg BME suspended in a ternary porogenic solvent (60/20/20 (%v/v) mixture of acetonitrile/ethanol/5 mM pH 7.0 phosphate buffer) that allows formation of a porous polymeric network. Upon homogenization and sonication, the polymerization mixture was flushed for two minutes into the separation capillary, sealed with septa and allowed to photopolymerize completely for 25 minutes under the action of the mercury lamp source.

The poly(GMA-co-TRIM) monolith was also fabricated through photoinduced copolymerization (30 minute irradiation) of glycidyl methacrylate (199 μL),

trimethylolpropane trimethacrylate (84 μL) crosslinker and BME (15 mg) photoinitiator suspended, vortexed (15 sec), sonicated (30 sec) and degassed (2 min) in isooctane (698 μL) and toluene (238 μL) porogenic solvent in a pre-silanized capillary. After photopolymerization, the polymer was conditioned hydrodynamically with toluene then acetonitrile using a high-pressure bomb (1000 – 1500 psi) for a minimum of 30 minutes each. Application of high-pressure resulted in a significant volumetric flow indicative of a high monolith permeability.

For smaller poly(GMA-co-TRIM) monoliths, employed as proteolytic microreactors, fabrication was achieved in polyimide-coated capillaries of 200 μm I.D. and 365 μm O.D. but with a 1.5 cm long window. The polyimide coating was removed by exposure to the flame of a lighter and washed with methanol to eliminate all carbonized polyimide residues.

For photografting experiments, only the poly(AMPS-co-BAC-co-BDDA) monolith was employed. Briefly, 19 cm acetonitrile washed monoliths were grafted with GMA for 2-10 minutes of UV exposure using BME as photoinitiator. The photografting solution consisted of 199 μL GMA, 15 mg BME suspended in 1 mL of acetonitrile. Acetonitrile allowed suspension of both GMA and photoinitiator while swelling the monolith (Section 4.3). The photografted capillaries were washed with ACN, immobilization buffer then trypsin/buffer, sealed and stored at 4 ^{o}C for a fixed duration. Unreacted trypsin and $CaCl_2$ was removed with NH_4HCO_3 Unless otherwise specified unreacted GMA was quenched with extended storage (1-2 days) in 50 mM TRIS.

Digestions were either performed at 25 or 38 °C at various linear flow rates. Due to potential hydrolysis of epoxide when exposed to water, extended exposure of GMA-grafted monoliths, not functionalized with trypsin, to aqueous solutions or buffers was avoided. Thus, grafting and conditioning were immediately followed by immobilization of the substrate of interest. To improve homogeneity of the grafting process, rotation of the capillary was incorporated in the photografting process at a rate of 1 rotation per minute. Hilder *et al.* [144] demonstrated enhanced surface distribution of grafted moieties, thus homogeneity, using rotation.

Flushing of polymerized monoliths was performed using a high-pressure bomb featuring five vertical ports as shown in Figure 2–1.

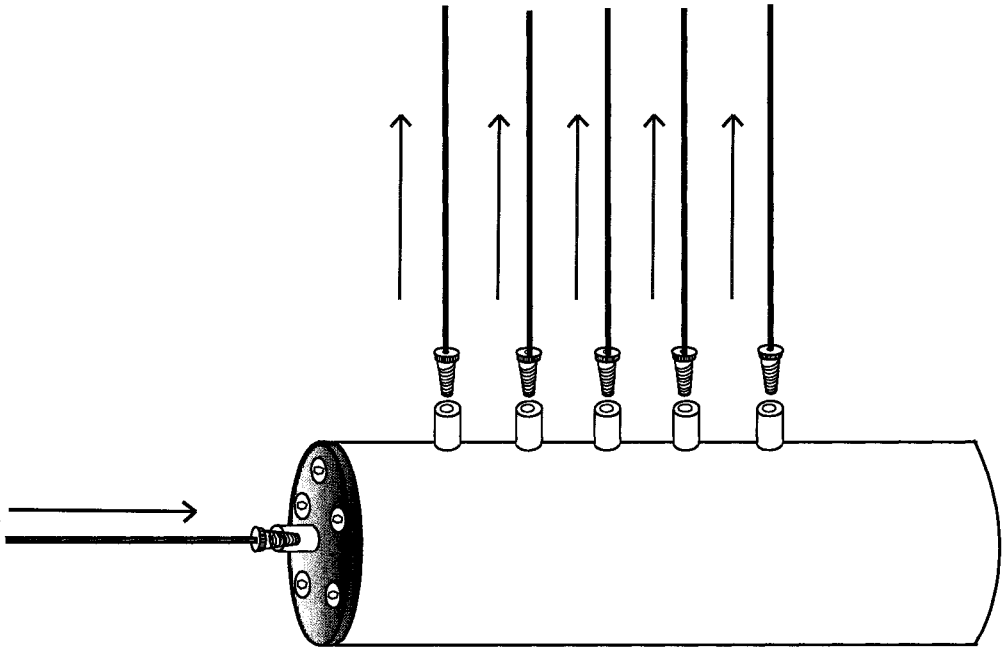

Figure 2–1: Design of a 5-port pressure-bomb for flushing of grafting or functionalization solution or for washing at high-pressure of the *in-situ* polymerized monolithic stationary phase.

Solutions in 0.75 or 1.5 mL Eppendorf tubes, without their caps, were placed under the individual ports and capillaries were inserted and sealed using finger-tight fittings. The bomb was operated at a fixed pressure of 2,000 psi and all unused ports were plugged using regular HPLC column caps.

Photopolymerization and photografting were carried out using a General Electric H85A3 high-pressure Mercury vapour lamp (General Electric, Toronto, ONT, Canada). Spectral output was 4.1 mW/cm^2, with the lamp placed 50 cm above the capillary. Calibration and measurement of the lamp intensity was achieved using an Indicator Model 154BT power meter (Laser Instrumentation, Chertsey, UK).

2.4 Instrumentation for Morphological and Surface Characterization

2.4.1 Atomic Force Microscopy

AFM experiments were conducted and analyzed with a Dimension 3100 Nanoscope III multimode AFM instrument (Digital Instruments - Veeco, Woodbury, NY, USA). Images acquired in tapping mode used an etched Silicon probe model RTESP (Veeco). Experiments carried out in contact mode used a Silicon Nitride (Si3N4) probe model NP-20 placed on a wafer capable of atomic resolution imaging (Veeco) [202].

To expose the monolith for AFM imaging, monolithic materials were expelled from the unsilanized capillaries by applying a high pressure flow of acetonitrile through the capillary. To generate this flow, the capillary was connected in parallel with a 5 μm Spherisorb C18 HPLC column (CSC, Saint-Laurent, QUÉ, Canada) using a zero dead

volume tee (Valco Instruments, Brockville, ONT, Canada). A Waters HPLC pump model 486 (Milford, MA, USA) set at 0.2 mL/min allowed a controlled hydrodynamic pressure of about 250 psi to be applied to the capillary. The polymer was deposited directly onto a microscope slide and rinsed at least five times with acetonitrile and finally dried under nitrogen flow. For AFM liquid phase imaging, the monolith was completely immersed in a specially designed cell from Digital Instrument containing HPLC-grade water.

For imaging the monolith in-capillary, a 0.5-1 mm length of the capillary column was vertically immobilized with epoxy glue exposing the monolith surface to the AFM probe.

2.4.2 Scanning Electron Microscopy and Elemental Surface Analysis

For SEM imaging, monoliths were either imaged directly at the end of the capillary or expelled using an HPLC pump. In both cases, samples were dried under vacuum at room temperature, gold coated using a Polaron PS3 Mini Sputter Coating Unit (Polaron – Quorum Technologies, East Sussex, UK) and imaged at 5 or 7 kV. The gold coatings usually did not exceed a thickness of 200 Å [203]. The high uniformity of the gold coating should not bias the porosity measurements accessible through SEM imaging. The scanning electron microscopes (Models S-2300 and S-4300 SE/N, Hitachi, Japan) were equipped with secondary-electron and retro-diffused electron detectors. Energy Dispersive (EDX) and Wavelength Dispersive (WDX) X-ray analysis were done on the

S-4300SE/N instrument. Both systems were coupled to a Kevex image analyzer (Kevex, Thermo-Fisher Scientific, Rockford, IL, USA)).

2.4.3 Mercury Intrusion Porosimetry

Measurements of the monolith's pore size were done with an Autopore IV 9510 mercury intrusion porosimeter (Micromeritics, Norcross, GA, USA). In order to measure pore diameters from 0.003 to 6 μm, the instrument was operated in high-pressure mode. A 5 cc "powder" penetrometer was used for all measurements. Sample masses, around 200 mg, were weighted precisely. Before measurements, extruded monoliths were washed three times with 50 mL of methanol on a sintered glass frit under vacuum then dried under vacuum at room temperature for 2 days to remove residual solvent from pores. Residual solvent prevents accurate pore size determination by partial filling of the pore during mercury pressurization.

2.4.4 Nitrogen Adsorption and Desorption (BET) and Differential Scanning Calorimetry (DSC) Measurements

Pore size, volume and surface area values from monoliths were acquired utilizing a Gemini surface area analyzer from Micromeritics (Norcross, GA, USA). Prior to analysis, samples were dried under vacuum at 220 ^{o}C for 4 hours then accurately weighed with masses close to 0.1 g.

A DSC Q1000 micro differential scanning calorimeter (Thermal advantage, New Castle, DE, USA) was utilized to measure the thermal stability of the monolith using a

ramp of 10 to 120 °C. Monoliths, dried as described previously, were placed within an aluminium microcupule and accurately weighed with a mass close to 3 mg.

2.4.5 RAMAN and NMR Spectrometry

Raman measurements were carried-out using a RFS 100/s FT-Raman Spectrometer from Bruker (Billerica, MA, USA) operated with a laser power of 450 mW, an aperture setting of 3.5 mm, scan range from 0 to 3500 cm^{-1}, a scan resolution of 4 cm^{-1} and 64 scans. The peak positions and intensities were verified using sulphur and tetrachloromethane (CCl_4) standards. Raman spectra were treated with OPUS NT (V3.1) software.

To obtain a sufficient amount of polymer for solid-state Raman measurements, samples were prepared as described in Section 2.3 but in Eppendorf tubes without prior silanization. Upon polymerization, samples were removed and rinsed under vacuum using ashless 7 cm filter paper from Whatman (Florham Park, NJ, USA). The sequential rinsing procedure consisted of 30 mL of decanol, 40 mL of methanol and 50 mL of HPLC-grade water. To remove unreacted reagents, including monomers, the polymer was agitated and ground against the filter during rinsing. Following this extensive washing, samples were air dried at room temperature for at least an hour in a fume hood and packed in a 2 mm diameter metal sample holder.

An Inova-300 from Varian (Palo Alto, CA) was used to perform ^1H NMR measurements using a sweep width of 4000 Hz, acquisition time of 3.744 seconds and 32 scans per sample. Internal lock was obtained with deuterated-chloroform, containing

TMS, as the solvent for all samples. Samples were prepared as for Raman experiments but were frozen at –84 °C for 30 minutes and ground into a fine powder. Sample (4 mg) was dissolved in 1 mL of deuterated-chloroform and filtered into NMR tubes for analysis.

2.5 Mass Spectrometry Analytical Instrumentation

Protein sequencing through peptide identification was performed on a Spec E MALDI-TOF mass spectrometer from Micromass (now part of Waters, Milford, MA, USA) equipped with a 337 nm N_2 laser. For calibration and analysis, the instrument was run in reflectron positive ion mode. Digested samples were lyophilized, resuspended and sonicated in 10 to 25 μL of 60% CAN / 0.1% trifluoroacetic acid (TFA, Supelco) solution (%v/v) and mixed with an equal volume of a 10 mg/mL α-cyano-4-hydroxy cinnamic acid (CHCA) solution in 50% ACN / 50% ethanol (%v/v). For sample deposition, the dried-droplet method originally described by Karas [204] was employed which consisted, after 60 seconds of sonication, of depositing 1.5 μL of samples in duplicate on a MALDI PrepTarget stainless steel plate which was then allowed to dry. When specified, on-plate desalting was achieved through sequential deposition and siphoning of 1 μL of HPLC grade water.

Assessment of proteolytic reactor efficiencies was accomplished by evaluating sequence coverage and mass spectrometric peak intensities from the peptide maps. Proteins were proteolytically digested without any prior denaturation or reductive alkylation that would cleave disulfide bridges. Fixed aliquot volumes of 60 μL were taken from the digest and lyophilized for each analysis. Protein sequences were obtained

from Swissprot [205] while expected proteolytically-generated peptides were determined via a proteolytic algorithm available on-line [206].

In order to determine the level of either glycosylation of myoglobin and bovine serum albumin (BSA) achieved through Maillard's reaction as well as deglycosylation of RNase B achieved enzymatically, electrospray ionization mass spectrometric (ESI-MS) analyses of initial and modified proteins were carried out on a Micromass QTOF with an ESI interface (Milford, MA, USA) equipped with a quadrupole time-of-flight mass analyzer. Capillary voltage was set at 3.3 kV, cone voltage at 40 V, source temperature was at 80 °C and desolvation temperature at 200 °C. Direct sample injection was achieved at an average flow rate of 5 μL/min and ions were analyzed in positive ion mode. Data analysis was performed with Waters MassLynx™ 4.0 SP1 (Milford, MA, USA). To improve signal intensity, samples were prepared according to a procedure outlined by Weinglass *et al.* [207]. In the first step, 300 μL of methanol was combined with 100 μL of sample solution containing 100 μg of protein and the resultant mixture was vortexed for 5 seconds. Afterwards, 100 μL of chloroform was added to the sample mixture followed by another vortexing step. A volume of 200 μL of HPLC water was added and the resultant mixture again vortexed, which lead to the formation of a precipitate. Upon centrifugation of this mixture at 10,000 rpm for 5 minutes, the collected precipitate was allowed to air-dry for 5 minutes. It was then washed with 300 μL of methanol, followed by vortexing for 5 seconds and centrifugation for 5 minutes at 10,000 rpm. Methanol was subsequently removed and the precipitate was

again allowed to air-dry. This final pellet was reconstituted in 50% ACN / 50% HPLC-grade water / 0.05% TFA (%v/v).

2.6 Materials and Reagents

Unless otherwise specified, all chemicals, solvents, standards and reagents were purchased from Sigma-Aldrich (Oakville, ONT, Canada).

2.6.1 Proteins for CEC and Proteolytic Digestion

Proteins were stored according to the manufacturer specifications. Proteins employed for the monitoring of the CEC behaviour of new monoliths were myoglobin (horse heart), transferrin (human), α-lactalbumin (bovine milk) and β-lactoglobulin A (bovine milk). Stock solutions were prepared daily in 5 mM pH 7.0 phosphate buffer and diluted prior to injection to the appropriate volume in the mobile phase.

For in-solution and solid-phase proteolytic digestion, bovine serum albumin (BSA), β-casein (bovine milk) and lysozyme (chicken egg white) were prepared daily in various digestion buffers that will be specified throughout the thesis. A non biological substrate, Nα-Benzoyl-L-arginine ethyl ester hydrochloride (BAEE) prepared as with the protein solutions.

2.6.2 Trypsin Immobilization

To prevent trypsin autodigestion resulting in immobilization of autolytic peptides and lowering the apparent proteolytic efficiency for in-solution and solid-phase digestions trypsin solutions were prepared just before use by dissolving 1 mg of trypsin

(from bovine pancreas, ≥10,000 BAEE units/mg protein) in 1 mL of 50 mM ammonium bicarbonate (NH_4HCO_3) at pH 8.5 or 50 mM HEPES at pH 7.5 both with 20 mM calcium chloride ($CaCl_2$) incorporated to reduce autolytic digestion.

For linker-mediated trypsin immobilization, N-succinimidyl-S-acethylthioacetate (SATA) was purchased from Pierce Biotechnology (now part of Thermo-Fisher Scientific, Rockford, IL, USA). Briefly, SATA and trypsin were reacted by initially dissolving 6-8 mg of SATA in DMSO while dissolving 10 mg of trypsin in 1 mL of PBS (0.1 M sodium phosphate, 0.15 M NaCl, pH 7.5). Trypsin was reacted to SATA at a 9 to 1 protein to SATA molar ratio by mixing 10 μL of the solutions and reacting for 30 minutes at room temperature. The reaction mixture was desalted through centrifugation with a Microcon YM-3 Centrifugal Filter Unit from Millipore with a molecular cutoff of 3000 Da. Conjugated trypsin was resuspended in 1.5 mL PBS via a backwash of the filter at 7000 rpm for 2 minutes. Incubation of 1 mL of this solution at room temperature for 2 hours with 100 μL of 0.5 M hydroxylamine, 25 mM EDTA in PBS, pH 7.5 deacetylated the SATA sulfhydryl moiety. Purification of deacetylated SATA-trypsin was through the same centricon methodology using 1 mL of 50 mM HEPES, 20 mM $CaCl_2$, pH 7.5 buffer for rinsing and elution.

Immobilization was achieved by flushing the SATA-trypsin or trypsin solution for a minimum of 48 hours at room temperature through the monolith capillary. In certain cases, longer immobilization durations were achieved by blocking both capillary ends with septa and storing at 4 °C to diminish trypsin proteolytic activity.

Following the immobilization reaction, residual epoxide moieties were opened by conditioning in 200 mM glycine solution and the reactor was kept sealed in 50 mM pH 8.0 TRIS buffer at 4 °C for storage.

2.6.3 PAH

Stock solutions of each PAH (acenapthalene, anthracene, benzo[k]fluoranthene, benzo[a]pyrene, chrysene, fluoranthene, naphthalene and pyrene) were prepared weekly in acetonitrile while standard solutions were diluted before injection in the mobile phase.

2.6.4 Boronate Immobilization and Protein Glycosylation and Deglycosylation

Boronate immobilization was achieved by dissolving 50 mg of APBA and 1 mg of sodium tetraborate in 0.5 mL HPLC-grade water in a 1.5 mL eppendorf tube and vortexing for 2 minutes prior to flushing for 20 minutes through a polymerized capillary using a syringe. Capillary ends were sealed with GC septa and placed in a Fisher Scientific Isotemp® incubator model 630D (Nepean, ONT, Canada) at 55 °C for 2 hours. After immobilization, the functionalized capillary was flushed at a flow rate of 5 μL/min with HPLC-grade water using the ESA pump.

Chemical protein glycosylation was carried-out using two different schemes of the Maillard reaction. In the first Maillard scheme, adapted from Chevalier [208], myoglobin and BSA were dissolved in 500 μL of 100 mM pH 6.5 phosphate buffer and glucose was added at a 90:1 sugar to protein molar ratio. After degassing with nitrogen

for 5 minutes, these solutions were incubated, along with blank solutions without added glucose, at 60 °C for 64 hours. Following incubation, samples were cooled to room temperature and dialyzed as described below.

The second Maillard reaction scheme was adapted from Sun [209]. Myoglobin and BSA were dissolved in 30 μL 20 mM pH 9 borate buffer and glucose was added at a 100:1 sugar to protein molar ratio. The resulting solution was vortexed for 3 seconds and then centrifuged for 5 seconds at 2000 rpm. The 1.5 mL Eppendorf tubes containing these solutions, along with blank solutions without added glucose, were pierced and inserted into a larger capped vial partly filled with 6 mL of saturated potassium iodide solution. These were incubated at 60 °C for 36 hours at a relative humidity of approximately 65% [210]. Following incubation, samples were cooled to room temperature and dialyzed as described below.

Samples generated though both Maillard reaction schemes were dialyzed for 2 hours against 2 L of HPLC-grade water to remove unreacted glucose. To accomplish this, 200 μL of protein solution was placed in the cap of a 1.5 mL Eppendorf tube after removal of the tube body. A 2.5 cm^2 section of Spectra/Pur cellulose ester membrane, 1000 Da molecular weight cutoff, from Spectrum Laboratories (Rancho Dominguez, CA, USA) was placed over the tube cap, and the remaining bottom was closed over the cap forming a sealed volume that was floated on the buffer membrane side down.

Enzymatic deglycosylation was performed with a GlycoProfile II enzymatic in-solution N-deglycosylation kit. The deglycosylation reaction mixture consisted of 90 μL

of 1.1 mg/mL Rnase B, a glycosylated protein used as the sample, dissolved in 20 mM ammonium bicarbonate (reaction buffer) mixed with 5 μL of 2% octyl β-D-glucopyranoside in 100 mM 2-mercaptoethanol (denaturing solvent). This reaction mixture was mixed, centrifuged down for 5 seconds at 2000 rpm, then heated/incubated at 100 °C in a water bath for 10 minutes, after which it was cooled to room temperature. Following the manufacturer recommended protocol, upon cooling, 5 μL of reaction buffer was added to the reaction mixture, mixed and centrifuged at 2000 rpm for 5 seconds. A 50 μL aliquot of this solution was mixed with 5 μL of HPLC-grade water and used as a control, a second 50 μL aliquot of the same solution was mixed with 5 μL of 0.5 unit/mL PNGase F and employed as a deglycosylated sample. As for previous solutions, these two latter solutions were centrifuged at 2000 rpm for 5 seconds, and incubated at 37 °C for 1 hour. To quench the reaction samples were placed in a 100 °C water bath, cooled and centrifuged down at 2000 rpm. Samples were dialyzed and analyzed through mass spectrometry (ESI-QTOFMS) as described previously.

2.6.5 Other Reagents

Sodium dodecyl sulphate (SDS) was from Schwarz/Mann biotech. Gamma-hydroxybutyrate (GHB) and gamma-butyrolactone (GLB) solutions were donations from the Laboratoire de Sciences Judiciaires et de Médecine Légale (affiliated with the Sûreté du Québec) while the injectable heparin solution (from porcine pancreas) was donated by Le Centre de Dialyse Semi-Autonome du Bois-de-Boulogne.

Six amino acids (alanine, arginine, aspartic acid, glutamine, glycine and histidine) were labelled with anthracene-2,3-dialdehyde (ADA), a fluorogenic dye from Molecular Probes (part of Invitrogen, Carlsbad, CA). Derivatization of the amino acids was performed at room temperature by combining within 1.5 mL microcentrifuge tubes 100 µL of sample solution, 700 µL of a 100 mM borate buffer (pH 9.5), 100 µL of a 100 mM KCN solution (pH 9.5) and 100 µL of 1 mM ADA in EtOH.

2.6.6 Buffers

All buffer salts as well as EDTA (ethylenediamine tetracetic acid) were Sigma Ultra grade purity. These buffers were ammonium bicarbonate, N-(2-hydroxyethyl)piperazine-N'-(2-ethanesulfonic acid) (HEPES), sodium tetraborate decahydrate, tris(hydroxymethyl)aminomethane (TRIS), mono and dibasic sodium phosphate. Dropwise addition of 0.1 or 1 M sodium hydroxide (NaOH) or hydrochloric acid (HCl) was used to adjust buffer pH, while in about 60% of the solution final volume followed by dilution to volume. All buffer solutions were filtered manually or under vacuum on 0.45 µm nylon filters from Millipore and kept at 4 °C or frozen (PBS and phosphate buffers) to prevent proliferation of biological matter.

2.7 Capillary Zone Electrophoresis Analysis of Peptides

In order to determine the relative amount of peptide generated through on-reactor digestion, a Beckman Pace MDQ capillary electrophoresis system was employed. The separation buffer consisted of 75 mM borate buffer with 0.8 mM EDTA adjusted at pH

9.25. Separation was achieved in normal polarity at 20 kV following hydrodynamic injection at the inlet at 34.5 mbar for 10 s in a 50 μm I.D. polyimide-coated capillary of 40 cm total length.

Chapter 3

Practical Aspects of Consideration for CEC Operation

This chapter is an expansion of a short communication detailing our work on the characterization of UV-transparent capillaries for capillary electrochromatography and capillary electrophoresis [201]. The text has been reformatted and is presented here in a thesis format. This publication described features of UV-transparent capillaries employed for capillary electrochromatography (CEC) and capillary electrophoresis (CE). A waveguide effect is observed when using UV-transparent capillaries. Through imaging with scanning electron microscopy (SEM), the UV-transparent coating is found to be highly porous unlike polyimide-coating, which does not exhibit any porosity at all. Unpublished material on prolonged exposure to several commonly employed solvents with elevated pH showed abrasion of the coating at the capillary tip but no swelling of the UV-transparent coating is observed. Lastly, four different cutting techniques are compared in order to obtain smooth capillary tips.

The vast majority of researchers in the field of CE and CEC employ polyimide-coated, fused-silica capillaries as their separation vehicle of choice [145]. A shortcoming of these capillaries is that a section of the protective polyimide-coating has to be removed to create a detection window. The same shortcoming occurs if one intends to create a monolith inside a polyimide-coated capillary through photopolymerization [87,131,218]. This latter aspect results in highly fragile capillaries since it typically requires the removal of several centimeters of coating. As an alternative, fused-silica capillaries

possessing a UV-transparent outside layer do not require removal of their protective coating [211]. Although their use has now been described for more than a decade [212,213], no publication has thus far characterized them in terms of waveguide effect, swelling or porosity of the coating. This short communication therefore reported a brief investigation of these aspects and also compared different cutting techniques in order to obtain smooth capillary endings. For polyimide-coated capillaries, smooth tips have long been recognized by the CE and CEC community as crucial in order to minimize band broadening [215, 216].

A previous publication from our group described the observation of a waveguide effect for UV-transparent capillaries [87]. Room lights (or other light sources in close proximity to the instrument) gave rise to a significant disturbance in the baseline. In the publication we compared two different types of detectors typically used in CE/CEC. The Unicam 4225 does not require any bending of the capillary in order to install the capillary in the detector, whereas the ISCO CV4 necessitates bending of the capillary by approximately 90° at both the detector inlet and outlet. Illumination in the laboratory consisted of standard fluorescent lamps on the ceiling. Figure 3–1 depicts the results obtained by sequentially turning the lamps on and off. Almost no waveguide effect is seen when using the ISCO CV4 detector as opposed to the Unicam detector. Total internal reflectance allows light to be guided into the detector but this phenomena is very sensitive to bending of the waveguide. If the curvature of the capillary exceeds a critical angle, total internal reflectance is lost and the waveguide effect is absent [214].

Consequently, one benefit of using the ISCO CV4 detector is that light levels remain relatively constant and are minimized in order to maximize signal-to-noise ratios and to reduce baseline fluctuations.

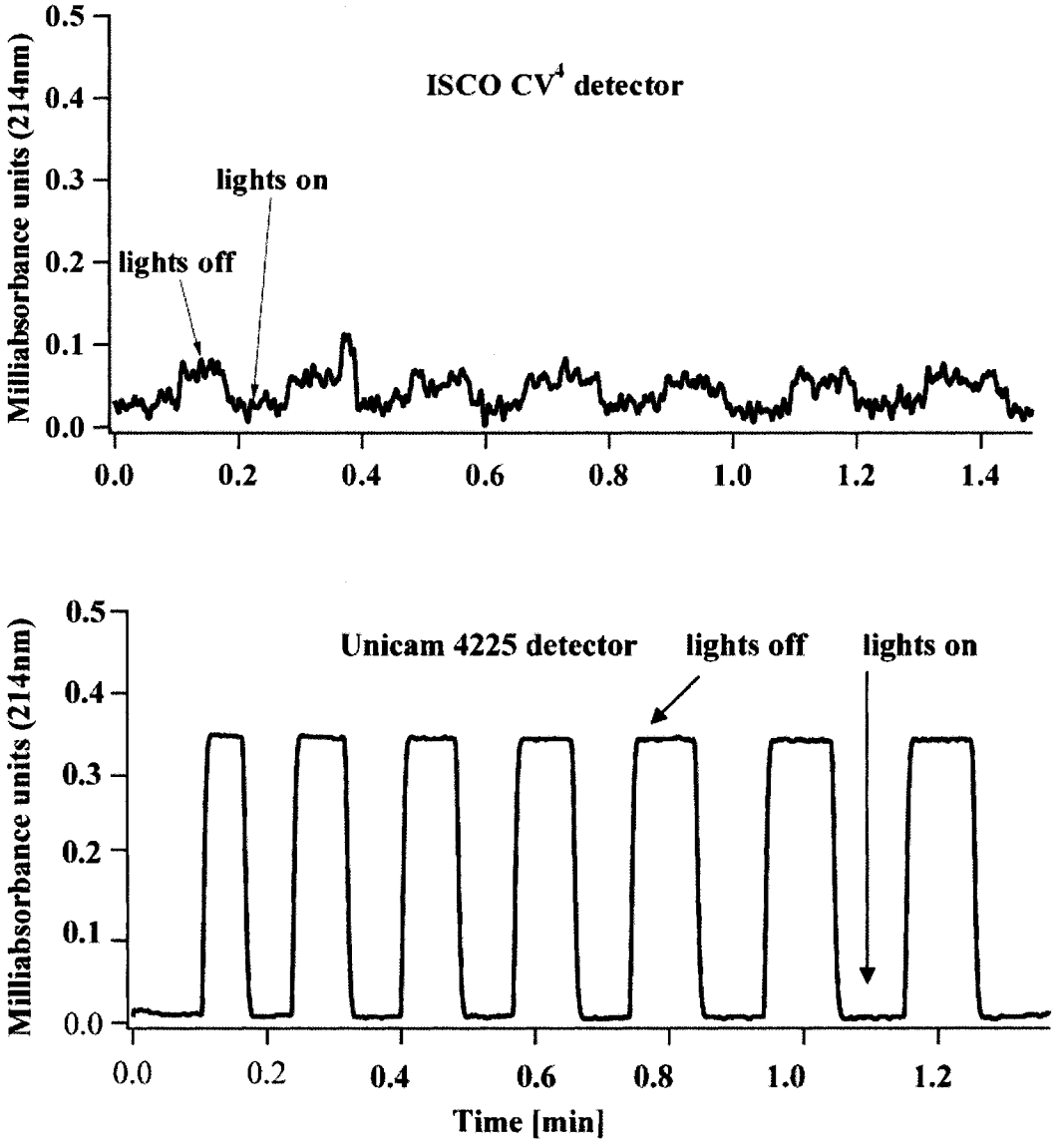

Figure 3–1: Visualizing the waveguide effect in UV-transparent capillaries between two different detectors by sequentially switching the room lights on and off.

Figure 3–2 compares the porosity between UV-transparent coatings and polyimide-coatings using SEM imaging of two capillaries that had not been in contact with any type of solvent. Higher porosity is observed in the UV-transparent coating while essentially no porosity in the polyimide-coating even at twice the magnification. However, the porosity of the coating should not have any deleterious effects on separations. For both coatings, delamination is observed between the coating and the fused-silica capillary tip. Research is currently under way in our laboratory to determine if this relates to the sporadic formation of bubbles at the inlet and outlet end of both UV-transparent and polyimide-coated capillaries in CEC.

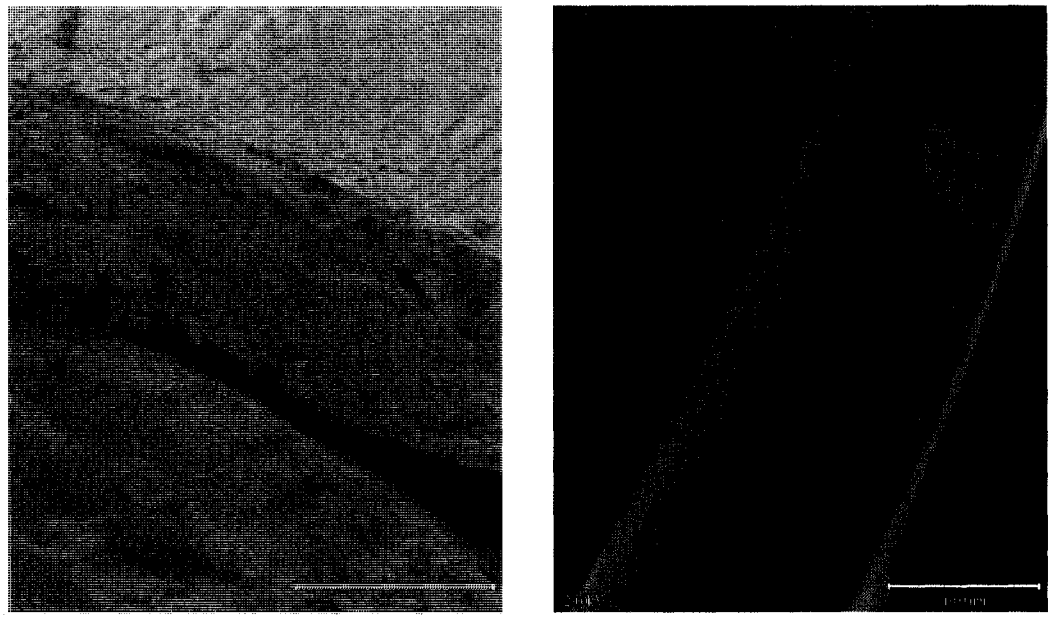

Scale bar is 20 μm Scale bar is 10 μm

Figure 3–2: Comparison of the porosity between capillaries with a UV-transparent coating and polyimide-coated capillaries.

Another point of interest is potential swelling of the protective coating upon prolonged exposure to solvents as was recently described by Baeuml and Welsch for

polyimide-coated capillaries from different vendors [145]. Our group investigated potential swelling of UV-transparent capillaries in five different solvents and one binary solvent system. All of them are commonly used for experiments conducted in the laboratory: (a) acetonitrile, (b) 5 mM pH 10.0 borate buffer, (c) 1 M NaOH, (d) water, (e) 1% (v/v) acetic acid, (f) 50% acetonitrile / 50% 5 mM borate buffer pH 10.0 (v/v).

The binary solvent system (f) was selected since it typifies a widely used mobile phase for CEC. Solvents a and b are the principal ingredients. The 1 M NaOH was selected since it is commonly used to precondition capillaries. To investigate response to lower pH, acetic acid was chosen, also a common ingredient of mobile phases in CEC. For each analysis, three UV-transparent and three polyimide-coated capillaries of approximately 3 cm length were kept in the solvents for five weeks and then subjected to SEM imaging. The analysis was complemented by three blank measurements, *i.e.*, freshly cut capillaries (both UV-transparent and polyimide-coated capillaries) that had not been exposed to solvents. Figure 3–3 shows the results for the UV-transparent capillaries (blank, solvents a-e).

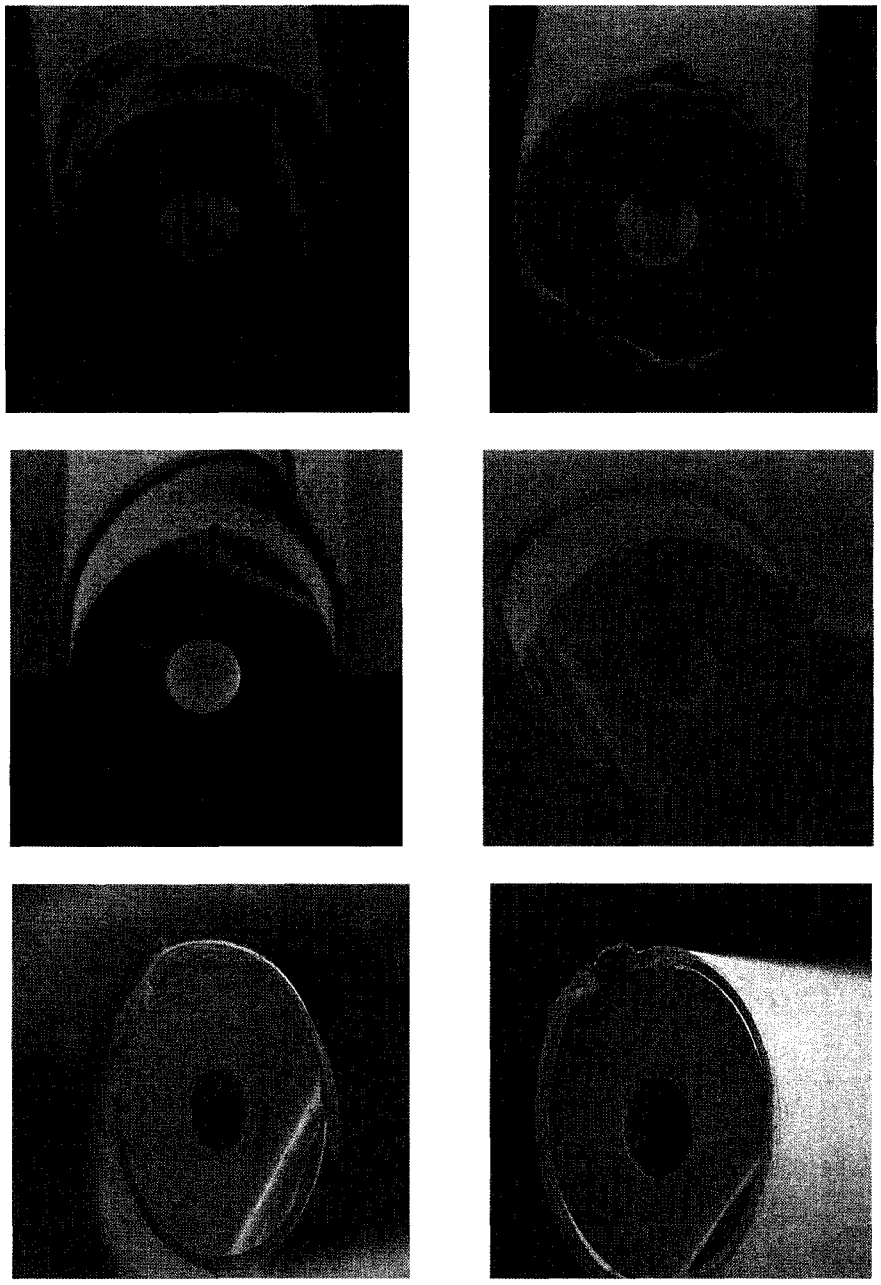

Figure 3–3: Comparison of a UV-transparent blank capillary and five UV-transparent capillaries exposed to solvents for five weeks: native (upper left), acetonitrile (upper right), borate buffer (middle left), NaOH (middle right), water (lower left) and acetic acid (lower right). All capillary images acquired at 250X magnification.

None of the capillaries show any form of irreversible swelling as observed through SEM imaging. The capillaries exposed to borate buffer and NaOH have parts of their coating that either delaminated over time or more likely the coating has pulled back along the capillary. Since little change is observed in either the blank capillary or the one exposed to acetonitrile, it appears that the elevated pH of both the borate buffer and the NaOH is responsible for this. The polyimide-coated ones did not show delamination in response to solvent exposure (results not shown). Thus, delamination seems to be inherent to UV-transparent capillaries.

Capillaries immersed into the binary solvent system (d) additionally had a the poly(AMPS-co-BAC-co-BDDA) monolith incorporated. Figure 3–4 illustrates the effect of the solvent system on both the UV-transparent coating and the monolith for this capillary. The UV-transparent coating exhibits the same delamination or "pulling back" that was seen in Figure 3–3 for NaOH and borate buffer. The monolith appears to be swollen after exposure for six weeks without any recognizable fine structure or porosity (images of a capillary with monolith that had not been exposed to mobile phase can be found in reference [87]). Also, cracking of the fused-silica is observed. Prolonged exposure to this particular mobile phase should therefore be avoided if one attempts to use the capillary over an extended period of time.

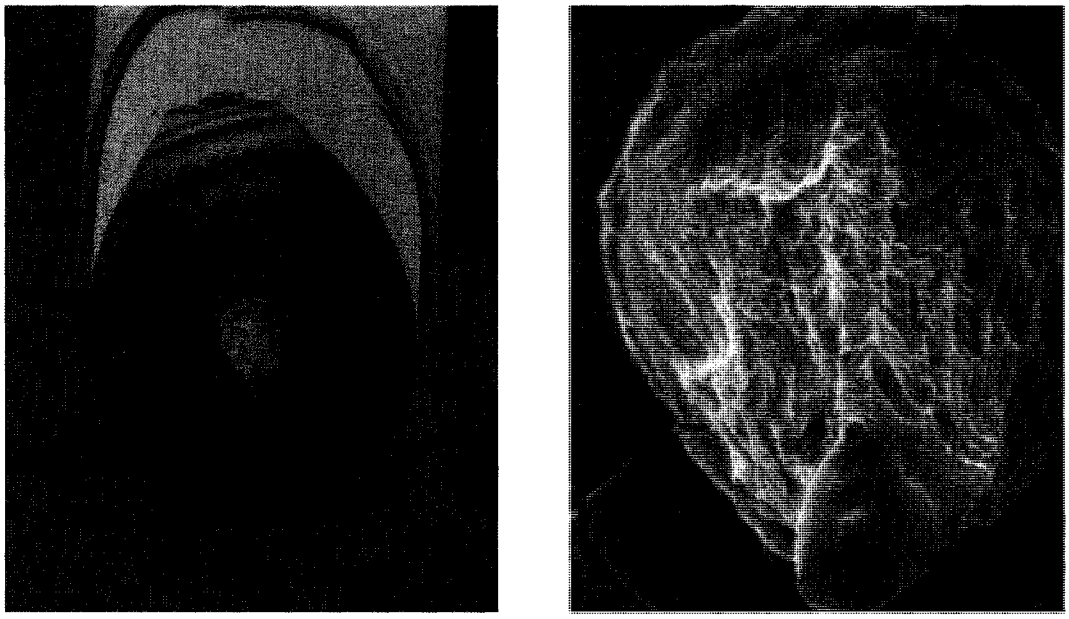

Figure 3–4: UV-transparent capillary containing a monolith after exposure to 50% acetonitrile / 50% 5 mM pH 10.0 borate buffer (v/v) for five weeks (left) and magnification of the monolith at the capillary tip (right). Magnification: 100X (left) and 250X (right).

Independent from whether a capillary is intended to be used in CE or CEC, clean cuts at the capillary tips are preferred in order to keep extra-column band broadening or inhomogeneities in the applied electric field as low as possible [215,216]. Since the UV-transparent coating appeared to be a rather soft material, different cutting techniques might be preferable compared to the ones applied for polyimide. We investigated the following four different cutting techniques and recorded SEM images of four trials for each technique:

a) Scratching the capillary with a conventional cutting stone used for CE and then bending the capillary at the groove until it breaks into two pieces;

b) Same as (a) but pulling the two pieces apart;

c) Same as (a) but "flicking" one piece off using the middle finger;

d) Using the Shortix™ column diamond cutter [217].

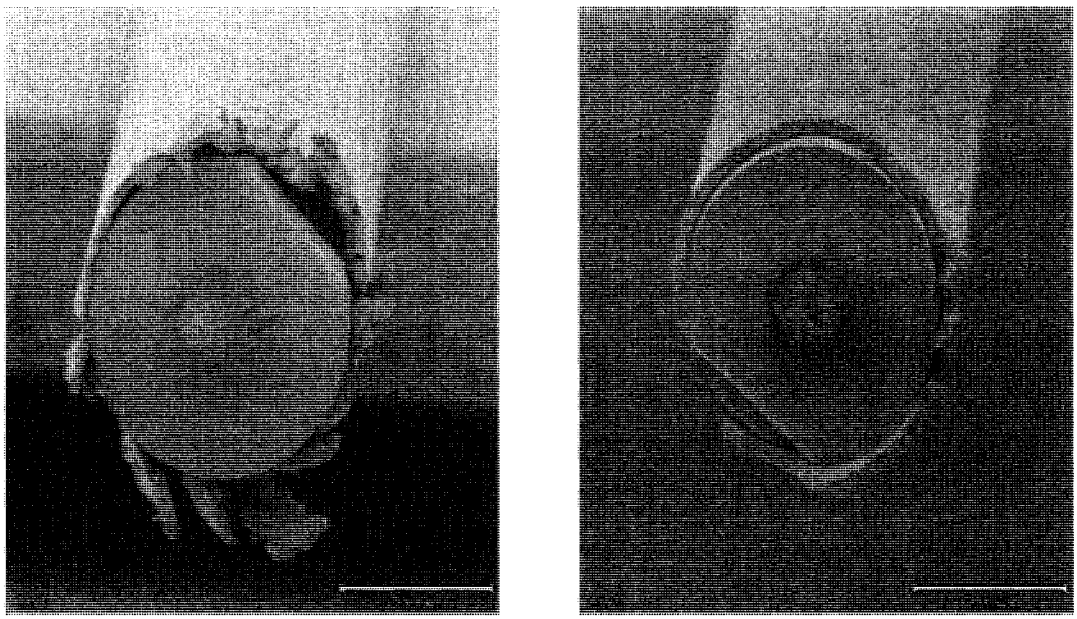

Figure 3–5: SEM images of two capillaries after using two different cutting techniques: "pulling" (left) and "breaking" (right).

The cleanest results were obtained using either the Shortix™ device (d) or by pulling the two pieces of capillary apart (b). Figure 3–5 shows one example of a relatively "clean cut" using the "pulling technique" (b) and one example of a less desirable cut using the "breaking" technique (a).

Summarizing the results, it was observed that the deleterious waveguide effect of UV-transparent capillaries can be decreased by sufficient bending of the capillary. The UV-transparent coating was found to be highly porous unlike the polyimide that does not exhibit any porosity. The chemical inertness of Teflon employed as a coating on the UV-transparent coating prevents bonding with the silica creating a gap at the silica-Teflon

interface while not with polyimide-coated capillaries. Indeed, UV-transparent capillaries were prone to breakage, delamination of the external coating and suffered from lower stability than polyimide-coated ones. Monolith incorporated in the capillary swelled significantly upon prolonged exposure to mobile phase consisting of 50% 5 mM pH 10.0 borate buffer and 50% acetonitrile (%v/v) with "pulling-back" of the coating observed in borate buffer, NaOH and mobile phase. The "pulling technique" or using the Shortix™ capillary cutter yielded the smoothest capillary tips.

As explained previously, a poorly cut capillary cut can potentially result in a heterogeneous electrical field close to the capillary end resulting in distorted a peak shape, especially if the inner wall of the capillary end is not flat. It can also yield increased dead volumes if connected to other capillary tubing through external connection. Although not proven, the presence of loose pieces of the external polymeric capillary coating can potentially trap and/or act as nucleation sites for bubbles when the capillaries are moved in and out of vials for injection, conditioning and separation. During operation, these bubbles can migrate into the capillary and act as a high-impendence zone that dissipates excessive power that leads to "cooking" of the monolithic stationary phase. Thus, an appropriate cutting technique resulting in both a flat capillary end without any residual external polymeric coating close to the capillary end should be employed.

Chapter 4

Fabrication and Characterization of a Monolithic Stationary Phase

Following the work of a laboratory colleague, Dirk Bandilla, who devoted his thesis research work to CEC separation of proteins using a model monolithic stationary phase, the initial goal of this thesis was to deepen the knowledge of the monolith morphological properties under working conditions. Since no experiments had been performed at that time to corroborate morphological values from flow-measurement techniques to more accurate and direct probing methods, developing an AFM methodology to measure the monolith properties in both wetted and dry conditions was the initial focus of this work. The methodology developed as well as the results were published and are detailed in the second section of this chapter. Special attention was given to illustrate the benefits and hazards associated with AFM measurements of very convoluted surfaces, such as the one investigated in this study.

The original paper did not include a detailed comparison against other common characterization techniques, namely MIP and BET, which is presented here to provide a better understanding of the variation in morphological results extrapolated from the different characterization techniques.

4.1 Fabrication of a Model Monolithic Stationary Phase

The literature flourishes with types of monolith that can easily be implemented by any research laboratory possessing the right facilities. Our laboratory has employed two basic monoliths because their high consistency, interesting (electro)chromatographic properties and ease of production. However, only one of these monoliths inherently possesses ionizable groups making its use in electrochromatographic conditions possible. Originally described by Ngola *et al.* [218], followed by Bandilla [87], this monolith consists of a poly(AMPS-co-BAC-co-BDDA) porous polymer fabricated through photoinitiation.

4.1.1 Description of Polymerization Scheme

The fabrication of this monolith is consistent with most other protocols from the literature where the inner walls of the silica capillary are initially functionalized with a silanization agent, (3-methacryloyloxypropyl)trimethoxysilane (MTS), through an acid catalyzed reaction as shown in Figure 4–1 below.

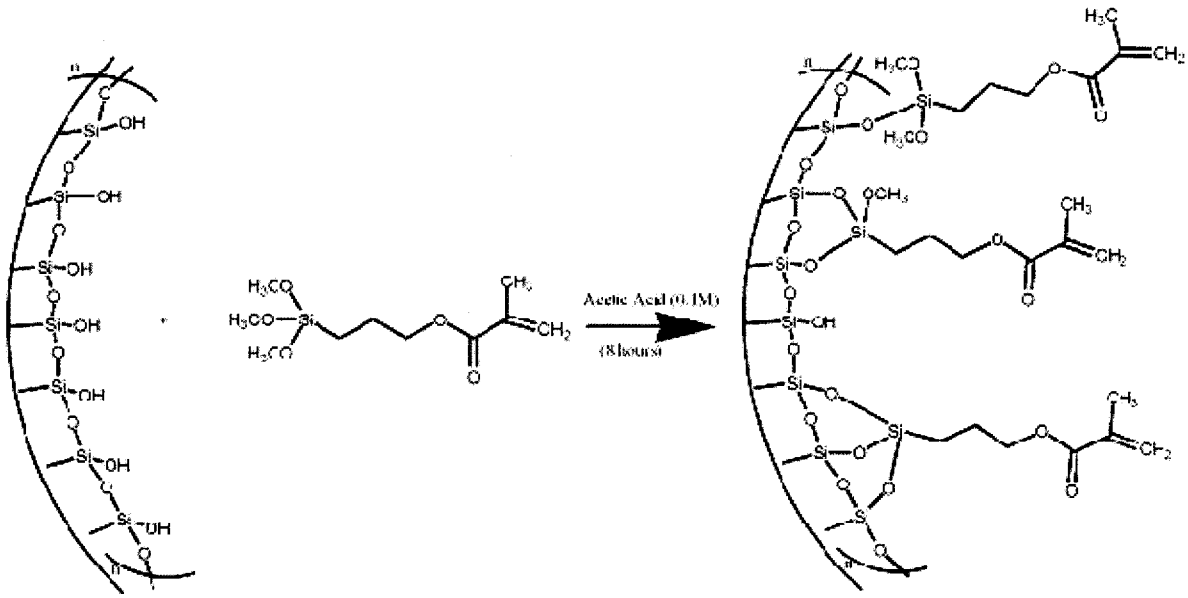

Figure 4–1: Silylation reaction on the capillary inner walls between free hydroxyls from surface silanols and the silanization agent through acid catalysis.

Photoinitiated polymerization provides many advantages over other modes of initiation, such as thermo-initiation. The benefits of photoinitiators are numerous but their main advantage for the *in-situ* polymerization of stationary phases is their ability to induce polymerization selectively in regions exposed to UV light allowing stationary phase length to be defined. Most common photoinitiators are not thermolabile at ambient temperatures so photopolymerization is easily stopped by simply removing the light source. Polymerization is usually completed quickly due to the high efficiency of photoinduced cleavage of the sensitive initiators that produce free radicals. This specific feature has been of a key importance for grafting procedures on existing stationary phase as it will be detailed later.

The BME initiator employed in this thesis induces polymerization through α-cleavage upon absorption of a high energy photon to yield two available free radicals as shown in Figure 4–2.

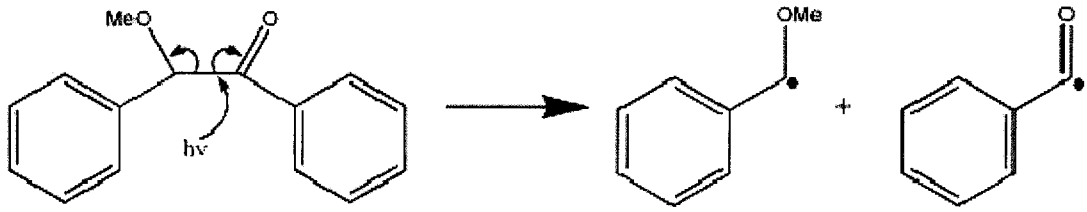

Figure 4–2: Photoinduced α-cleavage of benzoin methyl ether to yield two radical species.

Generation of free radical species in the vicinity of acrylate monomers induces the rapid formation of polymeric radicals leading to rapid propagation of the polymer chain. The growth, or propagation, of the polymer chain ceases upon combination of free radicals, trapping of free radicals in the polymer matrix (quenching), through stabilization of the free radicals or complete polymerization of all available monomeric and crosslinking species.

In order to validate that BME does not induce polymerization thermally, filled capillaries were completely masked using opaque electrical tape and subjected to increasing temperature. Even at 70 °C, no polymerization was observed for one hour while bubble formation occurred at higher temperatures due to solvent degassing.

When dealing with polymerization mixtures containing more than one monomer and crosslinker(s), the resulting polymeric chain will consists of a random branched

copolymer with non-homogeneous number of repeating units of each monomer and crosslinker.

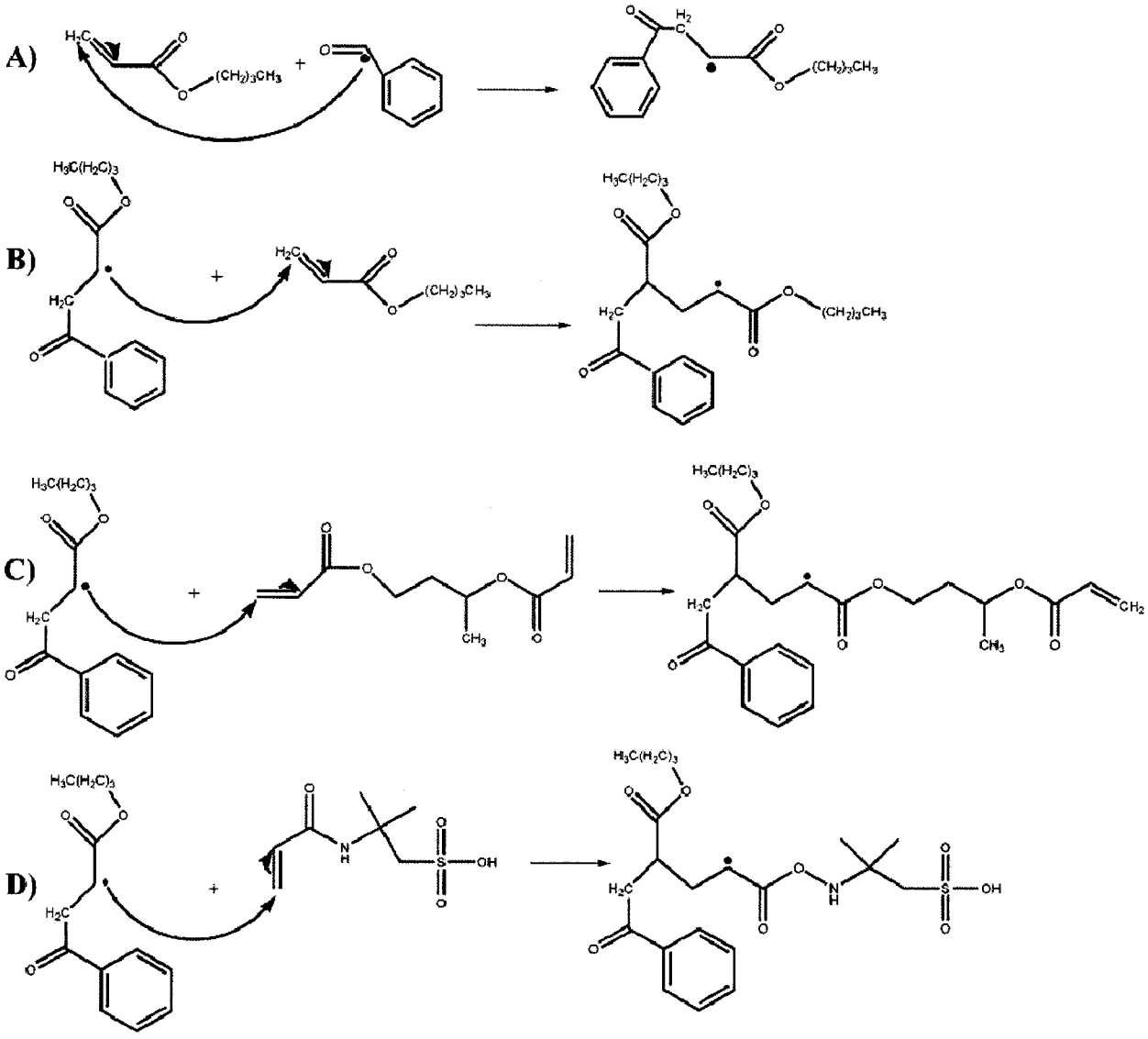

Figure 4–3: Initiation of the polymer chain propagation by (A) transfer of a free radical to BAC from benzoyl peroxide free radical and propagation from the radical BAC with another BAC monomeric subunit (B), the crosslinker (BDDA) (C) and AMPS (D).

This is the case with the present polymer where the relative abundance of each unit in the final polymeric backbone should theoretically be 0.5% AMPS, 75% BAC and 25% BDDA upon complete reaction of all individual constituents yielding a relatively hydrophobic polymer.

As introduced in Section 2.3, monoliths were either hydrodynamically washed following polymerization successively with water, ACN and the separation buffer or electrokinetically with the separation buffer. Hydrodynamic conditioning provided a very rapid and efficient washing method especially for "fresh" monolithic stationary phases that were to be used for grafting experiments. On the other hand, electrokinetic conditioning provided a convenient way of determining if any major issues occurred during polymerization that would impact the chromatographic behaviour of the column. Through monitoring of both current and UV absorbance signal during electrokinetic conditioning it was possible to verify that both signals became constant after 30 minutes conditioning. Typical current signals such as shown in Figure 4–4 are characteristic of a "good" capillary. On the other hand, the current signal of a "problematic" monolith usually demonstrates significant current drifts resulting ultimately in a complete loss of current. A "problematic" monolith usually consists of a monolith that has been partly polymerized along its axis in a heterogeneous manner resulting in a discontinuous monolith or can be a homogenous continuous monolithic bed where a section has dried resulting in cooking of the section upon voltage application.

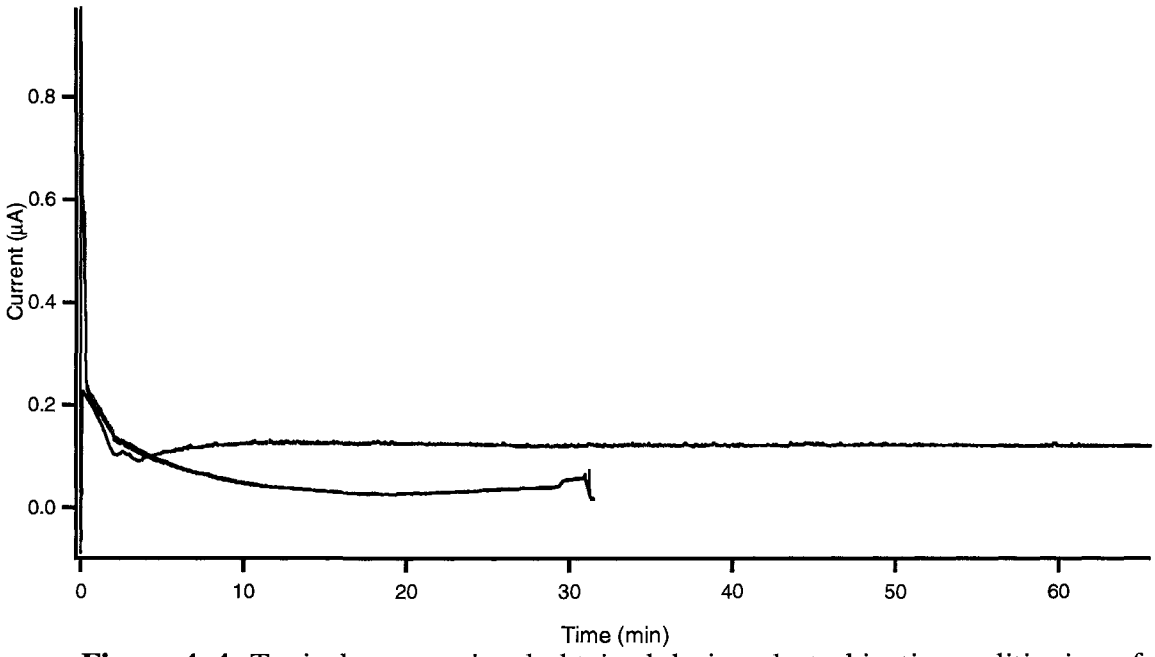

Figure 4–4: Typical current signal obtained during electrokinetic conditioning of a new poly(AMPS-co-BAC-co-BDDA) monolith with the first 30 minutes conditioning in 80/20 (%v/v) ACN/5 mM borate pH 10.0 (lower trace) and 240 minutes in 50/50 (%v/v) ACN/5 mM borate pH 10.0 (upper trace, only 65 minutes shown).

The complete polymerization resulted in a porous monolith as shown in Figure 4–5.

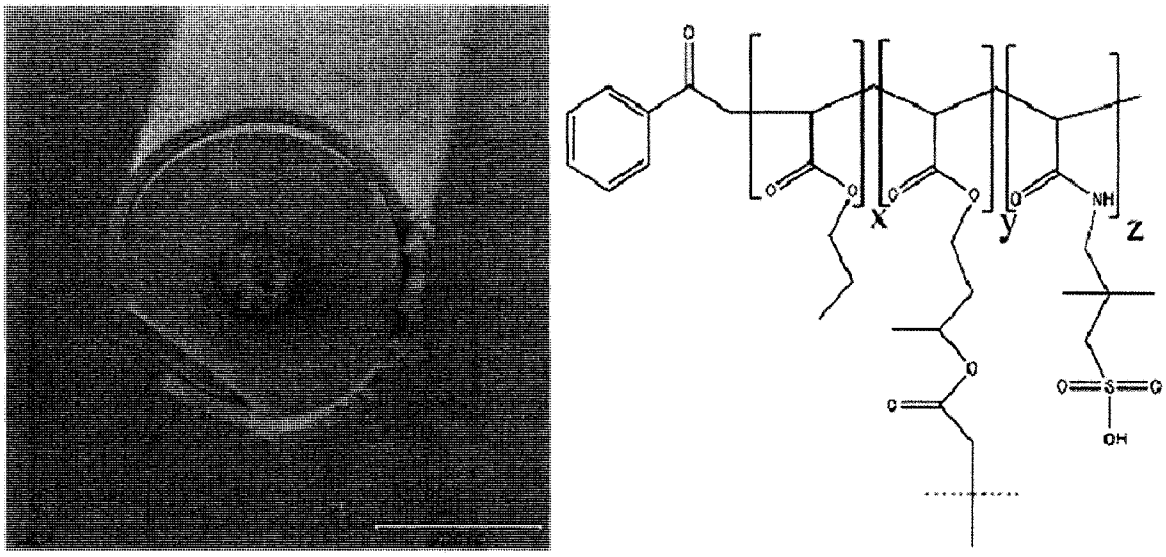

Figure 4–5: (A) SEM photograph of the poly(AMPS-co-BAC-co-BDDA) monolith and (B) its molecular structure consisting of randomly branched polymer with alternating monomeric units, *i.e.* where x, y and z represent the total number of individual monomeric units present in the final polymer.

4.1.2 Fabrication Process Reproducibility

Unfortunately, there is little information dealing with the assessment of manufacturing reproducibility and the factors that can affect monolith robustness. Bandilla examined the inter-monolith reproducibility of this specific polymer through compilation and comparison of electrokinetic measurements and electrochromatographic separation of model proteins with thiourea as a neutral unretained internal standard (I.S.) and EOF marker [16,87]. In these studies, the author investigated the migration time and peak area calculating intra and intercapillary reproducibility. While intracapillary reproducibility is obtained by measuring the variation in a model analyte migration time

and peak area obtained by multiple injections on individual monoliths, the intercapillary reproducibility corresponds to the variation in the same parameters but between different capillaries. Intracapillary reproducibility provides information on the reproducibility of the separation process while intercapillary reproducibility is associated with the variations in the fabrication process.

Employing 10 capillaries with five consecutive injections, he demonstrated intercapillary RSD's for thiourea, myoglobin, transferrin and α-lactalbumin between 7.7 and 18.4% using migration times while RSD's for peak areas were between 8.3 and 18.9%. It was also found that correction of migration time against the I.S. significantly improved reproducibility by rectifying changes in the EOF. Unfortunately, the same correction did not improve reproducibility for peak area.

The first project of this thesis was to validate if similar monoliths could be reproduced employing the same fabrication methodology. The study was conducted over a two-week period based on five daily runs of protein standards performed on 10 different monoliths. Compilation and comparison of peak areas and migration times for both operators are shown in Table 3. Even though capillary column dimensions were not identical between this study and Bandilla's, statistical analysis for equality of variances (F-test) revealed that intracapillary reproducibilities remained similar between the two operators illustrating the robustness of the fabrication protocol, with the exception of thiourea migration time reproducibility. As noted by Bandilla, part of the migration time fluctuation can be explained by the absence of capillary thermostatting resulting in

changes of solvent viscosity. Moreover, variations in temperature also lead to variations in the electroosmotic mobility as it is related to the electric double-layer thickness thus to the temperature, as previously shown in Equations 1 to 3. During the measurements, the laboratory temperature varied between 18 to 25 °C. Alternatively, peak area fluctuations can also be affected by changes in temperature, injection technique, sample preparation and stability but it is thought that the small, and not statistically-significant, difference between the two operator values can largely be explained by variations in peak integration procedures. In fact, since peak area calculations are achieved through a manual-based integration, interuser reproducibility can vary depending on the user's judgement on the location of baseline.

Table 3: Average of intracapillary reproducibilities based on 5 runs on 10 different capillaries

Parameters	Operator	Thiourea	Myoglobin	Transferrin	β–lactoglobulin A	α-lactalbumin
%RSD (Peak Area)	JLC	4.3	8.8	8.8	6.2	6.3
	DB	5.6	9.3	10.7	N.A.*	8.5
%RSD (Migration Time)	JLC	**7.0**	4.7	4.6	4.3	4.2
	DB	**2.1**	2.5	2.8	N.A.*	3.1

*Not available as β–lactoglobulin A was not measured.
Bold values: statistically different (F-test)

An efficient way to improve peak area and migration time reproducibility is the inclusion of an I.S. allowing compensation for small fluctuation in operational conditions. As depicted in Table 4, using the thiourea peak area and migration time as an I.S. permitted a clear improvement for values obtained by both operators except for β-

lactoglobulin A. On average, the use of the I.S. permitted a 50% and 60% improvement for peak area and migration time, respectively.

Table 4: Average of intracapillary reproducibilities with I.S. correction based on 5 consecutive runs on 10 different capillaries

Parameters	Operator	Thiourea	Myoglobin	Transferrin	β–lactoglobulin A	α-lactalbumin
%RSD (Corr. Peak Area)	JLC	N.A.	**2.5**	**2.6**	5.7	**2.5**
	DB	N.A.	**6.9**	**10.0**	N.A.	**6.1**
%RSD (Corr. Migration Time)	JLC	N.A.	1.2	1.2	2.9	1.5
	DB	N.A.	1.4	1.6	N.A.	1.7

Bold values: statistically different (F-test)

Interestingly, smaller %RSD values for corrected peak areas were obtained than for the previous study that could, as explained previously, be related to a difference between operator integration procedures. Alternatively, the higher protein concentrations employed in this study, *i.e.* 2 to 2.5 fold increase in comparison to Bandilla's measurements, could have generated these deviations between the two studies. Smaller RSD's are normally expected from larger peaks since variations in the manual assignment of the peak start and end required for integration become less significant.

Comparing all data accumulated without correction by the I.S., only minor deviations in %RSD were observed for intercapillary reproducibility from the two operators.

Table 5: Intercapillary reproducibilities based on compilation of 10 capillaries with 5 consecutive runs

Parameters	Operator	Thiourea	Myoglobin	Transferrin	β–lactoglobulin A	α-lactalbumin
%RSD (Peak Area)	JLC	5.0	9.5	11.3	8.9	10.6
	DB	8.3	7.1	18.9	N.A.	7.9
%RSD (Migration Time)	JLC	5.7	9.9	9.3	8.9	10.4
	DB	7.7	13.4	14.4	N.A.	18.4

Table 6: Intercapillary reproducibilities with correction by an I.S. based on compilation of 10 capillaries with 5 consecutive runs

Parameters	Operator	Thiourea	Myoglobin	Transferrin	β–lactoglobulin A	α-lactalbumin
%RSD (Corr. Peak Area)	JLC	N.A.	3.7	**4.6**	8.8	**5.9**
	DB	N.A	6.6	**15.7**	N.A.	**11.6**
%RSD (Corr. Migration Time)	JLC	N.A.	4.4	4.8	5.5	**5.0**
	DB	N.A.	5.4	6.9	N.A.	**11.6**

Bold values: statistically different (F-test)

As was the case for intracapillary reproducibility, the enhancement from using an I.S. correction was clearly significant for the intercapillary %RSD where daily fluctuations in working conditions were more likely to have an important impact. The use of an I.S. also presented the advantage of reducing the impact caused by variations in the final monolith bed lengths due to capillary breakage or polymerization issues.

Taking these results into consideration, it is possible to conclude that, the reproducibility for the fabrication of the CEC columns was within the same range as accomplished by Bandilla and was largely limited by the working conditions achievable with the lab-built system used. The addition of an I.S. was essential to obtain reproducible electrochromatographic behaviour.

4.1.3 Improvement of Fabrication Process Reproducibility

It is important to underline that these results were obtained using the same batches of reagents and capillary. As discovered, not without pain over the course of this work, the use of older reagents resulted in either no polymerization or non-stable and irreproducible polymeric stationary phases. Usually detected because of their non-homogeneous polymeric beds, these stationary phases yielded oscillating and heterogeneous current measurements as well as different chromatographic patterns for the separation of the four model proteins. On some occasions, sporadic monolith delamination from the interior wall was seen but was rectified by replacing the silanization agent. In the case of older monomers, polymerization can be hampered by the high amount of oligomers formed over time directly within the monomer bottles, even in the presence of inhibitors. Thus, monomers were aliquotted into smaller bottles of approximately 5 to 10 grams and replaced if any problems were encountered in polymerization and fresh stocks of monomers were purchased every 3 to 4 months.

Occasionally, deviations from the usual monolith electrochromatographic properties such as strength of the electroosmotic flow and/or electrical current in constant separation conditions were observed even after reagent replacement. Upon investigation, recalibration of the lamp intensity resulted in restoration of the initial polymer properties (data not shown).

Early in this thesis work, it was found that deaeration of the polymerization mixture prior to photoinitiation did not result in either better looking columns or electrochromatographic properties of the monolithic stationary phase.

4.1.4 Bubble Formation

One of the major drawbacks of electrodriven separation techniques is the problem associated with bubble formation within the separation channel. Bubbles, which can result from a non-homogeneous polymeric bed, local drying during polymerization or solvent degassing at high currents due to Joule heating effects, can lead to loss of the column if not quickly detected and responded to during an electrokinetic run.

Bubble formation is commonly detected by unusual spikes in both the current and absorbance signal or current breakdown. The main problem with bubbles is that they present an extremely high electrical resistance such that the electric field across the bubble rises up to nearly that of the applied voltage. At some field strength the bubble undergoes electrical breakdown, dissipating a large amount of power that can create more bubbles and/or destroy the stationary phase. Many researchers have blamed packing uniformity for this phenomenon due to higher current densities observed in very densely packed sections and non-uniform flow resulting in solvent shearing that leads to solvent degassing [219,220].

Introduction of an air bubble at the inlet of the polymeric bed during sample introduction nearly always results in "cooking" of the monolith. For bubbles appearing at the outlet, or within the stationary phase, column damage can usually be prevented by

immediately turning off the separation voltage before there has been extensive arcing within the capillary.

Three different methods to eliminate bubbles employing aqueous buffers are known: electrokinetic rinsing, hydrodynamic rinsing using a μ-HPLC pump as well as hydrodynamic (siphoning) rinsing [16]. All methods were able to regenerate packed beds where microbubbles were observed. All these methods were applied to eliminate bubbles when present at the outlet end of the capillary column. Siphon driven rinsing was not practical for packed columns due to the inherently high resistance to flow requiring either very high external pressure or long conditioning duration. Electrokinetic flushing with ACN required a minimum of 1 hour, however, longer electrokinetic rinses (>2 hours) are usually required to completely eliminate smaller bubbles. These bubbles are difficult to observe directly but are detected by persistent current drifts. Drifting current can be caused by microbubbles that remained trapped within the smaller pores of the stationary phase. Bandilla noted that bubbles can travel in any direction during electrokinetic rinsing [16]. This problem was avoided simply by raising the inlet side of the capillary upon application of the electric potential, which seemed to be sufficient to prevent the air bubble from moving towards the outlet end of the capillary. Not surprisingly, this approach is very practical for high-throughput applications.

Hydrodynamic flushing with a low viscosity solvent, such as ACN, thus appeared much more promising for bubble removal. To accomplish this, capillaries were either flushed with degassed ACN using a μ-LC as described by Bandilla [16] or using the 5-

port high-pressure bomb through application of positive pressure to the inlet end of capillary columns. Flushing of the polymeric bed with the separation buffer (50% /50% ACN/5 mM borate buffer pH 10.0 (v/v)) was also investigated in order to accelerate the rinsing/rejuvenation procedure but always resulted in reoccurrence of bubbles. The high-pressure hydrodynamic washing methodology was adopted throughout this thesis for the elimination of bubbles in capillary columns since elimination in less than 20 minutes was possible.

Validation of the reproducibility of *in-situ* polymerization was achieved through intra and intercapillary comparisons of electrochromatographic separations. Special attention was directed at identifying factors having an impact on the polymerization reproducibility. These results lay the foundation for all further evaluations of the modification and characterization investigations provided that any intentional alterations of monolith properties produce a response larger than the observed random variations.

4.2 Electrochromatographic Properties of the Model Monolith

CEC has yet to fulfill its promise as a very efficient separation technique not only for the differentiation of biomacromolecules such as proteins but also for differentiation of smaller molecules. An important advantage of the stationary phase that was used in this work is its dual chromatographic nature. The C4 and sulfonate functionalities are able to provide an interacting substrate for both reversed-phase and ion-exchange chromatography. This monolith has been extensively examined for protein separations [16,87]. In this section of the thesis other operational modes and applications will briefly

be investigated. Since part of the work described in Bandilla's Ph.D. thesis was done in collaboration with this thesis author, a brief review of these applications will also be presented. These studies will demonstrate the versatility of this monolithic stationary phase.

4.2.1 Biomolecule Separations: Proteins and Amino Acids

High efficiency protein separations are commonly achieved through ion-exchange or reversed-phase chromatography [221], while size-exclusion differentiation is mainly employed for isolation and purification purposes. For the separation of proteins, the use of a wide selection of classic hydrophobic through to hydrophilic stationary phases has been reported in the literature [222]. Recently, there has been an increasing interest for HILIC (hydrophilic interaction chromatography) for the separation of more polar peptides and proteins [223,224], but the great majority of protein separations are still achieved using C18 functionalities. Complimentary to RP separations, ion-exchange chromatography based on quaternary ammonium or sulfonate functionalities for strong anion or cation exchange, respectively, is a powerful technique for separating poly-ionic proteins.

Proteins consist of varying numbers of hydrophobic and charged amino acids, some exposed to the surrounding media while others are embedded within the three-dimensional protein structure. It follows that proteins can be separated chromatographically by either ionic or hydrophobic interactions or a combination of these mechanisms. Naturally in the case of a CEC separation, an additional

differentiation mechanism, the electrophoretic separation, will also influence the final chromatographic pattern. As Bandilla demonstrated for three model proteins [16], these three separation mechanisms are all involved in the separation. The influence of solvent strength on protein retention/capacity factor is a good way to determine if the primary separation mechanism is through RP interactions. Unfortunately, the protein three-dimensional structure is also affected by solvent composition which can result in modified protein hydrophobicity, making interpretation of retention vs. solvent composition difficult. Since Bandilla investigated this specific aspect of CEC protein separations, this topic was not further examined.

A crucial stationary phase property that has to be taken into consideration for protein separations is the pore diameter. The pores have to be wide enough to allow unrestricted movement within and across the pore thus improving the available surface area for retention and avoiding resistance to mass transfer, both crucial for high resolution and efficiency separations. It is recognized that in order to enable sufficient interaction of proteins or polypeptides within pores, the stationary phase should possess a pore size diameter at least 10 times the protein hydrodynamic radius [221]. For this reason, most HPLC protein separations are achieved with stationary phase characterized by 30 to 50 nm pore diameters. However, sorbents with pore diameters ranging between 100 to 1,000 nm, resulting in perfusive flow and described as gigaporous materials, have also been successfully employed for protein separations [225]. To analyze the pore

structure of stationary phases, destructive characterization techniques are commonly employed which will be the topic of Section 4.3.

However in the present study, taking into consideration the conclusion drawn by Bandilla, the electrochromatographic pattern of model proteins different size as well as small amino acids were used to determine if hydrophobic or ionic interactions were predominant, as described below.

The four model proteins selected for the current investigation covered a wide pI (isolectric point) and two size ranges, *i.e.* three proteins with molecular weight around 17 kDa and one at 77 kDa, as shown in Table 7, to demonstrate that there was no apparent sieving mechanism (in the size range investigated) during separation. These proteins pI's also enabled electrophoretic and ion-exchange differentiation at pH values above 8.5.

Table 7: Properties of the four standard proteins

Proteins	**Molecular Weight (Da)**	**PI**
Myoglobin	17,083	7.4
Transferrin	84,871	7.3
β-lactoglobulin A	19,883	5.0
α-lactalbumin	16,247	4.9

As seen in Figure 4–6, the electrochromatographic separation of these four standard proteins did not show a predominant sieving mechanism as transferrin, the largest protein, eluted after myoglobin. Although this finding is indicative, it might also imply

that the absence of size-exclusion differentiation could be the result of very small pores hampering penetration of all proteins, at least those larger than 16 kDa, into the chromatographic porous structure.

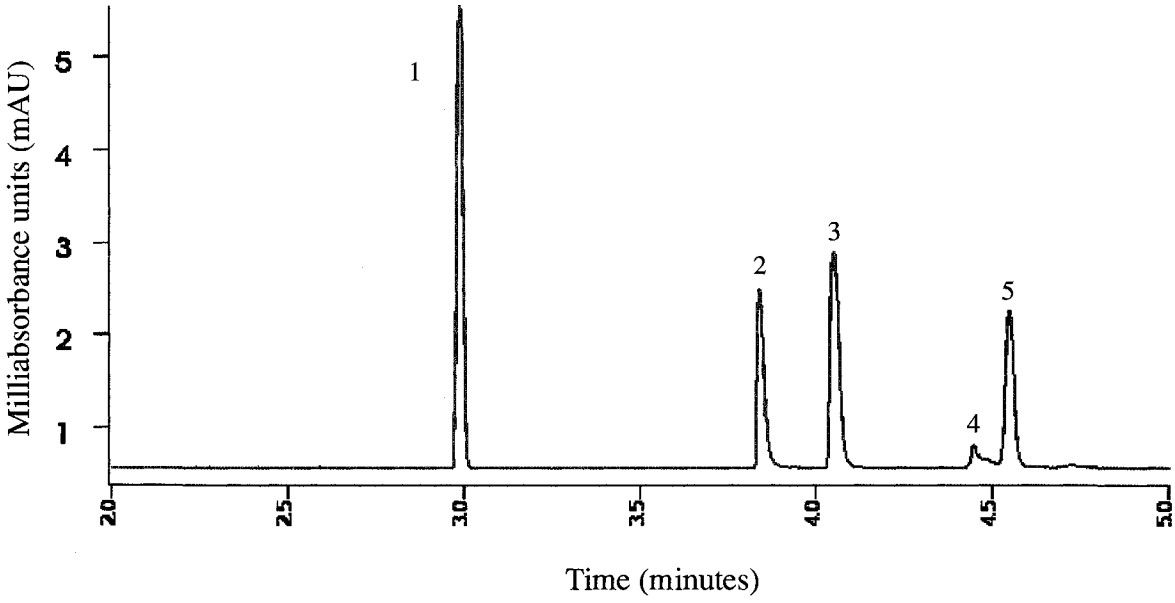

Figure 4–6: Electrochromatographic separation of four model proteins on poly(AMPS-co-BAC-co-BDDA) monolith. Peak identification: (1) thiourea (150 μg/mL), (2) myoglobin (300 μg/mL), (3) transferrin (300 μg/mL), (4) β-lactoglobulin A (150 μg/mL), (5) α-lactalbumin (300 μg/mL). Separation conditions: injection at 5 kV for 2 s, separation at 10 kV at room temperature, mobile phase consisted of 50/50 (%v/v) ACN/5 mM borate buffer pH 10.0, detection at 214 nm. The monolith segment was 21 cm long, total length of 35 cm and I.D. of 100 μm.

Ms. Marie-Ève Beaudoin, a project student cosupervised by Bandilla and I, worked on analyzing bovine milk by CEC [226]. Her work is explained in greater detail in Bandilla's Ph.D. thesis but the highlights are presented here as they have bearing on

the issue of the potential complex interplay of multiple differentiation mechanisms involved in the electrochromatographic separation of biomacromolecules. The five major proteins (shown in Table 8) commonly found in milk have similar size and pI values thus emphasizing the absence of size-exclusion differentiation.

Table 8: Properties of five major milk proteins

Proteins	**Molecular Weight (Da)**	**pI**
α-casein	24,529	5.5
β-casein	25,107	5.1
κ-casein	21,269	5.9
β-lactoglobulin A	19,883	5.0
α-lactalbumin	16,247	4.9

The electrochromatogram of standard milk proteins showed baseline resolution only for β-casein while all other proteins coeluted (Figure 4–7) into a large unresolved peak at around 4.5 minutes. It could be postulated that this lack of resolution is caused by lower chromatographic retention in addition to the small difference in protein sizes and electrophoretic mobility. However, this latter explanation might not hold as the charge states of these proteins were not known thus the relative difference in their mobility, which is dependent of a molecule's hydrodynamic radius and charge. The proteins also have different levels of hydrophobicity and ion-exchange interaction with

the stationary phase. Thus, further studies would be required to determine the respective influence of each chromatographic mechanism in this specific example.

In terms of applying this monolith for the analysis of a real sample, the electrochromatographic separation of diluted raw bovine milk proved to be feasible in a relatively short separation duration compared to published HPLC methodologies [227]. Unfortunately, as observed by Ms. Beaudoin, the abundance of fatty material within raw milk limited the number of direct injections on the monolith due to clogging of the column over time.

Less complex, and much smaller than proteins, amino acids are also a very important class of biomolecules. Certain amino acids (AA) are known as early biomarkers and progression markers of disease; for example, hydroxyproline is common to many inflammatory diseases such as osteoarthritis [228]. Their separation by CEC has been extensively described through both in-column and off-column derivatization strategies in order to enable their detection by LIF or direct UV detection [229,230].

Amino acids represent alternative model analytes for characterization of the monolith chromatographic properties due to their simple structure and established chromatographic behaviour. In order to demonstrate the predominant retention mechanism using smaller biomolecules, six amino acids with different charges and hydrophobicities were separated after labelling with a fluorogenic dye, anthracene-2,3-dialdehyde (ADA). Anthracene-2,3-dialdehyde (ADA) has gained attention in the last decade for the derivatization of compounds possessing primary amines [231,232]

allowing their sensitive detection either by chemiluminescence or laser induced fluorescence.

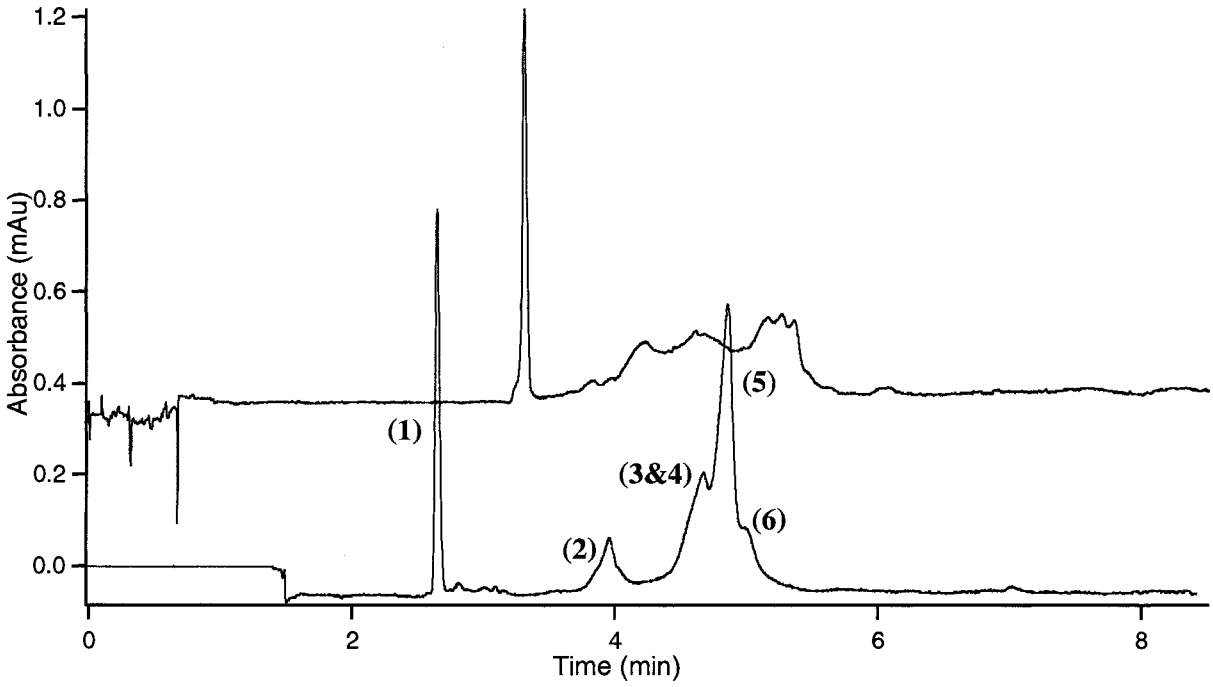

Figure 4–7: Electrochromatographic separation of a 10 fold diluted raw bovine milk spiked with thiourea as the I.S. (upper trace) and five standard bovine milk proteins (lower trace) on the poly(AMPS-co-BAC-co-BDDA) monolith. Peak identification confirmed by spiking: (1) thiourea (50 μg/mL), (2) β-casein (100 μg/mL), (3) κ-casein (100 μg/mL), (4) β-lactoglobulin A (100 μg/mL), (5) α-lactalbumin (100 μg/mL), (6) α-casein (100 μg/mL). Separation conditions: injection at 5 kV for 2 sec, separation at 10 kV at room temperature, mobile phase consisted of 50/50 (%v/v) ACN/5 mM borate buffer pH 10.0, detection at 214 nm. The monolith segment was 21.5 cm long with a total capillary length of 36.3 cm and an internal I.D. of 100 μm and O.D. of 355 μm.

Over other labelling dyes, ADA has several advantages notably its relatively low cost and its quick, straightforward functionalization methodology. As shown in Equation

13, because the fluorescence emission of naturally, or labelled, fluorescent compounds is directly proportional to the intensity of the excitation light, laser-induced fluorescence theoretically allows great improvement in the limit of detection. The high specificity of induced fluorescence limits the detection to just the fluorescent molecules thus improving significantly the signal-to-noise ratio once again over absorbance detection.

(Equation 13) $F = kc\Phi$

> **Equation 13**: Linear relationship between fluorescence intensity (F), sample concentration (c), radiant intensity of the excitation source (Φ) and (k) a constant including the pathlength (detection), sample absorbtivity, and fluorescence quantum yield.

Derivatization of primary amine containing molecules, such as amino acids, was achieved as described in Section 2.6.5.

The initial setup employed for detection was based on a relatively inexpensive Helium-Neon laser matching the excitation wavelength of ADA at 543 nm. However, since the principal goal of this study was to investigate the electrochromatographic pattern of selected A.A. and not analyzing minute concentrations of A.A., the opportunity was taken to investigate the potential of a very inexpensive blue light-emitting diode (LED) as an excitation source for LED-induced fluorescence (Section 2.2).

At first glance, the electrochromatographic and chromatographic patterns differ significantly as shown in Figure 4–8. The pressure-driven separation almost permitted separation of all amino acids but switching to electrochromatographic separation resulted

in a major improvement in analyte resolutions. In both cases, the overall chromatographic interactions consisted of a combination of electrostatic and hydrophobic chromatographic differentiation as denoted by the A.A. order of elution. Indeed, the observed order of elution in CEC and μ-LC was as predicted from the individual A.A. structure.

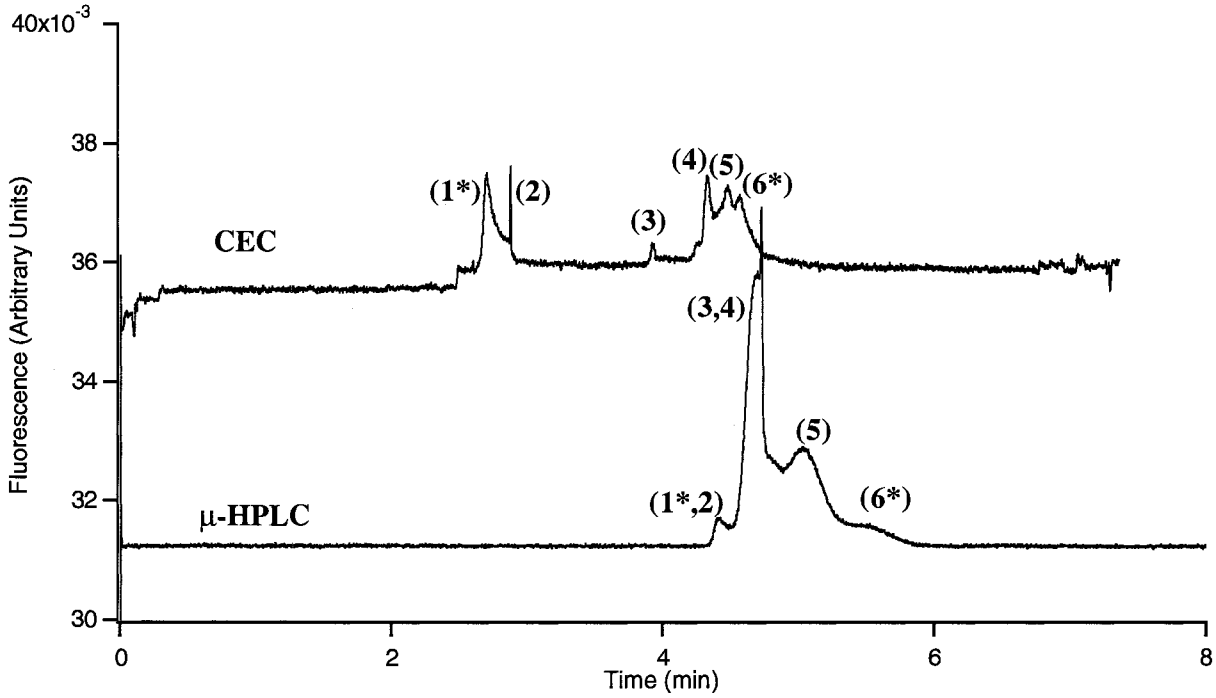

Figure 4–8: CEC and μ-LC separation of 6 ADA-labelled amino acids at 160 μM on the poly(AMPS-co-BAC-co-BDDA) monolith. Peak identification confirmed by spiking: (1* & 6*) labelling by-products, (2) Asn, (3) Gln, (4) Ala & Gly, (5) His, Not eluted: Arg. Separation conditions: injection at 5 kV for 2 sec, separation at 10 kV at room temperature, mobile phase consisted of 50/50 (%v/v) ACN/5 mM borate buffer pH 10.0, Fluorescence excitation and detection as described in experimental section. The monolith segment was 22 cm long with a total capillary length of 35 cm and an internal I.D. of 100 μm and O.D. of 355 μm.

In μ-LC, the extent of hydrophobic retention was high enough to differentiate only two of the four neutral A.A. (Asn & Gln, peaks 2 & 3) possessing both polar non-

charged lateral chains differed only in a single methylene group. Switching to CEC mode enabled the additional differentiation of Gln from the third & fourth neutral A.A. (Ala & Gly, peak 4), characterized by non-polar lateral chain groups (CH_3 & H). It is thought that the resolution of Gln from the two other A.A. was caused by the difference between Gln, Ala and Gly amino group pKa's (respectively 9.13, 9.78 and 9.87) resulting in difference in electrophoretic mobility at the working pH (10.0). It also appeared that the extent of hydrophobic interaction was not significant enough to induce differentiation of Ala and Gly.

In CEC and μ-LC, the most basic A.A. Arg was not eluted suggesting that electrostatic interactions prevailed for this specific compound, explained by the relatively high pKa of its lateral chain (12.48). A similar phenomena, resulting in longer elution times, was observed by Freitag [233]. In the case of His, another basic A.A. but characterized with a lower lateral chain pKa (6.04), there was no major shift in migration between the chromatographic and electrochromatographic separation. From this rapid experiment, it was concluded that the simple transfer from a pressure-driven to electrokinetically-driven separation enabled a net gain in resolution even though one of the compounds did not elute from the capillary nor was baseline resolution achieved. However, care must be exercised when interpreting the order of elution of labelled A.A.'s as the addition of ADA results in a significant increase in their hydrophobicity. Clearly improvement in the mobile phase is required and gradient elution would be a significant benefit. These results thus demonstrated that both the ionic (AMPS) and hydrophobic

(butyl acrylate) monomers used in the monolith's fabrication confer significant chromatographic properties to the monolith that can be exploited for other types of analytes. It also demonstrated that AA's could be used to monitor the impact of further modifications on the specific chromatographic properties of the monolith.

4.2.2 Separation of Small Hydrophobic Molecules from an Injectable Drug

The separation of amino acids and proteins only represents a small class of typical analytical targets. Even today, most major quality control analytical laboratories are focused on the analysis of small neutral molecules usually separated with well established C18 HPLC separations. In order to demonstrate the versatility of this monolithic stationary phase for similar separations, two simple analytical cases were investigated involving small neutral analytes.

The first sample consisted of a heparin solution, a linear polysaccharide found in all animal tissues and employed medically to control angiogenesis and blood coagulation [175]. Stable at room temperature for an extended period of time, heparin solutions contain two neutral antimicrobial preservatives, methyl and propyl paraben. These two species are also commonly employed together in many other injectable drugs due to their antimicrobial synergistic effect [234]. Another preservative, benzyl alcohol, is also added to heparin solutions to ensure sterility. Generally analyzed by HPLC [235], CE [236] and GC [237] methods have also been described. However, no detailed, or even crude, separation of these three compounds in a heparin solution by CEC has been

reported in the literature. Figure 4–9 illustrates the resulting electrochromatogram for the injection of the diluted heparin solution.

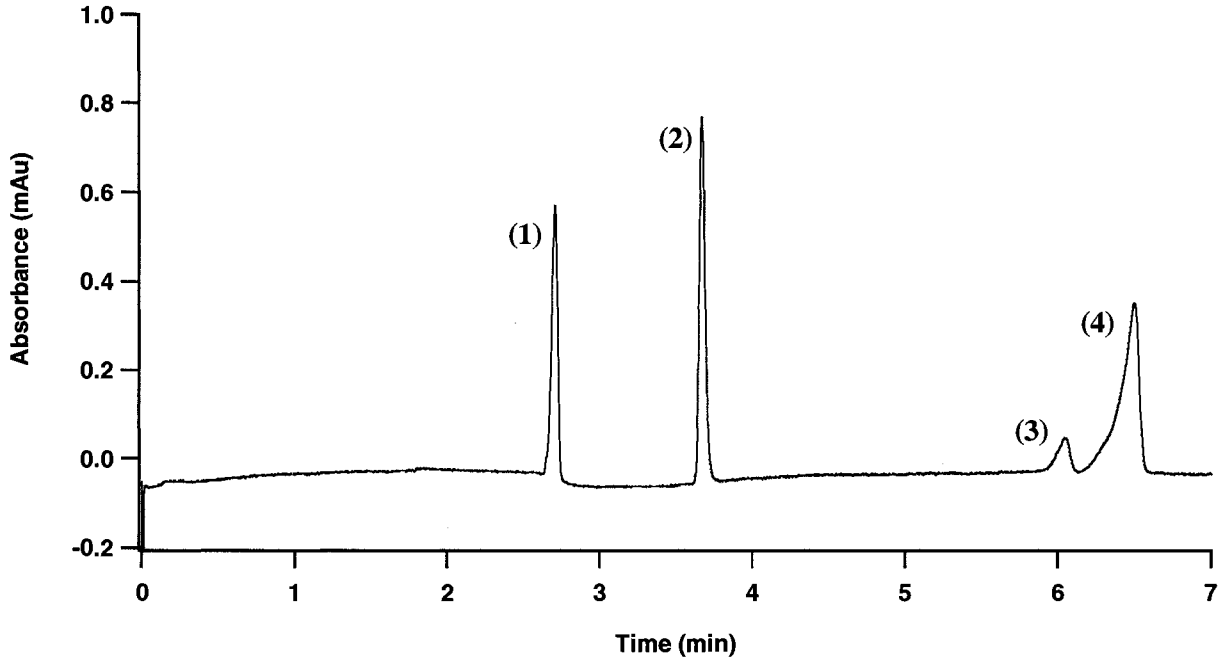

Figure 4–9: CEC separation of 3 drug preservatives found in a ten-fold diluted injectable heparin solution. Peak identification confirmed by spiking: (1) thiourea, (2) benzyl alcohol, (3) methyl paraben, (4) propyl paraben. Separation conditions: injection at 5 kV for 5 sec, separation at 10 kV at room temperature, dilutant and mobile phase consisted of 50/50 (%v/v) ACN/5 mM borate buffer pH 10.0, detection at 214 nm. The monolith segment was 21.5 cm long with a total capillary length of 36.3 cm and an internal I.D. of 100 μm and O.D. of 355 μm. Peak resolution: $R_{s(1-2)}$= 7.6; $R_{s(2-3)}$= 14; $R_{s(3-4)}$= 1.5.

In comparison to the two previously described CEC separations, the neutrality of the analytes greatly facilitates interpretation of the electrochromatogram. Although baseline resolution of all peaks was achieved without tuning the mobile phase composition, peak fronting was observed for the methyl and propyl paraben while not

predominant for the two other neutral compounds. This could have been caused by the high ionic strength of the sample solution; however this would also have resulted in distortion of all other peaks. Alternatively, peak fronting could result from column overload but given the sample size this was not the case. Thus, fronting was thought to be caused by induced dipole interactions of methyl paraben and propyl paraben with the stationary phase and is indicative of a non-linear adsorption isotherm suggesting a non reversed-phase interaction. An increase in ionic strength could have reduced potential ionic interaction and by a change in the mobile phase composition.

Because baseline resolution was achieved, further experiments were conducted to decrease run duration required for separation. However, increasing the separation voltage also resulted in current breakdown while increasing the organic content yielded coelution of methyl and propyl paraben (data not shown).

In this section, the complex interplay of electrostatic and hydrophobic interaction was demonstrated for several classes of molecules. Due to the small size and simple structure of amino acids, their separation allowed a clear demonstration of the dual chromatographic nature of the poly(AMPS-co-BAC-co-BDDA) model monolith, *i.e.* ion-exchange and reversed-phase chromatography, combined with electrophoretic differentiation. However, further studies are required to assess if the difference in retention mechanisms between the A.A. and proteins can be related to the monolith's pore size. The complexity of the interactions prevents a simple and systematic understanding of the retention mechanisms when biological analytes are involved. The

two following sections will detail the research work achieved towards methods of characterizing the pore size without the limitations imposed by the chromatographic methods.

4.3 Morphological Characterization of Monoliths in Dry and Wetted States using Physical Characterization Techniques

The following section details the use of scanning electron microscopy (SEM) and atomic force microscopy (AFM) for the characterization of the poly(AMPS-co-BAC-co-BDDA) monolith as a model CEC monolith. Although the majority of this section has already been published [150], we also report additional investigations that were carried to compare the published AFM and SEM results with the values obtained with two other destructive techniques, *i.e.* mercury intrusion porosimetry (MIP) and nitrogen adsorption-desorption isotherm (BET).

4.3.1 Description of the AFM Methodology

Air phase AFM imaging was performed in intermittent contact mode (tapping) with a 15 to 20 μm high pyramidal tip that was scanned over the monolith surface with a resonance frequency of 200 – 400 KHz. Collecting AFM images in the liquid phase had to be performed in contact mode due to unwanted resonances typically encountered with acoustic excitation in liquid media [238]. Furthermore, it has been shown that acoustically excited tapping probes generate vibrations of the detector components leading to a loss in sensitivity [239,240]. In both scanning modes, 512 points were

acquired per line. To ensure that deep penetration of the soft polymer surface did not occur, surface contact was established at low drive amplitude before imaging. The scan rate was first set to a high value (typically 1.5 Hz) to verify contact with the surface. In order to maximize scan rate while maintaining resolution the scan rate was optimized to an approximate value of 1.0 Hz for all surfaces. In contact mode, particular attention must be paid to avoid drifting, manifested as lines, misshapen features or shape bias depending on the scan direction, caused by a scan rate that is too high. Since scan size plays an important role in image quality, fine-tuning of the scanning parameters was necessary for each scanned size.

To avoid dislodging and floating in the liquid phase measurement, the samples were glued onto a metallic disc covered by a thin film of silicon cement, allowed to dry and immersed in the liquid cell. Subsequently, the tip and sample were brought together using the same approach as in tapping mode. AFM images were treated using the first-order flattening function and surface characterization methods provided by the Nanoscope III software.

The monolith was observed at both its external surface ("walls" of the monolith) and its inner layers represented at the extremities of the monolith. Since surface characteristics were very similar in both SEM and AFM for the monolith walls and extremities probably due to the highly crosslinked characteristics of the skeleton, the monolith was not sectioned using a microtome for investigation of inner layers properties as frequently used for characterization of biological materials [241].

4.3.2 Comparison of SEM and AFM images

In the present experiments, the SEM was comparable with AFM in terms of lateral (horizontal), or depth, information but AFM was superior in terms of quantitating information in the vertical dimension. The information collection strategies for these two techniques are significantly different even though both result in "images." SEM is effectively an imaging technique whereas AFM is actually a probing technique with the resulting information compiled and presented as an image. The intra- and inter-skeleton images obtained by both AFM and SEM were found to be highly reproducible in terms of pore and particle sizes.

From the SEM image in Figure 4–10 the macropores are readily visible but features smaller than about 50 nm (mesopores) are not resolved by the instrumentation. Surface charging due to the reticulated surface and thermal degradation of the polymer prevents further magnification that would allow features in the mesoscopic range to be imaged. Scanning electron microscopy, working on the principle of secondary electron emission, needs a conductive surface capable of emitting the secondary electrons. As explained before, the monolith surface had to be covered by a thin layer of gold to provide sufficient conductivity for imaging of the morphology. However, this coating method has to be performed on clean and dry surfaces to obtain a uniformly coated surface. In this particular case, we found that the optimal coating procedure required the use of high sputtering voltages (10 kV) in order to obtain a gold layer as homogeneous as possible while preventing thermal degradation of the monolith.

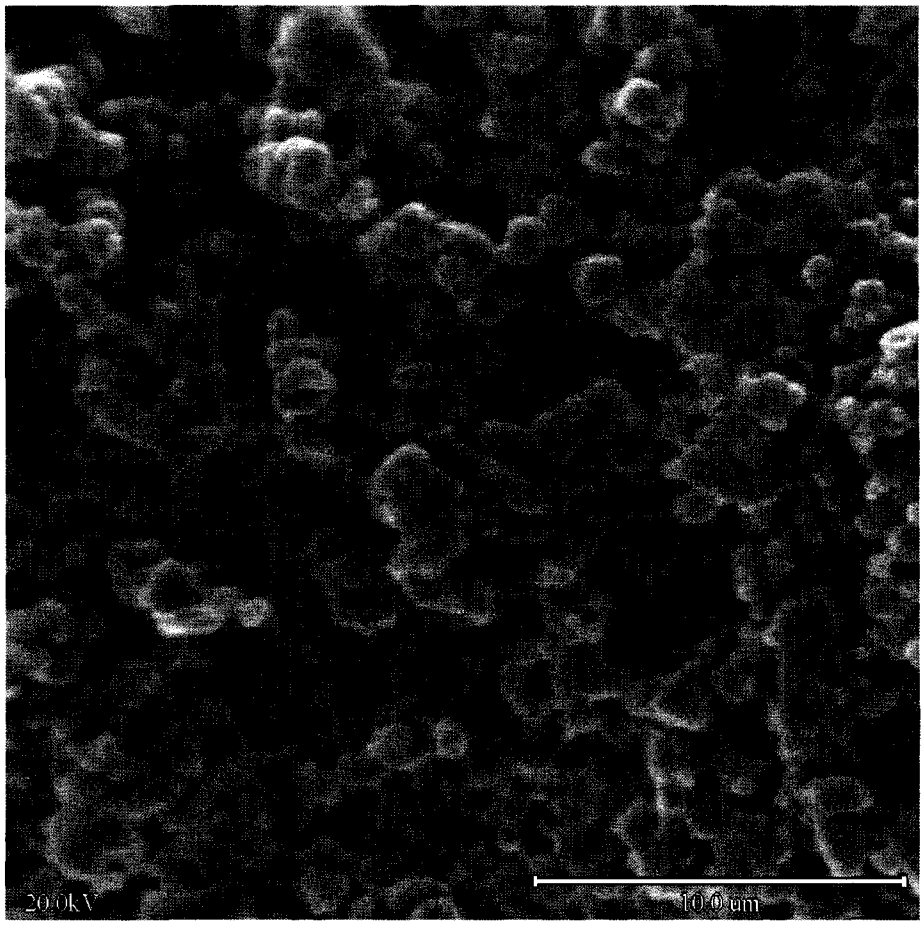

Figure 4–10: CEC Topographic images of a 25x25 μm^2 section of the monolith showed by SEM (detection voltage: 20.0 kV).

In the tapping mode AFM image shown in Figure 4–11, an area of the same size is imaged as in Figure 4–10 and the same general features are observable. Additional information about features in the mesoscopic range is present, but is not visible in the image shown, due to the 10 nm tip size and $\approx$ 50 nm step size attained on 25x25 μm^2 surfaces. This information is accessible at lower area of scan size and can be used to

compute surface areas and estimate pore sizes. Thus, the AFM image provides more detailed information about pore sizes at equivalent image sizes.

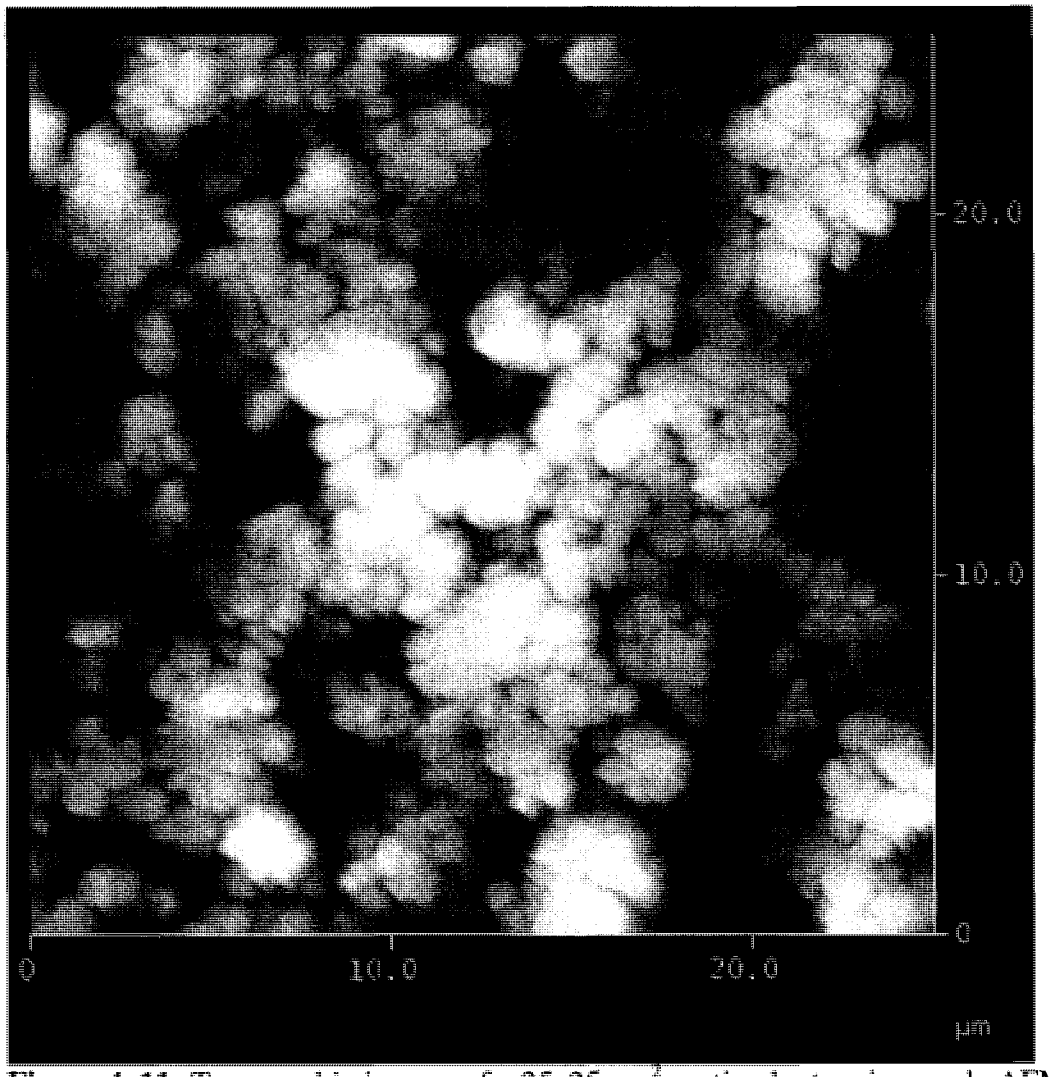

Figure 4–11: Topographic images of a 25x25 μm^2 section by tapping mode AFM in air.

Figure 4–12 shows a 5x5 μm^2 AFM image of the monolith collected in tapping mode. This image demonstrates that very subtle information is accessible by AFM at

scan sizes not accessible by SEM. In this case, AFM was able to show clearly defined pores as narrow as 25 nm on the monolith surface using a smaller scan size. Given that the tip was 10 nm, this is approximately the smallest pore size that can be imaged without biasing the resulting image. With even finer AFM tips, higher resolution should become possible.

Since AFM is based on the movement of a tip on a relatively rough surface, fine-tuning of the probing parameters is very important in order to obtain reproducible images and also to insure that the extrapolated topographic values extrapolated are representative of the convoluted surface. Nonetheless, while AFM pictures can illustrate very fine details of the convoluted structure, these fine tuning procedures are usually more time-consuming than the imaging methodology in SEM. AFM provides topographic images from which surface area, roughness and direct pore-sizes can be calculated. Since the surface of our photo-polymerized monolith is soft, drifting of the probes was observed at a drive amplitude (1V) and at relatively high scan rate (> 1.2 Hz) usually used for flatter surfaces. The scan rates also had to be lowered to values as low as 0.5 Hz to prevent dragging of the tip over the highly reticulated polymer surface. Drifting of the tip was observed as non-characterized scanning lines in the images and by particles being reoriented in the same direction as the movement of the AFM probes (from left to right on all AFM images). Using tapping mode causes less damage to the surface than contact mode because there is less interaction, fewer particles are dragged by the tip and the tip is better able to follow the surface features.

The AFM methodology was limited to pores with diameters larger than 100 Å due to the combination of the AFM probe angle at its tip and convoluted nature of the polymeric particles. This limitation is well illustrated by looking at an AFM tip and a topographic AFM image, as shown in Figure 4–12 (A &B) where the image of the surface is the result of the convolution between the spherical shape of particles and the pyramidal topographic features due to side contact with of the AFM tip during scanning.

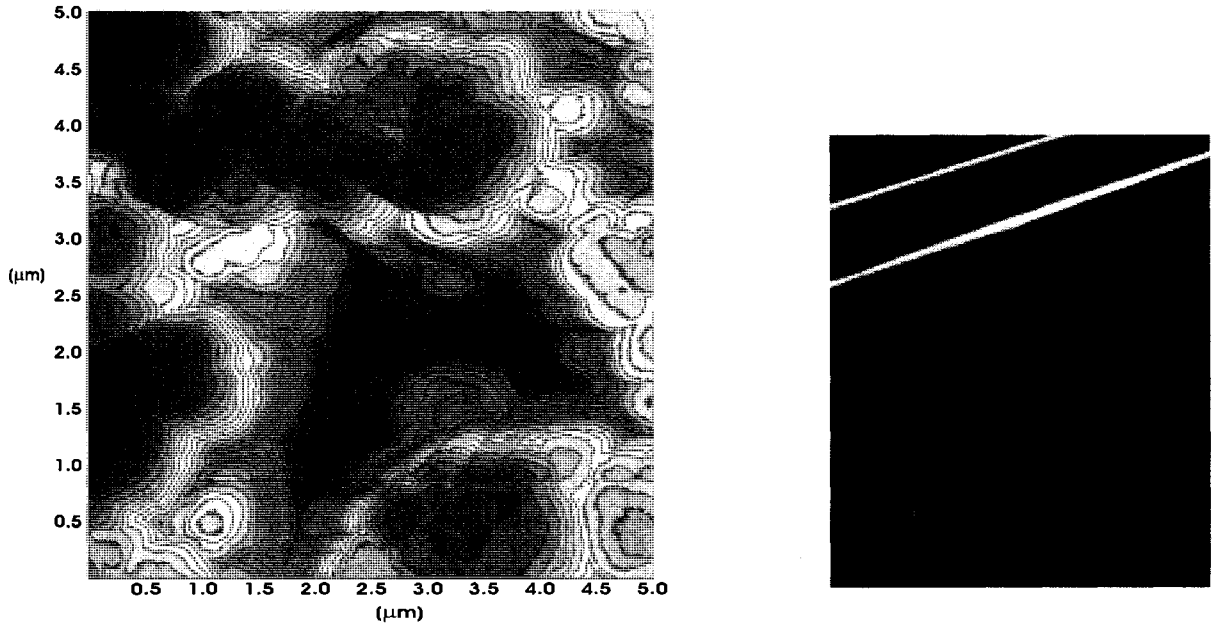

(A) (B)

Figure 4–12: (A) Contour plot of a 5x5 μm^2 monolith's section imaged by contact mode AFM in water, each contour line represents a 100 μm vertical step and (B) SEM photograph of an AFM probe where the triangular shape of the tip apex limits the actual accessible pore size due to side contact of the tip within very convoluted surfaces.

AFM also provides a direct method for the calculation of surface area and roughness. Therefore, primary measurements of root-mean-square roughness and surface area were carried out using the AFM data and the Nanoscope III software V5.12 as shown in Table 9. These measurements also demonstrated the necessity of using identical step sizes and scan rates to provide reproducible results as discussed by others [242]. Changes in step size alter the lateral resolution while changes in scan rate affect the magnitude of drifting artefacts in the data.

Table 9: Porosity parameters calculated from AFM imaging (25x25μm^2 section, N=3).

	AFM			
System	**Air**	**ACN**	**ACN / Water (50/50)**	**Water**
Channel size (μm)	2-3	2-3	2-3	3-5
Particle size (μm)	0.3-2	0.2-1.5	0.2-1.5	0.2-1.5
Porosity (%)	50	50	50	70
ISAD (%)	33 ± 2	32.1 ± 0.1	32.4 ± 0.3	43.8 ± 0.7
RMS (Rq) (nm)	727 ± 7	701 ± 7	710 ± 10	780 ± 10

ISAD (%): Image surface area difference between the projected area surface and the scanned surface area (related to total surface convolution).
Porosity (%): Estimated from the AFM images.
RMS (Rq): Root-mean-square roughness is the standard deviation of the surface height.

Artefacts present in AFM images associated with scanning of very rough surfaces inevitably lead to errors in calculation of a true surface area and roughness. As explained by Irene *et al.* [243], the AFM tip cannot faithfully reproduce the surface because the edges of the tip make contact before the apex. This distorts the image and introduces

artefacts. Such artefacts are usually represented by ladders of identical steepness surrounding very convoluted surfaces, such as those observed in Figure 4–12. Most experimentalists avoid such details by not including data under a certain z-axis cut-off. This approach approximates to an even greater extent the true surface area of a microscopically convoluted surface. The use of computational algorithms that could discard data associated with such false roughness characteristics would improve the accuracy of surface area calculations. Nonetheless, such mathematical treatment can distort the data and the values obtained would probably remain biased compared to the true surface area.

4.3.3 AFM liquid phase imaging of monolith

Liquid phase imaging is less susceptible to noise caused by non-uniformly dried surfaces and dust contamination than contact mode. Additionally, tapping mode has the advantage of using an oscillating probe which only contacts the surface at the end of its modulation cycle [244]. Therefore, this method minimizes frictional forces that are important sources of drifting artefacts (noise) on AFM images. Unfortunately, tapping mode imaging is not readily accomplished in liquid media because of unwanted disturbances in the liquid media that introduces noise on the measured signal. As such, we only used contact mode imaging in the liquid phase. The structures obtained from the wetted monolith showed that the volume of the particles that make up the monolith changed dramatically with solvent type as shown in Table 10. In water, the particles

contracted resulting in the expansion of the macropores by approximately a factor of 2, as shown in Figure 4–13. We were not capable of observing mesopores in the wetted polymer, probably because they had "contracted" to a size below the accessible limit of the 10 nm tip, *i.e.* in air they were roughly 25 nm and were observed. No clear swelling of the particles was observed in 50/50 (%v/v) acetonitrile/water and acetonitrile, *i.e.* under conditions expected when these polymers are used chromatographically. Imaging in very polar solvents such as THF was not possible due to quick evaporation of the solvent. Exposure to such solvents should lead to particle expansion and would probably also lead in a loss of macropore volume. Loss of macropore volume is explained by the polymer network expanding uniformly in all directions and closing off macropore spaces. Thus the volume of individual mesopores would expand by the same fraction that the particle expands. Additionally, some micropores would be sufficiently expanded to now be considered mesopores and successfully probed by the AFM tip.

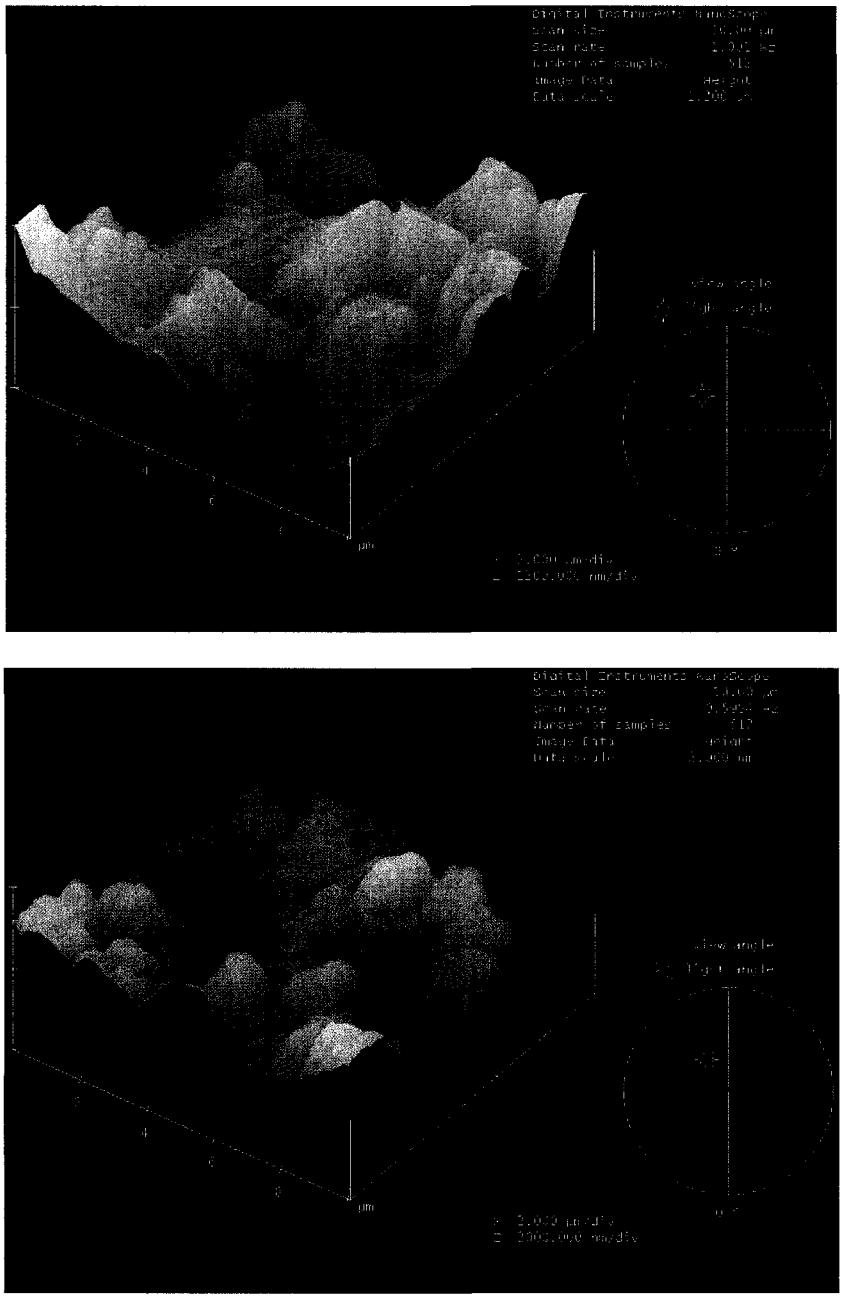

Figure 4–13: AFM images acquired in Millipore-grade water by contact mode (top image) and in air by tapping mode (bottom image).

The monolithic material studied here consists of a mixture of both hydrophobic (acrylate) and hydrophilic (sulfonate) functionalities. The results obtained by AFM could

indicate that the outer corpus of the monolithic beads shows a higher density of hydrophobic functionalities than hydrophilic ones as exposure to aqueous solutions resulted in shrinkage of the polymeric bead. This is corroborated by the chromatographic separation of polyaromatic hydrocarbons performed in our lab, on the same monolithic stationary phase that demonstrated a combination of both hydrophobic interactions and by dipole-induced dipole interactions exemplified by the influence of pH on the separation pattern. Nonetheless, such explanations would have to be confirmed with methods such as electron probe microanalysis [245] or the use of derivatized AFM tips to map the chemical properties of the skeleton through measurements of tip/surface interaction forces. Further studies aimed at this swelling effect under the influence of different solvents, such as mixed organic and aqueous buffer systems used in electrochromatography could demonstrate opposite trends due to different solvating properties and are the subject of further study.

4.3.4 BET Nitrogen adsorption Isotherm

Due to its ease of operation and high accuracy, adsorption and desorption isotherms of nitrogen on solid surfaces based on Brunauer-Emmett-Teller (BET) theory remains the preferred method for the physical characterization of solid substrates. This method allows calculation of the surface area and determination of the total pore volume as well as pore size distribution by deconvoluting the nitrogen adsorption and desorption isotherms. Details on the surface and internal pores are also obtained through shape analysis of the isotherms.

The accuracy of this technique depends on the "cleanliness" of the characterized surface, *i.e.* no solid impurities, residual solvents or adsorbed gasses present which might result in biased results due to a heterogeneous surface. In such cases, the ability of the probe gas molecules to adsorb and desorb from the surface will vary greatly affecting the pattern of the isotherms. Additionally, it is important that the probe gas has easy access to the bulk of the sample. For this reason, solid substrates are ground, homogenized and subjected to multiple washing and drying steps, usually at high temperature to eliminate all liquid trapped within the solid porous network, prior to their analysis. These physical procedures are not problematic for most inorganic materials such as particulate silica or activated carbon but these conditioning steps can significantly alter the physical properties of organic polymers.

Instead, a study was conducted using a different conditioning procedure as for the AFM imaging to demonstrate if similar results could be obtained between the two techniques without damaging the polymer. Since BET measurements require a higher amount of solid material, compared to AFM, polymerization of the monolith was achieved in an empty 1.5 mL cylindrical glass centrifuge tube and expelled through inversion of the tube followed by gentle centrifugation. As mentioned previously, all washing and drying steps were performed at room temperature.

Following these manipulations, the samples were placed within a sample tube and heated at 200 ^{o}C for 3 hours following a protocol established by the research laboratory operating the BET instrument. Upon cooling, the samples were subjected to analysis.

It was quickly noticed that none of the sample analyses provided meaningful data as both adsorption and desorption curves oscillated randomly during successive pressurization and depressurization of nitrogen. To explain these erratic data, measurements by differential scanning calorimetry (DSC) on dried monoliths were carried-out and are shown in Figure 4–14. The calorimetric data acquired through heating of the monolith demonstrated that two major changes occurred respectively at 100 °C and 160 °C. While the first inflection point was due to water desorption from the monolith, the second inflection temperature was thought to be the polymer critical temperature (T_c) at which crosslinked polymers lose their strength through improved flexibility of the polymer chain. In such cases, loss of monomer units can occur as well as irreversible denaturation of the polymer, which is a particularly important problem with a porous polymer. Based on these measurements, the conditioning temperature was lowered to 120°C and BET measurements reinitiated. Unfortunately, the same erratic BET isotherms were observed which were thought to be due to water remaining within the micropores (data not shown). Methanol washes were thus tried but did not yield improvement in BET isotherms. Due to the limited access to the BET instrumentation as well as the long workup, *i.e.* 2 to 3 days, for the production, conditioning and analysis of the required amount of samples, no further measurements were achieved.

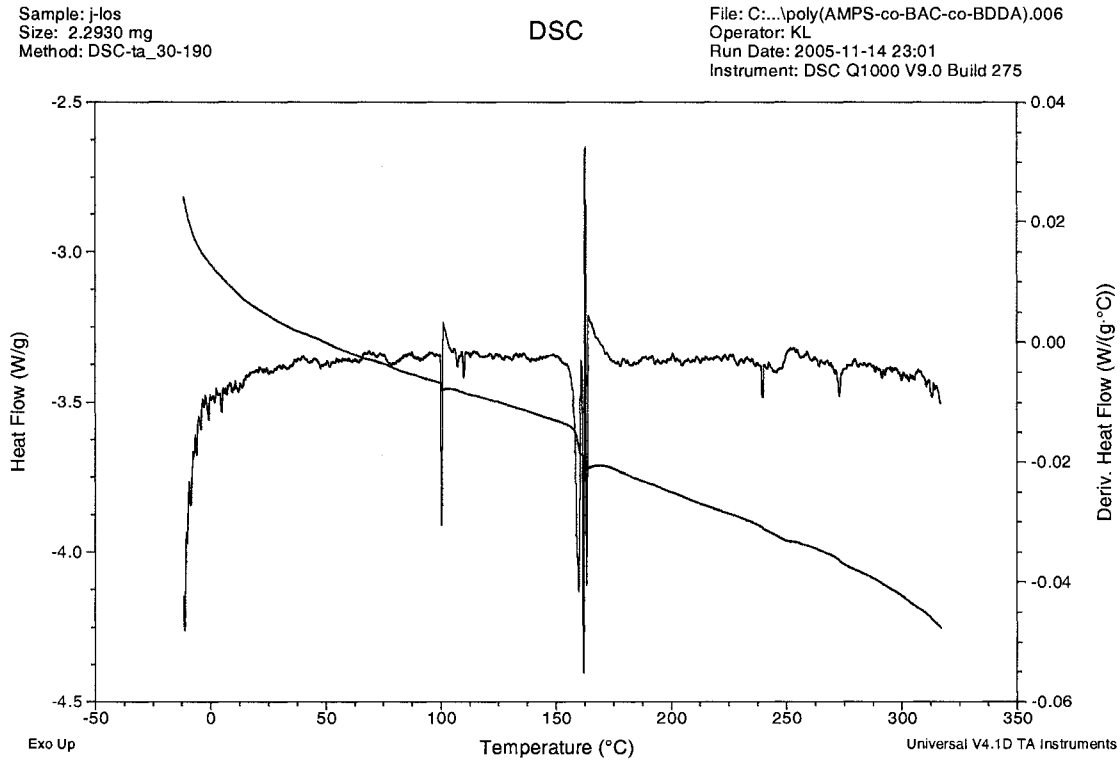

Figure 4–14: Differential scanning calorimetry of a dried poly(AMPS-co-BAC-co-BDDA) monolith performed on a Perkin Elmer JADE DSC (Waltham, MA).

4.3.5 Mercury Intrusion Porosimetry

Mercury intrusion porosimetry (MIP) theoretically avoids this specific issue due to its limitation to mesopore and macropore probing. As its name implies, MIP is based on high-pressure intrusion of mercury as a non-wetting inert liquid for the calculation of a solid pore diameter, total pore volume and surface area. Nevertheless, MIP is subject to some of the same limitations as BET, *i.e.* probed surfaces must be clean and free of liquid to allow accurate measurements. Normally, sample preparation for MIP requires the

samples to be washed and ground in order to homogenize the sample for measurement. However, the monolith samples were not ground in order to obtain information about the interstitial pore size or interparticle distance. Accordingly, the monolith samples were prepared as for BET measurements but they were not subjected to any heating before MIP analysis.

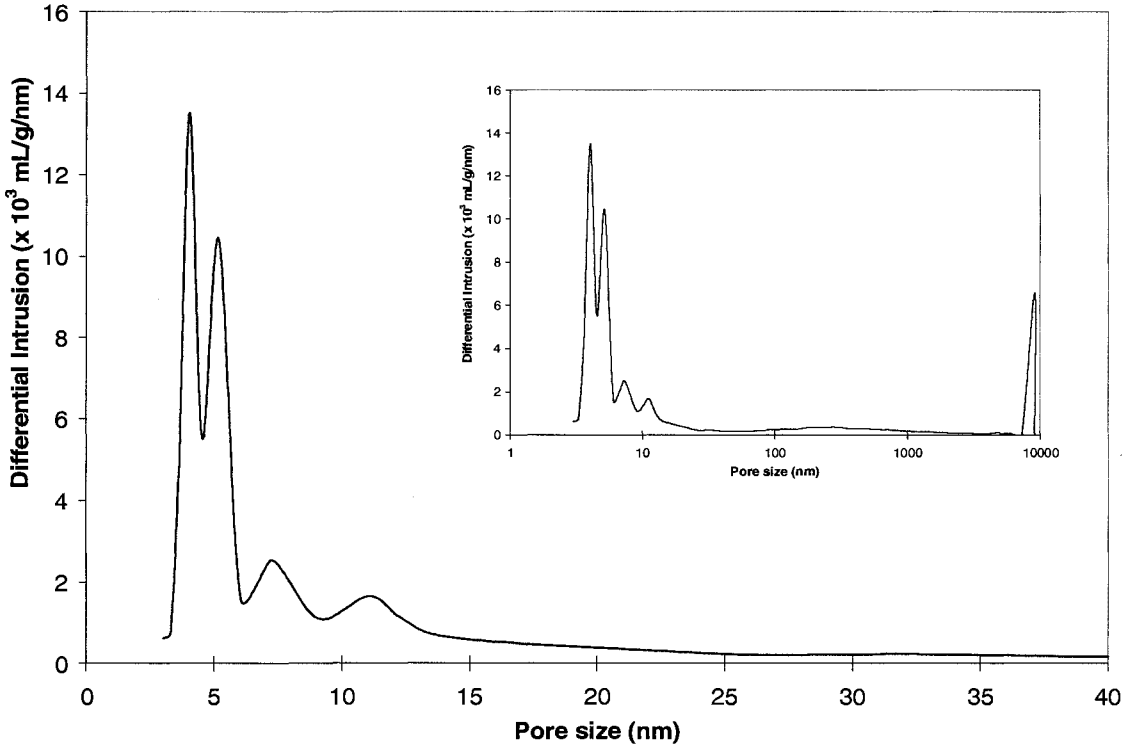

Figure 4–15: Pore size distribution of the poly(AMPS-co-BAC-co-BDDA) monolith by mercury intrusion porosimetry. Calculated porosity: 38.9%.

In Figure 4–15, the compiled intrusion data exhibited a bimodal pore size distribution with a majority of surface area situated within pore diameters smaller than 12 nm. A second, but minor, set of pores was also observed around 300 nm which could

account for a significant portion of the chromatographic interactions between the stationary phase and proteins.

4.3.6 Comparison of Surface and Porosity Values

While the techniques described and employed in the previous sections of this section were based on direct measurement of pore dimensions, distribution and general monolith structure, the overall porosity of the monolith can be assessed with non-destructive techniques. The total porosity (ε_{total}) of a porous media can be calculated according to the procedure published by Rathore *et al.* based on Archie's Law [155]. It relates ε_{total} to the conductivity ratio between a capillary containing monolith and an open capillary of the same length:

(Equation 14) $$\frac{\sigma_{packed}}{\sigma_{open}} = \varepsilon_{total}^{m}$$

Equation 14: Archie's Law; ε_{total} represents the total porosity of the monolith (dimensionless), σ_{packed} is the conductivity of a monolithic column in $A*V^{-1}*m^{-1}$, σ_{open} refers to the conductivity of an open section capillary $A*V^{-1}*m^{-1}$ and m is an empirical constant that is usually approximated as 1.5 for media with porosities higher than 0.2 [155].

The total porosity values calculated in Table 10 with this technique are similar to the ones obtained by AFM imaging using the same solvent system, as shown in Table 9. However, it is important to mention that Archie's law measures the entire porosity of a porous media, that includes the porosity of the outer corpus as well as the porosity associated with flow-through pores within the stationary phase particles. These latter

pores are not fully accessible by AFM imaging and could potentially lead to a bias between the AFM and the conductivity porosity values. The results in Table 10 do not indicate a significant difference between the AFM and the conductivity measurements in 50/50 (%v/v) acetonitrile/water.

Table 10: Porosity parameters calculated from conductivity measurements.

	Conductivity (ε_{total})	
System	**ACN / 5mM borate pH 10.0 (50/50)**	**5mM borate pH 10.0**
Porosity (%)	51 ± 2	68 ± 4

Since the BET measurements, a robust technique, did not prove successful, it was not possible to determine if the computed data (Table 9) were consistent with BET. Still, the data obtained should remain comparative and be used as semi-qualitative values. Even with the specific limitations of AFM, pore diameters exceeding 250 Å were observed with both MIP and AFM. Similarly, calculation of the monolith porosity by MIP (38.9%) corroborated the value approximated by AFM (~50%). AFM imaging of the monolith in conditions similar to those required by another destructive technique, MIP, resulted in similar porosity values but without destruction of the monolithic stationary phase.

With a simple AFM methodology, we found by direct observation that the same material exhibits mesopores in the nanometer range while SEM could not resolve these features. Thus AFM was capable of demonstrating the morphological differences between wet and dried monolithic materials that are not possible by other imaging

methods at micrometer resolution. With the AFM developed methodology, it was shown that the type of solvent has a dramatic effect on the macropore volume and is in agreement with flow measurements. The observations made with regard to BET analysis of this monolithic stationary phase indicate that special attention has to be directed in order to prevent alteration of the monolith which could potentially result in biased pore information.

Further experiments should aim at improving the accuracy of roughness values obtained from AFM images and following calculations. Also, AFM characterization of other monolithic surfaces, or other types of surfaces, presenting similar convoluted characteristics, might help in developing a better understanding of the swelling properties of these monolithic stationary phases.

Chapter 5

Modification of Monolith Chromatographic Properties

Initially driven by the input of polymer chemists who developed an extensive knowledge of the factors affecting the morphological properties of monolithic stationary phases, the CEC literature is rich in publications investigating specific relationships between polymerization conditions and the resulting monolith properties [246, 247, 248].

The complex interplay between morphological and (electro)chromatographic properties and how they are affected by tuning the polymerization conditions is a research thesis on its own and a complete investigation is well beyond the scope of this thesis. Instead this section will briefly report the author's work demonstrating the limitations of modification of the polymerization conditions, in particular the temperature and porogenic solvent ratio. An interesting alternative to this approach, namely copolymer grafting using photoinitiation, will be described in the last section of this chapter and compared to the classic approach.

5.1 Modification of Polymerization Conditions

Polymerization conditions play a symbiotic role in the formation and growth of the monolith. While modification of the monomers changes the type and/or extent of chromatographic interactions, the average particle and pore sizes are likely also affected due to the difference in the solubility of the growing polymer in the porogenic solvent

system. Polymerization temperature is an easy to investigate critical polymerization factor related not only to particle and pore size due to its influence on polymer solubility but also on solubility of the individual monomers resulting in slightly different chromatographic properties.

5.1.1 Polymerization Temperature

Svec and Fréchet [136] used BET and MIP measurements to carry-out one of the first proper investigations of morphological properties of a macroporous polymer as a function of temperature. They discovered that an increase of temperature responded by a decline in pore size and a corresponding increase in surface area of their model monolith, poly(glycidyl methacrylate-co-ethylene dimethacrylate) synthesized in bulk format.

A study similar to that of Svec and Fréchet was performed using the present monolith; however, the *in-situ* polymerizations were achieved in a filled capillary rather than in bulk to avoid the potential bias of the bulk. Temperature control was accomplished by using a Chipmaster SMD-6000 thermostating unit (APE, Key Largo, FL, USA).

As depicted in Figure 5–1, the present results showed an increase in EOF with temperature. However, an increase in EOF could result from multiple factors such as an increase in the sulfonate surface density, change in porosity or a change in pore size distribution that leads to reduction of electric double-overlap occurrence. A very straightforward approach to measure porosity was to compare the total current obtained

from each individual monolith as a measure of the electrokinetic porosity as explained in the previous chapter.

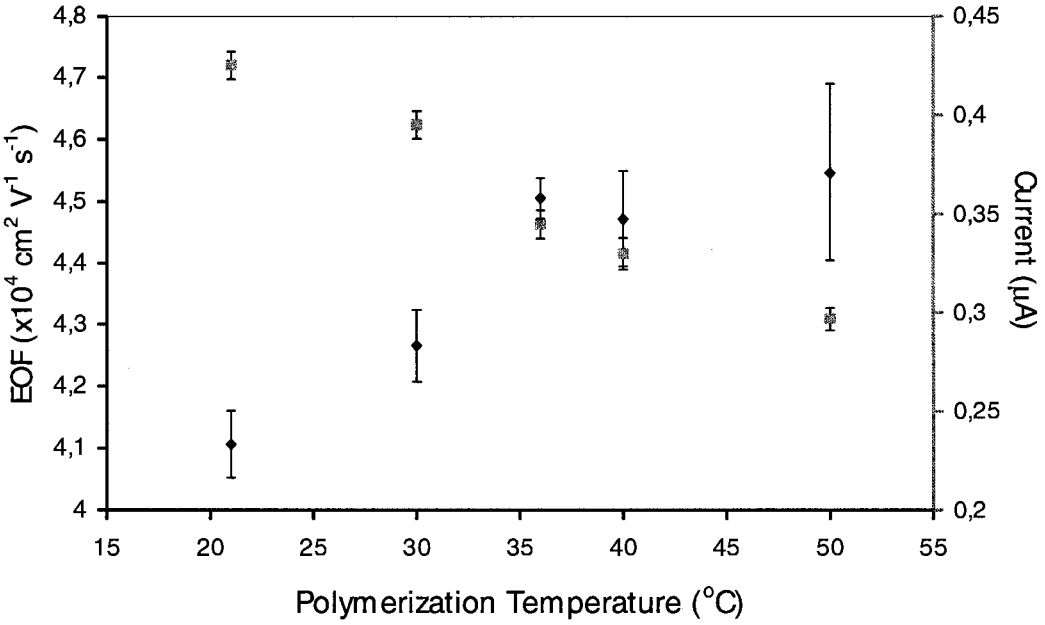

Figure 5–1: Relationship between polymerization temperature and EOF (circles) for the *in-situ* polymerized poly(AMPS-co-BAC-co-BDDA) with measured current (squares) upon initial polymer conditioning. EOF measured in 50/50 (%v/v) ACN/5 mM borate buffer pH 10.0. The monolith segments were 23 cm long with a total length of 40.5 cm and an internal I.D. of 100 µm.

The current measurements detailed in Figure 5–1, performed after initial polymer conditioning, revealed a decline in total porosity, measured as the electrokinetic porosity, of the monolithic bed with temperature. Since the electrokinetic porosity is the summation of both interstitial (flow-through) and intraparticle porosity, it is not possible to determine if the loss in the monolith porosity corresponds to a decrease in both interstitial and intraparticle porosity from this data. There was no observable decrease in

interparticle distances by SEM imaging (data not shown) which leads to the conclusion that the loss of porosity comes from changes in intraparticle porosity. This implies that there should be a decrease in either, or both, number and size of pores in the mesopore range and that columns prepared at lower temperatures may provide greater access to proteins whereas columns prepared at higher temperatures are better suited to smaller molecules. In fact, as explained by Svec and Fréchet [136], polymerization kinetics are usually accelerated at higher temperatures which favours the formation of higher numbers of smaller polymerization nuclei resulting in smaller pores and higher surface area, as confirmed experimentally.

Even though no further investigations of the (electro)chromatographic property changes with temperature were carried-out, it was demonstrated that slight modifications of the physical properties achieved through tuning of the temperature also alter other properties of the monolithic stationary phase, as shown here for the EOF.

5.1.2 Nature and Concentration of Monomers

While temperature enables the easy modification of a monolith morphology, adjustment of its monomer nature and concentration theoretically fosters the creation of various chromatographically and morphologically different stationary phases. For example, the hydrophobicity of the monolith can be increased through replacement by, or addition of, more hydrophobic monomers. This was achieved here via the gradual substitution of BAC, a C4 monomer, for lauryl acrylate (LAC) a significantly more

hydrophobic monomer due to its longer alkyl chain (C12) while the solvent system was kept constant.

As shown in Figure 5–2, addition of LAC correlated with a decrease in EOF together with an increase in the overall porosity (and loss of surface area) reflected in the current measurements.

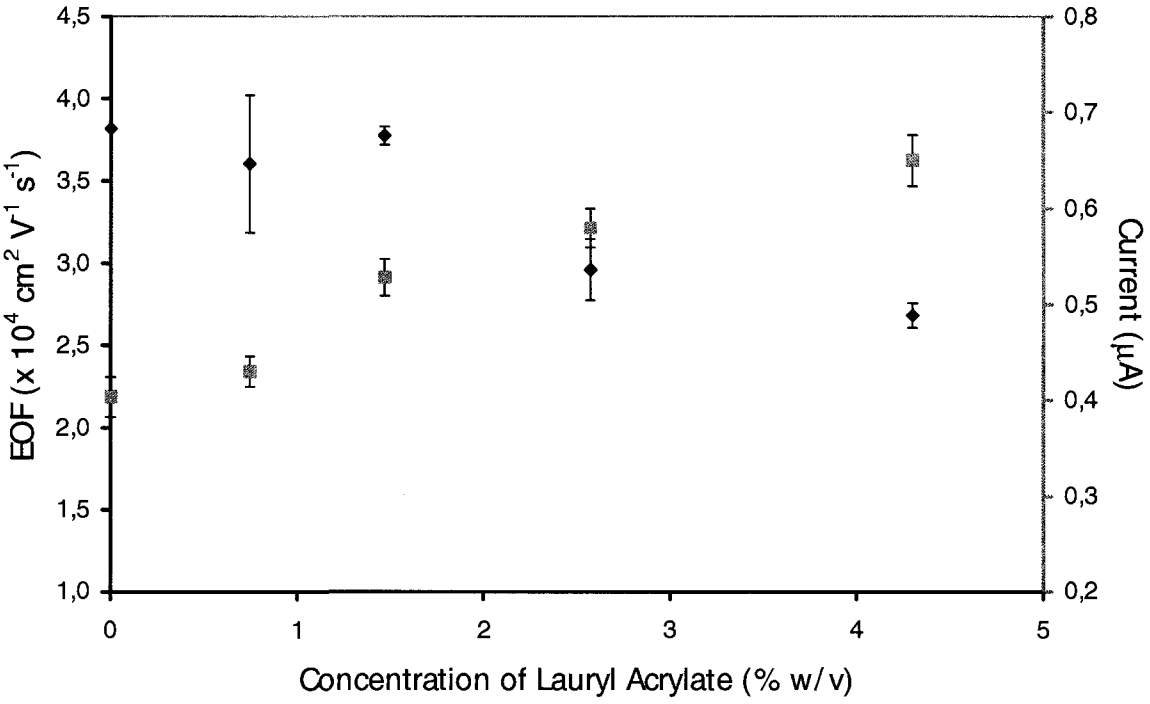

Figure 5–2: Relationship between EOF (diamonds) and measured current (squares) as a function of concentration of LAC in the polymerization mixture for the *in-situ* polymerized poly(AMPS-co-BAC/LAC-co-BDDA). The total concentration of BAC and LAC was kept constant (20 %w/v). EOF measured in 50/50 (%v/v) ACN/5 mM borate buffer pH 10.0. The monolith segments were 23 cm long with a total length of 38 cm and an internal I.D. of 100 µm.

At total LAC concentrations above 7% (w/v), polymerization was still observed but current breakdown resulted in the loss of all monoliths. Due to phase separation from the porogenic solvent prior to polymerization at LAC concentration above 12% (w/v) no polymerization was observed. An important point highlighted by Figure 5–2 is that the modification of the monomeric content resulted in changes of the same magnitude as the temperature on both EOF and current, thus monolith porosity. This could theoretically give a researcher the ability to compensate for variations in the monolith morphological properties via further adjustment of the polymerization temperature. However, to confirm this hypothesis, one would have to characterize the variations in dead-end and flow-through pores.

As expected, the gradual increase in monomer hydrophobicity also turned out to affect significantly the extent of RP interactions with naphthalene, a neutral hydrophobic molecule. In order to represent the strength of chromatographic interaction between the analyte and the stationary phase, the capacity factor (k') for naphthalene was measured for monoliths with increasing initial LAC content. First, as the EOF strength decreased with LAC concentration, longer retention times were required to elute naphthalene out of the column. From Figure 5–3, there is an increase in capacity factor but it is not linear with increasing polymer hydrophobicity. This is likely due to the loss in porosity with increasing LAC concentration which should correlate with the loss in surface area.

Alteration of the monomer nature and concentration predictably resulted in morphological variations of the monolith as well as of its EOF velocity as previously

demonstrated by polymerization temperature. Adjustment of LAC content resulted in a significant modification of the monolith (electro)chromatographic properties monitored with naphthalene, while not assessed for modification of the polymerization temperature. Thus, fine optimization of the monomer nature and concentration would be required to adjust an existing monolith in order to obtain desired physical and chemical properties.

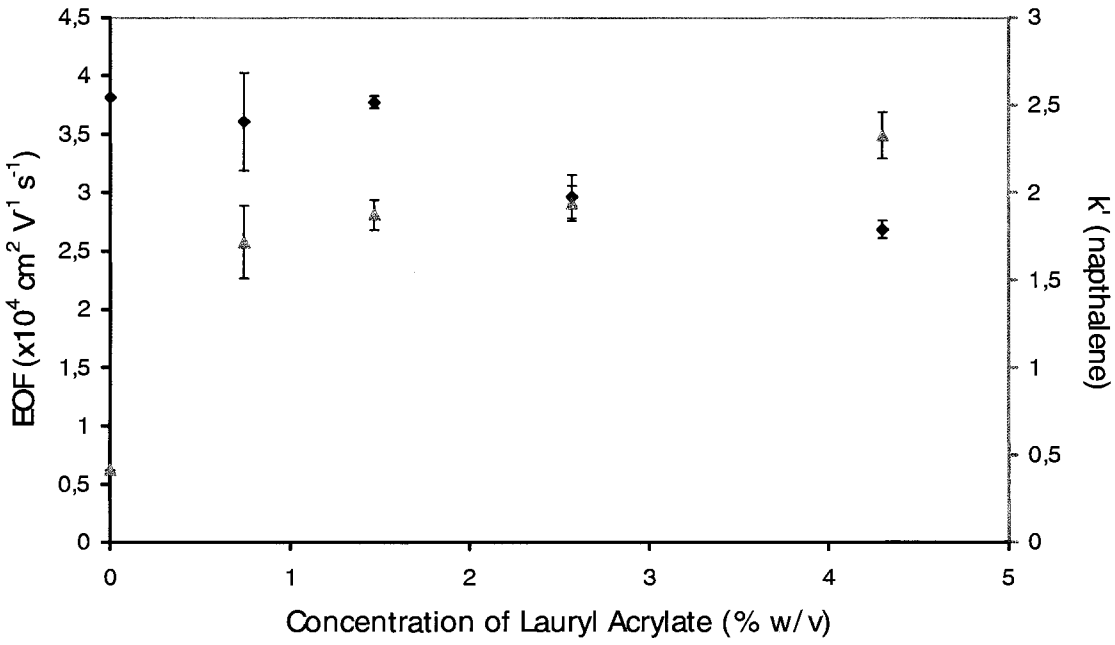

Figure 5–3 : Relationship between naphthalene retention, expressed as its capacity factor ($k'_{napthalene}$) (triangles), EOF (diamonds) and concentration of LAC in the polymerization mixture for the *in-situ* polymerized poly(AMPS-co-BAC/LAC-co-BDDA). Separation at 10 kV, room temperature, mobile phase consisted of 80/20 (%v/v) ACN/5 mM borate buffer pH 10.0. The monolith segments were 23 cm long with a total length of 38 cm and an internal I.D. of 100 μm.

5.1.3 Porogenic Solvent

From the two previous sections, adjustments of temperature and monomer concentration/nature revealed their significant potential to modify a monolith's

properties. One final parameter to explore is the porogenic solvent since this parameter is also critical in a monolith's properties. The solubility of the polymer in the porogenic solvent dictates the pore size and particle size. As the porogenic solvent does not participate directly in the polymerization process, it occupies a fixed volume that cannot be occupied by the newly formed polymer. Thus, solvent volume becomes a valuable tool for adjusting the overall porosity of a monolith, especially for *in-situ* polymerization due to the constrained environment compared to classic bulk polymerization. This parameter is not investigated in most publications because most new monoliths are fabricated through bulk, in-solution polymerization, or in larger cells, to meet the needs of larger amounts of polymer for destructive morphological analyses. Nevertheless, adjustment of the porogenic solvent nature and concentration has proven very successful in modifying the *in-situ* fabricated morphological properties [246].

During polymerization porogens do not take part in the polymerization reaction scheme but only plays a role in solubilization and precipitation of the forming polymer. This implies that in the *in-situ* method, the total pore volume is usually very close to the initial porogen volume. For this reason, the amount of porogenic solvent plays an important role in fixing the *in-situ* polymer void volume. To demonstrate this, the volume of porogenic solvent was modified and EOF measurement and SEM images of the resulting monoliths taken.

The SEM photographs in Figure 5–4 suggest that particle size were not affected to a great extent by variation in the amount of porogen. However, the space between

particle agglomerates, the interstitial or flow-through pore size, increased with the volume occupied by the porogen. This is confirmed by the current measurements where the monolith formed at 0.9 mL porogen yielded the lowest current indicative of a lower overall porosity and a visually very dense polymeric packing. Variation in porosity was most probably caused by an increase in both micro- and macroscopic porosity. Once again, the use of destructive characterization technique could most likely provide sufficient information to answer this question.

As demonstrated by modification of polymerization temperature, monomer nature and concentration as well as of the porogenic solvent volume, the outcome from any single modification is difficult to predict due to the complex interplay between solubility, polymer and condensation kinetics. This inherent complexity thus requires optimization for individual polymer systems to obtain the desired properties. Also evident is that extensive characterization of the physical and chemical properties are required in order to accurately determine the effects of modification of polymerization conditions.

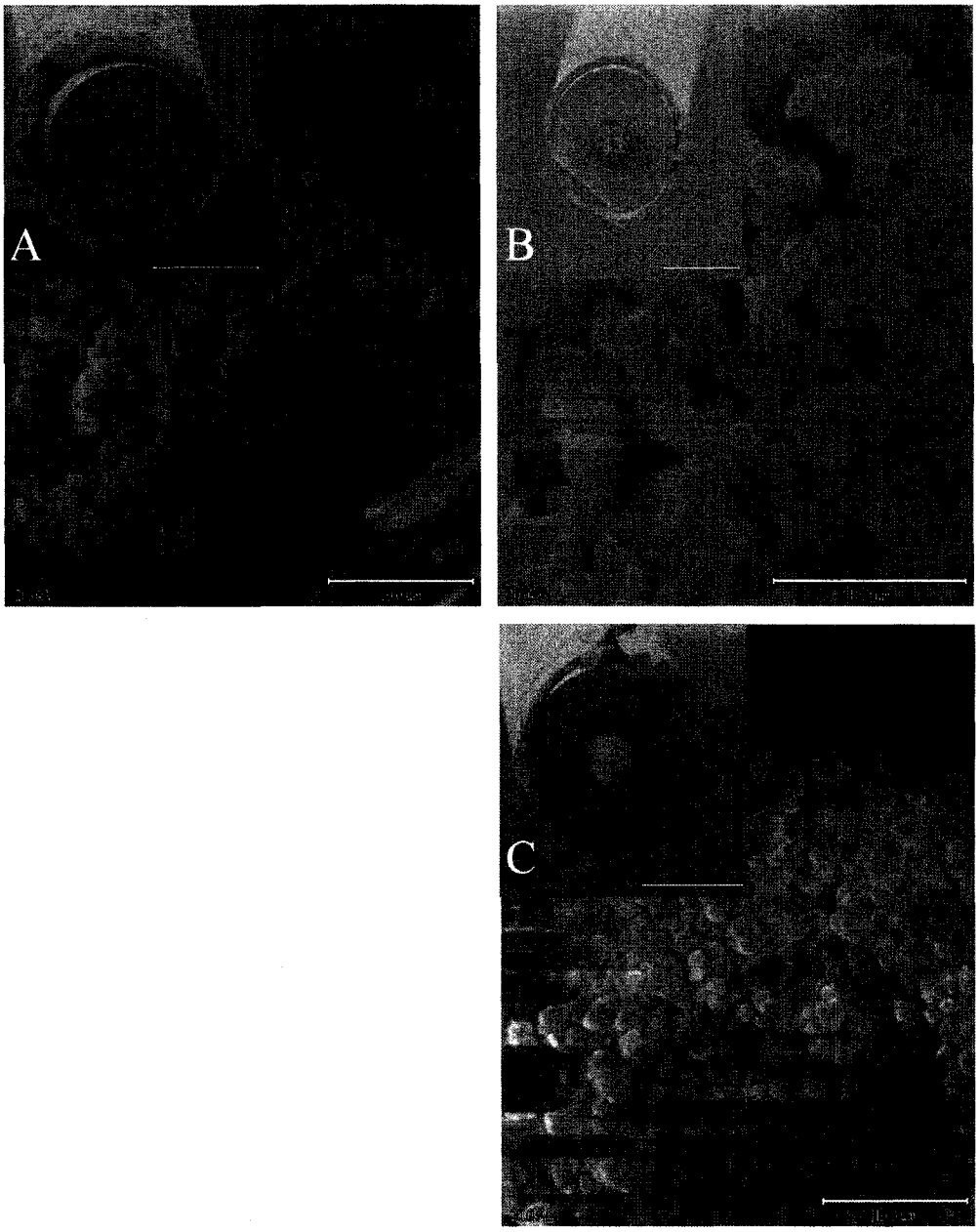

Figure 5–4 : SEM photographs of the poly(AMPS-co-BAC-co-BDDA) with various volumes of porogenic solvent (60/20/20 (%v/v) mixture of acetonitrile/ethanol/5 mM pH 7.0 phosphate) in the initial polymerization mixture. Porogenic solvent (Section 2.3) and magnification of inner/larger SEM images: (A) 1.1 mL, 250X/4000X, (B) 1.0 mL, 200X/5000X, (C) 0.9 mL, 250X/4000X. Current measured in 50/50 (%v/v) ACN/5 mM borate buffer pH 10.0: (A) 0.57 μA, (B) 0.40 μA, (C) 0.37 μA. The monolith segments were 23 cm long with a total length of 38 cm and an internal I.D. of 100 μm.

In order to avoid the complexity associated with optimization of individual polymerization conditions, adjustment of a monolithic stationary phase's (electro)chromatographic properties could be achieved by first creating a monolith backbone followed by its coating with a desirable moiety. With appropriate selection of the coating conditions, such a process will maintain the monolith physical integrity while only altering the chemical properties at its surface.

5.2 Preliminary Investigation of Copolymer Grafting

Copolymer grafting is a polymer modification technique that has been used extensively in commercial polymer production to introduce new functional groups that enable the tuning of the final polymer properties [249,250,251]. Recognized as a promising alternative for the easy *in-situ* modification of monolithic stationary phases, initial experiments were required to determine if the present polymer could be subjected to copolymer grafting. At the same time this study was started, Hilder *et al.* [144] published the results of a similar study but for the shielding of an hydrophobic polymer, poly(butyl acrylate-co-ethylene dimethacrylate), through sequential grafting of AMPS and BAC.

The model monolith, poly(AMPS-co-BAC-co-BDDA), was subjected to photomediated copolymer grafting of AMPS. This initial study was designed to determine the influence of grafting time on the resulting EOF and to assess wether there was an EOF "plateau" phenomenon associated with saturation of the monolith surface

with AMPS functionalities. As shown in Figure 5–5, increasing grafting duration surprisingly yielded a reduction in EOF. In fact, in a previous attempt to increase EOF with the same model monolith through an increase in the amount of AMPS during polymerization, Bandilla [16] observed a plateau region while similar studies with other monoliths have resulted in constant increase in EOF [6]. This phenomenon was thought to be caused either by the incomplete integration of increasing amount of AMPS in the polymer during formation or by a change in the monolith porosity and/or tortuosity resulting in longer elution time of the unretained marker.

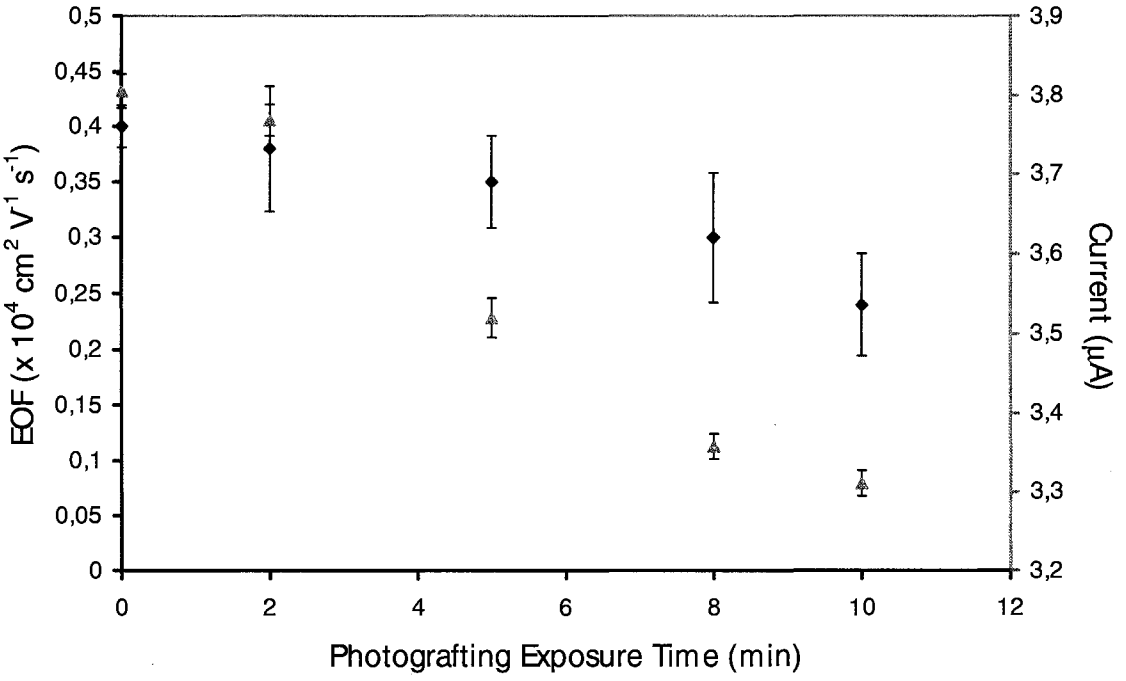

Figure 5–5: Relationship between EOF and photografting duration of AMPS on the *in-situ* polymerized poly(AMPS-co-BAC-co-BDDA) with measured current after individual grafting duration Each point represents three monoliths. EOF measured using same conditions as previous figures.

Bearing in mind that the base polymer already contains AMPS and its EOF was already large, the addition of AMPS via photographing did not increase the EOF since it was already close to its maximum value. In Hilder's report, an EOF increase was observed for a monolith characterized with low intitial EOF [144]. Given that the base polymer has extensive micropore volume (Figure 4–15), increasing surface sulfonate density likely resulted in increased electrical double-layer overlap and/or plugging of the smaller pores. This hypothesis is corroborated by the decrease in current and overall polymer porosity. Ideally, the formation of an AMPS monolayer would be desirable as it would have minimum impact on the monolith porosity. However, during the photographing process AMPS oligomers can be formed in solution and react with the monolith surface. The data presented in Figure 5–5 suggest that AMPS photografting caused the formation of multilayers on the monolith surface.

Intrigued by these results, photografting duration was later extended to 30 minutes to confirm this hypothesis but all monoliths failed due to bubble formation and current breakdown which might have resulted from very low total porosity thus high electrical resistance. This suggested that the actual AMPS photografting scheme resulted mostly in plugging of the pore rather than a uniform surface coating process as expected.

The main goal of this preliminary investigation was not the determination of the electrochromatographic properties of the monolith as a function of AMPS grafting but was the demonstration of the feasibility of photografting using this monolith, as such separations of model analytes were not attempted. It is clear that photografting of AMPS

resulted in considerable modification of the monolith EOF without requiring complex redesign of the polymer as required by the classical approach. It is expected that in conditions designed to favour formation of a graft monomer monolayer on the monolith surface, *i.e.* shorter grafting duration, lower concentration of graft monomer and reduced lamp intensity, minor reduction in the overall porosity could be obtained. Ideally, this would enable adjustment of the monolith surface chemistry without altering its overall physical properties.

In addition to confirming that grafting is possible using this monolith, this study has shown that the grafting process resulted in reproducible monoliths based on variability in the EOF. It has been reported that the grafting process is susceptible to various experimental conditions, including monomer purity [252,253] highlighting the need for careful control of experimental variables. To minimize variability, particular attention was given to control of the initial polymerization and grafting conditions (grafting temperature, duration, concentration of monomer and photoinitiator). Exploiting this process over a long-term would require additional characterization of the grafting process and the relevant experimental variables such as monomer purity, solvents and temperature.

From the results presented in this section, one will easily understand the complex interplay of individual experimental factors during the polymerization process individually or through a synergistic mechanism. Both the chemical and morphological properties of a monolith change simultaneously and not necessarily in an easily predicted

manner. An increase in temperature yielded a 1.5-fold difference in electrokinetic porosity but did not obviously modify the monolith's chemical properties. Using LAC significantly changed the both the physical properties and its electrochromatographic characteristics. In contrast to modifying the polymerization process, grafting unveiled a new set of possibilities that avoid the complexity of multifactorial optimizations. Further work is required optimize and provide appropriate characterization on the actual porous properties of the monolith. Copolymer grafting appears as a promising method for tuning a monolith surface while being able to establish its physical properties at the time of polymerization. As was demonstrated, copolymer grafting can be achieved with the poly(AMPS-co-BAC-co-BDDA) model monolith and will be extended in the following chapters to more complex applications.

Chapter 6

An Electrochromatographically Active Proteolytic Reactor: Direct and Linker-Mediated Enzyme Immobilization

The inherent enhanced mass transfer kinetics and high pH stability of monoliths have attracted attention not only for their role as (electro)chromatographic stationary phases but also as supports for wide classes of biologically mediated reactions and biomolecular recognition for chromatographic applications. Biologically mediated reactions are designated as enzymatically driven reactions, or molecular mechanisms, while biomolecular recognition in chromatography refers to the selective affinity of immobilized biological substrates toward specific molecular targets.

The potential benefits of immobilized enzymes have been noted in the literature [254,255]. The greatest interest has been, and still is, directed towards the potential of immobilized proteolytic enzymes for proteomic applications. The primary advantages are simplification over and an increase in sample-throughput compared to conventional in-solution digestion. In comparison to manual in-solution procedures, proteolytic reactors are expected to reduce autolytic peptides that are specifically important in the case of dilute protein solutions and for identification of minor proteins. If proper conditioning, operating and storage conditions are used, reactors also have the advantage of being reusable. Moreover, their use in a direct in-line approach prior to and/or after chromatographic differentiation, opens a new door towards high efficiency, high sample-throughput proteomic investigations.

Most proteolytic enzymes, such as trypsin (24 kDa), are large biomacromolecules that upon immobilization on solid substrates can lose much of their activity as a result of steric hindrance *in the* active site. Loss of activity can also be caused by poor orientation of the immobilized enzyme preventing *access to* the active site. Proximity to the supporting surface can also inhibit activity through non-specific interactions with the enzyme and/or substrate, especially in the case of hydrophobic support surfaces [256]. In such cases, different approaches can reduce non-desirable interactions. One very common approach relies on the introduction of a molecular linker arm of a defined length between the surface and the enzyme [257]. The linker increases enzyme mobility and reduces surface effects by moving the enzyme away from the surface. Alternatively, or together with the linker, deactivation of the surface by introduction of hydrophilic moieties, such a polyethylene glycol, can also reduce the extent of non-specific interactions.

The work reported in this chapter was the result of discussions with Dr. Karen C. Waldron from Université de Montréal who has developed enzymatic reactors on controlled-pore glass beads [188]. An extended research project with three undergraduate students (Anda Vintiloiu, Navneet Kaur and Bobby Boursiquot) under the supervision of the author was set up with Dr. Waldron. In parallel to this project, a somewhat similar reactor was developed using a photografting scheme to take advantage of the photografting methods detailed in previous chapters. The main goal of these

projects was to design an "easy-to-manufacture" monolith with a proteolytically-active surface to be used as a microreactor for high-throughput proteomic investigations.

6.1 Fabrication of a Proteolytically-Active Monolith

The fabrication and characterization of the modified monolith will be described using both direct immobilization of trypsin and immobilization mediated with a novel linker, N-succinimidyl-S-acethylthioacetate (SATA). Subsequently, both reactors will be compared for their proteolytic conversion efficiency while placing an emphasis on the overall fabrication reproducibility and ease of use.

6.1.1 Fabrication of Two Monolithic Proteolytic Reactors

The basic monolithic stationary phase employed for this study consisted of a poly(glycidyl methacrylate-co-trimethylolpropane trimethacrylate) previously described in the literature [258]. The advantage of this monolith resides in the reactivity of the epoxide ring incorporated within the polymeric backbone through the glycidyl methacrylate monomer. Preparation of this monolith is described in Section 2.3.

Photopolymerization resulted in the formation of a rigid porous randomly branched poly(GMA-co-TRIM) monolith, with a significantly higher porosity as depicted in Figure 6–1 by SEM than the poly(AMPS-co-BAC-co-BDDA) monolith.

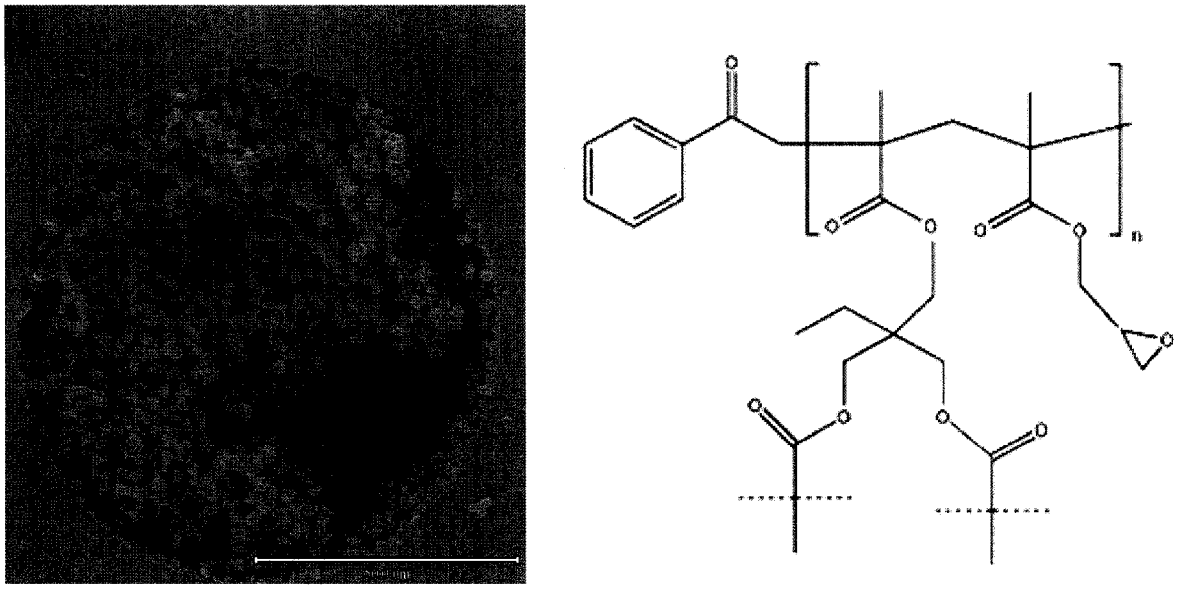

Figure 6–1 : SEM image of the poly(GMA-co-TRIM) monolith (50 µm scale) and its molecular structure consisting of randomly branched polymer with alternating monomeric units.

The monolith larger particle size (2-3 µm) and interparticle distance resulted in higher permeability that enabled manual pressure conditioning using a syringe and appropriate fittings (rather than the bomb).

Derivatization of this highly permeable monolith was achieved using either direct trypsin immobilization or via prior functionalization of the monolith surface with the SATA linker (Section 2.6.2). Figure 6–2 shows these two different immobilization reaction schemes.

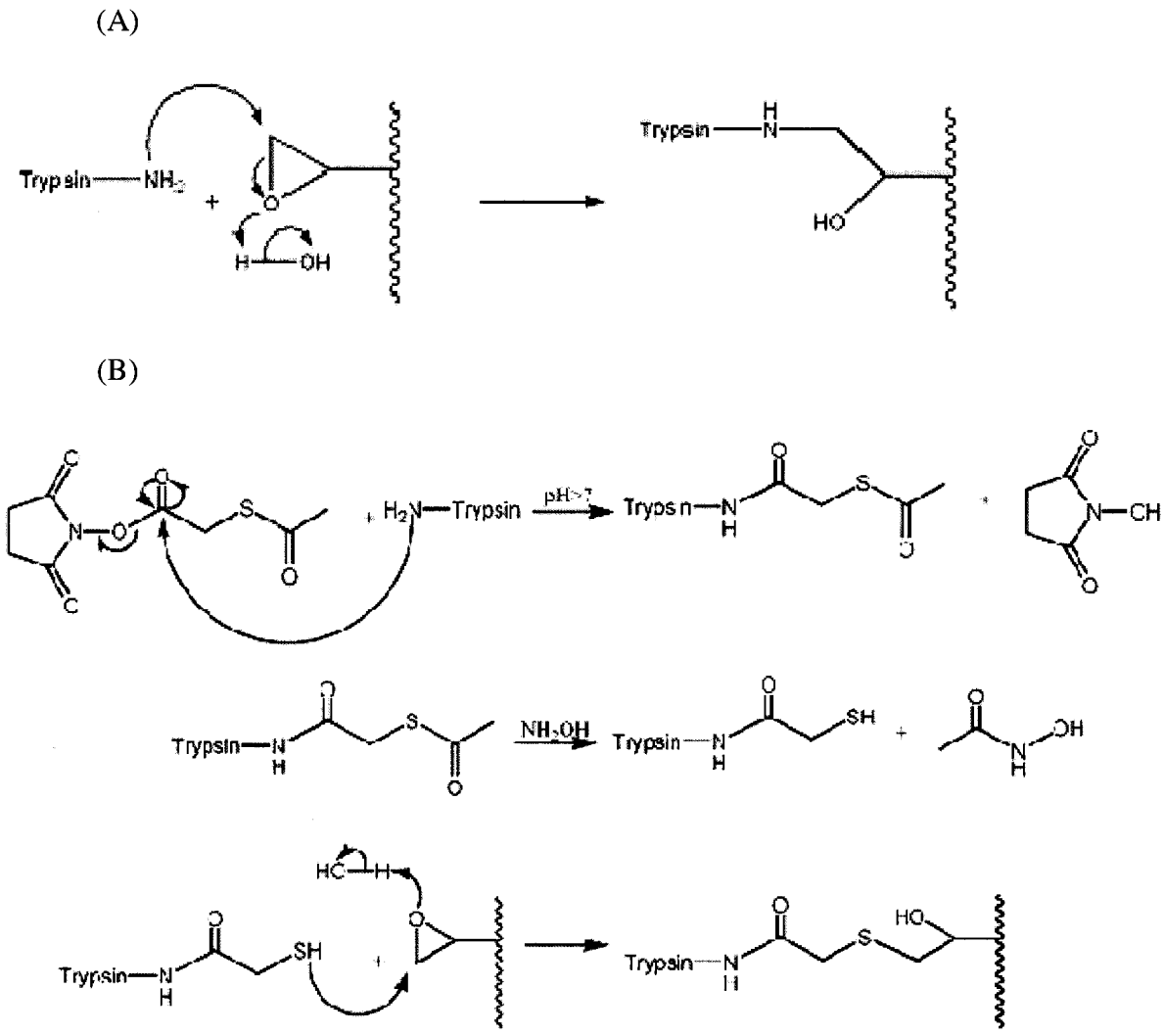

Figure 6–2 : Trypsin immobilization via (A) direct reaction with the surface and (B) SATA-mediated derivatization.

Derivatization with the SATA linker gave two important advantages over direct trypsin immobilization. First, SATA introduced a sulfhydryl (SH) moiety on the trypsin that is a stronger nucleophile than primary amines, and can theoretically increase reactivity with the oxirane (epoxide) ring [259]. Secondly, its insertion between the monolith surface and the trypsin also provides a little additional space, about 3 Å, from

the 3 additional atoms. This extra space can provide increased motion/flexibility potentially alleviating hindered access to the active catalytic site.

With regards to the reaction kinetics, opening of the epoxide ring is an acid-catalyzed reaction but due to the limited stability of trypsin in these conditions an immobilization buffer (pH 7.5 HEPES) was selected at the cost of the kinetics. Considering this, long reaction times of 48 hours were chosen to mitigate the lower reaction kinetics, as were also described by Peterson *et al.* [189].

The proteolytic reactors were highly permeable even after functionalization and could be operated manually, via a fitted syringe, but the pressure bomb combined with a medium pressure regulator was employed to drive protein and wash solutions through the reactors reproducibly. Figure 6–3 shows the volumetric flow rate as a function of applied pressure with a functionalized monolith. Large digestate volumes, for further MALDI-TOF experiments, could be collected in a short duration.

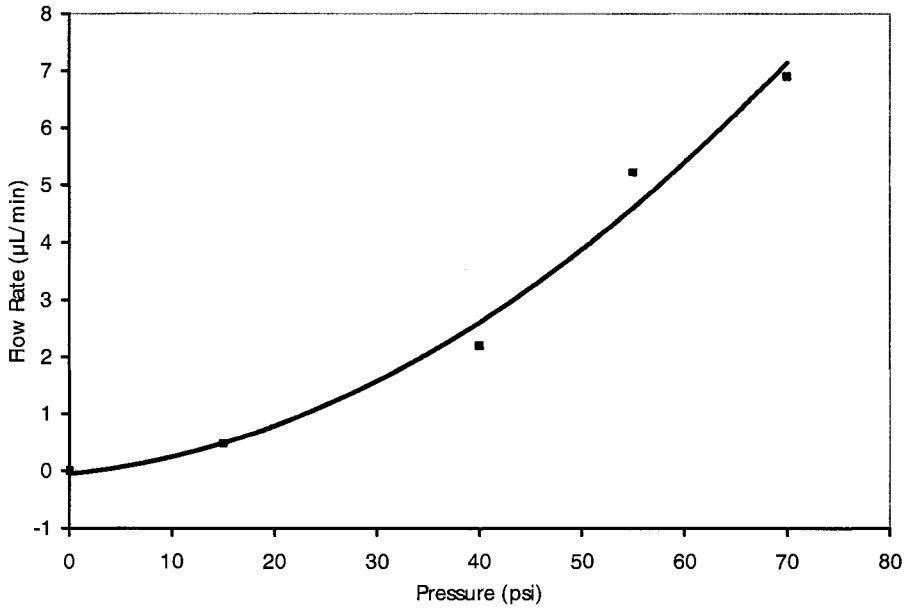

Figure 6–3: Flow rate through a 1.5 cm directly functionalized trypsin-monolith within a 40 cm long 200 µm I.D. capillary with a 5 mM pH 8.0 TRIS buffer.

6.1.2 Proteolytic Efficiency of the Two Reactors

The first set of experiments, employing the directly functionalized monolith, were to assess proteolytic efficiency for the digestion of two proteins, β-casein and bovine serum albumin (BSA), selected due to their large size difference (24 kDa vs. 60 kDa) as a function of the linear flow rate/contact time. The proteolytic efficiency was monitored by assessing the number of peptides observed together with the number of missed cleavages within these peptides, *i.e.* the number of arginines or lysines that were not cleaved by the trypsin per observed peptide. The experimental sequence coverages were calculated by dividing the number of amino acids from the observed peptides (only from the digested protein) into the total number of amino acids from the protein sequence. As a general rule, any amino acid at a specific site within the protein primary structure can only be

considered once in the calculation even though it may appear in two detected peptides. This can occur for instance in the case of peptides with at least one missed cleavage site.

The relationship between proteolysis efficiency and linear flow rate (Figure 6–4) showed a clear decrease for the two proteins, which agrees with other studies [260], and is a result of shorter contact time. Enzymatic proteolysis requires the protein to migrate, or diffuse, close to the enzyme active site, shorter contact times inevitably result in lower digestion efficiency. Thus, digestion conditions should be optimized to enable both optimal interaction with the immobilized enzyme and diffusion within its active site. Digestion of β-casein attained maximum sequence coverage of 19% while BSA yielded a maximum coverage of 13%, however the contact times were 45 and 10.8 seconds respectively. Interestingly, with a uniform contact time of 10 seconds, β-casein resulted in a lower sequence coverage than for the larger BSA. Homolytic digestions of the two proteins, performed in standard conditions (37°C for 10 hours) using the same digestion buffer resulted in sequence coverages of 25% for β-casein and 41% for BSA. This data suggests that the protein structure, perhaps accessibility of the cleavage sites, rather than the overall size is a significant parameter in determining the sequence coverage.

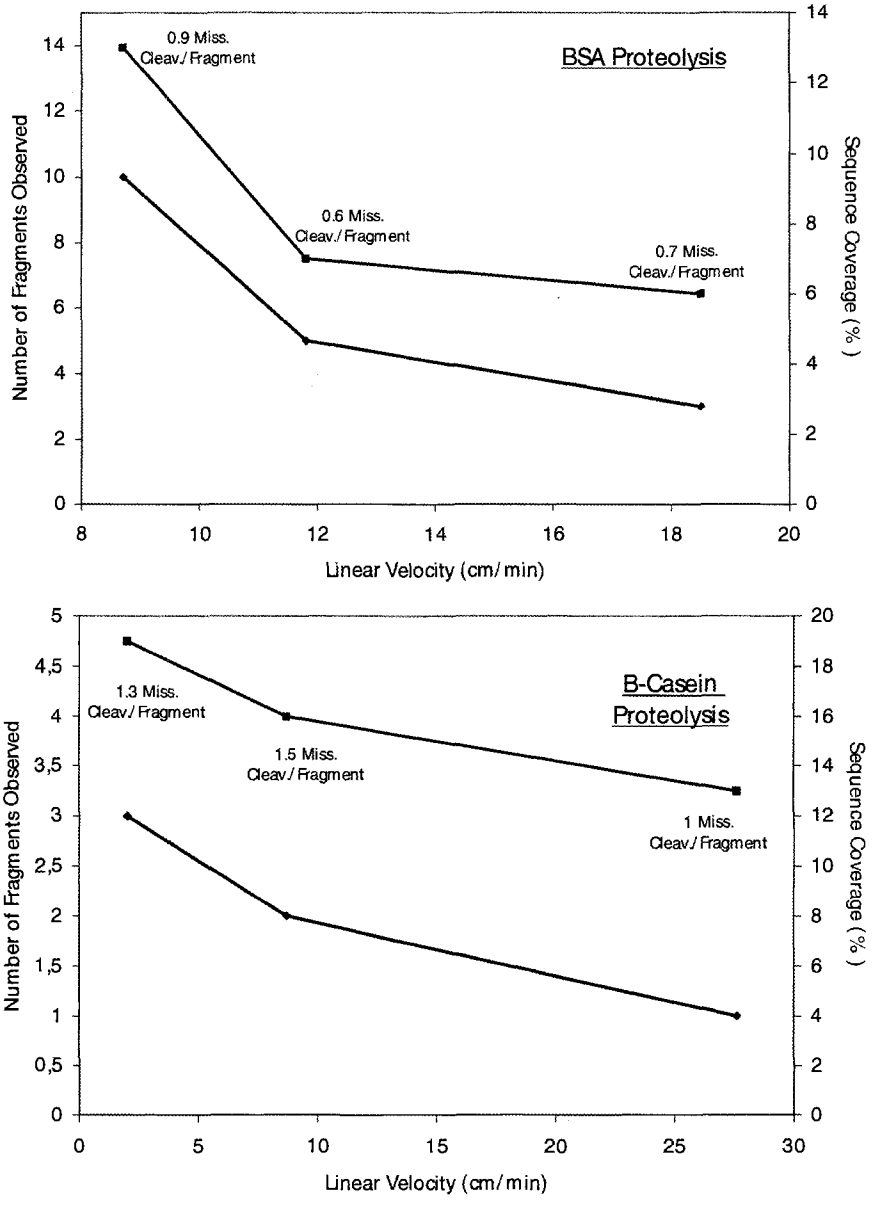

Figure 6–4: Relationship between proteolytic efficiency expressed as the percentage of sequence coverage (squares/upper curves) and the number of fragments as a function of linear flow rate (diamonds/lower curves) on the same directly functionalized reactor for the digestion of 1 mg/mL BSA and 5 mg/mL β-casein in 50 mM TRIS buffer pH 8.0 (n=2). Conversion: 1 μL/min = 6.4 cm/min.

The important point to note is that the on-column digestions are orders of magnitude faster than homolytic digestion and would probably have higher sequence coverage with longer contact time. While a longer contact time should improve the digestion this strategy is not appealing in the high-throughput application context where time efficiency is critical. In sharp contrast to homolytic digestions that yielded many trypsin-specific peptides, all peptide maps generated with the proteolytic reactor were free of trypsin autolytic peptides. This specific advantage of the proteolytic reactor is particularly important for the analysis of low-abundance proteins where autolytic peptides create a high background on mass spectrometric maps and can confound the analysis.

In order to improve the reactor efficiency, it was initially thought that the introduction of a linker should have a beneficial impact on its proteolytic activity even though trypsin is a relatively small enzyme (24 kDa) with a lower potential of steric hindrance compared to other common enzymes. To verify this hypothesis, reactors fabricated through immobilization of SATA-acetylated trypsin were compared to those made via direct immobilization approach. As shown in Table 11, sequence coverages obtained from reactors were employed as the assessment parameter.

Table 11: Proteolytic efficiency of direct and linker-mediated trypsin reactors for the digestion of β-casein (n=2)

Parameters	**SATA-acetylated Trypsin Reactors (Digestion 1)**		**Direct Trypsin Reactors (Digestion 2)**	
Reactor #	1	2	3	4
Flow velocity (cm/min)	0.8	3.7	2.7	3.6
Contact time (sec)	113	24	33	25
Sequence Coverage (%)	18	75	93	53
Number of Fragments	4	12	11	10
Missed Cleavages/Fragment	0.75	1.0	2.0	0.90

These results show increased sequence coverages in comparison to the previous experiments employing direct immobilization. But, these data also demonstrate that there is a significant issue with immobilization/sequence coverage reproducibility between reactors and experiments. As there is a general lack of information in the literature on both direct and linker-mediated enzyme immobilization reproducibility, it is plausible that other researchers may have also experienced issues with regards to immobilization reproducibility. The two direct-linked reactors yielded much higher sequence coverage in comparison to what was attained in Figure 6–4. From the experimental linear flow velocities described in Table 11 and the data from Figure 6–4 the expected sequence coverages should have been between 16 and 19% in sharp contrast to the observed coverages of 53 and 93%. Even though the magnitude of these variations was significant, all of the direct immobilization reactors yielded very similar peptide maps with the

additional appearance of a very low intensity peptide in Reactor 3 characterized by 4 missed cleavages. For the SATA-acetylated trypsin reactors, the large variations were thought to be caused by precipitation of the SATA acetylated-trypsin as was observed in the final purified solution even after several filtrations. This precipitate could have caused blocking of the monolith during protease immobilization resulting in poor immobilization and irregular flow rates.

The results show that for Reactors 2 and 4, which had very similar flow rates, a small gain in proteolytic efficiency was attained using SATA-mediated immobilization, which might have been caused by the slight difference in flow velocity. Furthermore, this difference was not considered significant as the mass spectrometric maps were not distinctive in terms of intensity or number of observed peptides. The best reactor provided a sequence coverage of 93% for β-casein digestion. This suggested that there was, in principle, no steric hindrance in the active site nor blocked access to the enzyme but rather a major issue with regards to reproducibility of the immobilization process or insufficient contact time. Thus, optimization of the enzymatic microreactor would first require improved control of the immobilization reproducibility. Higher trypsin density and longer contact times may be necessary in order to increase the number of interactions with the trypsin. Increasing trypsin density could be accomplished through adjustment of immobilization conditions or modification of the monolith structure to increase surface area accessible for immobilization. Contact time is an inverse function of linear velocity. A simple method of increasing contact time is to reduce velocity but if a fixed volume of

sample is required this has time costs. Alternatively, increasing the capillary diameter while maintaining the volumetric flow rate also increases the contact time. Increasing the distance between the supporting surface and the immobilized protease can also reduce the risk of non-specific interactions with the protease. A much longer flexible tether, such as aminated polyethylene glycols should also be investigated. For instance, Zare's group has worked on the development of a tryptic reactor based on immobilization of trypsin on a hydrophilic PEG monolith resulting in over 2000 times enhanced proteolytic efficiency, as assessed through conversion of a synthetic substrate, compared to in-solution digestion [261].

6.1.3 Further Characterization of the Directly-linked Proteolytic Microreactor

Due to ease of preparation of the directly-linked proteolytic reactor over its trypsin-SATA counterpart, further characterization of the properties of this reactor was undertaken to better assess intra and inter-reactor reproducibility. Additional attention was directed to the identification of potential factors that could affect its stability. Immobilization of chymotrypsin was also investigated to validate that the results were applicable to other enzymes.

Two microreactors were fabricated and operated in parallel for the proteolytic digestion of lysozyme. In addition to MALDI-TOF analysis (experimental conditions described in Section 2.5) of collected eluates, separation by capillary electrophoresis (CE) (experimental conditions described in Section 2.7) was used to establish the relative

abundance of undigested proteins and peptides from digest solutions and eluates from interdigestion washes. Peptides were analyzed at 194 nm, characteristic of peptide amide bond, and proteins at 280 nm specific to aromatic amino acids. The first point to note is that the average sequence coverage from on-reactor lyzosyme digestion was lower than for homolytic digestion, *i.e.* 55% sequence coverage (data not shown). In this set of experiments the digestion had a longer contact time (45 s) but still resulted in lower digestion efficiency than in the previous experiment for β-casein and BSA (Table 11). This is suggestive that individual proteins will exhibit different degrees of digestion as for in-solution digestion.

Reactor digestion efficiency was reproducible in regards to the number and relative amount of peptides generated with a small increase with subsequent digestions (*e.g.* Table 12, digestions 1-4 for Reactor 1: 13, 17, 18, 21 %).

Table 12: Intra and inter-reactor proteolytic sequence coverage, reproducibility and carry-over. For each run one sample was measured one each of the two reactors.

Reactor Number	Sample Number	Run Type/Digested Enzyme	Sequence Coverage (%)	Analysis by CE	
				Protein (280 nm)	Peptide (194 nm)
1	1	**Lyzosyme**	13	**	*****
2	2	**Lyzosyme**	12	**	*****
1	3	Wash	14	-	**
2	4	Wash	19	-	**
1	5	Wash	18	-	*
2	6	Wash	23	-	*
1	7	**Lyzosyme**	17	**	*****
2	8	**Lyzosyme**	24	**	*****
1	9	Wash	13	-	**
2	10	Wash	23	-	**
1	11	**Lyzosyme**	18	**	*****
2	12	**Lyzosyme**	14	**	*****
1	13	Wash	33	-	**
2	14	Wash	38	-	**
1	15	**Lyzosyme**	21	**	*****
2	16	**Lyzosyme**	18	**	*****

Digestion conditions: 0.3 μL/min (for 50% monolith porosity, extrapolated to a 45 sec contact time), 37 °C, 1.5 cm long monolithic reactor section, 50 mM HEPES pH 7.5, 1 mg/mL Lyzosyme. Collection volume: 60 μL (~200 min/sample).
CE conditions: As described in Section 2.7
* The number of *'s represents the relative total peak intensity from peptides and undigested protein separated measured by CE and is indicative of their relative abundance.

It was postulated that the increased reproducibility over that achieved in the previous sections was due to an improved control of immobilization conditions. These improvements included improved monitoring and control of immobilization duration, temperature as well as rejection of any monoliths showing unusual liquid permeability

(backpressure). Carry-over of generated peptides due to retention on the monolithic backbone was observed in the post-digestion wash samples where sequence coverage was comparable to those from the sample digestion. However, CE separations of the blank (wash) runs showed that the total amount of peptides (peak areas) obtained were lower than from the sample digestions. Interestingly, the higher sensitivity of MALDI-TOF, compared to CE-UV detection, revealed an increased number of low-abundance peptides that eluted in the wash solutions. Combination of the CE and MALDI-TOF findings suggested that carry-over was caused primarily by slow but continuous elution of a small amount of strongly bound peptides. Since no protein carry-over was shown by CE, it can also be postulated that these peptides were not originating from adsorbed proteins being slowly digested.

As no protein was observed by CE in the wash runs, it appeared that the extent of interaction with the relatively hydrophobic monolith was more significant for peptides than undigested proteins. Addition of an organic modifier during washing could reduce the extent of peptide carry-over due to hydrophobic interactions with the monolith but might also result in denaturation of the immobilized protease as it will be discussed in a later section. On the other hand, the use of a hydrophilic monolith or modification of the current monolith surface chemistry could also reduce carry-over.

The enzyme is key to overall reactor efficiency through its specificity, sensitivity to immobilization and stability. Trypsin is the most widely used enzyme in proteomics but chymotryspin, another serine protease specific toward phenyl-containing AA

(tyrosine, tryptophan and phenylalanine) may also serve as a benchmark for reactor efficiency. This was achieved via immobilization of chymotrypsin through the same immobilization procedure as trypsin followed by the digestion of BSA and Lyzosyme.

It can be seen from Table 3 that immobilization of chymotrypsin yielded similar digestion efficiencies as trypsin, but the resulting microreactors differed in many aspects. For the digestion of BSA, peptides generated via chymotrypsin exhibited a stronger affinity toward the monolithic backbone as the sequence coverage and intensity of peptide peaks increased for wash runs over those from the trypsin microreactor. Trypsin and chymotrypsin are both serine proteases but chymotrypsin cleaves proteins at hydrophobic residues (such as tryptophan, tyrosine, phenylalanine) producing peptides with hydrophobic terminal AA's. Trypsin, on the other hand, acts on lysine and arginine, producing peptide with less hydrophobic terminal groups.

It was interesting to note that the chymotrypsin microreactor suffered from relatively low stability as its associated sequence coverage dropped dramatically after only 10 consecutive runs, while the trypsin-microreactor remained stable in the same conditions. This suggests that surface induced effects such as slow denaturation, or product induced hindering, of the enzyme may play an important role in reactor stability.

Table 13: Efficiency of a chymotrypsin reactor in comparison to a trypsin reactor achieved simultaneously in parallel

Run Number	Reactor type (Immobilized Enzyme)	Run Type/Digested Enzyme	Sequence Coverage (%)	Analysis by CE	
				Protein (280 nm)	Peptide (194 nm)
Digested Protein: BSA					
1	Chymotrypsin	**BSA**	21	-	*****
	Trypsin	**BSA**	12	-	*****
2	Chymotrypsin	Wash	29	-	**
	Trypsin	Wash	12	-	-
3	Chymotrypsin	**BSA**	16	-	*****
	Trypsin	**BSA**	24	-	*****
4	Chymotrypsin	Wash	13	-	**
	Trypsin	Wash	5	-	**
5	Chymotrypsin	**BSA**	19	-	*****
	Trypsin	**BSA**	12	-	*****
Digested Protein: Lyzosyme					
6	Chymotrypsin	**Lyzosyme**	13	**	*****
	Trypsin	**Lyzosyme**	9	**	*****
7	Chymotrypsin	Wash	13	-	**
	Trypsin	Wash	22	-	**
8	Chymotrypsin	**Lyzosyme**	6	**	*****
	Trypsin	**Lyzosyme**	22	**	*****
9 (22.5°C)	Chymotrypsin	Wash	4	-	**
	Trypsin	Wash	20	-	-
10 (22.5°C)	Chymotrypsin	**Lyzosyme**	0	***	-
	Trypsin	**Lyzosyme**	33	**	*****

Digestion conditions: 0.3 µL/min, 37 °C (22.5 °C for runs 9 & 10), 1.5 cm long monolithic reactor section (for 50% monolith porosity, extrapolated to a 45 sec contact time), 50 mM HEPES pH 7.5 with 20 mM $CaCl_2$, 1 mg/mL BSA/Lyzosyme, Collection volume: 60 µL (~200 min/sample).
CE conditions: As described in Section 2.7

Findings in this section have demonstrated the potential of the direct immobilization method for the fabrication of a monolithic enzymatic reactor. Immobilized trypsin demonstrated improved stability over chymotrypsin and its immobilization enabled relatively high sequence coverages in a reproducible scheme. It is thought that the monolith hydrophobic backbone was responsible for carry-over of generated peptides and that optimization of washing conditions and/or modification of the backbone should reduce this phenomenon. Special attention would have to be directed toward preservation of the immobilized enzyme activity due to the potential for irreversible denaturation in stronger washing solutions or with the monolith surface.

6.2 Implementation for Automated High-Throughput Proteolytic Digestion

Many research groups have directed their efforts towards the development of high-throughput proteolytic reactors using either complex liquid handling systems or electrophoretically-driven microreactors [262, 263]. Implementation of high-throughput proteolytic reactors requires that a significant number of samples can be digested efficiently as quickly and cleanly as possible. Hence, minimal or no carryover should be observed between runs. In addition, enzymatic reactors should exhibit high digestion reproducibility, be reusable and easily implemented on existing analytical instrumentation.

The directly-bound trypsin microreactor was investigated for its potential for automated proteolytic digestion on a Beckman Pace MDQ capillary electrophoresis instrument as a stand-in for automated high-throughput instrumentation.

6.2.1 Modification of the Monolithic Support

In the previous study, pressures ranging between 15 and 70 psi were employed to drive the protein solutions through the microreactor monolithic network. The Beckman Pace MDQ generates a maximum 14 psi pressure by action of a syringe pump and would require a very long period (>1 hour) before an injection sample could be eluted. Thus, two solutions were possible. One would have consisted of using a shorter reactor bed length but would have naturally yielded lower proteolytic efficiency in terms of sequence coverage and possible protein breakthrough due to shorter contact time and lower total enzyme mass. On the other hand, an increase in the porosity/permeability of monolith would result in a smaller back-pressure and/or shorter elution time but could also result in a decrease in enzyme mass due to lower surface area accessible for immobilization. This second option was investigated by modifying the porogenic solvent to favour formation of larger flow-through pores thus higher monolith permeability. In the poly(GMA-co-TRIM) polymerization isooctane favours lower porosity since little phase separation occurs during polymerization in a good solvent environment. Toluene, the poor solvent, increases pore sizes through the inverse mechanism.

Table 13: Modification of the porogenic solvent and resulting hydrodynamic porosity for the poly(GMA-co-TRIM) unfunctionalized monoliths (n=3)

Modified Parameter	Monolith #	Isooctane (%v/v)	Bed Length (cm)	Backpressure @ 0.2 mL/min (bar)
% Isooctane	1	70	1.0	54 ± 3
	2	50	1.0	28 ± 2
	3	30	1.0	22 ± 2

Experimentally, the increase in porosity with decreasing isooctane (and increasing toluene) was confirmed as shown in Table 13. SEM images of Monoliths 1 to 3, shown in Figure 6–5, also corroborate this trend in hydrodynamic permeability with an increase in the flow-through pore dimension together with larger particle sizes.

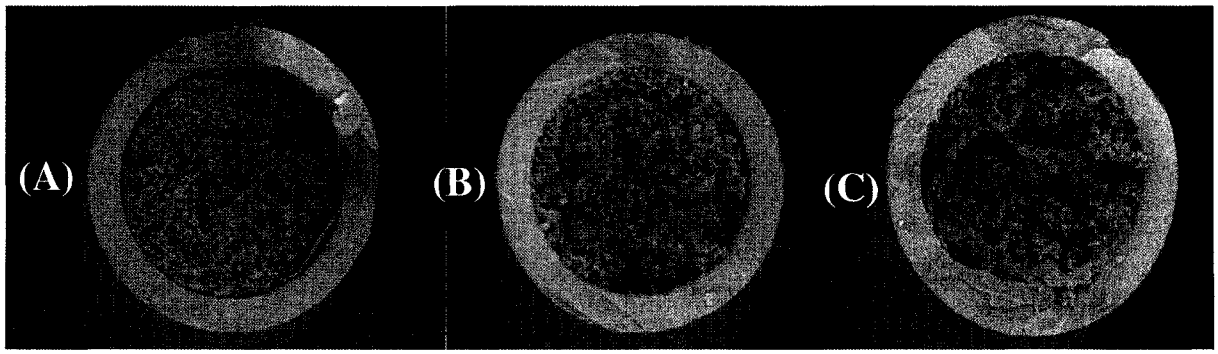

Figure 6–5 : SEM images of the poly(GMA-co-TRIM) monoliths with decreasing isooctane content in the porogenic solvent: (A) 70%, (B) 50%, (C) 30% (v/v) isooctane.

It can be seen that Monolith 1 (A) had the least porous monolithic network with smaller flow-through pores resulting in the highest resistance to flow but would also have the highest surface area. Alternatively, flow-through pores increase in size and surface area decreases, from Monoliths 1 to 3.

In order to use the modified monolith on the automated instrument, 2.5 cm of the polyimide coating was removed but only 1.0 cm was used for photopolymerization. The additional 1.5 cm window was employed for post-monolith on-capillary UV detection. Practically, operating the Beckman instrument at its maximum pressure (90 psi) (JL, I

don't think our Beckman can go to 90 PSI?? Ask Wei) yielded no elution of an injected BSA sample plug even after 170 minutes for Reactor 1 (made using a Monolith 1 subsample) while BSA eluted in 86 minutes for Reactor 3, as seen in the following elution pattern.

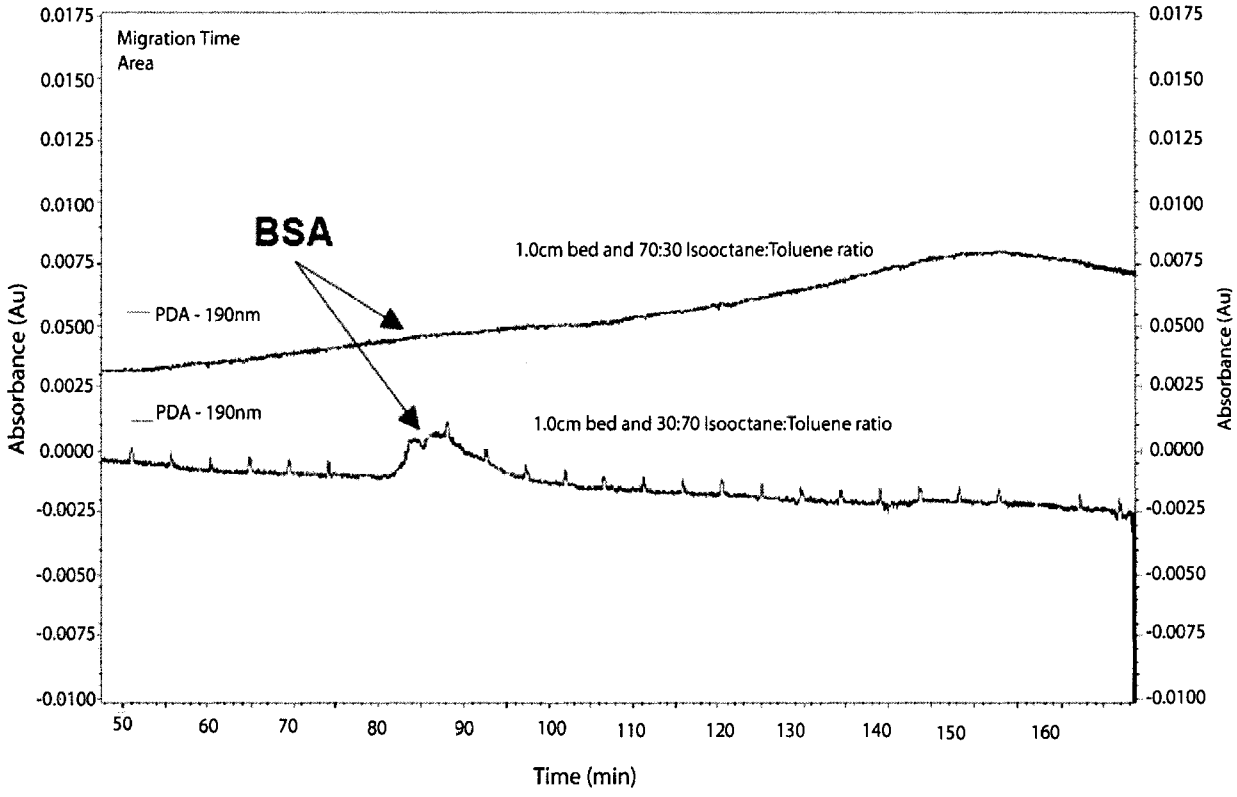

Figure 6–6 : Elution pattern of a 30 sec 1.5 mg/mL BSA injection at 14 psi and 25 °C in 50 mM HEPES buffer pH 7.5 on microreactors with different Isooctane:Toluene ratio (Above: 70/30 %v/v, Below: 30/70 %v/v). L_{total} = 40 cm, L_{bed} = 1.0 cm, detection at 190 nm.

From the above data it is clear that the modified monolith (Reactor 3) was sufficiently permeable to enable elution within the pressure limitations imposed by the current instrumentation despite the relatively long time required to elute the injected

BSA. The bottom trace exhibited baseline spikes caused by the periodic cycling of the syringe pump due to an apparent slow pressure leak, probably at a seal. All the following monoliths were fabricated using a 30/70 (%v/v) isooctane:toluene porogenic solvent.

6.2.2 Optimization of the Monolithic Support: Proteolytic Digestion

While investigating elution pattern reproducibility, it was discovered that a significant time drift occurred with the directly immobilized trypsin reactor at 25 °C but not at 37 °C. This suggests that the BSA was interacting with, perhaps accumulating on, the surface and slowly changing the porosity. By raising the operating temperature to 37 °C, conventionally employed for in-solution tryptic digestion, reproducible elution times were achieved for BSA injection as shown below. The improved elution of BSA could be explained by one, or more, of the following factors: a decrease in solvent viscosity, swelling of the monolith and a shift to lower retention, all as a result of the increased temperature.

As depicted in Figure 6–7, running the reactor at 37 °C allowed improved inter-injection elution time reproducibility of 3.3 %, all further experiments were thus performed at 37 °C. This temperature effect was also observed in a previous experiment (Table 13) indicated by an increase in sequence coverage upon consecutive use of the trypsin reactor at 22.5 °C, most probably caused by significant peptide carry-over.

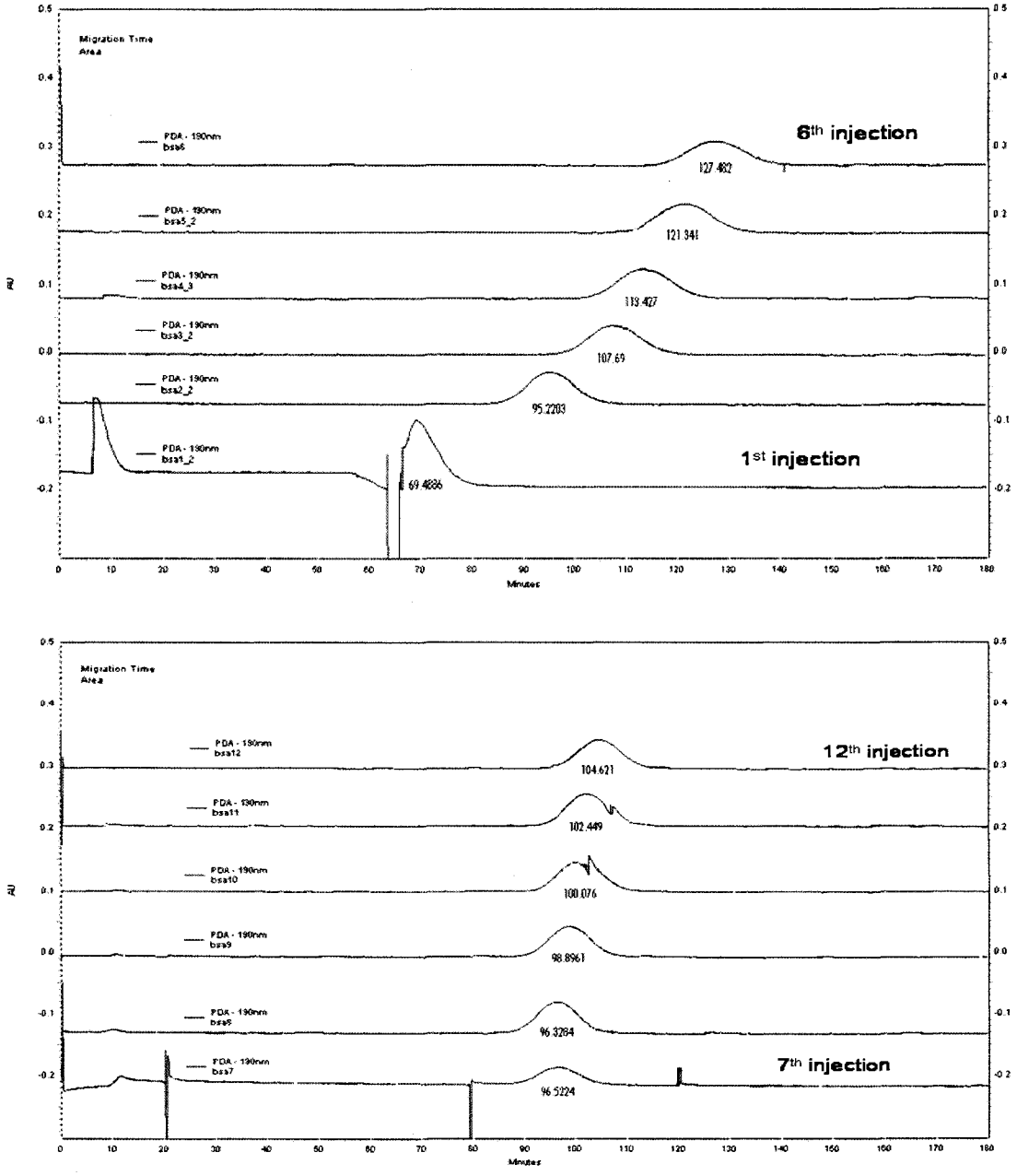

Figure 6–7 : Reproducibility of elution time upon sequential injection of 1.5 mg/mL BSA in 50 mM NH_4HCO_3 buffer pH 8.5 at 25 °C (left) and 37 °C (right) on a 30/70 isooctane/toluene (%v/v) microreactor. L_{total} = 40 cm, L_{bed} = 1.0 cm, detection at 190 nm.

Choice of digestion buffer also plays a pivotal role in the digestion efficiency due to the pH sensitivity of most proteases as well as potential interferences with the enzyme active site. The nature and concentration of digestion buffers also have a marked effect on mass spectrometric measurements due to ionization suppression, formation of buffer adducts and high/noisy background. In order to use this type of microreactor for direct on-line mass spectrometric use of volatile buffers becomes absolutely necessary. Ammonium bicarbonate, a volatile buffer, can limit mass spectrometric signal suppression phenomenon and is the usual choice for trypsin digestions. The HEPES buffer was thus replaced by ammonium bicarbonate (NH_4HCO_3) for the microreactor proteolytic digestion of BSA as shown in Figure 6–8.

Contrary to what was expected, preliminary sequence coverage obtained with the more volatile buffer, *i.e.* NH_4HCO_3 was lower than with HEPES. This was despite the observation that NH_4HCO_3 seemed to yield more uniform crystallization. As expected, a reduction in baseline noise was observed from samples generated with a NH_4CO_3 digestion buffer and "cleaner" MALDI mass spectra were measured as shown in Figure 6–8.

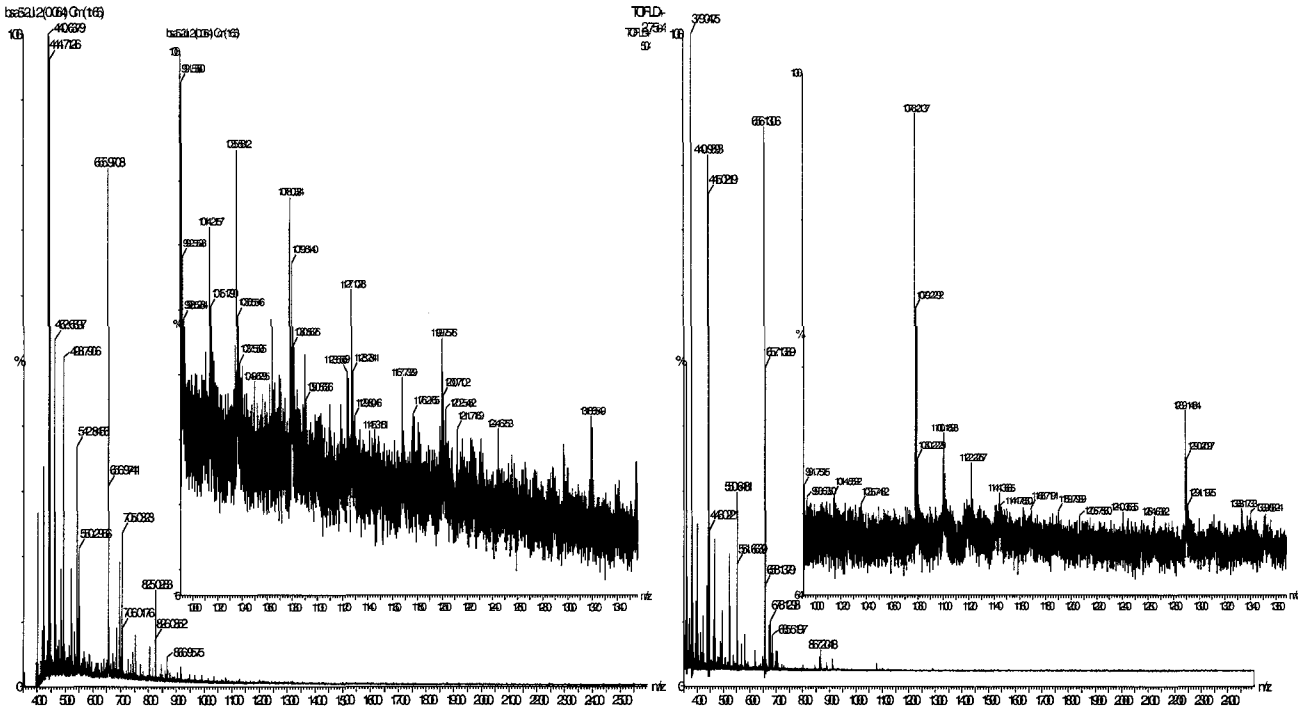

Seq. Cov.: 26%Seq. Cov.: 14%

Figure 6–8 : MALDI-TOF analyses in (+ve) mode of BSA (1.5 mg/ml) infusion in 50 mM HEPES pH 7.5 (left) and 50 mM NH_4HCO_3 pH 8.5 (right) used as digestion buffers at 14 psi, at 37 °C.

Because no experiments were performed in order to assess buffer influence on homolytic digestion efficiency, the variation in signal could also be due to different trypsinolysis rates at the different pH's. Even with the reduction in sequence coverage obtained with NH_4HCO_3 this buffer was used in further studies due to its improved compatibility for subsequent MALDI-TOF and eventual ESI-MS analysis.

Previous digestion experiments used continuous injection of protein through the reactor and would definitely not be in the high-throughput realm given the long elution time of the reactor. Instead short duration injections of protein, similar to that of

chromatographic peaks, or those that would provide sufficient mass of protein for direct MS analysis were investigated. This strategy of plug digestion is especially relevant as a great number of biological samples under proteomic investigation are only available in minute quantities thus requiring analytical techniques able to handle such small volumes.

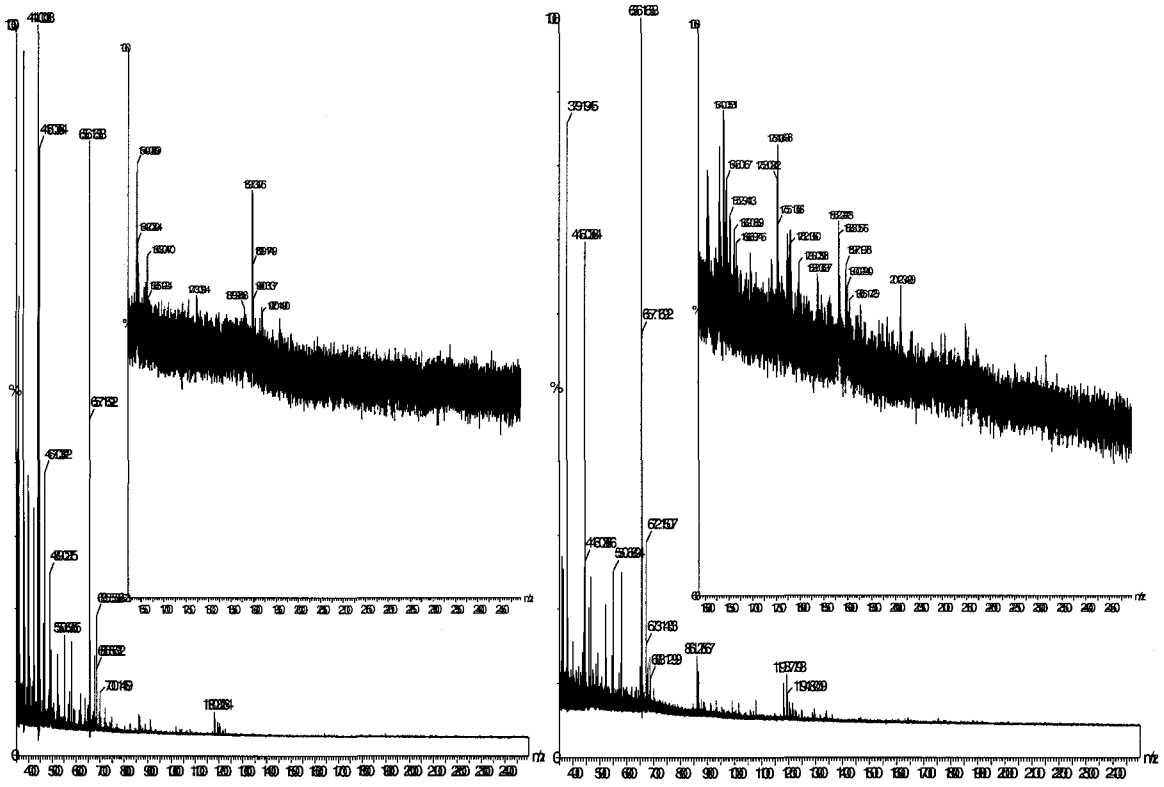

Seq. Cov.: 25%Seq. Cov.: 35%

Figure 6–9 : MALDI-TOF analyses in (+ve) mode of BSA (1.5 mg/mL) 30 sec injection or plug flow (left) and continuous flow digestion (right). Digestion buffer was 50 mM NH_4HCO_3 pH 8.5 at 14 psi, at 37 °C. Collection time: 120 minutes.

Not surprisingly, a greater number of peptides were detected by MALDI-TOF with the 120 minutes continuous injection than for the single 30 seconds injection of

BSA. Considering that the injection introduced only 1/240th the sample mass the results attained make plug injection very appealing for applications where protein amount is limited. It also would be possible to use a direct capillary to MALDI plate spotter [264] or an in-line ESI-MS strategy.

Digestion of model proteins, such as BSA and lysozyme, in conditions close to those used in real proteomic scenarios demonstrated the potential of the reactor. However it is difficult to decouple the effects of the protein from those of the reactor when evaluating reactor efficiency. Methods based on the conversion of an arginine containing low-molecular weight substrate are used extensively in the literature to establish and compare the proteolytic activity of bound, or free, trypsin [190,197,265,266]. Two different substrates (N-α-benzoyl-L-arginine ethyl ester (BAEE) and N-α-benzoyl-DL-arginine p-nitroanilide (BAPNA)) were tested here but no elution peaks were observed with the digestion buffer and an elution buffer containing 25% of acetonitrile (%v/v). The lack of elution was thought to be due to strong interaction between the substrate and/or its products with the monolith.

At this point, a summary of the findings described and explained in the two previous sections will be given to guide the reader through the upcoming sections where photografting will be used. It was shown that direct linkage of trypsin compared to SATA-mediated trypsin immobilization yielded improved proteolytic efficiency as demonstrated by MALDI-TOF MS analysis of digest solutions. Immobilization of chymotrypsin yielded similar efficiency as trypsin, but lower reactor stability.

Considering that the directly immobilized trypsin reactor offered the best performance, modification and optimization of porosity allowed the production of microreactor compatible with a commercial analytical instrument demonstrating the potential for automated analysis.

Even though an improvement in baseline noise was observed with NH_4HCO_3 it did not result in improved sequence coverage. It was confirmed that the use of continuous flow for the digestion of a model protein resulted in improved digestion efficiency but the plug injection approach was also functional and promising for on-line analysis. One significant advantage provided by all fabricated microreactors was the absence of trypsin autolytic peptides particularly important for the analysis of low-abundance protein.

One of the major issues that were observed was the strong retention of peptides leading to both carry-over and potentially to low sequence coverages. There is a need to reduce retention on the monolith as it will increase sequence coverages, reduce carry-over and potentially increase reproducibility and column stability. Likely candidates are hydrophilic polymers that also have the potential benefit of probably stabilizing the enzyme.

It was thus hypothesized that strong retention of peptides on the hydrophobic monolith backbone was one of the major impediment for this specific proteolytic microreactor. As the main purpose of this project was to demonstrate the ease of fabrication and efficiency of such microreactors over other type of microreactors as it

will be described later, no further optimization was achieved to reduce the extent of peptide retention. The central goals of demonstrating the practicality of the reactor, assessing its efficiency, stability and versatility toward model proteins were demonstrated. To carry this work forward the issues of reduction of protein/peptide interaction with the monolith, increasing the efficiency via increased contact time and/or enzyme density should be addressed. To implement the reactor in a practical situation would benefit from implementation with direct elution to an ESI-MS interface for the continuous analysis of the eluting peptides. This configuration would be the gateway to developing the reactor for high-throughput applications.

6.3 Copolymer Grafting of a Proteolytically and Electrochromatographically Active Monolith

One of the major issues associated with parallel proteolytic analyses, *i.e.* shotgun approaches, where a mixture of proteins is digested simultaneously is the complexity of the mass spectra which consist of all the generated peptides. As the number of proteins, and the number of generated peptides increases, the shotgun approach can lead to excessively complicated mass spectra interpretation. In the case of low-abundance proteins, this strategy can become very problematic due to signal suppression. A common way to improve the quality and simplicity of peptide maps relies on the fractionation/separation of the proteins followed by digestion or post-digestion separation of generated peptides. Automating these strategies requires complex liquid handling systems similar, or equivalent, to multidimensional HPLC instrumentation with the

addition of a proteolytic reactor system. The most sophisticated systems should enable sequential protein chromatographic separation, proteolytic digestion and final chromatographic differentiation of the peptides.

An approach based on a single multifunctional chromatographically and proteolytically-active column would seem to be a very promising alternative to complex interfaced instruments. A major benefit of such multifunctional columns would be their simplicity, ease of use and lack of complex liquid interfacing such as liquid switching valves. A single multifunctional column would require two characteristics: 1- very high separation efficiency to enable separation of proteins and generated peptides, and 2- rapid proteolysis so that proteins peaks are converted into peptides without destroying the chromatographic efficiency. Hand-in-hand with the previous, the column should also have sufficient versatility to enable efficient tuning and optimization of chromatographic separations while preserving the immobilized protease activity and stability.

This section will demonstrate copolymer grafting on the poly(AMPS-co-BAC-co-BDDA) monolith as a proof-of-principle bifunctional chromatographic/proteolytic microcolumn. The experimental design includes optimization of the grafting procedure, immobilization conditions and assessment of proteolytic efficiency. Simultaneous digestion and electrochromatographic separation will be illustrated with the potential of this methodology for the fabrication of fully integrated (microfluidic) proteomic interfaces in mind.

6.3.1 Copolymer Grafting Procedure for Introduction of Reactive GMA

The same general scheme employed for sequential grafting and trypsin immobilization on the model poly(AMPS-co-BAC-co-BDDA) was used here (see Section 2.3 for experimental details).

Immobilization kinetics could have been increased through increased temperature and lower pH. But, to avoid potential loss of trypsin viability and reduce autolysis immobilization was performed at 4°C. Lower temperatures also lead to an increase in solvent viscosity and reduction of trypsin diffusion necessitating longer immobilizations. By lowering the immobilization pH, nucleophilic substitution at the epoxide ring can be enhanced but trypsin activity is known to degrade under these conditions so this procedure was carried-out at pH close to neutrality.

6.3.2 Reactor Optimization: Grafting and Immobilization Duration

The relatively high complexity and physical fragility of multiply modified monoliths fabricated in UV-transparent capillaries limited the number of factors selected for optimization. The capillary fragility is a particularly difficult problem to overcome because the Teflon coating is easily damaged, and lost, because of the high pressure HPLC fittings used to connect the capillary to the bomb for flushing. The first factor optimized was the grafting duration and its effect on proteolytic efficiency for the digestion of BSA. Proteolytic digestion of BSA on monoliths photografted with GMA for 2, 3, 5, 7 and 10 minutes yielded different sequence coverages as shown in Table 14 Sequence coverages, based on three grafted monoliths at each duration, show that a five

minute GMA photografting resulted in maximum sequence coverage, seven and ten minute GMA-grafting did not yield any further improvement in proteolytic efficiency (not shown).

Table 14: Effect of GMA Grafting duration on on-column proteolytic efficiency (n=3)

Grafting Duration (min)	Sequence Coverage (%)
1	37.4 ± 0.5
3	39.9 ± 0.5
5	44.7± 1.4
7	44.7± 1.4
10	44.7± 1.4

* More details and example of an on-column BSA digest MALDI-TOF spectra in Appendix A

The significant and reproducible improvement in sequence coverages, over those obtained in the previous sections, can be explained by combination of a longer reactor bed length (1.5 *vs.* 19 cm) and a longer contact time (30 sec *vs.* 3 min). The higher pressure attainable with the HPLC instrument, even on this much longer column, facilitated control of contact time. There may have also been an increase in trypsin surface density or a reduction in trypsin interaction with the surface as the photografting process partly shields the monolith surface with hydrophilic diol groups. Once again, no autolytic peptides were observed in the MALDI-TOF MS analysis.

Table 15 details the relationship between digestion efficiency and trypsin immobilization duration at 4 °C.

Table 15: Effect of trypsin immobilization duration on on-column proteolytic efficiency (n=3)

Immobilization duration (day)	Sequence Coverage (%)
2	21.0 ± 2.0
3	39.9 ± 0.5
4	44.7± 1.4
5	40.0± 2.0
6	38.0± 2.0

* More details and example of an on-column BSA digest MALDI-TOF spectra in Appendix A

From Table 15, three days of immobilization duration was required to reach maximal sequence coverage. Interestingly, as immobilization was extended to periods exceeding five days, a net reduction in sequence coverage from 45 to 38% was observed (not shown). This phenomenon was probably caused by digestion of immobilized trypsin by unbound trypsin. However, autolytic peptides were detected at similar levels in the first wash solutions of the 3 days and 5 days immobilized monoliths. Alternatively, a reduction in activity could have also been associated with a significant increase in surface-bound trypsin density resulting in a decrease in trypsin accessibility. If true, an increase in column backpressure or decrease in the monolith permeability would have

been expected. Backpressure values did not confirm this hypothesis has illustrated in Table 16.

Table 16: Proteolytic digestion on a 19 cm GMA-grafted trypsin-functionalized monolith by μ-LC. Mobile phase was HPLC grade water at 0.1 mL/min

Monolith #	Grafting duration (min)	Immobilization duration (days)	Total Backpressure (bar)	Increase in Backpressure vs. Control (%)
*Control	0	0	28	-
1	1	3	32	14.3
2	3	3	35	25.0
3	5	3	35	25.0
4	5	3	34	21.4
5	5	5	35	25.0
6	5	6	34	21.4
7	2.5	2	33	17.9
8	2.5	4	34	21.4
9	2.5	5	34	21.4

*Control: unmodified base monolith

The backpressure measurement data indicated that the GMA grafting step was mainly responsible for the decrease in monolith permeability. The restriction caused by trypsin immobilization was responsible for only 25% of the loss in permeability. This suggests that GMA photografting resulted in formation of multiple layers of GMA on the monolith surface obstructing some of the pores of the monolith. In order to minimize blockage of pores, formation of a GMA monolayer would be desirable enabling improved conservation of the monolith porous properties. The subsequent decrease in permeability resulting from trypsin immobilization reduced further accessibility to the

porous system. The overall decrease in porosity is thought to cause a reduction in potential proteolytic activity.

6.3.3 Microreactor Versatility: Manual Utilization

Many have seen proteolytic microreactors as a good alternative to complicated and time-consuming homolytic digestion and with significant potential for simplified high-throughput sequencing and identification of proteins. With this in mind, developed microreactors were operated with well-controlled high-pressure bombs, CE instruments or HPLC pumps capable of mimicking automated protein sequencing instrumentation that provide consistent and accurate liquid flows.

Outside of the high throughput environment there are vast numbers of researchers who only require occasional proteolysis. The microreactors inherent simplicity of use, high efficiency, absence of autolysis peptides make it appealing for such occasional use. In addition, the microreactor can be used without sophisticated high pressure liquid handling equipment. To investigate manual utilization of these microreactors, a short section of a GMA-grafted trypsin-immobilized microreactor was fabricated and connected to a 5 cc syringe with a commercially available luer-lock fitting designed to hold capillary tubing (Figure 6–10).

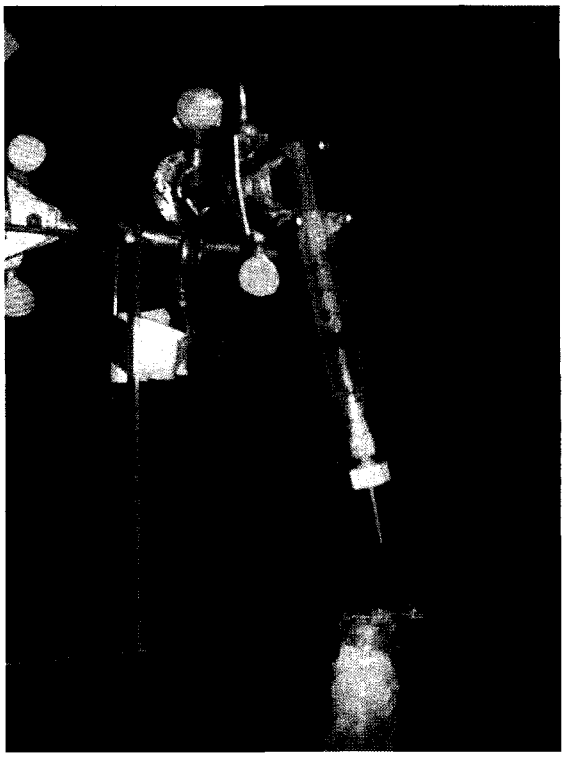

Figure 6–10: Manual application of low pressure to a 5cm monolithic microreactor via a luer-lock adapter connected to a fingertight fitting where a capillary sleeve is inserted to hold the microreactor capillary by pressure.

Even though this was a very simple setup it is was easy to perform the digestion and washing steps. The syringe is sufficiently strong and resilient that the system can be pressurized, and maintain the pressure, for the required digestion and washing steps. Surprisingly, the digestion of 1.5 mg/mL lysozyme resulted in an enhanced efficiency compared to the 19 cm long monolithic microreactors (*i.e.* 51% *vs.* 41% coverage), as shown in the following mass spectra.

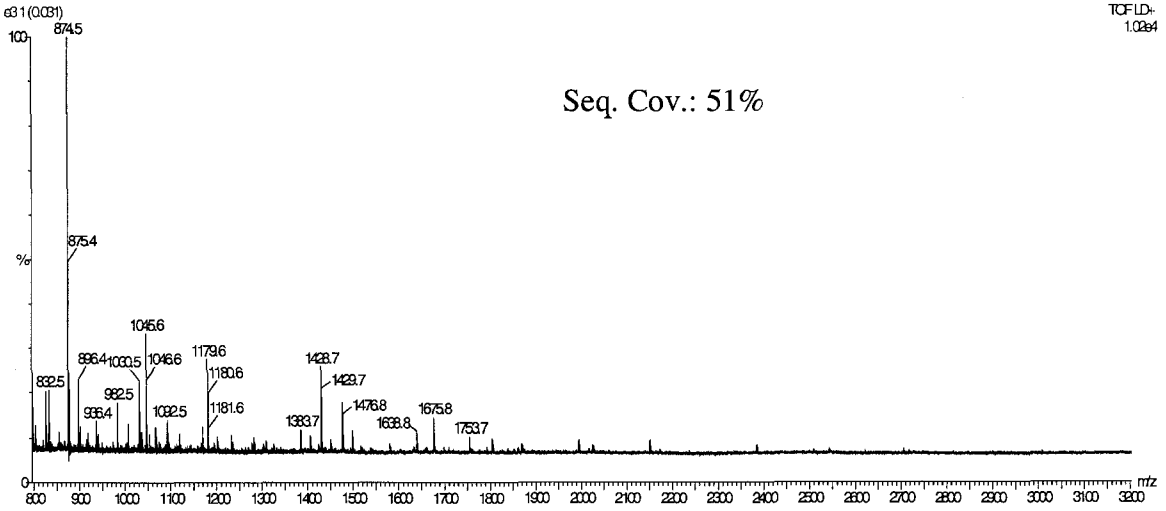

Figure 6–11: Digestion of a 1.5mg/mL lysozyme solution in 50mM NH_4HCO_3 pH 8.5 at ~0.5 uL/min for 60 minutes at room temperature measured by MALDI-TOF MS analysis in (+ve) on a manually operated 5cm long trypsin-functionalized (3 days), GMA-grafted (5 minutes) monolith.

This unexpected result was verified by repeating the experiment which also showed similar gains in efficiency. A potential cause for this apparent enhancement was thought to be breakthrough of the two newly observed peptides on the shortened monolith. This was further corroborated as the intensity for these two peptide fragments was relatively small compared to the other peptides. Indeed, these two peptides were found in the acetonitrile wash of the 19 cm long monolith at higher relative intensities supporting this latter hypothesis. Thus, manually operation of these reactors is practical and offers an interesting possibility for researchers who need the advantages of the microreactor but do not want to be burdened with the liquid handling instrumentation.

6.3.4 Assessment of the Proteolytic Microreactor Properties

Several publications have used a variety of immobilization strategies on different types of substrates and reported their proteolytic efficiency [267,268]. Unfortunately, few of these publications focused on assessment of reproducibility and stability of developed microreactors [267]. This information is essential to developing a rational methodology for optimization of monolithic and/or capillary microreactors. These two parameters were investigated here.

Table 17: Reproducibility of proteolytic digestion based on 5 grafted monoliths each in 50 mM NH_4HCO_3 pH 8.5 at room temperature, 6.5 cm/min

Protein Digested	Monolith length (cm)	Number of Fragments	Sequence Coverage (%)	Autolytic Peptides
Lysozyme	10	8 ± 2	41 ± 2	-
BSA	10	15 ± 1	21 ± 0.2	-
	19	26 ± 4	44 ± 0.5	-

Table 17 shows the relatively high and significantly more reproducible proteolytic efficiencies for the digestion of lysozyme and BSA. Sequence coverages were very reproducible. The number of fragments varied significantly but most of the newly observed peptides were the proteolysis products of previously observed peptides, *i.e.* peptides with at least one missed cleavage were the source of the newly generated peptide(s). In addition, no trypsin autolytic peptides were detected.

Microreactor stability would play an important role in the adoption and acceptability of microreactor technology for real laboratory and research work. The

following reports on an initial stability study of proteolytic digestions carried-out over 8 weeks with the same monolith.

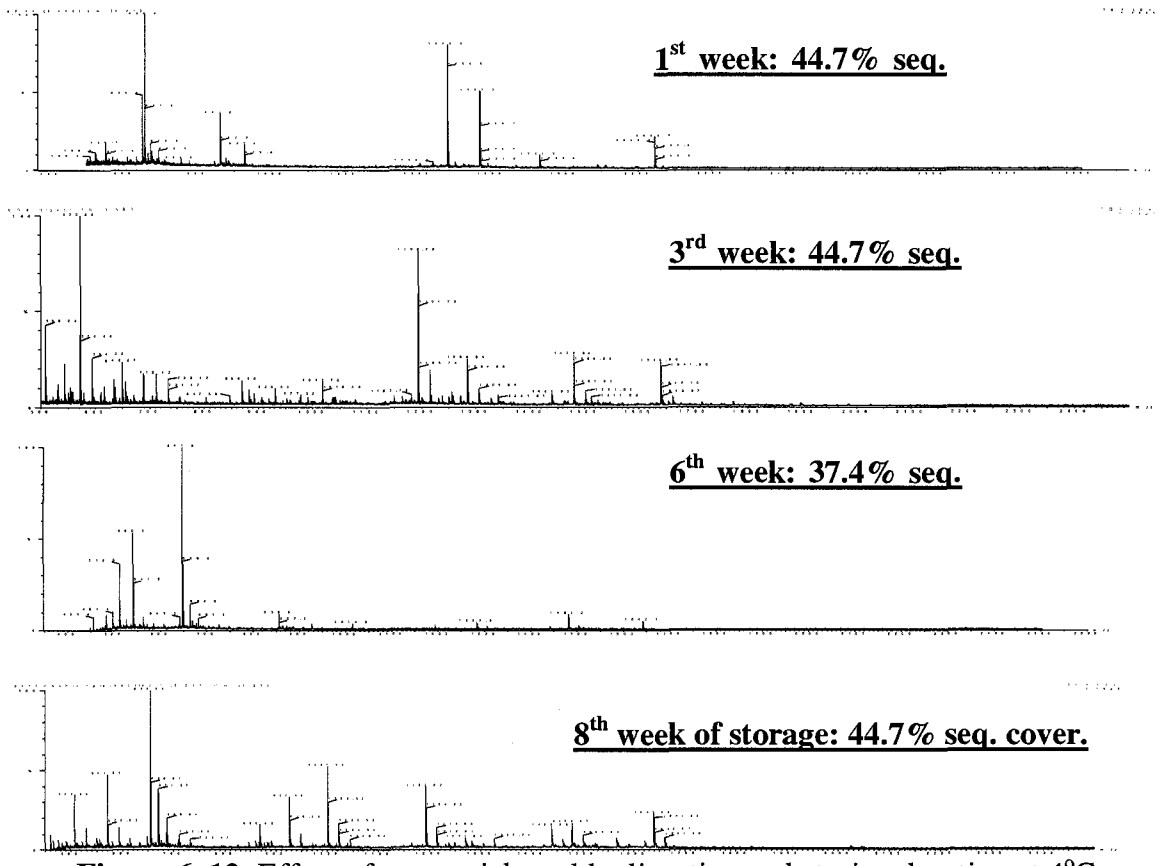

Figure 6–12: Effect of sequential weekly digestion and storing duration at 4°C on digestion of 1mg/mL BSA. Not all data shown. (5 minutes GMA-grafting, 3 days trypsin-immobilized). Relative peak intensity variations were observed and were due to quality of individual MALDI sample spots (salt effect) as peak intensities varied between sample spots generated from the same digest samples.

The monolith showed a decline in digestion efficiency after 6 weeks of weekly usages that consisted of four proteolytic digestions separated by an hour washing with the digestion buffer. Interestingly, digestion performed on a monolith stored at 4°C for 8 weeks prior to its first proteolytic use yielded the same digestion efficiency as "fresh" microreactors. It was concluded that reduction of the microreactor activity was likely

caused by the limited, and fixed, number of proteolytic cycles that an immobilized enzyme could undergo *i.e.* catalytic lifetime. Build-up of peptide fragments or undigested proteins due to the hydrophobic characteristic of the base monolith was not considered a major factor in the microreactor inactivation because a steady, or even rapid, drop in efficiency would have been expected once the build-up "poisoned" the surface. In principle, adsorption of proteins and peptides could have resulted in additional interactions between immobilized trypsin and the surface reducing the overall microreactor activity.

To investigate if peptides were building-up on the column, the inter-digestion wash solution hydrophobicity was increased by addition of acetonitrile to increase elution of adsorbed hydrophobic peptides.

Inclusion of acetonitrile during washing did not enable detection of any new peptides not already observed in digest or wash eluates. It also appeared that by replacing the initial washing solution with an acetonitrile/ NH_4HCO_3 buffer irreversible denaturation of trypsin occurred resulting in complete loss of the microreactor proteolytic activity even after multiple conditionings in NH_4HCO_3 buffer.

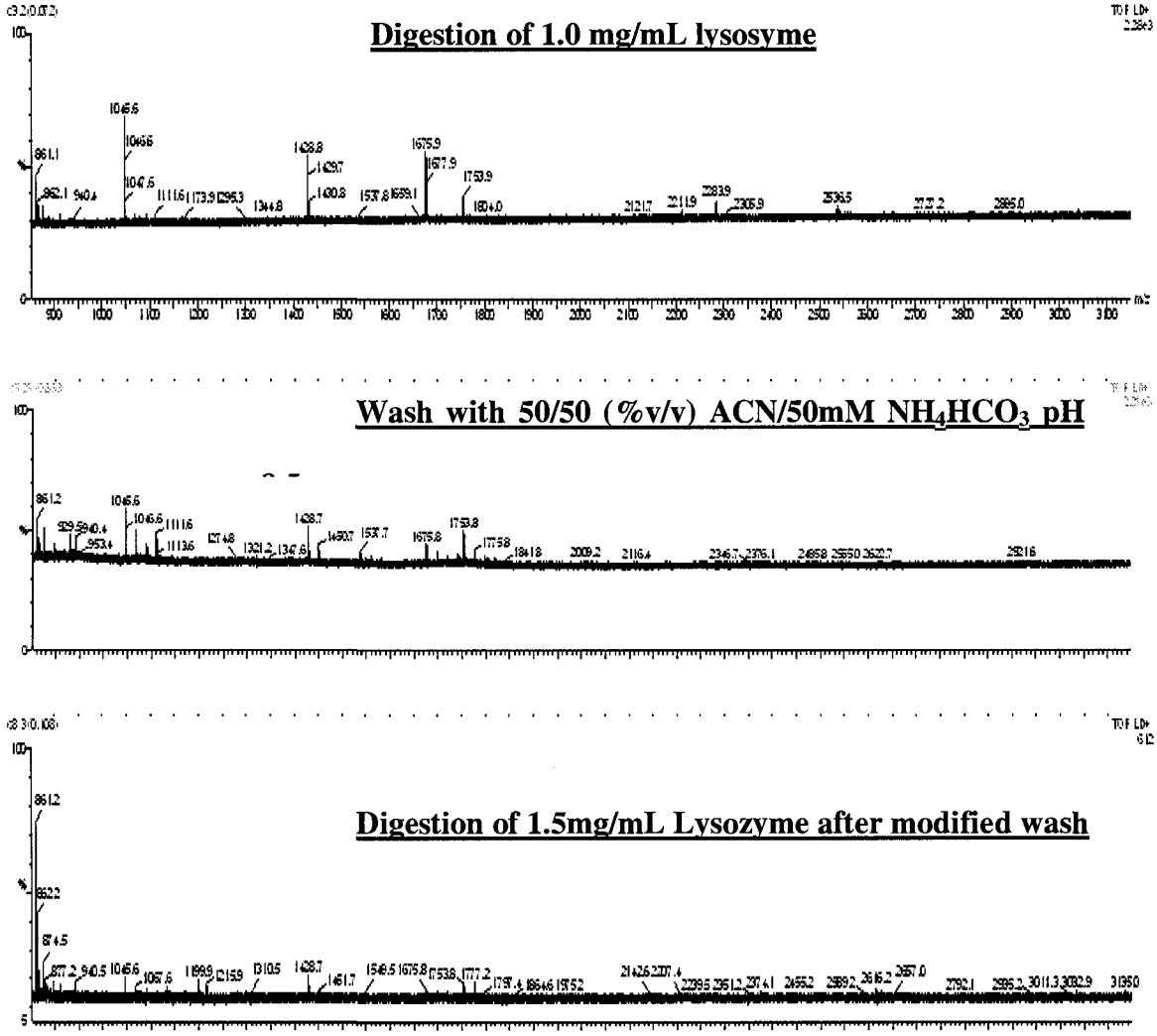

Figure 6–13 : Loss of activity resulting from washing with a more hydrophobic solvent as measured by the digestion of 1 mg/mL lysozyme solution in 50mM NH_4HCO_3 pH 8.5 at ~0.5 uL/min (~6.5 cm/min) for 60 minutes at room temperature measured by MALDI-TOF MS analysis in (+ve) on a 5 minutes GMA-grafted 3 days trypsin-immobilized poly(AMPS-co-BAC-co-BDDA) monolith.

As with many other enzymes, trypsin is known to be solvent sensitive resulting in its denaturation [269]. Given that the supporting monolith is relatively hydrophobic,

exposure to acetonitrile probably resulted in the trypsin unfolding but strong interaction with the monolith surface prevented successful refolding. As acetonitrile is relatively hydrophobic, the same procedure was repeated by replacing acetonitrile with methanol but resulted in the same loss in activity even when added at 20% in the mobile phase.

Retention of peptides and slow loss of activity could limit the usage of the microreactor to a fixed number of digestions and demand a better cleanup procedure. Analysis of wash eluates has shown that carry-over was efficiently prevented between digestions through a one hour hydrodynamic conditioning with the digestion buffer but is not ideal for high-throughput applications.

The grafted microreactor has demonstrated the potential for reproducible and rapid proteolytic digestion of model proteins. To demonstrate if the microreactor could be used for on-line mass spectrometric analysis the microreactor was used as the column on a μ-HPLC system connected to an ESI-QTOF mass spectrometric system. To start, continuous infusion was used to determine if it was possible to detect peptides in real-time.

Figure 6–14 shows the peptide mass spectra of the eluted peptides and subsequent buffer washes. It clearly demonstrated that the microreactor provided relatively good proteolytic efficiency and functioned in an on-line mode. Protein identification was achieved based on an automated protein identification algorithm combined with an integrated peptide map database (ProteinLynx), but required at least a 15 second integration resulting in a sequence coverage of 31%.

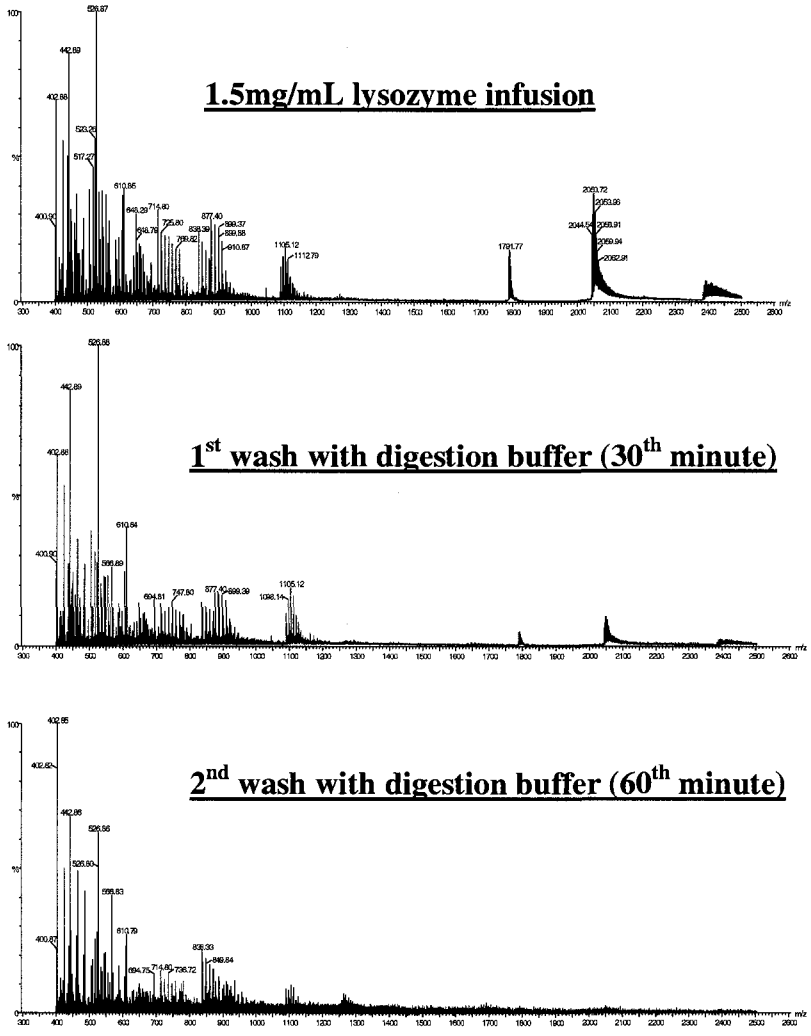

Figure 6–14: Continuous direct infusion on a 19 cm GMA-grafted trypsin-functionalized monolith at room temperature of 1.5 mg/mL lysozyme in 50mM NH_4HCO_3 pH 8.5 (top trace) sampled at 30 minutes into wash (middle trace) and at 60 minutes wash (lower trace) All ESI-QTOF MS spectra in (+ve) mode but non-optimized conditions (Section 2.5). Mass spectra are from an accumulation of 15 seconds of data.

Deconvolution of heavier ions enabled detection of undigested lysozyme as well as multiply charged fragments in both MS spectra collected during infusion of lysozyme

and washing with the digestion buffer. The necessity for an hour-long reconditioning with the digestion buffer was confirmed by averaging of the last 5 minutes of conditioning which did not exhibited signs of either lysozyme peptides or protein fragments.

Even though these findings might appear not very exciting with regards to the microreactor capacity in high-throughput applications, these experiments clearly showed that the microreactor could be employed in an on-line mass spectrometric approach. The next step was to try the microreactor for the on-line digestion of (electro)chromatographic protein peaks followed by their on-line detection by ESI-QTOF. The lysozyme data suggests that to digest and detect the proteins in a complex mixture would require that the chromatographic peaks have a minimal width of 15 seconds with concentrations over 1.5 mg/mL.

6.3.5 Eletrochromatographic Microreactor

Initial experiments with electrokinetic injection of proteins onto a trypsin-functionalized monolith showed a decrease in EOF based on the longer IS migration time (Figure 6–15). Recall that EOF is generated at the liquid-surface interface and immobilized trypsin (pI of 10.1 to 10.5 [270]) acts as a poly-ionic surface that will also participate in EOF generation and at a pH of 8.5 will generate a reverse EOF and slow the overall EOF as shown.

When operating in CEC mode, these monoliths suffered frequent occurrence of bubble formation leading to failure of the monolithic microreactor. Bubble formation is

generally thought to be induced by discontinuities in the chromatographic bed resulting in high electric field gradients that cause localized Joule heating of the solvent [271]. This phenomenon never occurred with non-grafted monoliths so a disruption of the monolith morphology appears to be associated with the grafting and/or immobilization process. Even though capillary rotation was employed to improve homogeneity of grafting, it appeared that the monolith surface included discontinuities. Joule heating is related power dissipation and the higher current generated with the 50 mM NH_4HCO_3 digestion buffer was mitigated by using 5 mM NH_4HCO_3 pH 8.5. With this buffer, electrochromatographic digestion of BSA was achieved. Comparison of the electrochromatographic pattern obtained from separation of the undigested BSA and its homolytic digest on a control monolith is shown in Figure 6–15.

From these results it is clear that there was significant decomposition of BSA into a smaller, broader unresolved multiplex of peaks relative to the control column. On-line generated peptides were not observed as new major peaks most probably because of their low concentration and coelution with BSA. This demonstrated that proteolytic digestion was achieved during elution of BSA on the modified monolith. Because digestion occurred while BSA traveled along the modified monolith, the resulting peptide peaks are broad and overlapping. This can be contrasted to the electrochromatogram from the homolytic digest of the same BSA solution (Figure 6–15) on the control column that shows separation of many peptides and potentially undigested BSA.

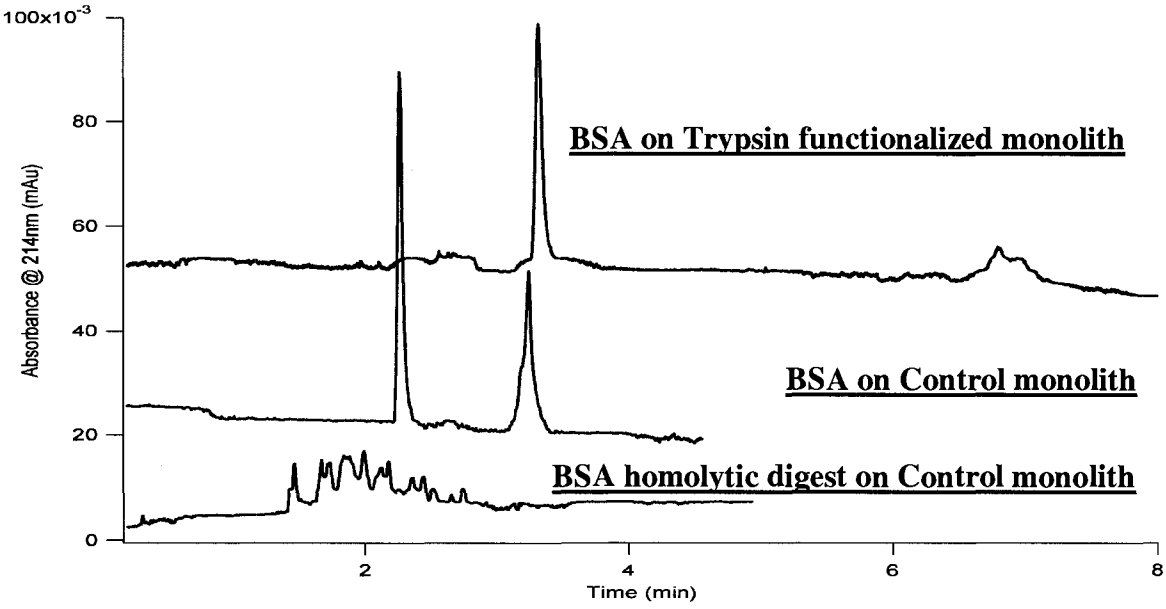

Figure 6–15: CEC digestion/separation of a 0.5 mg/mL BSA sample with thiourea as an I.S. on a trypsin-functionalized (top electrochromatogram) and control monolith (middle electrochromatogram) as well as CEC separation of the homolytic digest of the same solution on the control monolith (lower trace). Separation conditions: injection at 5 kV for 2 sec, separation at 7 kV at room temperature, mobile phase consisted of 5 mM NH_4HCO_3 pH 10.0, detection at 214 nm. The monolith segment was 19 cm long with a total length of 35 cm and an internal I.D. of 100 μm.

Enhancement of resolution on the trypsin column would be beneficial as multiple proteins could be injected/separated and digested on the same monolith. This could be achieved with the current monolith through applying the following strategies alone or in combination. First, improvement of digestion conditions (temperature, buffer, trypsin density) specifically to enhance a more rapid and complete generation of peptides early enough on the microreactor to enable their electrochromatographic differentiation on the remainder of the column. Second, using a digestion pause between injection and

application of the separation voltage could allow the necessary contact time while restricting the peptides to a smaller geometric/chromatographic zone. Third, increasing the monolith bed length and optimizing the separation conditions is a simple method of resolution enhancement.

If alternate column designs are considered the first place to start is to significantly reduce the peptide interaction with the monolith. As previously noted, this is the major limitation to the current monolith. With reduced retention there will be less bandbroadening but at the cost of chromatographic differentiation. The electrophoretic separation mechanism would still act on the peptides and there is ample CE literature to show that high-efficiency peptide separations are possible. In fact, several reviews have already been dedicated to such application in addition to the previously cited one from Bandilla [272, 273,274]. Alternatively just a short section of the top of the column could be photografted and immobilized with trypsin and the remainder grafted with "good" chromatographic moieties but these would need to function in aqueous mobile phases.

To summarize the findings presented in this chapter, on-line electrochromatographic digestion and differentiation of model proteins has been described. The proteolytic efficiency and reproducibility, which is critical to any analytical method was 1 to 5 % in terms of sequence coverage which were obtained respectively for BSA and lysozyme. Reproducibility was affected by many factors not only from the sequential manufacturing processes but also from the digestion procedure.

Particular attention was directed to consistently using the same grafting and immobilization process and providing adequate washing in-between runs.

Efficient digestion and identity confirmation of model proteins was possible using both manual application of pressure on a short microreactor as well as high-pressure from a bomb or HPLC pump. Consistent digestion activity, as monitored through MALDI-TOF MS, was possible for at least 10 consecutive digestions. Peptides retained on the microreactor could not be washed with organic solvent without destroying trypsin activity so a long washing procedure with the digestion buffer had to be performed between runs.

These findings show the versatility of reactive monolithic stationary phases as both a reactor and reactor/chromatographic system. Employing the reactor in a high-throughput proteomic application demands lower peptide retention either through better column washing/elution procedures or modification of the monolith. Further issues associated with bubble formation in electrochromatographic conditions would have to be investigated even though they are not problematic for hydrodynamic applications.

Chapter 7

Boronate Immobilized Monoliths for Glyco-protein Affinity Electrochromatography

In the previous sections, the results were devoted to the characterization and modification of two model monolithic stationary phases to demonstrate the potential of monolithic stationary phases for (electro)chromatographic applications and efficient proteolytic supports. This section explores a modified reactive monolithic stationary phase for the separation of glycosylated proteins. Protein glycosylation introduces, usually selectively, sugar moieties and polysaccarides onto the polypeptide but usually produces only slight variations in a protein structural properties and thus poses a formidable challenge to the separation scientist. The kinetic advantage of monolithic stationary phases over other types of packings should make them a better choice for efficient glycosylated protein separation methods.

A wide number of applications involving chromatographic differentiation of simple and complex carbohydrates have employed the non-specific interaction between aminated ($-NH_2$) functionalized chromatographic stationary phases and sugar moieties [275,276]. Able to provide sufficient resolution for the separation of small glycosylated molecules, the bond strength between amines and carbohydrate hydroxyls is neither strong nor selective enough to enable resolution of glycosylated proteins from their non-glycosylated counterparts. On the other hand, boronate moieties have high selectivity for the affinity extraction and separation of glycosylated proteins [277].

This chapter describes the production of a boronate-functionalized monolith, its spectroscopic characterization followed by its (electro)chromatographic properties with glycosylated proteins.

7.1 Fabrication of a Monolithic SP with Boronate Moieties

Preparation of boronate modified poly(GMA-co-TRIM) monolith is described in Section 2.6.4. Already reported for separation of glycosylated proteins [278,279] aminophenyl boronic acid (APBA) immobilization proceeds via an SN_2 substitution in neutral or basic conditions [280,281], a scheme similar to those described for the direct and linker-mediated trypsin microreactors (see Figure 6–2).

One major advantage of the APBA reaction in comparison to trypsin is its thermal stability allowing higher reaction temperatures that promote rapid epoxide reactions with APBA. Also, APBA immobilization can be tuned through adjustment of pH to acidic conditions, which is not possible with trypsin.

7.1.1 Spectroscopic Characterization

Spectroscopic analysis of the boronate-modified monolith was performed to probe the immobilization of the boronate. The volume requirements of the spectrometers required larger monoliths that were prepared, and modified, in eppendorf tubes using the same procedures as within capillary columns.

^{1}H-NMR analyses were performed on unmodified monolith, boronate-modified monolith as well as pure APBA (typical NMR spectra are shown in Appendix B). NMR experimental details are described in detail in Section 2.4.5.

Fourier-Transform Raman spectroscopy was used for detection of immobilized boronate. Thus a series of unmodified, boronate-immobilized as well as aniline-modified monoliths were measured (Section 2.4.5)

Analysis of the boronate-modified monolith ^{1}H-NMR spectra revealed contamination peaks from toluene, a porogenic solvent, as denoted by the characteristic peaks at 2.173, 7.160, 7.184, and 7.234 ppm. Thus, a more careful and extended washing procedure would have been beneficial. Other solvent peaks arose from both chloroform (7.3 ppm) and water (1.6 ppm) used in the final conditioning and washing of the modified monolith. No resonance frequencies from APBA were observed in the modified monolith but contamination from chloroform could have masked the APBA. In addition to the spectral background introduced by solvent contamination, the low solubility of the monolith resulted in formation of a highly scattering aggregate in the NMR solvent over time.

As the accessible NMR system did not have solid state cross-polarization magic angle spinning (CP/MAS) nor a boron detector, APBA immobilization could not be confirmed through this analytical methodology. The lack of APBA signal could also have been caused by low sensitivity so the APBA concentration was doubled during immobilization but did not improve the ^{1}H-NMR spectra (data not shown).

Raman spectroscopy is known to be effective for the rapid analysis of highly scattering solid samples using a very simple instrumental setup. It was thought that this technique could provide a more sensitive approach for detection of immobilized boronate. The Raman measurements (Section 2.4.5) confirmed the presence of APBA on the modified monolith as shown in Figure 7–1 as highlighted by the appearance of several bands over the bare unmodified monolith.

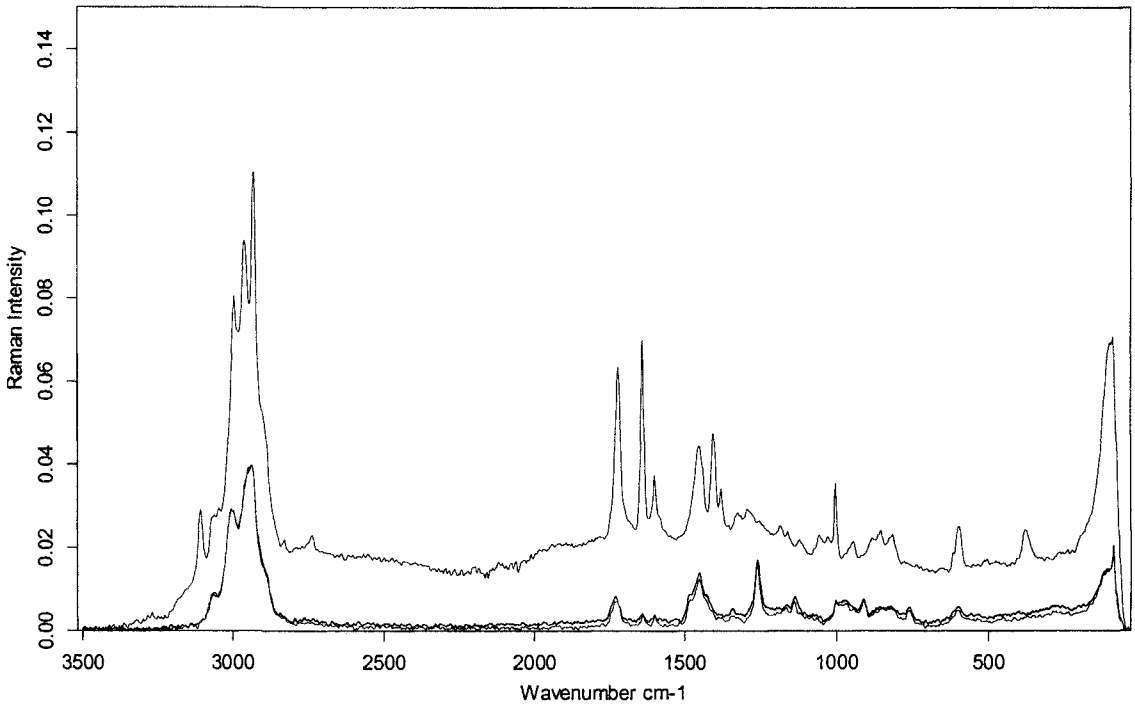

Figure 7–1: Raman spectra of two unmodified (two lower/blue traces) and boronate-immobilized monoliths (upper/pink trace).

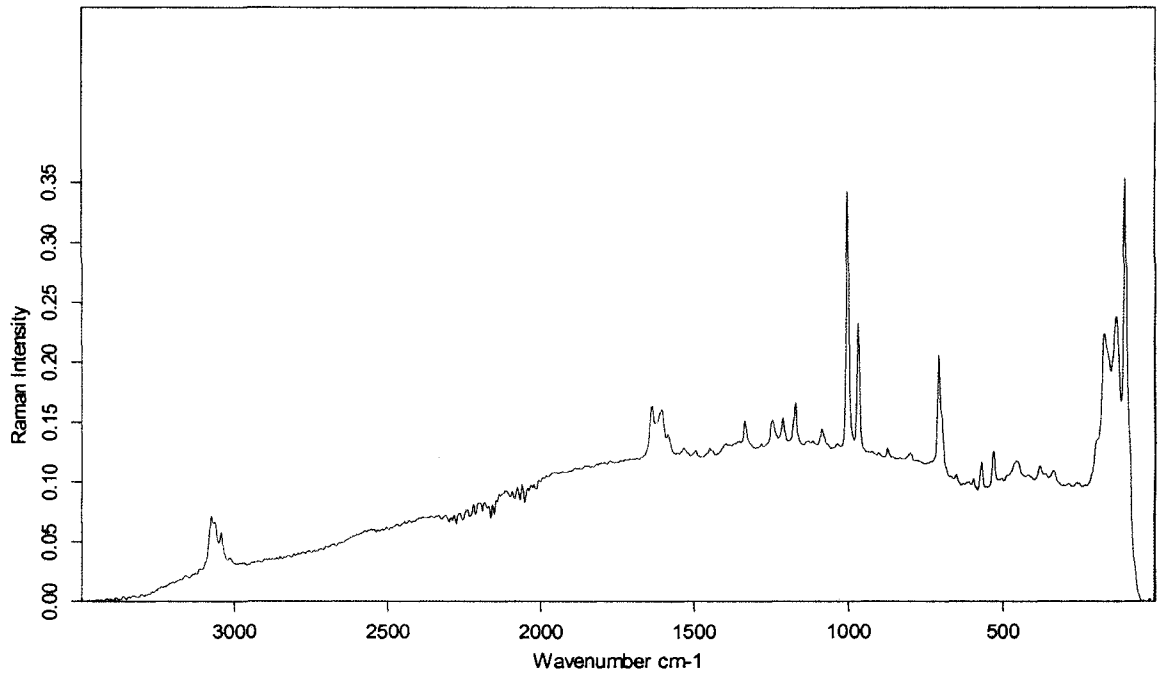

Figure 7–2: Raman spectrum of pure APBA.

A Raman spectrum of APBA confirmed that bands observed on the APBA-functionalized monolith at 3095 cm^{-1}, 1637 cm^{-1} and 1003 cm^{-1} were from APBA. Other weaker bands (1605, 969, and 710 cm^{-1}) were not observed very clearly on the modified monolith, most probably because of diminished molecular vibration associated with immobilization.

One could argue that some of the observed bands could have been attributed to toluene and/or BME which both possess phenyl rings. In the case of BME, which is incorporated into the polymer, Raman signals would have be expected in both modified and unmodified monoliths. Toluene is also characterized by phenyl Raman bands, *i.e.* at 3160, 1215 and 1010cm^{-1} but would only be detected if insufficient washing was applied to all the monoliths, which was not the case. To validate that these phenolic bands could

be observed when a phenolic compound was introduced onto the monolith, aniline (phenylamine) was reacted with the monolith.

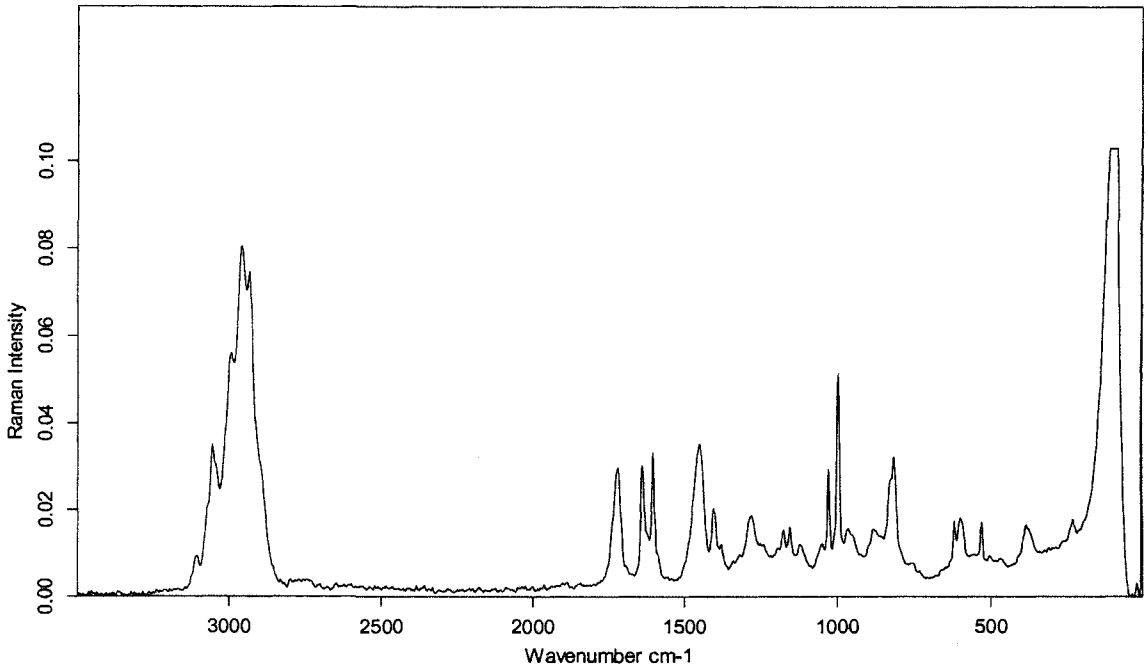

Figure 7–3: Raman spectrum of aniline- immobilized monolith.

Immobilization, via a similar synthetic scheme (Section 2.6.4), resulted in the appearance of several peaks also observed with the APBA-immobilized monolith. These peaks included a weak band at 3105 cm^{-1}, a strong band at 1638 cm^{-1}, a medium band at 1403 cm^{-1} and a last one at 597 cm^{-1}. Other bands that were found in pure aniline were also preserved at 1028 and 996 cm^{-1}.

Thus, the appearance and preservation of many bands associated with the introduction of the phenolic-immobilized compounds pointed to the successful immobilization of both APBA and aniline. The disappearance of a major peak at 1259 cm^{-1} from all modified monolith spectra, initially present in the bare monolith, in a

spectral region associated with oxirane ring vibrations, also confirmed the occurrence of surface immobilization. From these spectroscopic measurements, it was concluded that opening of the oxirane ring occurred through a SN_2 mechanism similar to that described for protein immobilization (Figure 6–2) resulting in the introduction of boronate moieties on the monolithic stationary phase.

Knowing that this strategy enabled the fabrication of a boronate-modified monolithic stationary phase through direct reaction with the monolith surface, the next step was to prepare glycosylated proteins and see if the stationary phase enabled differentiation of glycoprotein from its non-glycosylated counterpart.

7.1.2 Synthesis of Model Glycoproteins

Production and characterization of glycosylated and non-glycosylated proteins was carried out due to limited commercial access to such products and is presented in this section.

As detailed in the experimental section (Section 2.6.4), the first approach for the production of a glycosylated – non-glycosylated protein pair was based on the deglycosylation of RNase B, a 13.5 kDa protein with a total sugar mass of 1.5 kDa attached to its primary structure, through an enzymatic-mediated scheme.

Mass spectrometric analyses of both the intact and deglycosylated RNase B were carried out employing ESI Q-TOF mass analysis (Section 2.5). The soft ionization conditions and high-resolution provided a spectrum with a charge envelope characteristic

of multiple charged macromolecules. Generation of the charge envelope was caused by the formation of multiply charged protein ions in the ESI source, and this is employed to calculate the original protein mass as demonstrated in the following equation.

(Equation 15) $P_i = \frac{M + Z_i}{Z_i}$

Equation 15: Experimental mass for a peak P_i with a charge Z_i both relating to the protein actual mass M [282].

To calculate the protein mass M deconvolution is applied via an iterative calculation that computes a protein mass able to generate the experimental charge envelope.

The mass spectra for intact and deglycosylated RNase B show a definite loss in mass for the deglycosylated protein and deconvolution results indicate a loss of 1,367 Da. The deconvoluted protein masses were calculated to be 15,050 and 13,683 Da, a difference of 7 Da compared to the expected value. The 1,367 Da difference was associated with the loss of a 6-mannose unit oligosaccharide including 7 water molecules as RNase B is known to have a carbohydrate chain consisting of 2 N-acetyl-glucosamine units plus 5 to 9 mannose sugars. However, the 7 Da error could have been caused by the presence of multiple reaction impurities in the sample generated from the deglycosylation reaction yielding a noisy mass spectrum baseline. Noisy baselines hamper mass deconvolution and result in lower (calculated) mass accuracy. Such interferences usually produce a major peak and multiple smaller ones on deconvolution. As the protein primary structure exhibited at least a dozen ionizable amino acids, protonation of some of

these amino acid residues due to the addition of TFA to the protein solution could have also influenced the final calculated mass.

To further corroborate these results, both proteins were subjected to MALDI-TOF MS characterization which typically produces singly ionized species.

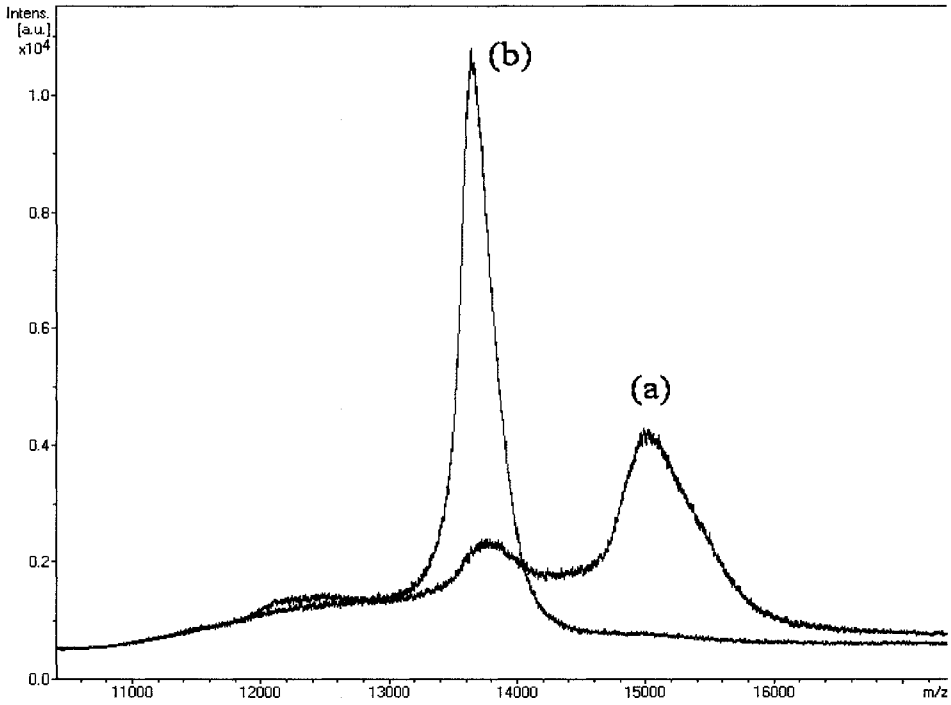

Figure 7–4 : MALDI-TOF spectra of (a) intact RNase B and (b) deglycosylated RNase B in (+ve ion) mode. No further investigation for identification of the minor peak in the intact RNase B was achieved.

From the MALDI-TOF MS spectras shown in **Figure 7–4**, the predominant masses for the intact and deglycosylated RNase B were respectively 14,988 and 13,641 Da, slightly lower than the masses calculated from the ESI-QTOF measurements. The resulting loss caused by enzymatic deglycosylation was very close to what calculated through ESI-QTOF with a loss of 1,347 Da, *i.e.* a difference of 20 Da. Indeed, this difference correlated with the first hypothesis extrapolated from the ESI-QTOF results

where protonation and formation of an aggregate in the ESI interface between the protein and heavier atoms such as potassium or sodium or simply the presence of these atoms in the protein structure would have caused a small deviation between expected and observed masses. Overall, both mass spectrometric techniques confirmed the efficiency of the enzymatic deglycosylation for the generation of deglycosylated RNase B. Interestingly, the intact RNase B MALDI spectra also presented a second less intense peak with a mass close to the deglycosylated RNase B. It was thus suspected that RNase B also contained naturally its deglycosylated counterpart.

A second, more general, approach was also employed for the generation of glycosylated/non-glycosylated myoglobin and BSA protein pairs. These proteins were selected to enable investigation of potential size-exclusion or size effects with the boronate-immobilized monolith. Glycosylation was attempted through two different Maillard reaction schemes as described in Section 2.6.4.

ESI-QTOF analyses of both glycosylated and intact myoglobin and BSA through the first Maillard reaction scheme did not reveal the addition of sugar moieties, expected through sequential addition of 180 Da with each sugar moiety.

As shown in Figure 7–5, the deconvoluted mass for myoglobin subjected to the first Maillard reaction scheme was 16,951 Da, identical to the intact myoglobin (not shown). Attempted glycosylation of BSA also failed to demonstrate any glycosylation.

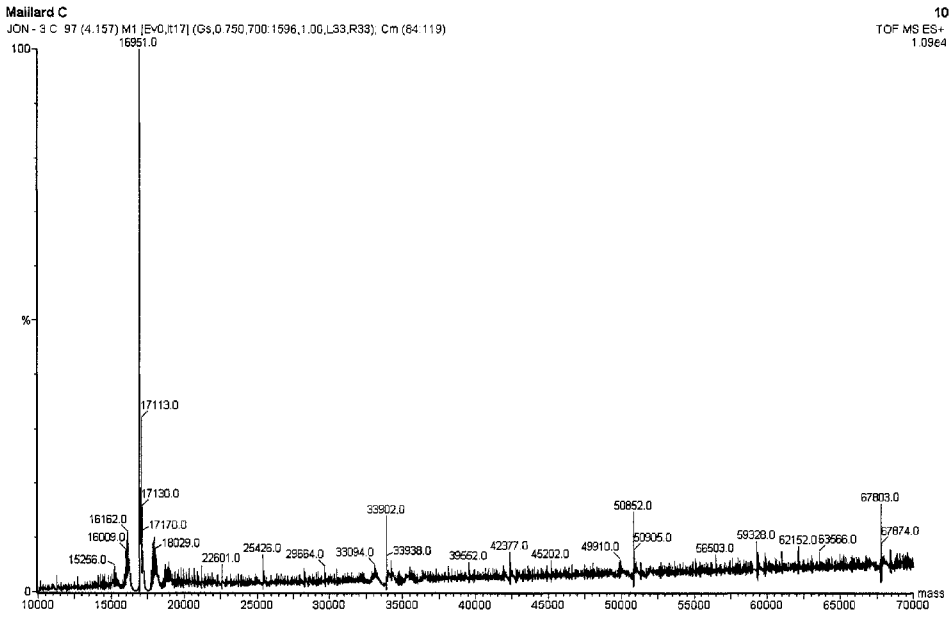

Figure 7–5 : Deconvoluted ESI-QTOF MS spectrum of myoglobin subjected to the first Maillard reaction scheme.

For the second Maillard scheme, ESI-QTOF analyses of glycosylated BSA and myoglobin resulted in noisy mass spectra hampering accurate mass deconvolution (not shown). The deconvolution algorithm is prone to spurious peaks because it tries to interpret them as members of the proteins charge envelope. These peak artefacts were probably caused by inefficient desalting and dialysis procedures resulting in cluster formation with unreacted sugars and Maillard reagents and are especially problematic for ESI-QTOF analysis performed through direct infusion.

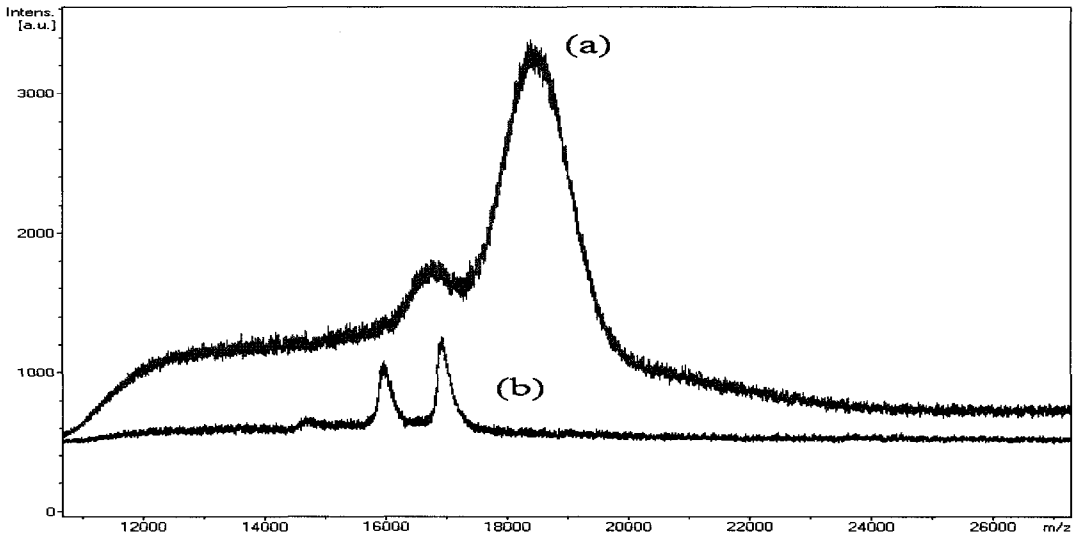

Figure 7–6: MALDI-TOF MS spectra of (a) myoglobin subjected to the second Maillard reaction scheme and (b) intact myoglobin.

MALDI-TOF analysis yielded the cleaner mass spectra shown in Figure 7–6 demonstrating an increased mass. MALDI-TOF is less susceptible to the presence of concomitant species such as salts and sugars. It allowed detection of two proteins in both intact and glycosylated protein mixtures. Even though the peaks observed in MALDI-TOF were relatively broad, their resolution was sufficiently high to confirm occurrence of glycosylation of both protein peaks albeit with a wide ranging gain in mass.

Overall, out of the three approaches employed for the generation of a glycosylated and non-glycosylated protein pair, the enzymatic deglycosylation of RNase B provided the most efficient and simple methodology and will be the protein used for the further assessment of the boronate-functionalized monolithic stationary phase chromatographic properties.

7.1.3 Electrochromatographic and Chromatographic Differentiation

One of the basic requirements of a stationary phase for its use as an electrochromatographic support is its ability to generate constant and sufficient EOF flow, along its entire surface, to enable movement of the mobile phase. Thus, the APBA-immobilized monolith was tested for its ability to generate and support constant EOF. The unmodified poly(GMA-co-TRIM) monolith is not able to generate EOF due the lack of ionizable groups so ionization of the boronate moiety was required.

Stronger affinity interaction between boronate and sugar cis-diols requires a pH close to, or over, APBA's pKa of 8.5. A 5 mM borate buffer pH 10.0 /ACN 75/25 (%v/v) was employed for this investigation. The HPLC system (described in Section 2.2) was used to make multiple injections of thiourea, a neutral marker, onto the column operating in CEC mode. Without application of external pressure on the APBA-modified monolith, a constant current (6.2 μA) was observed while elution of the neutral marker at 3.15 minutes in CEC conditions demonstrated that the modified monolith was able to generate a constant EOF, as depicted in Figure 7–7.

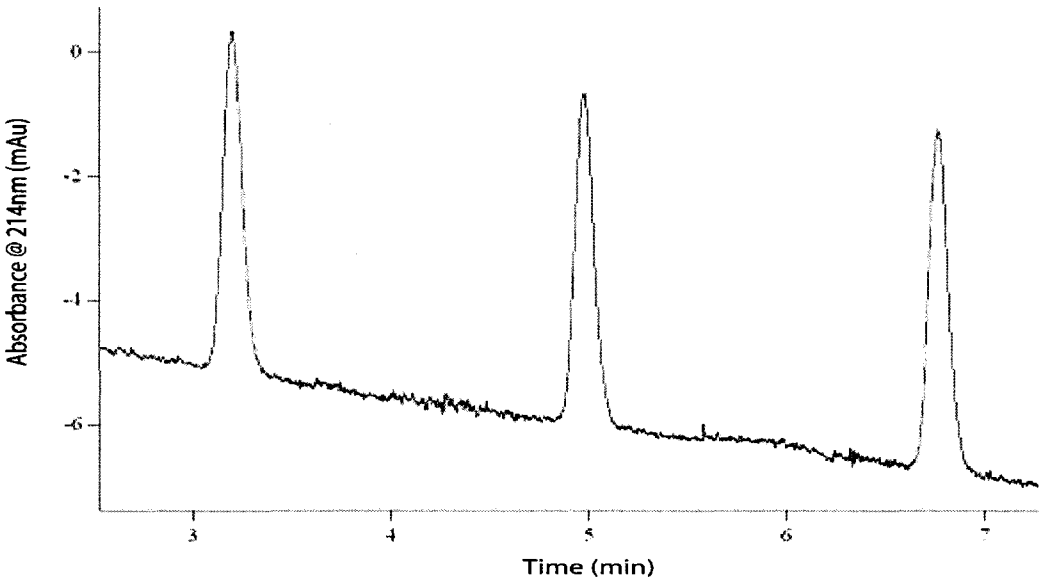

Figure 7–7: Three 10 µL sequential injections, separated by 1.81 minutes, of 1.8 mg/mL thiourea. Applied voltage of 13 kV. Separation in 5 mM borate buffer pH 10.0 /ACN 75/25 (%v/v) and detection at 214 nm.

As seen on Figure 7–8, multiple injections of thiourea (three per run) in electrochromatographic conditions resulted in a reduction of thiourea migration time representative of either a loss over time in the EOF caused by slow removal of APBA from the monolith or blocking of the porous network. The current increased by 0.15 µA from the first run to the last one which theoretically correlates with an increase in the monolith permeability or porosity. In repeated experiments it was observed that the occurrence of bubble formation increased significantly during the run. These findings are suggestive that the surface density of APBA was not high enough to support a strong EOF and that APBA may have been shed from the column.

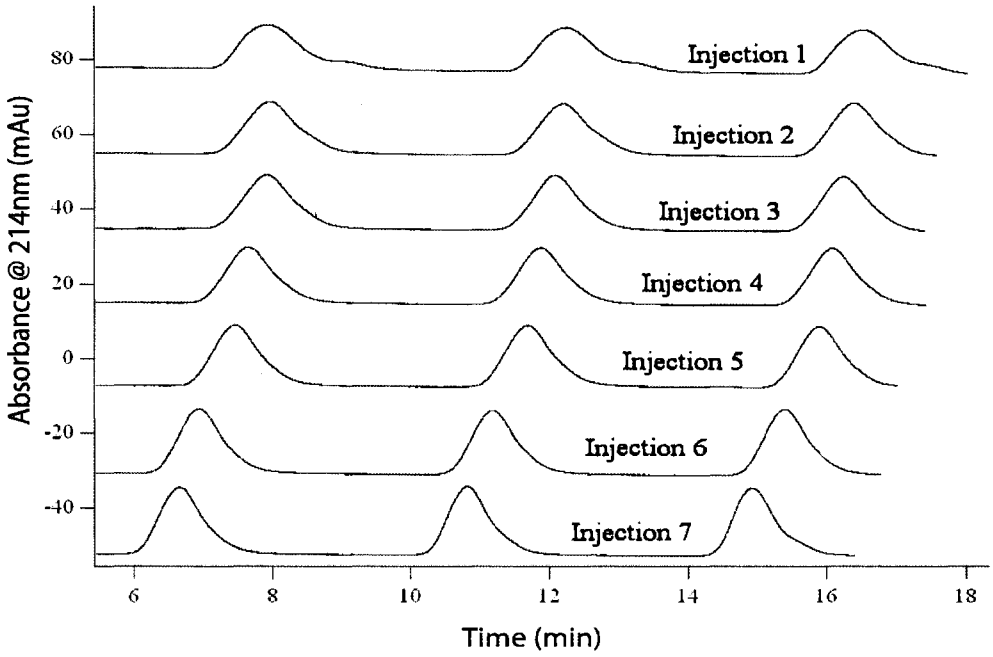

Figure 7–8: Reproducibility of thiourea elution over time in CEC conditions at 10 kV. Each electrochromatogram represented three serial injections of thiourea for a total of 21 injections in seven sequential runs. Separation in 5 mM borate buffer pH 10.0 /ACN 75/25 (%v/v) and detection at 214 nm.

Interestingly, injections of BSA (and pepsin) did not result in CEC elution even for total run times exceeding sixty minutes. Hydrodynamic injection, and elution, of pepsin was carried out and clearly showed elution. There are a few possible explanations for this difference in behaviour. It was thought that BSA and pepsin might not be eluting since APBA is known to undergo autopolymerization potentially leading to restriction or blockage of the porous system [279]. But successful flushing/conditioning, observation of CEC current and the EOF elution of thiourea eliminated this possibility. A much stronger argument would be that the APBA (phenyl rings) was acting as a strongly absorbing stationary phase and retained these species in the weak 5 mM borate buffer pH

10.0 /ACN 75/25 (%v/v) mobile phase but elution in pressure driven mode shows strong but not complete retention. The broad peak shapes also revealed potential interaction with the surface which could have been caused partially by the hydrophobicity of the poly(GMA-co-TRIM) monolithic skeleton.

The remaining explanation was ineffective electrokinetic injection. Recall that negatively charged proteins have a negative mobility and the EOF strength must be large enough to sweep these species into the column.

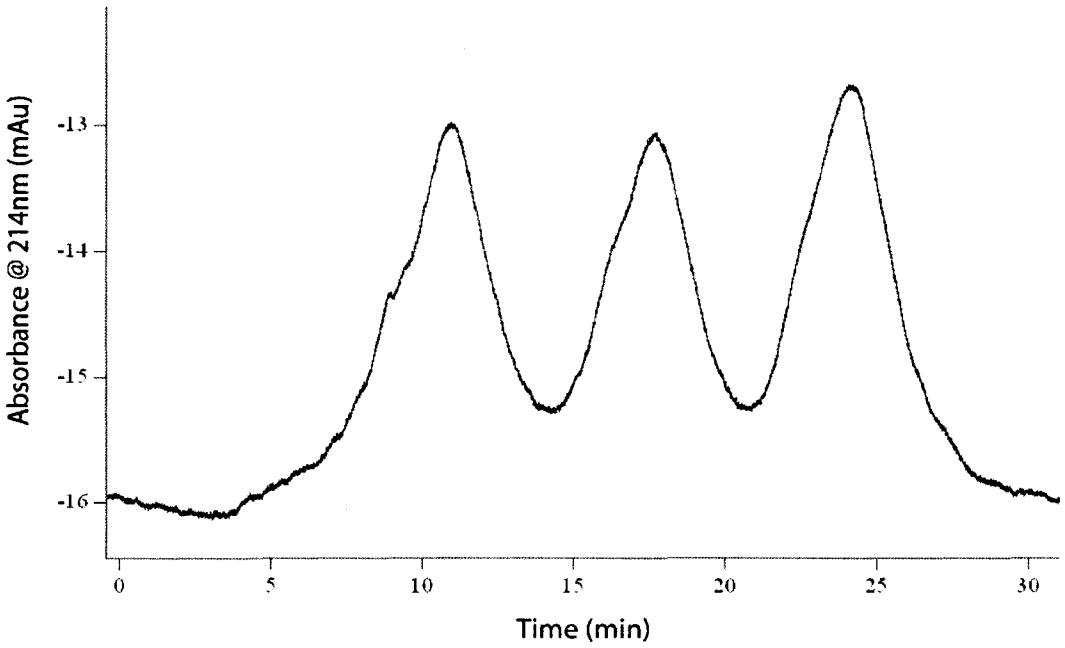

Figure 7–9 : Separation of three serial injections of pepsin (1 mg/mL) in μ-HPLC conditions separated by 6.81 minute intervals in 5 mM borate buffer pH 10.0 /ACN 75/25 (%v/v).

From the experimental data in Figure 7–7 the EOF velocity was +0.99 mm/s at 500 V/cm and previous experiments suggest that BSA would have a mobility of -

1.4 mm/s at 500 V/cm. It can thus be assumed that the proteins were not injected. In order to verify this hypothesis the electric field was reversed so that the higher mobility of the proteins would carry them to the detector. By doing so, the negatively charged BSA and pepsin finally eluted after 5.1 and 5.7 minutes respectively.

To overcome this limitation, pressure-assisted CEC and pure hydrodynamic injections and separations of thiourea (neutral), benzoic acid (negative) and thiamine (positive) were performed to establish if the additional flow created by the application of a hydrodynamic flow could enable both introduction and separation of the negatively charged proteins.

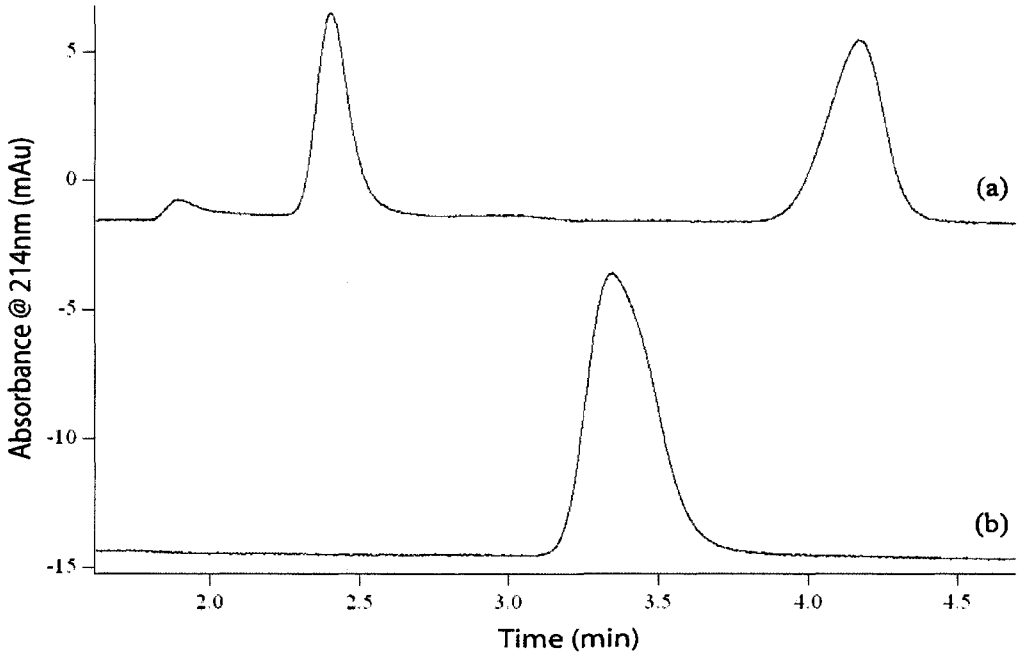

Figure 7–10: Assessment of separation mechanisms involved in (a) pressure-assisted CEC separation of thiourea, benzoic acid and thiamine at 13 kV. The first peak was assigned to thiamine, the second to thiourea and the last to benzoic acid and (b) pressure only separation (all analytes co-eluted). Separation in 5 mM borate buffer pH 10.0 /ACN 75/25 (%v/v). Absorbance measured at 254 nm.

As demonstrated in Figure 7–10, the separation of these three small model molecules was very informative in that the electric field component (electrophoresis) was required to enable the separation of the three molecules. Because the positive and negative compounds could only be separated through electrophoresis, it was concluded that no ion-exchange differentiation mechanism was associated with the introduction of the potential APBA cation exchanger.

Even though this additional information on the chromatographic properties of the monolith helped understanding its basic characteristic, it was still not known if the monolith was able to differentiate a glycosylated protein from its non-glycosylated counterpart. Pressure-assisted separations of deglycosylated RNase B and intact RNase B was investigated as shown in Figure 7–11.

Unfortunately, both the intact and deglycosylated RNase B samples resulted in an identical retention time meaning that the APBA moiety on the monolith did not provide sufficiently strong interactions with the glycosylated RNase B to enable the differentiation of the two proteins. Coelution might also been caused by the excessive amount of residual sugars in sample solution. Supporting this possibility is the negative peak at 2 minutes with the deglycosylated RNase B observed as the excess sugars eluted in the deglycosylated RNase B electrochromatogram.

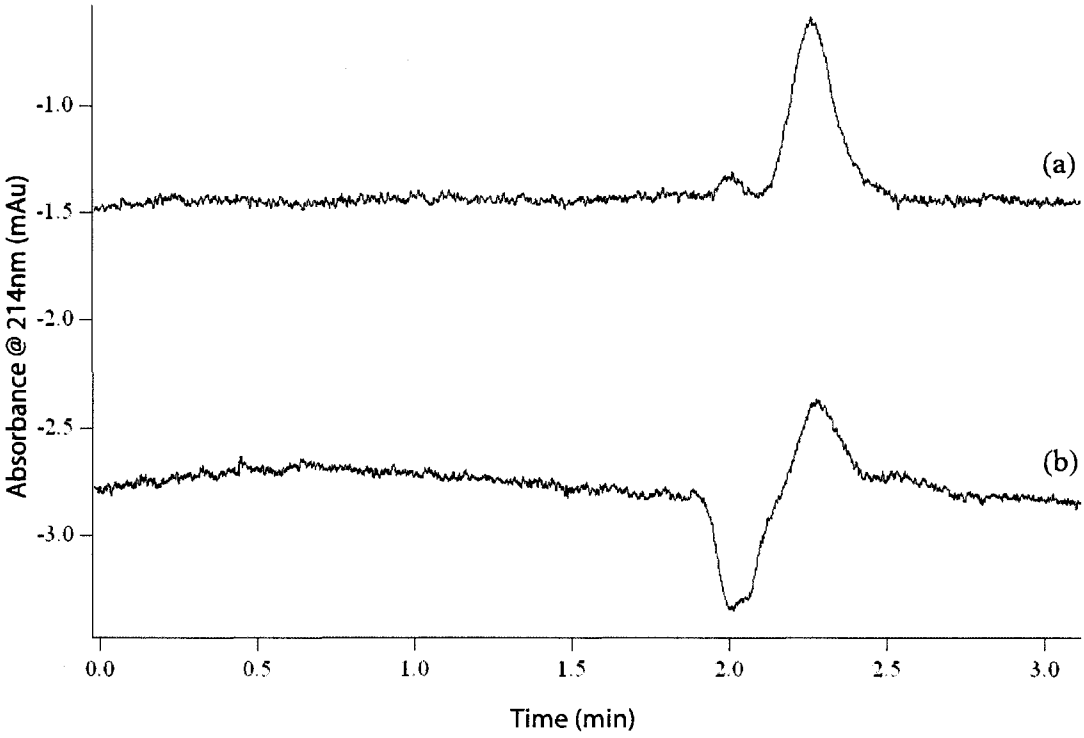

Figure 7–11: Pressure-assisted CEC separation of (a) intact RNase B and (b) deglycosylated RNase B at 13 kV. Separation in 5 mM borate buffer pH 10.0 /ACN 75/25 (%v/v). Absorbance measured at 214 nm.

Thus, it was clear that this monolith was not satisfactory for CEC of glycoproteins and that it would need further modifications to increase the surface density of the boronate and interaction with glycoproteins. Introduction of moieties possessing permanent charges able to generate a strong EOF flow would also be beneficial.

7.2 Other Immobilization Strategies

Motivated by the success achieved through photografting of proteolytic enzymes, a (summer undergraduate) research project was instigated in order to determine if the issues related to the immobilization of APBA could be solved through photografting.

Thus, APBA was reacted using the previously described GMA grafted poly(AMPS-co-BAC-co-BDDA) monolith (see Section 6.3.1 for GMA grafting procedure and Section 2.6.4 for APBA immobilization).

APBA immobilization on the monolith was confirmed through both ICP-MS and CE analysis of cleaved APBA from the GMA grafted monolith by washing with HCl to hydrolyze the bond between the APBA and the monolith surface. Through these measurements, the summer student, Wei Lin, was able to determine that the final monolith contained about 0.24% (w/w) of APBA. EDX analyses of the resulting monolith were performed to assess the surface homogeneity of the grafting process.

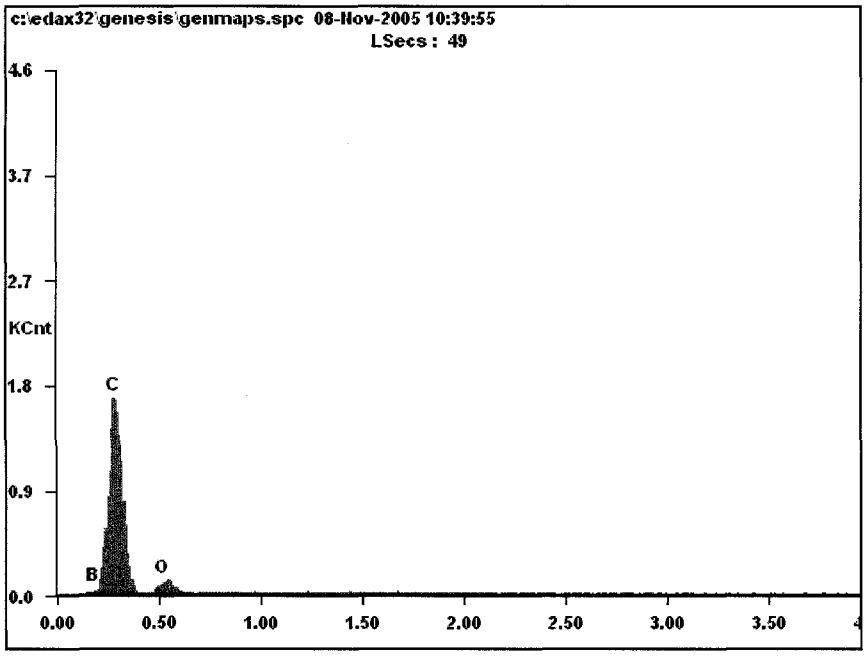

Figure 7–12: Assessment of the surface distribution of boron upon grafting on a poly(AMPS-co-BAC-co-BDDA) monolith through EDX elemental analysis.

While the ICP-MS and CE proved to be successful in determing the total immobilized boronate, EDX elemental analysis revealed an insignificant surface concentration of boron as shown in Figure 7–12. The EDX spectrum showed a higher surface concentration of carbon and oxygen (C & O peaks) in comparison to boron (B). However, EDX is more sensitive to heavier atoms so it was expected to be difficult to observe the presence of boron at the surface.

Later on, it was thought that the lack of chromatographic resolution might have been caused by an inefficient selection of substrates and/or elution conditions. Thus, CEC separation of ovalbumin, a naturally glycosylated and phosphorylated protein was attempted on the same photografted APBA functionalized monolith using a combination of loading and elution buffers.

The preliminary electrochromatogram obtained for ovalbumin in CEC conditions showed three peaks as shown in the following figure. The first two peaks correspond to thiourea, the internal marker, and excess ovalbumin. This data shows that excess ovalbumin was eluted in the loading buffer (Eluent I). When the pH was lowered (Eluent II), and the boronate-sugar ring was disrupted, the remaining ovalbumin was eluted. A similar separation with cytidine, a nucleoside consisting cytosine and a cyclic ribose moiety showed that elution occurred almost exclusively in the elution portion of the electrochromatogram (data not shown). These results are indicative of the interaction of diol sugars with the boronate moieties.

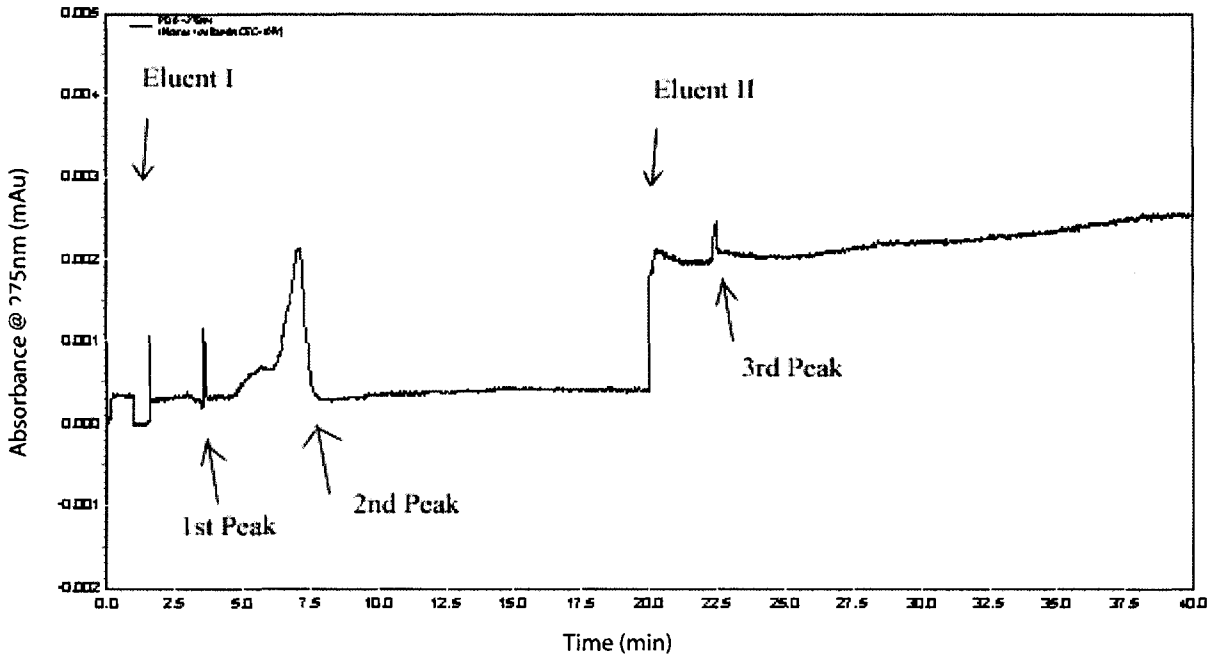

Figure 7–13: Boronate-affinity electrochromatography of ovalbumin at 10 kV with a high pH loading buffer (Eluent I: 10 mM ammonium acetate pH 8.8) and a low pH eluting buffer (Eluent II: 10 mM ammonium acetate pH 3.5). Peak identification: (1) thiourea, (2) excess ovalbumin, (3) retained ovalbumin.

These very promising, but preliminary, results showed that photografting will most probably lead to more robust stationary phases than those obtained through direct reaction of APBA on a monolithic stationary phase. As suggested by the previously developed photografted stationary phases, special attention will have to be directed toward monolith stability and reproducibility.

To summarize the findings described in this chapter, direct immobilization of APBA on a reactive poly(GMA-co-TRIM) monolith did not result in chromatographic differentiation of glycosylated and deglycosylated proteins. It was established that introduction of APBA did not provide a suitable surface for generation of strong, homogeneous, and constant EOF required for CEC. This limitation was overcome using

APBA immobilized GMA photografted poly(AMPS-co-BAC-co-BDDA) monoliths. This is the first description of the electrochromatographic retention and elution of a glycosylated protein through a photografting scheme.

Conclusions, Future Prospects and Thoughts

Throughout this thesis, different aspects of CEC were investigated, some in great detail but many were proof of principle experiments. At the time of writing, approximately ten years has passed since the first CEC applications appeared in the open scientific literature.

Briefly, three major aspects were investigated. First, modification of monolithic stationary phases was achieved through a conservative/conventional approach using modification of the polymerization conditions/solvents. This strategy has also been investigated in other research laboratories involved in the development of monolithic stationary phases. This demonstrated the complex interplay between the morphological and chemical properties of *in-situ* fabricated monoliths. Using these monoliths, separations of model proteins, bovine milk as well as the novel separation of preservatives from a diluted injectable drug were shown. A fair criticism of the CEC literature is the lack of reproducibility of the data, the cornerstone of analytical science. We report that reproducibilities of 5 to 10 % are routinely achievable for inter and intra monolith experiments.

The most extensively used method of monolith morphology characterization is with SEM but application of an innovative AFM characterization methodology in Chapter 3 provides more accurate morphological analysis in both dried and wetted conditions. The developed method should find wider use in the monolith research

community, especially in light of the fact that the monolith porosity can change by as much as 20 % between the dry and CEC solvent swollen state.

While many researchers focus on the potential (electro)chromatographic advantages of monoliths, monoliths were also employed for their great mass transfer efficiency as enzymatic microreactors. With additional work to reduce peptide retention these materials could find extensive use in high-throughput proteomic applications. Three different approaches were employed for the fabrication of trypsin microreactors. Proteolytically-active monolithic microreactors were demonstrated in both electrokinetic and hydrodynamic modes but the most intriguing results were obtained with long electrochromatographic / proteolytic monoliths. This represents the first demonstration of a photografted proteolytic reactor capable of simultaneous electrochromatographic differentiation.

Due to its simplicity, this grafting and immobilization approach can be employed for the integration of chromatographic functionalities and/or proteolytic enzymes within transparent devices such as microfluidic microchannels. High-throughput and high-efficiency applications will require better elution and washing procedures but the path is clear. As proof of principle, a directly-bound trypsin microreactor was used within existing (but not high-throughput) analytical instrumentation for proteomic applications. Experiments carried-out with a novel linker, SATA, did not prove useful but longer linkers should be investigated.

The limited amount of sample consumed with the proteolytic reactors is a considerable advantage for the analysis of minute of samples but is problematic when used in an off-line method due to the time required to collect sufficient amount digestate for mass spectrometric analysis. Considering the relatively short reactor length as well as the digestion efficiency achieved using β-casein as a model protein, the two proteolytic reactor fabrication strategies allowed preparation of efficient tryptic reactors able to handle minute amount of samples.

Returning to CEC, two strategies were employed for the fabrication of boronate-immobilized affinity monolithic stationary phases for the separation of glycosylated and non-glycosylated proteins. Immobilization of APBA was demonstrated spectroscopically for the directly immobilized monolith but did not yield sufficient EOF or interaction with the glycoproteins to be operated in a useful CEC mode. Photografting of GMA and immobilization of boronate increased retention and elution of a model nucleoside and partial retention of ovalbumin was demonstrated. Unfortunately, Eeltink *et al.* [143] just published a paper based on a similar strategy. Thus, future work will involve a different immobilization which is thought to provide a stronger boronate-surface bond as well as improved retention.

In terms of future projects, photografting appears to be a very interesting approach for the development of multifunctional stationary phases and is particularly appealing for microfluidic applications requiring integration of different types of surface chemistries and functions. Thus, many other applications that require the porous

properties of the monolith with the freedom to adjust the surface proprties can be implemented through this functionalization approach. The on-going projects in our research laboratory involving various immobilization strategies for boronate-affinity electrochromatography are a good example of such type of applications.

The AFM methodology developed during this Ph.D. work should be validated for other types of stationary phases. Also, functionalization of AFM tips with specific surface moieties mimicking those encountered in (electro)chromatographic interactions, such as proteins, could be used to better assess surface homogeneity and interactions.

In conclusion, the future prospects of CEC as a field are limited by the lack of instruments that allow an operator to easily switch from μ-HPLC to CEC to CE separation modes and limit the freedom of researchers to explore the possibilities. In parallel to instrumental limitations, the analytical community will have to develop new methodologies for the *reproducible in-situ* fabrication of monoliths especially on a larger commercial scale. The low durability and weak mechanical properties of Teflon-coated capillaries makes them an unlikely contender. Alternative, initiation techniques such as radiolytic initiation can be just as effective as photopolymerization in providing geometrically defined monoliths but in UV-opaque and mechanically resistant polyimide-coated capillaries.

CEC is also beginning to see challengers with the introduction of UPLC as a new highly efficient technique because the 1.8 to 2.3 μm functionalized silica particles produce a significant improvement in separation efficiency over conventional HPLC.

However, it is expected that the ever increasing requirements of faster and more efficient separations will keep CEC in the forefront as a separation technique.

Appendix A: MALDI-TOF Spectra of Digested Proteins

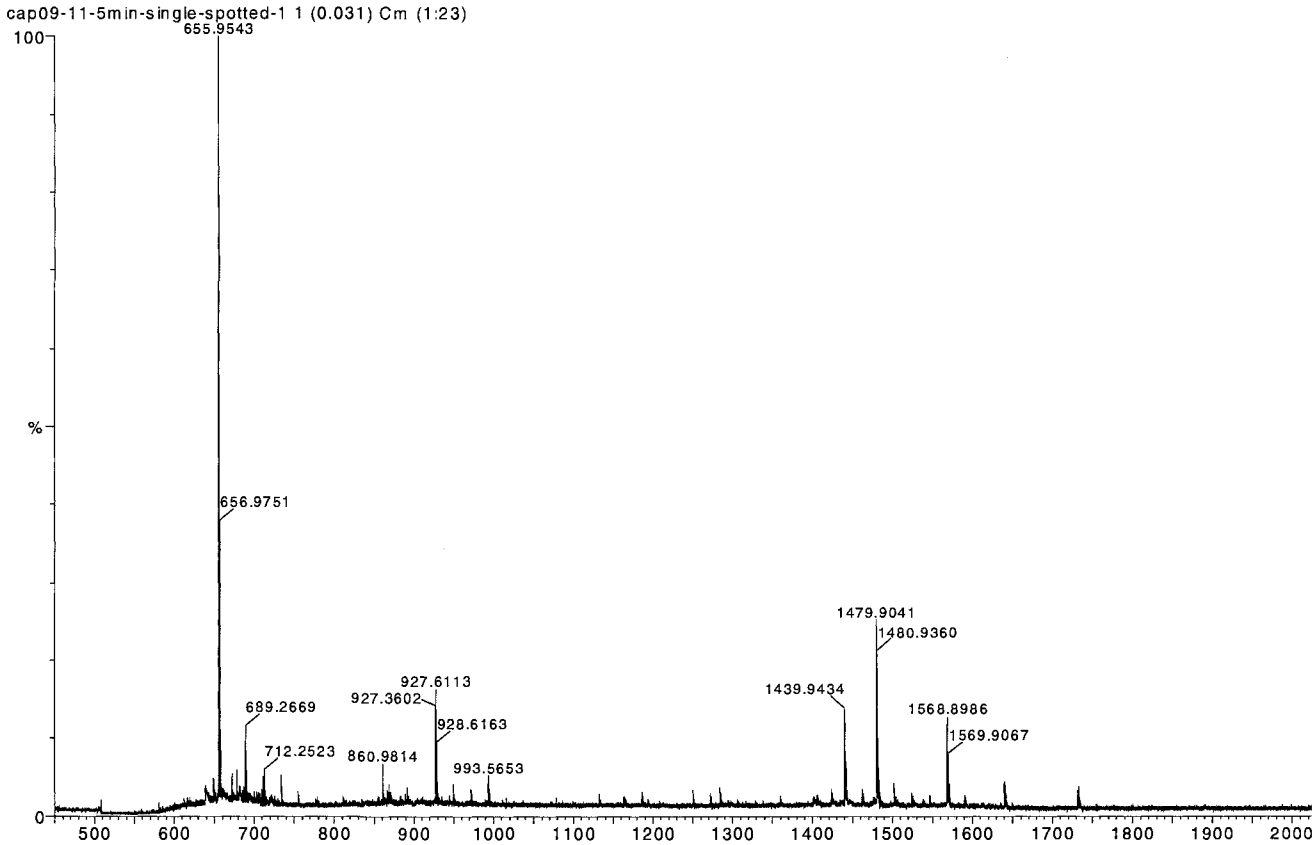

Figure A–1: MALDI-TOF MS analysis in (+ve) mode of on-column proteolytic digestion of 1mg/mL BSA solution in 50 mM NH_4HCO_3 pH 8.5 at ~0.5 µL/min (~6.5 cm/min, 2.9 min contact time). Monolith was GMA-photografted for 5 minutes followed by trypsin immobilization for 60 minutes at room temperature followed by 3 days at 4 °C.

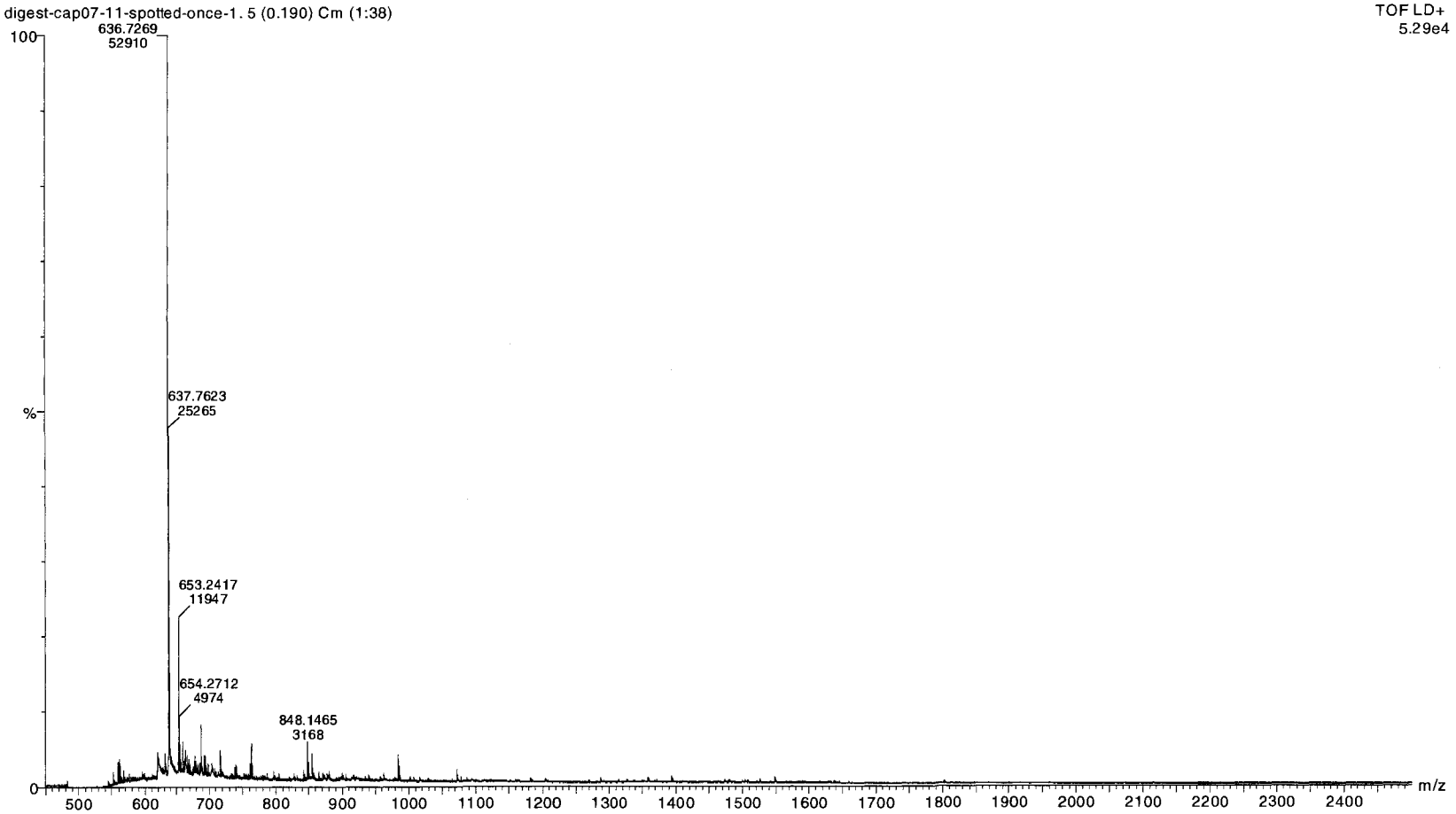

Figure A–2 : MALDI-TOF MS analysis in (+ve) mode of on-column proteolytic digestion of a 1 mg/mL BSA solution in 50mM NH_4HCO_3 pH 8.5 at ~0.5 µL/min (~6.5 cm/min). Monolith was GMA-photografted for 5 minutes followed by trypsin immobilization for 60 minutes at room temperature followed by 2 days at 4 °C,

Appendix B: NMR Spectra of Boronate-grafted modified

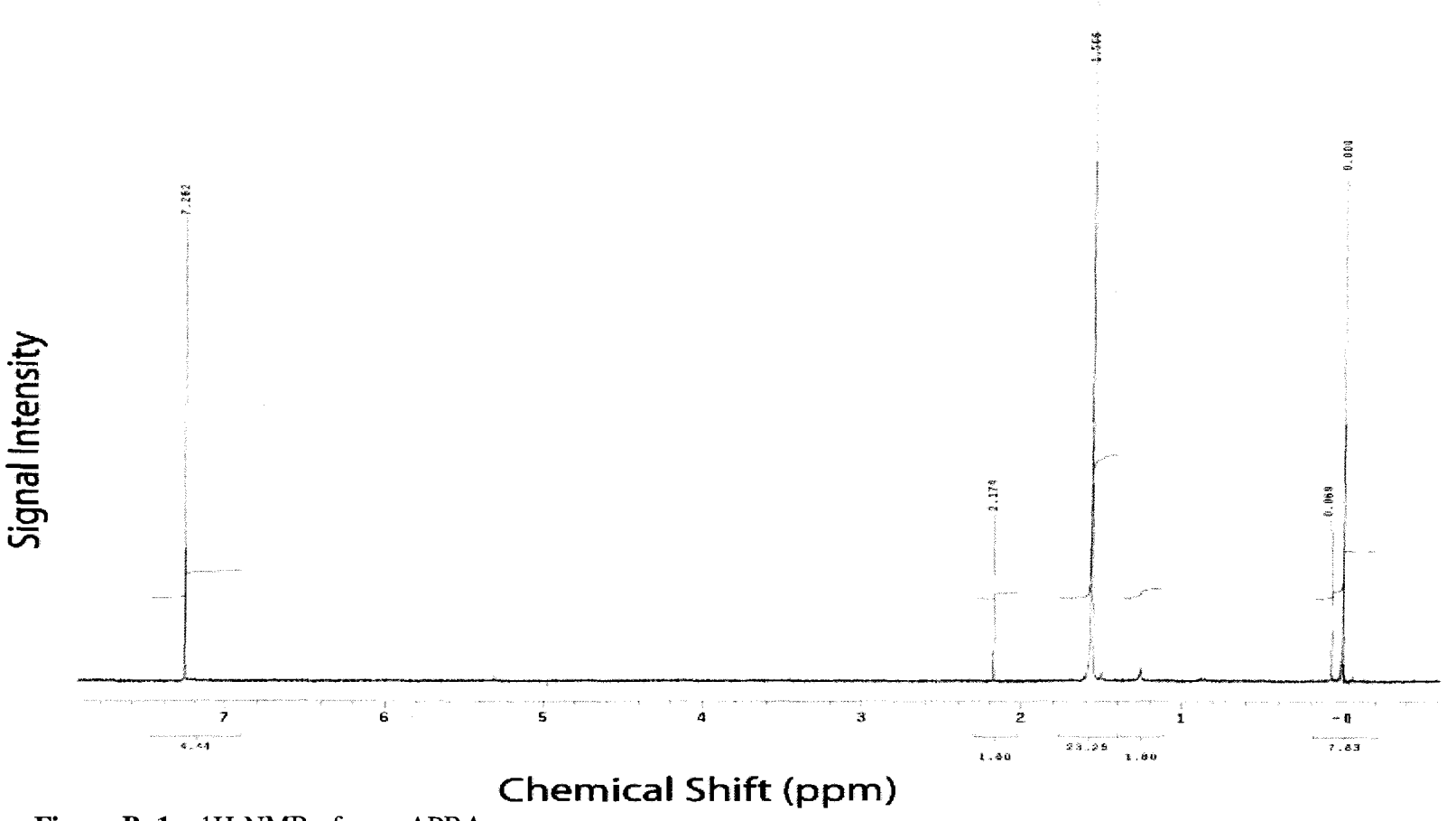

Figure B–1 : 1H-NMR of pure APBA.

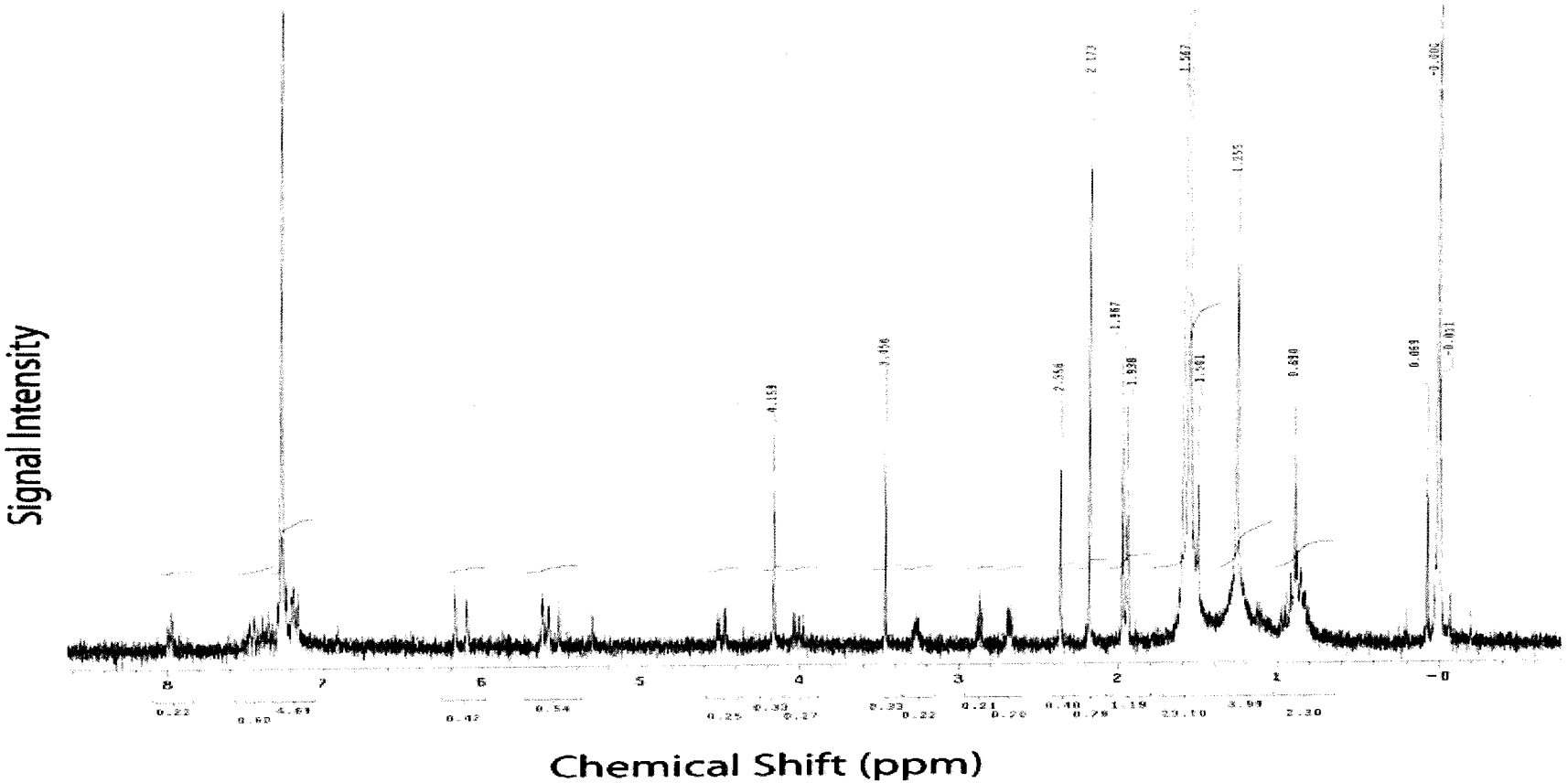

Figure B–2: ^{1}H-NMR of the boronate-modified poly(GMA-co-TRIM) monolith.

Appendix C: Van Deemter Equation

$$A = 2\lambda d_p$$

Equation A1: Eddy diffusion term where λ is the packing factor and d_p the average diameter of particles.

$$B = \psi D_M$$

Equation A2: Longitudinal diffusion term related to the obstruction factor (ψ) and diffusion coefficient of solute in the mobile phase (D_M).

$$C = C_S + C_M = \frac{qR(1-R)d_p^2}{D_S} + \frac{\omega d_f^2}{D_M}$$

Equation A3: Mass transfer term divided into coefficient of mass transfer in the stationary phase (C_S) and the mobile phase (C_M), df is the film thickness of the stationary phase, R is the retention ratio (t_m/t_R), D_s is the diffusion coefficient of solute in the stationary phase, q and ω are constants for the column.

A decrease in particle size causes an increase of the Eddy diffusion term (A) as well as a decrease in the mass transfer term (C). In CEC, since the Eddy diffusion is almost inexistent, it results in a net decrease in separation efficiency (N). In HPLC, the use of smaller particle is limited by attainable constant pressure of most commercial HPLC pumps. Only few HPLC systems, known as Ultrahigh Performance Liquid Chromatography systems are able to work with columns packed with silica particles smaller than 3 μm at flow rates similar to 5 μm silica particle packed columns.

Appendix D: Protein Sequences

β-Casein
Total Length: 208 Amino Acids
M_w: 23,583 Da

RELEELNVPGEIVESLSSSEESITRINKKEKFQSEEQQQTEDELQDKIHPFAQTQSL
VYPFPGPIPNSLPQNIPPLTQTPVVVPPFLQPEVMGVSKVKEAMAPKHKEMPFPK
YPVEPFTESQSLTLTDVENLHLPLPLLQSWMHQPHQPLPPTVMFPPQSVLSLSQSK
VLPVPQKAVPYPQRDMPIQAFLLYQEPVLGPVRGPFPIIV

Bovine Serum Albumin
Total Length: 607 Amino Acids
M_w: 69,293 Da

MKWVTFISLLLLFSSAYSRGVFRRDTHKSEIAHRFKDLGEEHFKGLVLIAFSQYL
QQCPFDEHVKLVNELTEFAKTCVADESHAGCEKSLHTLFGDELCKVASLRETYG
DMADCCEKQEPERNECFLSHKDDSPDLPKLKPDPNTLCDEFKADEKKFWGKYL
YEIARRHPYFYAPELLYYANKYNGVFQECCQAEDKGACLLPKIETMREKVLASS
ARQRLRCASIQKFGERALKAWSVARLSQKFPKAEFVEVTKLVTDLTKVHKECCH
GDLLECADDRADLAKYICDNQDTISSKLKECCDKPLLEKSHCIAEVEKDAIPENLP
PLTADFAEDKDVCKNYQEAKDAFLGSFLYEYSRRHPEYAVSVLLRLAKEYEATL
EECCAKDDPHACYSTVFDKLKHLVDEPQNLIKQNCDQFEKLGEYGFQNALIVRY
TRKVPQVSTPTLVEVSRSLGKVGTRCCTKPESERMPCTEDYLSLILNRLCVLHEK
TPVSEKVTKCCTESLVNRRPCFSALTPDETYVPKAFDEKLFTFHADICTLPDTEKQ
IKKQTALVELLKHKPKATEEQLKTVMENFVAFVDKCCAADDKEACFAVEGPKL
VVSTQTALA

Egg White Lysozyme
Total Length: 147 Amino Acids
M_w: 16,239Da

MRSLLILVLCFLPLAALGKVFGRCELAAAMKRHGLDNYRGYSLGNWVCAAKFE
SNFNTQATNRNTDGSTDYGILQINSRWWCNDGRTPGSRNLCNIPCSALLSSDITA
SVNCAKKIVSDG NGMNAWVAWRNRCKGTDVQAWIRGCRL

Appendix E: Prototype Capillary Holder

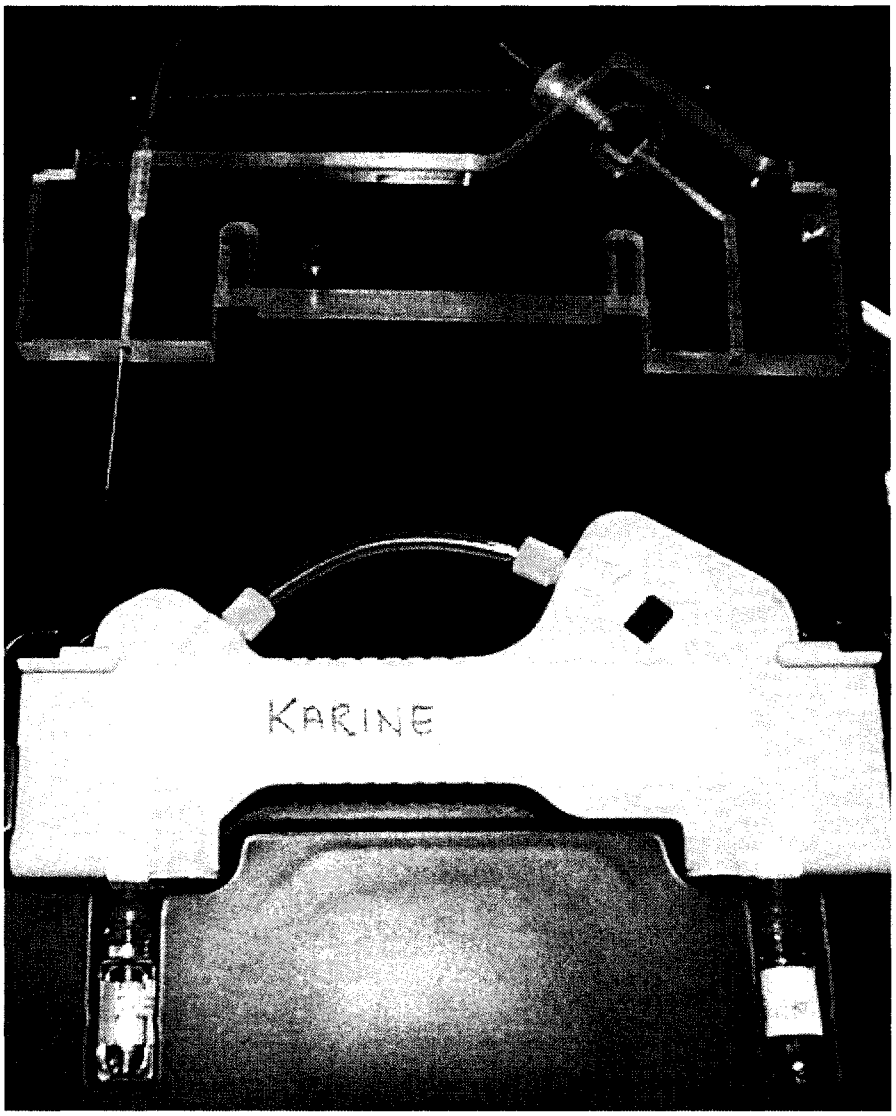

Figure E–1: Prototype capillary holder (above) adapted to avoid contact between fluorinated coolant and Teflon-coated capillary on a Beckman-Coulter CE system.

Appendix F: LEDIF Instrumental Setup

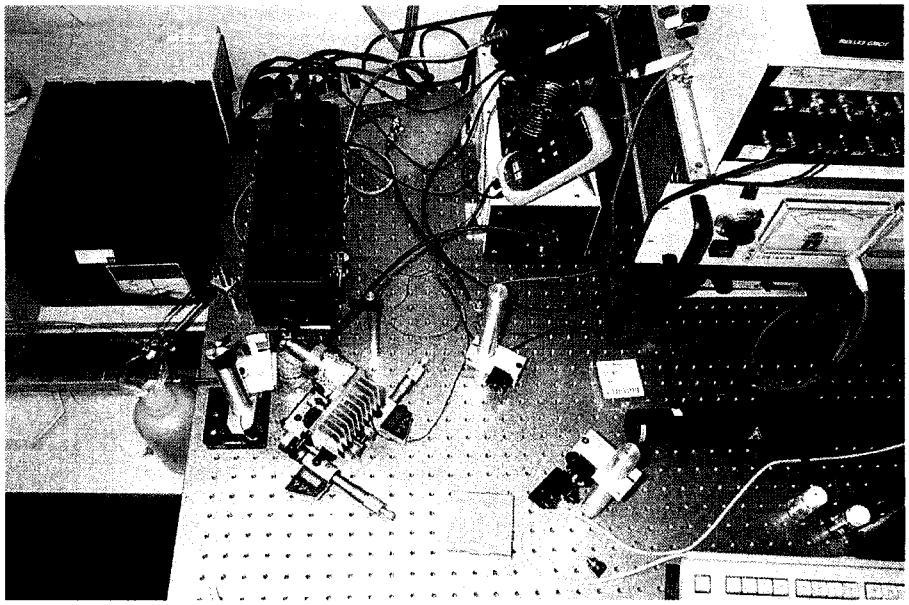

Figure F–1: Instrumental setup employed for Light-emitting diode induced fluorescence detection (LEDIF).

Glossary and List of Abbreviations

A.A.: Amino Acid
AFM: Atomic Force Microscopy
AMPS: 2-Acrylamido-2-methylpropane-1-sulfonic acid
BAC: n-Butyl acrylate
BET: Brunaeur-Elmer-Teller isotherm (used in Nitrogen adsorption-desorption porosimetry)
BDDA: 1,3-Butanediol diacrylate
CE: Capillary Electrophoresis
CEC: Capillary Electrochromatography
CIEF: Capillary Isoelectric Focusing
CGE: Capillary Gel Electrophoresis
CZE: Capillary Zone Electrophoresis
EOF: Electroosmotic flow
EDX: Energy Dispersive X-Ray Spectroscopy
ESI-MS: Electrospray Ionization Mass Spectrometry
GMA: Glycidyl methacrylate
HPLC: High-Performance Liquid Chromatography
I.S.: Internal Standard
LEDIF: Light-Emitting Diode Induced Fluorescence
LIF: Laser-Induced Fluorescence
MEKC: Micellar Electrokinetic Chromatography
μ-LC: Micro-Liquid Chromatography
MS: Mass Spectrometry
NACE: Nonaqueous Capillary Electrophoresis
PCEC: Pressurized Flow Electrochromatography (conventionally abbreviated PEC, designation also employed for Planar Electrochromatography)
PTM: Post-translational modification
Porosity: The porosity of a monolithic material is defined as the combination of its interstitial volume between stationary phase particles available for the mobile phase flow and the pores at and within these particles. There are three types of pores, based on their size (diameter): micropore (<2nm), mesopore (2nm<diameter<50nm) and macropore (>50nm).
RP: Reversed-Phase Chromatography
SP: Stationary Phase
WDX: Wavelength Dispersive X-Ray Spectroscopy
XPS: X-Ray Photoelectron Spectroscopy

References

[1]Pretorius, V., Hopkins, B.J., Schieke, J.D., *J. Chromatogr.*, **1974**, 99, 23-30.

[2]Jorgenson, J.W., Lukacs, K.D., *J. Chromatogr.*, **1981**, 218, 209-216.

[3]Knox, J.H., Grant, I.H., *Chromatographia*, **1987**, 24, 135-143.

[4]Breadmore, M.C., Palmer, A.S., Curran, M., Macka, M., Acdalovic, N., Haddad, P.R., *Anal. Chem.*, **2002**, 74, 2112-2118.

[5]Breadmore, M.C., Macka, M., Acdalovic, N., Haddad, P.R., *Anal. Chem.*, **2001**, 73, 820-828.

[6]Bedair, M., El Rassi, Z., *Electrophoresis*, **2002**, 23, 2938-2948.

[7]Tegeler, T., El Rassi, Z., *Anal. Chem.*, **2001**, 73, 3365-3372.

[8]Jiskra, J., Claessens, H.A., Cramers, C.A., *J. Sep. Sci.*, **2002**, 25, 1337-1345.

[9]Lämmerhofer, M., Svec, F., Fréchet, J.M.J., Lindner, W., *J. Chromatogr. A*, **2001**, 925, 265-277.

[10]Enlund, A.M., Andersson, M.E., Hagman, G., *J. Chromatogr. A.*, **2002**, 979, 335-344.

[11]Okanda, F.M., El Rassi, Z., *Electrophoresis*, **2006**, 28(1-2), 89-98.

[12]Scriba, G.K.E., *Electrophoresis*, **2003**, 24(15), 2409-2421.

[13]Carter-Finch, A.S., Smith, N.W., *J. Chromatogr. A*, **1999**, 848(1-2), 375-385.

[14]Smith, N.W., Evans, M.B., *Chromatographia*, **1995**, 41, 197-203

[15]Mistry, K., Cortes, H., Meunier, D., Schmidt, C., Feibush, B., Grinberg, N., Krull, I., *Anal. Chem.*, **2002**, 74(3), 617-625.

[16]Bandilla, D., Development of a Monolithic Stationary Phase for Capillary Electrochromatography and Microfluidic Separation of Proteins and Further Applications, Ph.D. Thesis, Concordia University, Montreal (Qc), Canada, **2004**.

[17]Siouffi, A.M., Tomao, V., Pesek, A., *Analusis*, **1999**, 27(2), 151-154.

[18]Majors, R.E., *LC-GC*, **1998**, 16(2), 96-106.

[19]Colón, L.A., Reynolds, K.J., Alicea-Maldonado, R., Fermier, A.M., *Electrophoresis*, **1997**, 18, 2162-2174.

[20]Simal-Gándara, J., *Crit. Rev. In Anal. Chem.*, **2004**, 34, 85-94.

[21]Altria, K.D., *Capillary Electrophoresis Guidebook: principles, operation, and applications*, Humana Press, Totowa (NJ), **1996**.

[22]Snyder, L.R., Kirkland, J.J., Glajch, J.L., *Practical HPLC Method Development 2nd Ed.*, Wiley & Sons, New York, **1997**.

[23]Pesek, J.J., Matyska, M.T., *J. Chromatogr A.* **2000**, 887(1-2), 31-41.

[24]Wu, J.T, Qian, M.G., Li, M.X., Zheng, K., Huang, P., Lubman, D.M., J. Chromatogr. A, **1998**, 794, 377-389.

[25]Pucci, V., Mandrioli, R., Raggi, M.A., Fanali, S., *Electrophoresis*, **2004**, 25(4-5), 615-621.

[26]Maruska, A., Pyell, U., *J. Chromatogr. A*, **1997**, 782(2), 167-174.

[27]Fu, H., Jin, W., Xiao, H., Huang, H., Zou, H., *Electrophoresis*, **2003**, 24(12-13), 2084-2091.

[28]Zhang, M., Yang, C., El Rassi, Z., *Anal. Chem.*, **1999**, 71, 3277-3282.

[29]Zhang, K., Yan, C., Zhang, Z., Wang, Q., Gao, R., *J. Liq. Chromat. & Rel. Tech.*, **2003**, 26, 2119-2131.

[30]Atkins, P.W., Physical Chemistry, 5th Edition, W.H. Freeman and Company, New York, **1996**, p.1007-1029.

[31]Knox, J.H., *Chromatographia*, **1988**, 26, 329-337.

[32]Bartle, K.D., Carney, R.A., Cavazza, A., Cikalo, M.G., Myers, P., Robson, M.M., Roulin, S.C., Sealey, K., *J. Chromatogr. A*, **2000**, 892(1-2), 279-90

[33]Biddiss, E., Erickson, D., Li, D., *Anal. Chem.*, **2004**, 76, 3208-3213.

[34]Choudary, G., Horváth, C., *J. Chromatogr. A*, **1997**, 781, 161-183.

[35]Bartle, K.D., Myers, P., *J. Chromatogr. A*, **2001**, 916, 3-23.

[36]Dittmann, M.M., Rozing, G.P., *Theory and Practice of Capillary Electrochromatography, Handbook of Capillary Electrophoresis*, ed. J.P. Landers, CRC Press, Boca Raton, **1997**, 139-152.

[37]Paul, P.H., Garguilo, M.G., Rakestraw, D.J., *Anal. Chem.*, **1998**, 70(13), 2459-2467.

[38]Snyder, L.R., Kirkland, J.J., Glajch, J.L., *Practical HPLC Method Development 2nd Ed.*, Wiley & Sons, New York, **1997**., p.47-50.

[39]Skoog, D.A., West, D.M., Holler, F.J., *Chimie Analytique*, Seventh Edition, De Boeck & Larcier, Paris, **1997**.

[40]Knox, J.H., *J. Chromatogr. A*, **1999**, 831, 3-15.

[41]Wen, E., Asiaie, R., Horvath, C., *J. Chromatogr. A*, **1999**, 855, 349-366.

[42]Yan, C., Schaufelberger, D., Ferni, F., *J. Chromatogr. A*, **1994**, 15-23.

[43]Dittmann, M.M., Rozing, G.P., *J. Chromatogr. A*, **1996**, 744, 63-74.

[44]Berek, D., Novák, I., *Chromatographia*, **1990**, 30(9), 582-590.

[45]Jiang, T., Jiskra, J., Claessens, H.A., Cramers, C.A., *J. Chromatogr. A*, **2001**, 923, 215-227.

[46]Mistry, K., Krull, I., Grinberg, N., J. Sep. Sci., **2002**, 25, 935-938.

[47]Rathore, A.S., Horváth, C., *Electroph.*, **2002**, 23, 1211-1216.

[48]Grimes, B.A., Lüdtke, S., Unger, K.K., Liapis, A.I., *J. Chromatogr. A*, **2002**, 979, 447-466.

[49]Liu, Z., Otsuka, K., Terabe, S., *J. Chromatogr. A*, **2002**, 959, 241-253.

[50]Xiang, R., Horváth, C., *Anal. Chem.*, **2002**, 74(4), 762-770.

[51]Girelli, A.M., Messina, A., Ferrantelli, P. , Sinibaldi, M. Tarola, A.M., *Chromatographia*, **2001**, 53(1), 284-289.

[52]MacDonald, A.M., Sheppard, M.A.W., Lucy, C.A., *Electrophoresis*, **2005**, 26(23), 4421-4428.

[53]Walhagen, K.; Unger, K.K., Hearn, M.T.W., *J. Chromatogr. A*, **2000**, 893(2), 401-409.

[54]Gförer, P.; Tseng, L.H., Rapp, E., Albert, K., Bayer, E., *Anal. Chem.*, **2001**, 73(14), 3234-3239.

[55]Rimmer, C.A., Piraino, S.M., Dorsey, J.G., *J. Chromatogr. A*, **2000**, 887, 115-124.

[56]Eimer T., Unger, K.K., Van der Greef, J., *Trends in Anal. Chem.*, **1996**, 15(9), 463-468.

[57]Eimer, T., Unger, K.K., Tsuda, T., *Fres. J. Anal. Chem.*, **1995**, 352(7-8), 649-653.

[58]Quirino, J.P., Dulay, M.T., Zare, R.N., *Anal. Chem.*, **2001**, 73, 5557-5563.

[59]Zhang, Y, Zhu, J., Zhang, L., Zhang, W., *Anal. Chem.*, **2000**, 72, 5744-5747.

[60]Zhang, Y., Zhu, J., Zhang, L., Zhang, W., *Anal. Chem.*, **2000**, 72, 5744-5747.

[61]Hilhorst, M.J., Somsen, G.W., de Jong, G.J., *Chromatographia*, **2001**, 53, 190-196.

[62]Stead, D.A., Reid, R.G., Taylor, R.B., *J. Chromatogr. A*, **1998**, 798, 259-267.

[63]Carney, R.A., Robson, M.M., Bartle, K.D., Myers, P., *J. High Res. Chromatogr.*, **1999**, 22(1), 29-32.

[64]Behnke, B., Bayer, E., *J. Chromatogr.*, **1994**, 680, 93-98.

[65]Robson, M.M., Bartle, K.D., Myers, P., *Chromatographia*, **1999**, 50(11-12), 711-715.

[66]Eimer, T., Unger, K.K., Tsuda, T., *Fresenius J. Anal. Chem.*, **1995**, 352, 649-653.

[67]Simal-Gándara, J., *Crit. Rev. Anal. Chem.*, **2004**, 34, 85-94.

[68]Klampfl, C.W., *J. Chromatogr. A*, **2004**, 1044, 131-144.

[69]Gfrörer, P., Schewitz, J., Pusecker, K., Tseng, L.-H., Albert, K., Bayer, E., *Electrophoresis*, 1999, 20, 3-8.

[70]Schewitz,J., Gfrörer,, P., Pusecker, K., Tseng, L.H., Albert, K., Bayer, E., Wilson, I.D., Bailey, N.J., Scarfe, G.B., Nicholson, J.K., Lindon, J.C., *Analyst*, **1998**, 123, 2835-2837.

[71]Lurie, I.S., Anex, D.S., Fintschenko, Y., Choi, W.Y., *J. Chromatogr. A*, **2001**, 924(1-2), 421-427.

[72]Wall, W., Juan, L, El Rassi, Z., *J. Sep. Sci.*, **2002**, 25(15-17), 1231-1244.

[73]El Rassi, Z., *Electrophoresis*, **1999**, 20(15-16), 3134-3144.

[74]Walbroehl, Y., Jorgenson, J.W., *J. Chromatogr.*, **1984**, 315, 135-143.

[75]Tjornelund, J., Hansen,S.H., *Chromatographia*, **1997**, 44, 5-9.

[76]Wright, P.B., Lister, A.S., Dorsey, J.G., *Anal. Chem.*, **1997**, 69, 3251-3259.

[77]Fritz, J.S., Breadmore, M.C., Hilder, E.F., Haddad, P.R. *J Chromatogr A*, **2002**; 942(1-2), 11-32.

[78]Miyama, J.H., Alasandro, M.S., Riley, C.M., *J. Chromatogr. A*, **1997**, 769, 145-153.

[79]Rozing, G.P., Dittmann, M.M., *J. Chromatogr. A*, **1996**, 744, 63-74.

[80]Smith, N.W., Evans, M.B., *Chromatographia*, **1995**, 41, 197-203.

[81]Spikmans, V., Lane, S.J., Smith, N.W., *Chromatographia*, **2000**, 51(1-2), 18-24.

[82]Bartle, K.D., Myers, P., *Capillary Electrochromatography.* RSC chromatography, London, **2001**.

[83]Eeltink, S., Rozing, G.P., Kok, W.T., *Electrophoresis*, **2003**, 24, 3935-3961.

[84]Huck, C.W., Stecher, G., Bakry, R., Bonn, G.K., *Electrophoresis*, **2003**, 24, 3911-3997.

[85]Zhang, J., Huang, X., Zhang, S., Horváth, C., *Anal.Chem.*, **2000**, 72, 3022-3029.

[86]Zhang, J., Huang, X., Zhang, S., Horváth, C., *J. Chrom. A.*, **2000**, 887, 465-477.

[87]Bandilla, D., Skinner, C.D., *J. Chrom. A.*, **2003**, 1004, 167-179.

[88]Klampfl, C.W., Haddad, P.R., *J. Chromatogr. A*, **2000**, 884, 277-285.

[89]Bandilla, D., Skinner, C.D., *J. Chrom. A*, **2004**, 1044, 113-129.

[90]Krull, I., Sebag. A., Stevenson, R., *J. Chromatogr. A*, **2000**, 887, 137-163.

[91]Simal-Gándara, J., *Crit. Rev. In Anal. Chem.*, **2004**, 34, 85-94.

[92]Kitagawa, F., Inoue, K., Hasegawa, T., Kamiya, M., Okamoto, Y., Kawase, M., Otsuka, K., J. Chrom. A., **2006**, 1130(2), 219-226.

[93]Hilhorst, M.J., Somsen, G.W., de Jong, G.J., *J. Chrom. A*, **2000**, 872(1-2), 315-321.

[94]Pucci, V., Mandrioli, R., Raggi, M.A., Fanali, S., *Electrophoresis*, **2004**, 25(4-5), 615-621.

[95]Valette, J.C., Demesmay, C., Rocca, J.L., Verdon, E., *Chromatographia*, **2005**, 62(7-8), 393-399.

[96]Yan, C., Dadoo, R., Zhao, H., Zare, R.N., Rakestraw, D.J., *Anal. Chem.*, **1995**, 67, 2026-2029.

[97]Ding, M., Vouros, D., *Am. Lab.*, **1998**, 30(12), 15-29.

[98]Kok, W.T., *J. Chromatogr. A*, **2004**, 1044(1-2), 145-151.

[99]Zeng, H.L., Li, H.F., Lin, J.M., *Anal. Chim. Acta.*, **2005**, 551, 1-8.

[100]Witsuba, D., Schurig, W., *J. Chromatogr. A*, **2000**, 875, 255-276.

[101]Schweitz, L., Andersson, L.I., Nilsson, S., *J. Chromatogr. A*, **1998**, 817, 5-13.

[102]Yamamoto, , H., Baumann, J., Erni, F., *J. Chromatogr. A*, **1992**, 593, 313-319.

[103]Stol, R., Mazereeuw, M., Tjaden, U.R., Van der Greef, J., *J. Chromatogr. A*, 2000, **873**, 293-298.

[104]Yan, C., *US Patent 5,453,163*, **1995**.

[105]Maloney, T.D., Colon, L.A., *Electrophoresis*, **1999**, 20, 2360-2365.

[106]Tang, Q., Xin, B., Lee, M.L., *J. Chromatogr. A,* **1999**, 837, 35-50.

[107]Reynolds, K.J., Colon, L.A., *Analyst*, **1998**, 123, 1493-1495.

[108]Chen, J.-R., Dulay, M.T., Zare, R.N., Svec, F., Peters, E., *Anal. Chem.,* **2000**, 72, 1224-1227.

[109]Matyska, M.T., Pesek, J.J., Sandoval, E., Parkar, U., Liu, X., *J. Liq. Rel. Techn.*, **2000**, 23(1), 97-111.

[110]Wu, J.T., Qian, M.G., Li, M.X., Zheng, K., Huang, P., Lubman, D.M., *J. Chromatogr. A,* **1998**, 794, 377-389.

[111]Hradil, J., Svec, F., Votavova, E., Bleha, M., Pelzbauer, Z., Brych, J., *Polymer*, **1992**, 33, 1731-1738.

[112]Horak, D., Labsky, J., Bleha, M., Pelzbauer, Z., Svec, F., *Polymer*, **1993**, 34, 3481-3489.

[113]Horak, D, Svec, F., Fréchet, J.M.J, *J. Polym. Sci., Polym. Chem.*, **1995**, 33, 2329-2338.

[114]Liang, Y.-C., Svec, F., Fréchet, J.M.J., *J. Polym. Sci., Polym. Chem,*. **1997**, 35, 2631-2643.

[115]Brinker, C.J., Scherer, G.W., *Sol-Gel Science: The Physics and Chemistry of Sol-Gel Processing*, Academic Press, San Diego, **1989**.

[116]Minakuchi, H., Nakanishi, K., Soga, N., Ishizuka, N., Tanaka, N., *Anal. Chem.*, **1996**, 68, 3498-3501.

[117]Nakanishi, K., Soga, N., *J. Am. Ceram. Soc.*, **1991**, 74, 2518-2530.

[118]Asiaie, R., Huang, X., Farnan, D., Horvath, C., *J. Chromatogr. A*, **1998**, 806, 251-263.

[119]Park, S.S., Ha, C.S., *Chem. Rec.*, **2006**, 6, 32-42.

[120]www.merck.de

[121]Allen, D., El Rassi, Z., *Electrophoresis*, **2003**, 23, 3-18.

[122]Lazar, I.M., Li, L., Yang, Y., Karger, B.L., *Electrophoresis*, **2003**, 24(21), 3655-3662.

[123]Bhattacharyy, S., Lelong, G., Saboungi, M.L., *J. Experim. Nanosc.*, **2006**, 1(3), 375-395.

[124]Hjerten, S., Eaker, D., Elenbring, C., Ericson, C., Kubo, K., Liao, J.L., Zeng, C.M., Lindström, Lindh, C., Palm, A., Srichiayo, T., Valcheva, L., Zhang, R., *Jpn. J. Electrophor.*, **1995**, 39, 105-118.

[125]Ericson, C., Liao, J.-L., Nakazato, K.I., Hjerten, S., *J. Chromatogr. A*, **1997**, 767, 33-41.

[126]Janson, J.C., Rydén, L., Protein Purification, Principles, high resolution methods and applications, Wiley, New York, **1998**.

[127]Adam, T., Lüdtke, S., Unger, K.K., *Chromatographia*, **1999**, 49, 49-55.

[128]Dittmann, M.M., Rozing, G.P., *J. Microcol. Sep.*, **1997**, 9, 399-408.

[129]Allen, P.E.M., Burnett, G.M., Downer, J.M., Melville, H., *Die Makromol. Chem.*, **2003**, 38(1), 72-84.

[130]Jenkins, R.K., *J. Polym. Sci. B*, **2003**, 2(12), 1147-1154.

[131]Yu, C., Xu, M., Svec, F., Fréchet, J.M.J., *J. Polym. Sci.Part A : Polym, Chem.*, **2002**, 40, 755-769.

[132]Yu, C., Davey, M.H., Svec, F., Fréchet, J.M.J., *Anal. Chem.*, **2001**, 73, 5088-5096.

[133]Sinner, F.M., Buchmeiser, M.R., *Angew. Chem. Inter. Ed.*, **2000**, 39(8), 1433-1436.

[134]Wuff, G., *Angew. Chem.*, **1995**, 34, 1812-1832.

[135]Cameron, N.R., Flook, K.J., Wren, S.A.C., *Chromatographia*, **2003**, 57, 203-206.

[136]Svec, F., Fréchet, J.M.J., Macromolecules, **1995**, 28, 7580-7582.

[137]Personal communications, Julien Courtois (Prof. K. Irgum's research group).

[138]Davies, M.P., De Biasi, V., Perret, D., *Anal. Chim. Acta*, **2004**, 504 (1), 7-14.

[139]Navarro-Villoslada, F., San Vicente, B., Moreno-Bondi, M.C., *Anal. Chim. Acta*, **2004**, 504 (1), 149-162.

[140]Hogendoorn, E.A., van Zoonen, P., *Anal. Chem.*, **1998**, 70, 1362-1368.

[141]Yang, W., Rånby, B., *Eur. Polym. J.*, **1999**, 35, 1557 – 1568.

[142]Battaerd, H.A.J., Tregear, G.W., *Graft Copolymers*. Polymer Reviews (vol. 16), Interscience Publishers, New York, **1967**.

[143]Eeltink,S., Hilder. E.F., Geiser, L., Svec, F., Fréchet, J.M.J., Rozing, G.P., Schoenmakers, P.J., Kok, W.T., *J. Sep. Sci.*, **2007**, 30, 407-413.

[144]Hilder, E.F., Svec, F., Fréchet, J.M.J., *Anal. Chem* . **2004**, 76(14), 3887-3892.

[145]Baeuml, F., Welsch, T., *J. Chromatogr. A*, **2002**, 961, 35-44.

[146]Doneanu, A., Chirica, G.S., Remcho, V.T., *J. Sep. Sci.*, **2002**, 25, 1252-1256.

[147]Kornyšova, O., Šurna, R., Snitka, V., Pyell, U., Maruška, A., *J. Chromatogr. A*, **2002**, 971, 225-235.

[148]Rouquerol, J., Avnir, D., Fairbridge, C.W., Everett, D.H., Haynes, J.H., Pernicone, N., Ramsay, J.D.F., Sing, K.S.W., Unger, K.K., *Pure & Appl. Chem.*, **1994**, 66, 1739-1758.

[149]Robens, E. Krebs, K.-F., Meyer, K., Unger, K.K., Dabrowski, A. *Coll. Surf. A.*, **2002**, 253-257.

[150]Cabral, J.L., Bandilla, D., Skinner, C.D., *J. Chromatogr. A.*, **2006,** 1108(1), 83-89.

[151]Maruška, A., Kornyšova, O., *J. Biochem. Biophys. Methods*, **2004**, 59, 1-48.

[152]Binnig, G., Gerber, C., Stoll, E., Albrecht, T.R., Quate, C.F., *Surf. Sci.*, **1987**, 189-190, 1-6.

[153]Jančo, M., Xie, S., Peterson, D.S., Allington, R.W., Svec, F., Fréchet, J.M.J., *J. Sep. Sci*, **2002**, 25, 909-916.

[154]Al-Bokari, M., Cherrak, D., Guiochon, G., *J. Chromatogr. A*, **2002**, 975, 275-284.

[155]Rathore, A.S., Wen, E., Horváth, C., *Anal. Chem*, **1999**, 71, 2633-2641.

[156]Chen, L., Chen, L., Yan, X., Wan, Q.H., *Anal. Chem*, **2000**, 74, 5157-5159.

[157]Pesek, J. J., Matyska, M. T., Capillary Electrochromatography, J. Chromatogr. Library v.62, Elsevier Science B.V., Amsterdam, **2001**.

[158]Pullen, P.E., Pesek, J.J., Matyska, M.T., *Anal. Chem.*, **2000**, 72, 2751-2757.

[159]Kornyšova, O., Šurna, R., Snitka, V., Pyell, U., Maruška, A., *J. Chromatogr. A*, **2002**, 971, 225-235.

[160]Hilder, E.F., Svec, F., Fréchet, J.M., *Electrophoresis*. **2002**, 23, 3934-3953.

[161]Eymann, W., *Chromatographia*, **1997**, 45(1), 235-242.

[162]Hercules, D.M., Houalla, M., *Fres. J. Anal. Chem.*, **1986**, 324(6), 589-600.

[163]Poncin-Epaillard, F., Beunet, J., Bulou, A., Bardeau, J.F., *J. Polym. Sc. A*, **2001**, 39(18), 3052-3061.

[164]Gillberg, G., *The J. of Adhesion*, **1987**, 21(2), 129-154.

[165]Bandilla, D., Skinner, C.D., *J. Chromatogr. A.* **2004,** 1044, 113-129.

[166]Zhang, S., Zhang, J., Horváth, C., *J. Chromatogr. A.* **2002,** 965, 83-92.

[167]Xu, W., Regnier, F.E., *J. Chromatogr. A.* **1999,** 853, 243-256.

[168]Throckmortin, D.J., Shepodd, T.J., Singh, A.K., *Anal. Chem* **2002**, 74, 784-789.

[169]Ericson, C., Hjertén, S., *Anal. Chem.* **1999**, 71, 1621-1627.

[170]Okanda, F.M., El Rassi, Z., *Electrophoresis*. **2006**, 28(1-2), p.89-98.

[171]Porath J., Carlson J., Olsson I., Belfrage G., *Nature*, **1975**, 258, 598-599.

[172]Slentz, B.E., Penner, N.A., Regnier, F.E., *J. Chromatogr. A.* **2003**, 984, 97-107.

[173]Tischer, W., Kasche, V., *Tibtech*, **1999**, 17, 326-335.

[174]Elbert, D.L., Hubbell, J.A., *Ann. Rev. Mater. Sci.*, **1996**, 26, 365-394.

[175]Voet, D., Voet, J.G., *Biochemistry 2nd Edition*, Wiley, New York, **1995.**

[176]Moses, R.G., *Diab. Med.*, **1994**, 11, 603.

[177]Madera, M., Mechref, Y., Novotny, M.V., *Anal. Chem.*, **2005**, 77, 4081-4090.

[178]Okanda, F.M., El Rassi, Z., *Electrophoresis*, **2006**, 27 (5-6), 1020-1030.

[179]Singh, N., Willson, R.C., *J. Chromatogr. A.* **1999**, 840, 205–213

[180]Cuatrecasas P., *Bio. Chem*, **1970,** 245, 3059-3067.

[181]Lorand, J.P., Edwards, J.O., *J. Org. Chem.*, **1959,** 24, 769-774.

[182]Sandanayake, K., Shinkai, S., *J. Chem. Soc., Chem. Commun.*, **1994**, 1083-1084

[183]DiCesare, N., Lakowicz, J.R., *Org. Lett.*, **2001**, 3(24), 3891-3893.

[184]Potter, O.G., Breadmore, M.C., Hilder, E.F., *Analyst*, **2006**, 131, 1094-1096.

[185]Bergström, K., Holmberg, K., *Biotech. Bioeng.*, **2004**, 38(8), 952-955.

[186]Nam, Y., Branch, D.W., Wheeler, B.C., *Biosens. Bioelec.*, **2006**, 22(5), 589-597.

[187]Kandimalla, V., Tripathi, V., Ju, H., *Crit. Rev. Anal. Chem.*, **2006**, 36(2), 73-106.

[188]Bonneil, E., Mercier, M., Waldron, K.C., *Anal. Chim. Acta*, **2000**, 404, 29–45.

[189]Peterson, D.S, Rohr, T., Svec, F., Fréchet, J.M.J., *Anal. Chem.*, **2003**, 75, 5328–5335.

[190]Peterson, D.S, Rohr, T., Svec, F., Fréchet, J.M.J., *Anal. Chem.*, **2002**, 74, 4081–4088.

[191]Peterson, D.S, Rohr, T., Svec, F., Fréchet, J.M.J., *J. Proteom.Res.*, **2002**, 1, 563–568.

[192]Petro, M., F. Svec, F., Fréchet, J.M.J., *Biotech. Bioeng.*, **1996**, 48, 355–363.

[193]Xie, S., Svec, F., Fréchet, J.M.J., *Biotech. Bioeng.*, **1999**, 62, 30–35.

[194]Palm, A.K., Novotny, M.V., *Rapid Commun. Mass Spectrom.*, **2004**, 18, 1374–1382.

[195]Massolini, G., Calleri, E., *J. Sep. Sci.*, **2004**, 28(1), 7-21.

[196]Slysz, G.W., Schriemer, D.C., *Rapid Commun. Mass Spectrom.*, **2003**, 17, 1044–1050.

[197]Calleri, E., Temporini, C., Perani, E., Stella, C., Rudaz, S., Lubda, D., Mellerio, G., Veuthey, J.-L., Caccialanza, G., Massolini, G., *J. Chromatogr. A*, **2004**, 1045, 99–109.

[198]Dolnik, V., Liu, S., Jovanovich, S., *Electrophoresis*, **2000**, 21, 41-54.

[199]Lazar, I.M., Trisiripisal, P., Sarvaiya, H.A., *Anal. Chem.*, **2006**, 78, 5513-5524.

[200]Ethier, M., Hou, W., Duewel, H.S., Figeys, D., *J. Proteome Res.*, **2006**, 5, 2754-2759.

[201]Bandilla, D., Cabral, J.L., Skinner, C.D., *Electrophoresis*, **2006**, 27(16), 3271-3276.

[202]Fischer, U.C., Scanning Probe Microscopy: Analytical Methods, Roland Wiesendanger (Ed.), Springer, Berlin, **1998**

[203]Mineau, R., "personal communication".

[204]Karas, M., Hillenkamp, F., *Anal. Chem.*, **1988**, 60, 2299-2301

[205]http://ca.expasy.org/sprot/

[206]http://prospector.ucsf.edu/prospector/4.0.8/html/msdigest.htm

[207]Weinglass, A.B., *EMBO Journal*, **2003**, 22, 1467-1477

[208]Chevalier, F., Chobert, J.-M., Dalgalarrondo, M., Choiset, Y., Haertlé, T., *Nahrung/Food*, **2002**, 46, 58-63.

[209]Sun, Y., Hayakawa, S.; Chuamanochan, M.; Fujimoto, M.; Innun, A.; Izumori, K., *J. Agric. Food Chem.*, **2004**, 52, 1293-1299

[210]http://www.nkhome.com/pdfs/k3_k35_k4_calkit_web.pdf

[211]www.polymicro.com

[212]Wang, T., Bruin, G.J., Kraak, J.C., Poppe, H., *Anal. Chem.* **1991.**

[213]Kim, S., Yoo, H.J., Nam, H.G., Hahn, J.H., *Chromatographia*, **1995**, 40, 345-349.

[214]Ingle, J.D., Crouch, S.R., *Spectrochemical Analysis*; Prentice-Hall, Inc., Upper Saddle River, New Jersey, **1988.**

[215]Guttman, A., Schwartz, H.E., *Anal. Chem.*, **1995**, 67, 2279-2283.

[216]Rozing, G.P., *Am. Laboratory*, **1998**, 30, 33.

[217]Geijels, V.L., *J. Am. Laboratory*, **2002**, 34, 9-10.

[218]Ngola, S.M., Fintschenko, Y., Choi, W.Y., Shepodd, T.J., *Anal. Chem.*, **2001**, 73, 849-856.

[219]Chen, L.; Chen, L.; Yan, X.; Wan, Q. H., *J. Chrom. A*, **2003**, 986, 297-302.

[220]Carney, R. A.; Robson, M. M.; Bartle, K. D.; Myers, P. J. High Res. Chromatogr., **1999**, 22, 29-32.

[221]Gooding, K.M., Regnier, F.E., HPLC of Biological Macromolecules 2nd edition, Chromatographic Science Series v.87, CRC Press, Boca Raton, **2002**, p.81-247.

[222]Boysen, R.I., Hearn, M.T.W., *Curr. Prot. In Mol. Biol.*, **2001**, Unit 10.13.

[223]Alpert, A.J., *J. Chromatogr.*, **1990**, 499, 177-196.

[224]Wang, X., Li, W., Rasmussen, H.T., *J. Chromatogr. A*, **2005**, 1083(1-2), 58-62.

[225]Chang, J.P., An, J.G., *Chromatographia*, **1988**, 25(4), 350-355.

[226]Beaudoin, M. E.; *Chem 450 Report*, Department of Chemistry and Biochemistry, Concordia University: Montreal, **2003**.

[227]Bobe, G., Beitz, D.C., Freeman, A.E., Lindberg, G.L., *J. of Agric. Food Sci.*, **1998**, 46, 458-463.

[228]Moseley, R., Stewart, J.E., Stephens, P., Waddington, R.J., Thomas, D.W., *Brit. J. Dermat.*, **2004**, 150, 401-413.

[229]Oguri, S., , Maeda, Y., Mizusawa, A., *J. Chromatogr. A.*, **2004**, 1044(1-2), 271-276.

[230]Veledo, M.T., de Frutos, M., Diez-Masa, J.C., *Electrophoresis*, **2006**, 27(15), 3101-3107.

[231]Kwakman, P.J.M., Koelewijn, H., Kool, I., Brinkman, U.A.T., De Jong, G.J., *J. Chromatogr.*, **1990**, 511, 155-166.

[232]Alba, F.J., Daban, J.R., *Electrophoresis*, **2005**, 18(11), 1960-1966.

[233]Freitag, R., *J. Chromatogr. A.* **2004**, 1033(2), 267-273.

[234]Mahuzier, P.E., Altria, K.D., Clark, B.J., *J. Chromatogr. A*, **2001**, 924, 465-470

[235]Garcia, I., Ortiz, M.C., Sarabia, L., Vilches, C. Gredilla, E., *J. Chromatogr.A*, **2003**, 992, 11-27

[236]Kuo, K.L., Hsieh, Y.Z., *J. Chromatogr. A*, **1997**, 768, 334-341

[237]W. Horwitz (Ed.), *Official Methods of Analysis of AOAC Inter., vol.2*, AOAC Inter., **2000**, Gaithersburg, Maryland, p. 9.

[238]Rogers, B., York, D., Whisman, N., Jones, M., Murray, K., Adams, J.D., Sulchek, T., Minne, S.C., *Rev. Sci. Instrum.* **2002**, 73, 3242-3244.

[239]Putman, C., VanderWerf, K., DeGrooth, B., VanHulst, N., Greve, J., *Appl.Phys.Lett.*, **1994**, 64, 2454-2456.

[240]Han, W., Lindsay, S., Tianwei, J., *Appl.Phys.Lett.*, **1996**, 69, 4111-4113.

[241]Matsko, N.; Mueller, M. *J. Struct. Biol.* **2004**, 146(3), 334-343.

[242]Simpson, G.J., Sedin, D.L., Rowlen, K.L., *Langmuir*, **1999**, 15, 1429-1434.

[243]Lai, L.; Irene, E.A.; *J. Vac. Sci. Technol. B*, **1999**, 17; 33-39.

[244]Hansma, P.K., Cleveland, J.P., Radmacher, M., Walters, D.A., Hillner, P.E., Bezanilla, M., Fritz, M., Vie, D., Hansma, H.G., Prater, C.B., Massie, J., Fukunaga, L., Gurley, J., Elings, V., *App. Phys. Lett.*, **1994**, 64, 1738-1740.

[245]Rohr, T., Hilder, E.F., Donovan, J.J., Svec, F., Fréchet, J.M.J., *Macromol.*, **2003**, 36, 1677-1684.

[246]Svec, F., Peters, E.C., Sýkora, D., Fréchet, J.M.J., *J. Chrom. A*, **2000**, 887, 3-29.

[247]Augustin, V., Jardy, A., Gareil, P., Hennion, M.C., *J. Chromatogr. A*, **2006**, 1119, 80-87.

[248]Svec, F., *J. Sep. Sci.*, **2004**, 27, 1419-1430.

[249]Burlant, W. J., Hoffman, A. S., *Block and graft polymers*, Reinhold, New York, **1961.**

[250]Lokensgard, E., Richardson, T.L., *Industrial PlasticsTheory and Applications, 3rd Edition*, Thompson Delmar Learning, Florence, **2004.**

[251]Chanda, M., Roy, S.K., *Plastics Technology Handbook, 4th Edition (Plastics Engineering vol. 72)*, CRC Press, Boca Raton, **2006.**

[252]Arayapranee, W., Rempel, G.L., *J. Appl.Polym. Sci.*, **2004**, 93(1), 455-463.

[253]Phadnis, S., Patri, M., Hande, V.R., Deb, P.C., *J. Appl.Polym. Sci.*, **2003**, 90(9), 2572-2577.

[254]Marconi, W., *React. Polym.*, **1989**, 11, 1-19.

[255]Guisán, J.M., *Immobilization Of Enzymes And Cells (Methods in Biotechnology)*, 2nd edition, Humana Press, New York.

[256]Gianfreda, L., Scarfi, M.R., *Mol. And Cell. Biochem.*, **1991**, 100, 97-128.

[257]Hermanson, G.T., Mallia, A.K., Smith, P.K., *Immobilized Affinity Ligand Techniques*, **1992**, Academic Press, San Diego.

[258]Viklund, C., Ponten, E. Glad, B., Irgum, K., Horstedt, P., Svec, F. *Chem. Mater.*, **1997**, 9, 463-471.

[259]Podgornik, H., Podgornik, A., *Enzyme and Microbial Tech.*, **2002**, 31. 855-861.

[260]Josie, D., Buchacher, A., *J. Biochem. Biophys. Methods*, **2001**, 49, 153-174.

[261]Dulay, M.T., Baca, Q.J., .Zare, R.N., *Anal. Chem.*, **2005**, 77, 4604-4610.

[262]Girelli, A.M., Mattei, E., *J. Chromatogr. B*, **2005**, 819, 1, 3-16.

[263]Temporini, C., Perani, E., Mancini, F., Bartolini, M., Calleri, E., Lubda, D., Felix, G., Andrisano, V., Massolini, G., *J. Chromatogr. A*, **2006**, 1120, 121-131.

[264]Keil, O., LeRiche, T., Deppe, H., Volmer, D.A., *Rapid Commun. Mass Spectrom.*, **2002**, 16, 814-820.

[265]Okubo, M., Kamei, S., Tosaki, Y., Fukunaga, K., Matsumoto, T., *Coll. Polym. Sci,*, **1987**, 265(11), 957-964.

[266]Walsh, K.A., Wilcox, P.E., *Methods Enzymol.*, **1970**, 19, 31.

[267]Freije, J.R., Mulder, P.P.M.F.A., Werkman, W., Rieux, L., Niederlander, H.A.G., Verpoorte, E.; Bischoff, R., *J.Proteome Res.*, **2005**, 4, 1805-13

[268]Sakai-Kato, K., Kato, M., Toyo'oka, T., *Anal. Chem.*, **2002**, 74, 2943-2949.

[269]Tyagi, R., Gupta, M.N., *Biotechnol. Tech.*, **1998**, 12, 569-570.

[270]Cunningham, L.W., *Biol. Chem.*, **1954**, 211, 13-19.

[271]Dadoo, R., Zare, R.N., Yan, C., Anex, D.S., *Anal. Chem.*, **1998**, 70, 4787-4792.

[272]Kasicka, V., *Electrophoresis*, **2006**, 27, 142-175.

[273]Kasicka, V., *Electrophoresis*, **2003**, 24, 4013-4046.

[274]Li, Y., Xiang, R., Wilkins, J.A., Horvath, C., *Electrophoresis*, **2004**, 25. 2242-2256.

[275]Picha, D.H., *J. Food. Sci.*, **1985**, 50, 1189-1190.

[276]Nikolov, Z., Jakovljevi, J.B., Bokov, M., *Starch – Stärke*, **1984**, 36, 97-100.

[277]Hage, D.S., *Handbook of Affinity Chromatography, 2nd Edition*, **2005**, CRC Press, Boca Raton.

[278]Li, Y., Linné-Larsson, E., Jungvid, H., Yu, Galaev, I.Y., Mattiasson, B., *.Biosep.*, **2001**, 9, 315-323.

[279]Bossi, A., Castelletti, L., Piletsky, S.A., Turner, A.P.F., Righetti, P.G., *J. Chromatogr. A*, **2004**, 1023, 297-303.

[280]Svec, F., Hrudkova, H., Horak, D., Kalal, J., *Die Angew. Makromol. Chem.*, **1977**, 912, 23-36.

[281]Kalal, J., Svec, F., Marousek, V., *J. Polym. Sci.*, **1974**, 47, 155-166.

[282]Gross, J.H., *Mass Spectrometry*, Springer, New York, **2004**